

# Journal of Energy

ISSN 1849-0751 (On-line)  
ISSN 0013-7448 (Print)  
UDK 621.31

**VOLUME 65 Number 1–2 | 2016 Special Issue**

- 03** Ž. Tomšić, I. Rajšl, M. Filipović  
Possible Role of NPP in Long Term Low Carbon Development Strategy – Case Study Croatia
- 15** G. Maronati, B. Petrović, N. Čavlina  
P<sub>2</sub>S-LWR Top-Down Differential Economics Evaluation Approach
- 24** J. Čeović, M. Širola  
Medium and Low Voltage Cable Measurements - TD, PD, LIRA
- 38** P. Mateljak, M. Budimir, M. Koštan, A. Mohimi  
High-Temperature Ultrasound NDE Systems for Continuous Monitoring of Critical Points in Nuclear Power Plants Structures
- 50** M. Pirc  
Cable Aging Management Program Implementation in Krško NPP-NEK
- 63** V. Čalić  
The Efficiency of Nuclear Ion Exchange Resins Applied in the Primary Circuit Demineralizers of NPP Krško
- 75** I. Rep, T. Tomašić, D. Barila  
Sludge Deposit Mapping for Steam Generators
- 83** A. N. Kilic, D. M. Ward, P. H. Lebreton  
Increasing Needs and Solutions for Non-Baseload Operation of Nuclear Power Plants
- 93** Š. Vlahović, D. Grgić, V. Benčik  
NPP Krško Post-UFC Transient Response during MSLB
- 105** M. Kromar, B. Kurinčič  
Validation of the CORD-2 System for the NPP Krško Nuclear Core Design Calculations
- 116** G. L. Ponomarenko  
Peculiarities of Neutronics Characteristics of Integral Reactor WWER of Small Capacity
- 127** J. Haščík, Š. Čerba, J. Lúley, B. Vrban  
Study of the Allegro Core Performance
- 138** M. Matijević, D. Pevec, R. Ječmenica  
I2S-LWR Activation Analysis of Heat Exchangers Using Hybrid Shielding Methodology With SCALE6.1
- 151** M. Matijević, R. Ječmenica, D. Grgić  
Spent Fuel Pool Dose Rate Calculations Using Point Kernel and Hybrid Deterministic-Stochastic Shielding Methods
- 162** R. Ječmenica, D. Grgić, M. Matijević, B. Petrović  
Nuclear and thermal hydraulic calculation of a representative I2S-LWR first core
- 173** V. Vo Van, P. Breitenstein  
Possible Used Fuel Management Options For A Single Reactor Utility

# Journal of Energy

Scientific Professional Journal Of Energy, Electricity, Power Systems

Online ISSN 1849-0751, Print ISSN 0013-7448, VOL 65-1

## Published by

HEP d.d., Ulica grada Vukovara 37, HR-10000 Zagreb

HRO CIGRÉ, Berislavićeva 6, HR-10000 Zagreb

## Publishing Board

**Robert Krklec**, (president) HEP, Croatia,

**Božidar Filipović-Grčić**, (vicepresident), HRO CIGRÉ, Croatia

## Editor-in-Chief

**Goran Slipac**, HEP, Croatia

## Associate Editors

**Helena Božić** HEP, Croatia

**Stjepan Car** Končar-Electrical Engineering Institute, Croatia

**Tomislav Gelo** University of Zagreb, Croatia

**Davor Grgić** University of Zagreb, Croatia

**Mičo Klepo** Croatian Energy Regulatory Agency, Croatia

**Stevo Kolundžić** Croatia

**Vitomir Komen** HEP, Croatia

**Marija Šiško Kuliš** HEP, Croatia

**Dražen Lončar** University of Zagreb, Croatia

**Goran Majstrovic** Energy Institute Hrvoje Požar, Croatia

**Tomislav Plavšić** Croatian Transmission system Operator, Croatia

**Dubravko Sabolić** Croatian Transmission system Operator, Croatia

**Mladen Zeljko** Energy Institute Hrvoje Požar, Croatia

## International Editorial Council

**Franco Barbir** University of Split, Croatia

**Tomislav Barić** J.J. Strossmayer University of Osijek, Croatia

**Anastasios Bakirtzis** University of Thessaloniki, Greece

**Frank Bezzina** University of Malta

**Tomislav Capuder** University of Zagreb, Croatia

**Ante Elez** Končar-Generators and Motors, Croatia

**Dubravko Franković** University of Rijeka, Croatia

**Hrvoje Glavaš** J.J. Strossmayer University of Osijek, Croatia

**Mevludin Glavić** University of Liege, Belgium

**Božidar Filipović Grčić** University of Zagreb, Croatia

**Dalibor Filipović Grčić** Končar-Electrical Engineering Institute, Croatia

**Josep M. Guerrero** Aalborg Universitet, Aalborg East, Denmark

**Dirk Van Hertem** KU Leuven, Faculty of Engineering, Belgium

**Žarko Janić** Siemens-Končar-Power Transformers, Croatia

**Igor Kuzle** University of Zagreb, Croatia

**Niko Malbaša** Ekoneg, Croatia

**Matislav Majstrovic** University of Split, Croatia

**Zlatko Maljković** University of Zagreb, Croatia

**Predrag Marić** J.J. Strossmayer University of Osijek, Croatia

**Viktor Milardić** University of Zagreb, Croatia

**Srete Nikolovski** J.J. Strossmayer University of Osijek, Croatia

**Damir Novosel** Quanta Technology, Raleigh, USA

**Hrvoje Pandžić** University of Zagreb, Croatia

**Robert Sitar** Končar-Electrical Engineering Institute, Croatia

**Damir Sumina** University of Zagreb, Croatia

**Elis Sutlović** University of Split, Croatia

**Damir Šljivac** J.J. Strossmayer University of Osijek Croatia

**Darko Tipurić** University of Zagreb, Croatia

**Bojan Trkulja** University of Zagreb, Croatia

**Nela Vlahinić Lenz** University of Split, Croatia

**Mario Vražić** University of Zagreb, Croatia

## INTRODUCTION

**J**ournal of Energy special issue: Papers from 11<sup>th</sup> International Conference of the Croatian Nuclear Society “Nuclear Option in Countries with Small and Medium Electricity Grids”

Welcome to this special issue, which is based on selected papers presented at the 11<sup>th</sup> International Conference of the Croatian Nuclear Society “Nuclear Option in Countries with Small and Medium Electricity Grids”, held in Zadar, Croatia, on June 5<sup>th</sup>–8<sup>th</sup>, 2016.

This International Conference was organized by the Croatian Nuclear Society in cooperation with International Atomic Energy Agency (IAEA), Croatian State Office for Nuclear Safety and University of Zagreb, Faculty of Electrical Engineering and Computing. The goal of the Conference was to address the various aspects of the implementation of nuclear energy for electricity production in the countries with small and medium electricity grids and in power system in general. The conference also focuses on the exchange of experience and co-operation in the fields of the plant operation, nuclear fuel cycle, nuclear safety, radioactive waste management, regulatory practice and environment protection.

The conference was organized in eight main topics covered in ten oral sessions and one poster session. In three Conference days authors presented 49 papers orally and 23 papers in poster session. 102 participants came from 16 countries representing equipment manufacturers and utilities, universities and research centres, and international and government institutions. Eight invited lectures were held and 72 papers were accepted by international programme committee.

The importance of international cooperation for the assessment of the nuclear option has been recognized by everybody planning to introduce nuclear power plant to the grid. That is even more important for small and medium countries having limited resources and specific requirements due to limited grid size. The Conference topics reflect some current emphasis, such as country energy needs, new reactor technologies (especially small reactors), operation and safety of the current nuclear power plants, move of the focus in nuclear safety toward severe accidents and accident management strategies, improvement in nuclear safety, reactor physics and radiation shielding calculation tools and ever increasing requirements for minimization of environmental impact.

From 72 papers presented at the Conference, 16 papers were accepted for publication in this number of Journal of Energy after having undergone the additional peer-review process. We would like to thank the authors for their contributions and the reviewers who dedicated their valuable time in selecting and reviewing these papers, both during the Conference and during the preparation of this special issue of Journal of Energy. It was very challenging to collect a balanced overview of the entire Conference. We decided to select 16 papers for this issue and additional 14 for the next one. We believe that the papers which were selected for this number represent some of the best research related to nuclear plant operation, energy planning, development of new reactors and technologies, reactor physics and radiation shielding. We hope this special issue will provide a valuable insight into different aspects of nuclear and electrical engineering and reactor physics, as well as a pleasant and inspiring reading.

## Guest Editors

*Dubravko Pevec*

*Davor Grgić*

*University of Zagreb, Croatia*

## Possible Role of NPP in Long Term Low Carbon Development Strategy – Case Study Croatia

Željko Tomšić\*, Ivan Rajšl, Matea Filipović

University of Zagreb, Faculty of Electrical Engineering and Computing  
Unska 3, 1000 Zagreb, Croatia

[Zeljko.tomsic@fer.hr](mailto:Zeljko.tomsic@fer.hr), [ivan.rajsl@fer.hr](mailto:ivan.rajsl@fer.hr), [matea.filipovic@fer.hr](mailto:matea.filipovic@fer.hr)

### ABSTRACT

The term low – emission development strategies (LEDS) was developed on the UN Framework Convention on Climate Change (UNFCCC) in 2008. LEDS is used to describe a long-term national economic development plans or strategies that include low emissions and economic growth resistant to climate change.

The concept of Low Carbon Development Strategies (LCDS) has been introduced by the Conference of Parties to the UNFCCC as a common but differentiated approach to meet the overall emissions reduction objectives:

*“All countries shall prepare Low Emission Development Strategies ...nationally-driven and represent[ing] the aims and objectives of individual Parties in accordance with national circumstances and capacities”* (Cancun Agreement).

Low Carbon Development Strategies (LCDS) in this way become an overarching framework to design and achieve Nationally Appropriate Mitigation Actions (NAMAs) reflecting the Common but Differentiated Responsibilities (CBDR) of all countries.

For Long-Term National Strategy and Action Plan for Low-Carbon Development the main objective of this programme is the development of a long-term national strategy and action plan for low-carbon development to enable country to fulfil its commitment to carbon obligations.

Low-carbon development strategy will become the fundamental for the development of the energy sector with low rate of carbon, but also for the entire economy. European Union is the leader in the effort to reduce emissions especially in the energy sector – sector with the highest rate of emission. With the goal of reducing emissions, necessary measures are accentuated for energy in the EU Countries, as well as in Croatia. The possibilities for realization of Croatian low-carbon development and particularly possible role and barriers for Nuclear power plants for Low carbon emissions development in the electricity sector until 2050 will be presented in this paper.

**Keywords:** *Low Carbon Development Strategies, Electricity Sector, Greenhouse Gasses, Energy Efficiency, Renewable Energy, Low Carbon Technologies, PLEXOS*

### 1 INTRODUCTION

In the aspects of financial and economic crisis, low carbon development, with the goal of predominant production from renewable sources, is becoming increasingly important. Positive changes in national and international policy making with the huge impact of low carbon development in long term strategic planning are also notable. The United Nations Framework Convention on Climate Change (UNFCCC), an agreement about the integration of policies and measures for the protection of the climate system from dangerous anthropogenic interference with

the climate system, also includes national development plans and programs. [1] It was the first step toward limiting global warming and to face future climate change with its effects. [2] Main objective of UNFCCC is stabilisation of greenhouse gas concentration in atmosphere at levels which will stop dangerous effect on the climate. [3] UNFCCC parties have signed the Kyoto Protocol and agreed to set internationally binding emission reduction targets. The main objective of last COP21 in Paris was to achieve a legal binding agreement on climate and to keep global warming below 2°C above pre-industrial levels. Implementation of this agreement will start in 2020.

The term Low Emission Development Strategies (LEDS) was first used by UNFCCC in 2008. The primary task was to enable the improvement of national climate change, to develop policies in more directing, coherent and strategic manner and to bring international impetus for climate action. Parties agree to commit to a maximum global temperature rise of 2°C and to prepare a low-carbon development strategy. National climate strategies include plans for mitigation of climate change with a focus to specific circumstances and development objectives of each country. LEDS, as a strong climate document, manages national development and national strategies.

The concept of Low Carbon Development Strategies (LCDS) has been introduced by the Conference of Parties to the UNFCCC as a common but differentiated approach to meet the overall emissions reduction objectives:

***All countries shall prepare Low Emission Development Strategies ...nationally-driven and represent[ing] the aims and objectives of individual Parties in accordance with national circumstances and capacities” (Cancun Agreement).***

## 2 OBJECTIVES AND GUIDELINES OF LEDS

Based on the LEDS it is possible to highlight disadvantages and to prioritize activities for founding on the national level. [4] Thereby, LEDS can be integrated and build on existing strategies (National Sustainable Development Strategies (NSDS), National strategy on climate change, Technology Needs Assessment and Nationally Appropriate Mitigation Action (NAMA)). Legal form of LEDS is a strategic plan to help countries in promoting their development pathway towards a low-carbon sustainable development based on the socio-economic development priorities of the country. There is a long-term component that includes a strategic vision and short- and medium-term components to show precise action to be undertaken. [5] Elementary guidelines adopted in LEDS Global Partnership workshops are stated in [6].

Strategy development process includes: high level of political support, identification of important interested groups and stakeholders, strengthening of the institutional framework and establishment of cross-sectoral coordination body, collection and analysis of data, identification of greenhouse gas emission scenarios and projections, identification of climate change mitigation policies and measures, political support for document adoption, and climate change measures application and monitoring. [7] LEDS developing process and comprehensive explanation can be found in [4].

## 3 NATIONAL CLIMATE POLICY

In year 2010 at COP16, Cancun UNFCCC members officially agreed on the preparation of low-carbon development strategies (LEDS), which will be developed at the national level and take a special place in the national considerations. [8] The national development strategy is usually based on the individual plans of each sector which are described by specific objectives and development strategies. According to the [9] following elements are basis for development of national climate plan: goals and objectives, sectoral plans and investment plans. Over the past two decades both,

developed and developing countries, have been active in the preparation of national plans for climate change and sustainable development strategy.

### 3.1 Low-emission development strategy in EU

Key elements of low-emission European policy framework for 2030 identified by European Commission can be found in [10]. Many strategies have already been launched in several countries, such as Great Britain, Germany, Sweden, Finland, France, Netherlands, Belgium and Ireland. Details can be found in [11].

### 3.2 Low-emission development strategy in Croatia

The main objective of Long-Term National Strategy and Action Plan for Low-Carbon Development is the development of a long-term national strategy and action plan for low-carbon development to enable country to fulfil its commitment to carbon obligations.

The Strategy is fundamental document in the field of climate change mitigation as well as a main economic, development and environmental strategy. [12] The objective of the Strategy is to achieve a competitive low carbon economy by 2050 in line with relevant guidelines such as [8] and [10].

At the end the Low-emission development strategy contains three scenarios [13]:

1. NUR – the referent scenario which represent the implementation of existing regulations;
2. NU1 – scenario of the gradual transition, reduction of the greenhouse gas emissions in Croatia to the binding level according to the European Union;
3. NU2 – scenario of the strong transition, 80% reduction of the greenhouse gasses emissions by 2050 compared to the 1990

### 3.3 Certain measures related to the energy sector

Technical measures that can be applied in the energy sectors are stated and discussed in [14]. The focus is on the following: energy efficiency of residential and non-residential buildings; energy audits in industry; metering and informative billing of energy consumption; construction of the cogeneration (CHP); labelling the energy efficiency of the appliance; eco-design of energy using products; RES; use of refuse-derived fuel to generate electricity and heat; carbon tax. [15]

### 3.4 Possible measures in electricity sector

List of possible measures in electricity sector consists of:

1. Increase energy efficiency in electricity production and consumption,
2. Renewable energy sources (wind, PV, geothermal, biomass & biogas),
3. **Croatian Nuclear Energy Program – CRONEP,**
4. Additional utilization of hydro potential and
5. Thermal power plants with CSS.

#### 3.4.1 Croatian Nuclear Energy Programme (CRONEP)

The Energy Strategy of the Republic of Croatia is the first document that indicates necessity for Croatian nuclear energy program (CRONEP) and the need to build nuclear power plant in Croatia.

Energy Strategy of the Republic of Croatia [16] predicted that by 2030 two nuclear power plants, about 1,000 MW each, will be in operation.

Assuming this decision is confirmed, nuclear power plants could start with operation between year 2030 and 2035, and corresponding investment will be 3-5 billion € for each of them. The main

constraints for this implementation are public acceptance public and the significant financial resources.

On the other hand, this option will significantly reduce greenhouse gasses emissions with annual production of electricity around 9,000 GWh by year 2030 and around 18,000 GWh by year 2035. with zero associated greenhouse gasses emissions.

This also means employment opportunity in Croatia: the construction will result in an average of about 1400 to 1800 jobs (with a peak around 2400 in the designated time) and 4000 of indirect employments. The operation of the power plant will generate directly about 500-700 permanent jobs. There will be also a huge number of additional jobs in the local community to supply goods and services.

Positive side effects can also be significant: the technological development of domestic industries, the advancement of science and education, economic benefits for the local community etc.

Certain disadvantages are also expected such as storage and disposal of nuclear waste (low, medium and high-radioactive).

## 4 CROATIAN POWER SYSTEM MODEL

For the purpose of this analysis Croatian power system is modelled in the „PLEXOS for Power Systems“. PLEXOS is product of the Australian company Energy Exemplar for simulations of the electricity market. For power system modelling specific data was collected on request for the purpose of research and from publicly available sources. The simulation model requires a large amount of input data: technical and economic parameters of power plants, power plants availability, system load; the key parameters for the power plants that are candidates for the expansion of the system. Parameters which are not available were estimated or assumed.

### 4.1 Basic assumptions

LEDS for Croatia was made for the period up to 2050. Following major assumptions are made:

- One of the assumptions is unavailability of the external market since 2020 because the determination of the Croatian CO<sub>2</sub> footprint in conditions of self-sufficient energy production. External market for period between 2015 and 2020 was modelled by using the hourly EEX prices from 2014. The ability to import and export is limited to model the restriction of cross-border transmission capacity.
- Power plants outages and new entries are also modelled.
- Predicted rise of installed renewable capacities is based on the key documents: Croatian Energy Strategy, National Renewable Energy Action Plan by 2020, and others.
- Possibility of CO<sub>2</sub> capture and storage technology in the scenario becomes available at the earliest by year 2035. Power plant Plomin C has the ability to upgrade the CCS technology (Retrofit) using a special restriction, but also after 2035.
- Wind power is possible from three areas, each has its own capacity factor which is obtained at the request for the Study. It is assumed that the intensity of the construction of wind power is equal in all three areas.
- For photovoltaic power generation three areas are also used which are presented with their capacity factors. It is assumed that the intensity of the construction of photovoltaic systems is equal in all three areas.
- Hourly electricity demand curve is based on the actual data. For each of scenarios (NUR, NU1 and NU2) separate curves were created based on the prediction of electricity consumption. It is

assumed that the growth of the peak load is in direct correlation with the growth of electricity load.

- System capacity margin is 15% without taking into account wind power and photovoltaic systems.
- It is assumed that the photovoltaic system and other renewable energy sources are connected to distribution network while other plants (and wind) are connected to transmission network. This is a reason for separate modelling of losses in electrical power transmission and distribution system.
- Hourly energy demand curve for heating (and steam) is based on the actual data. For each of scenarios separate curves were created based on the prediction of heating energy consumption by 2050. It is assumed that the growth of the peak load is in direct correlation with the growth of consumption of the heat energy.

## 4.2 Modelled objects

Croatian power system model in PLEXOS consists of Thermal Power Plants (gas, coal, oil), Cogenerations, NPP Krško, Hydro Power Plants, Pump-storage Power Plant Velebit, Wind Farms, Photovoltaic Power plant and other renewables (RES). Depending on the scenario there are different costs of emissions and different annual production limits of CO<sub>2</sub> emissions. Expansion candidates are modelled based on data from commercially available technologies. In addition to the cogeneration, heat boiler and heat storage tanks contribute in covering regional energy heat and steam demand. In this model secondary reserve are provided by thermal power plants (gas) and hydro power plants.

In the nuclear scenario, introduction of new nuclear power plant was forced.

## 5 RESULTS AND DISCUSSION

PLEXOS allows huge amount of output data and it is impossible to show all of them within framework of this work. Those shown are selected according to the importance represented by the LEDS RH.

### 5.1 Selected results from LEDS

Three different scenarios are compared based on the results shown in following figures. From Figure 1 it is obvious that total electricity load in 2050 is expected to be highest in scenario NU2 and lowest in scenario NU1. In scenario NU1 implementation of energy efficiency measures will result in decreased electricity demand during whole time period of interest. Further, in scenario NU2 implementation of energy efficiency measures will result in decreased electricity demand until 2040, but afterwards intensive electricity usage in transport sector is assumed that results in significant increase in electricity demand [12]. In accordance with the above data, installed capacity in scenario NU2 is larger, and in scenario NU1 slightly lower in comparison to NUR (Figures 2-4).

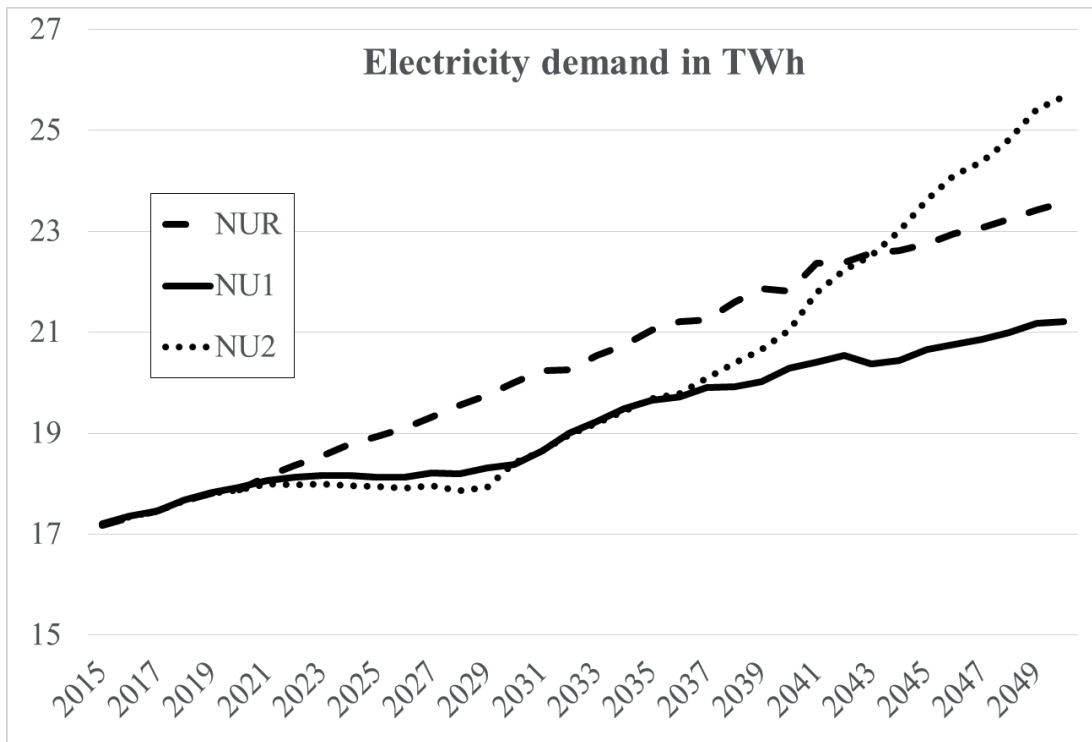


Figure 1 Total electricity demand comparison between scenarios

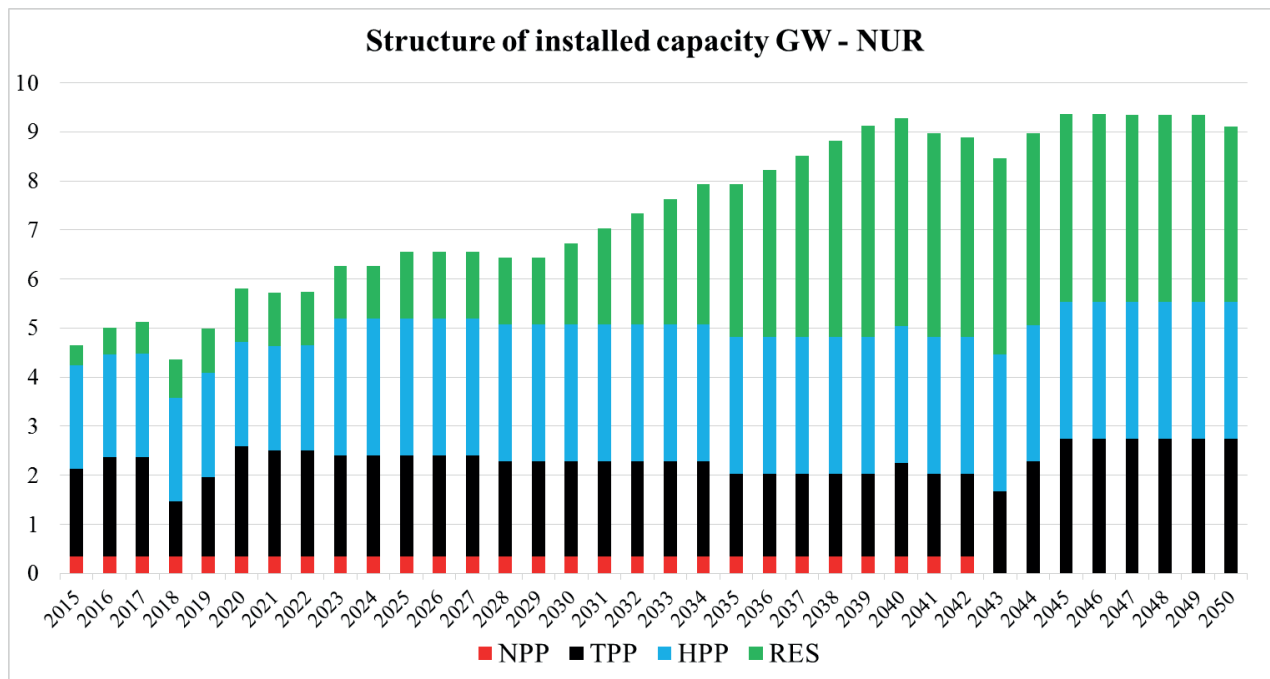


Figure 2 Structure of installed capacity for scenario NUR

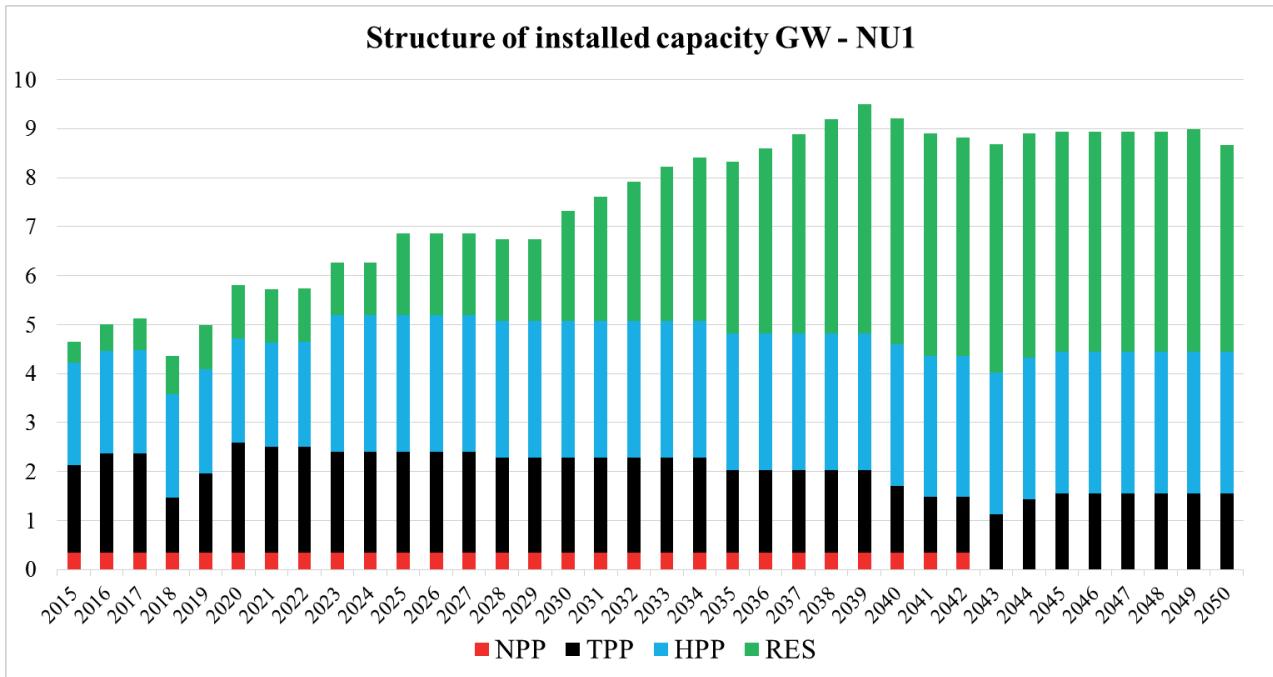


Figure 3 Structure of installed capacity for scenario NU1

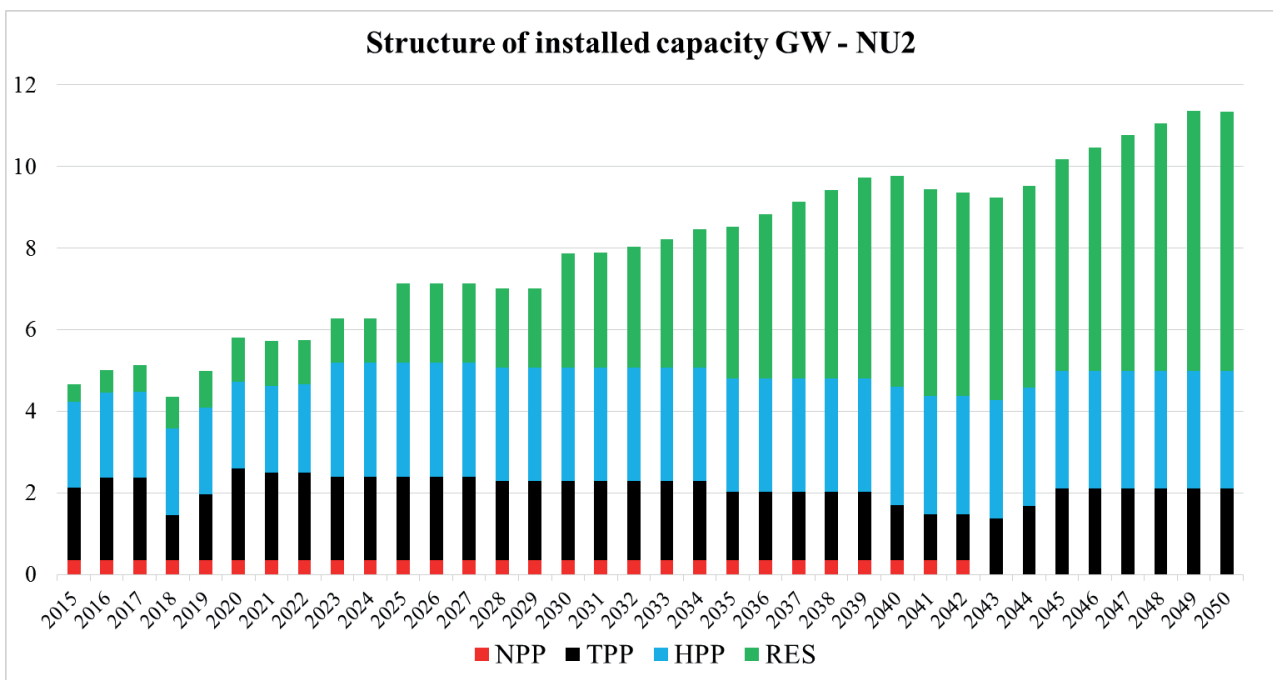


Figure 4 Structure of installed capacity for scenario NU2

From presented results it is obvious that there is no new NPP regardless of scenario of interest. Main reason for that is large increase in RES installed capacity that is partly due to current subsidies policy and partly due to increasing competitiveness of main RES technologies, wind and solar power. This large RES capacity is very volatile in nature and requires some kind of flexible power plants such as gas fired thermal power plants or pumped storage hydropower plants. Nowadays NPPs can't handle this volatile nature of RES and is therefore pushed out of future capacity schedule. But there are some strong reasons to take nuclear scenario into account as discussed in next paragraph.

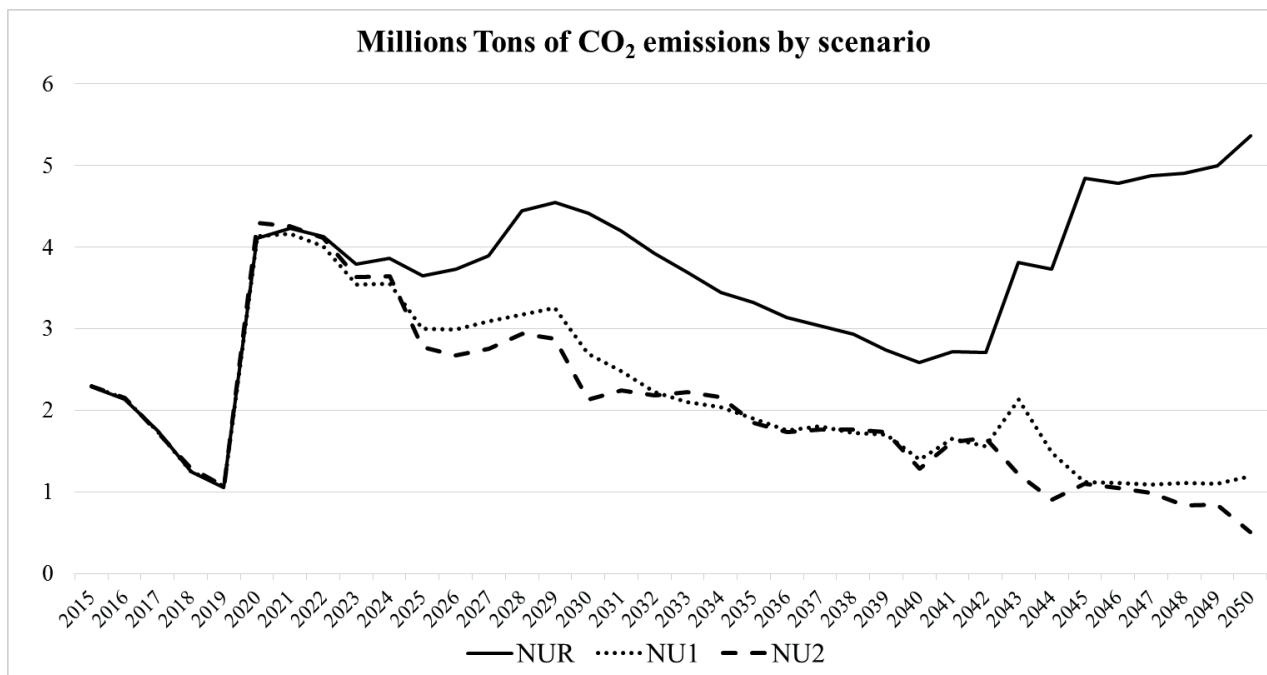


Figure 5 Greenhouse gasses emissions by scenario

Figure 5 shows total yearly CO<sub>2</sub> emissions generated in Croatian power system for each scenario. There are three main sources of CO<sub>2</sub> emissions: Gas (CO<sub>2</sub> emissions generated in gas fired thermal power plants), Coal (CO<sub>2</sub> emissions generated in coal fired thermal power plants) and Heating (CO<sub>2</sub> emissions generated for the heating purposes).

It is evident that measures taken in both scenarios, NU1 and NU2, significantly reduce CO<sub>2</sub> emissions in comparison to referent scenario NUR. By year 2050., it is expected that greenhouse gasses emissions will be more than 5 times lower in NU1 and NU2 compared to NUR levels. CO<sub>2</sub> emissions are high in NUR scenario during whole horizon due to relatively low emission prices (10 €/ton). Emission spike in NUR around 2040 (Figure 5) is because Krško NPP must be decommissioned in 2042 when its production is replaced with some greenhouse gasses production power plant.

## 5.2 Nuclear scenario

Why nuclear scenario?

- NPP is already a part of Croatian power system - Hrvatska Elektroprivreda - HEP (Croatian Power Utility) is co-owner of 696 MWe NPP Krško in Slovenia (NEK);
- The Energy Strategy Green Book indicates that energy system development scenarios with nuclear power plants provide the regional competitiveness in electricity generation, contribute to the security of energy supply, and that the nuclear power is the only one, along with the renewable energy sources, which contributes to reducing the CO<sub>2</sub> emissions in the atmosphere;
- National Energy Strategy is approved by the Croatian Parliament on October 16th, 2009;
- The Strategy decided in favour of launching the Croatian Nuclear Energy Program (CRONEP), consistent with the IAEA methodology (Milestones in the Development of a National Infrastructure for Nuclear Power) – entering into PHASE 1.

In the nuclear scenario one nuclear power plant with installed capacity of 1000 MW is forced to operation in year 2035.

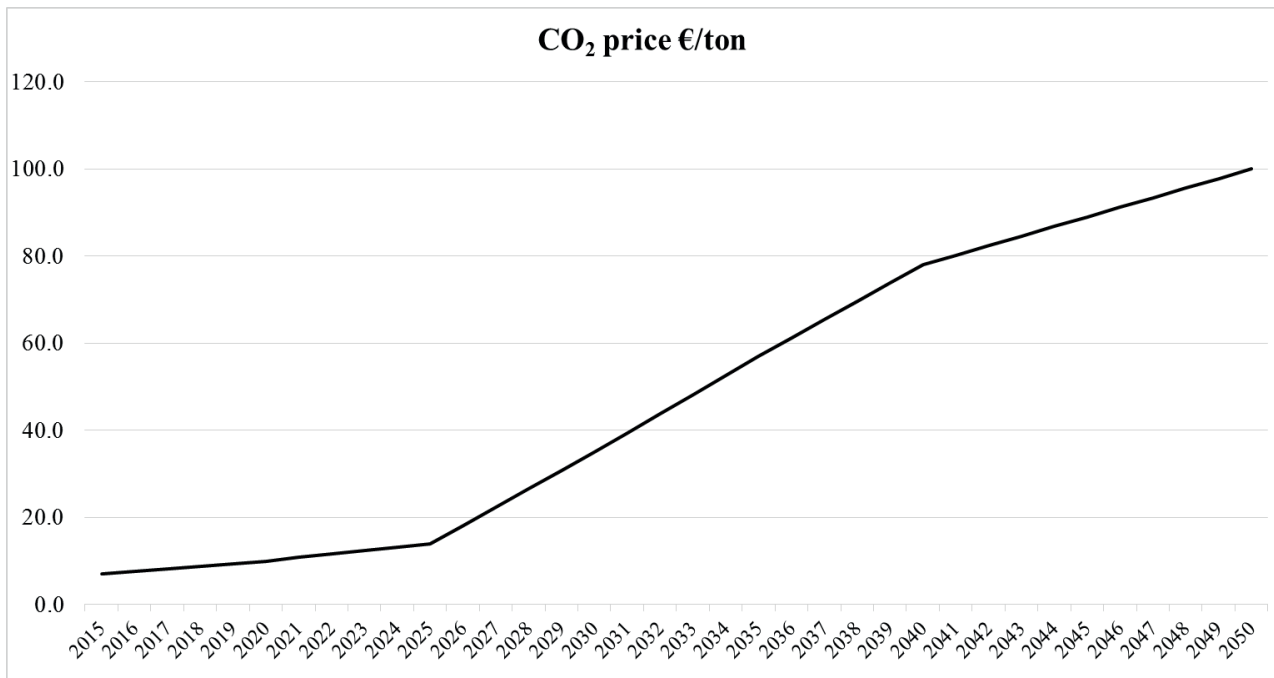


Figure 6 Increase of CO<sub>2</sub> price until 2050

One of the main barrier for new nuclear power plants is expected very slow growth of electricity demand (mainly because of very strong energy efficiency policy and high financial support to implementation of energy efficiency measures. Future electricity demand is assumed to be same as in NU2 scenario.

Further, expected high increase in CO<sub>2</sub> price until 2050 is highly in favour of nuclear technology (Figure 6).

Figure 7 shows total installed capacity in Nuclear scenario. It is obvious that introduction of new NPP resulted in decreased installed capacity of other base type power plants – thermal power plants. Installed capacity of RES and HPP are approximately the same as in NU2.

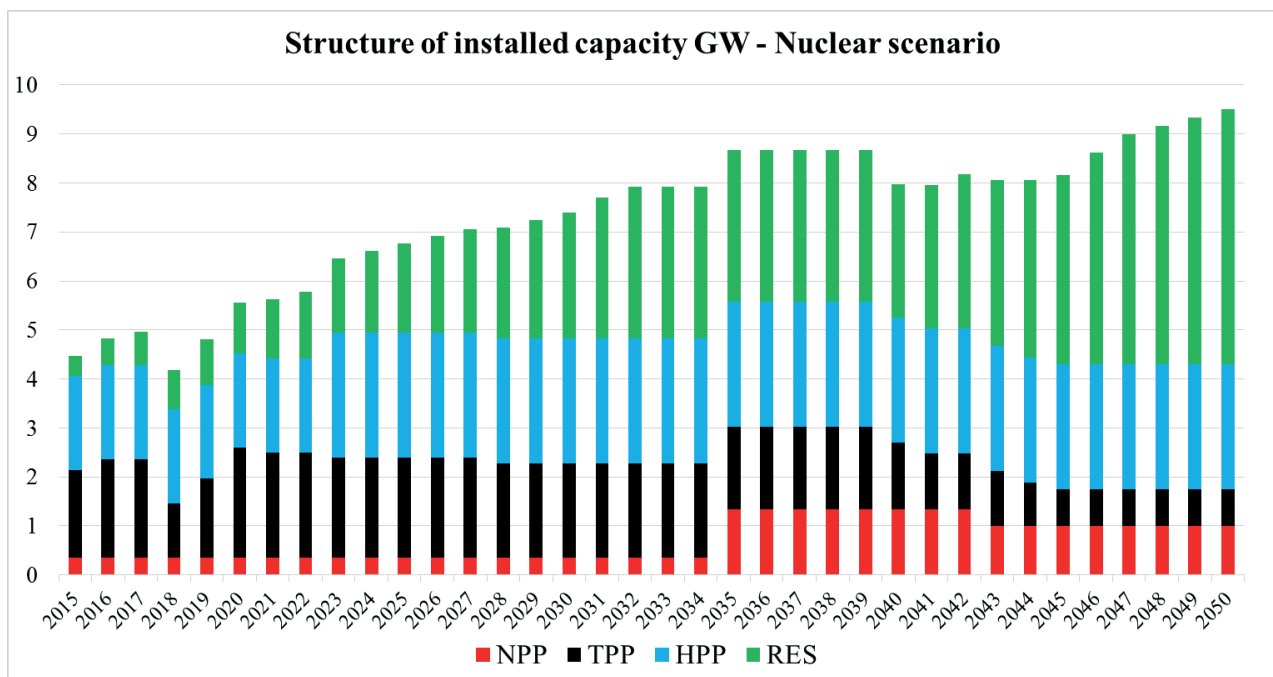


Figure 7 Structure of installed capacity for Nuclear scenario

Figure 8 shows CO<sub>2</sub> emissions in nuclear scenario compared to emissions in other scenarios.

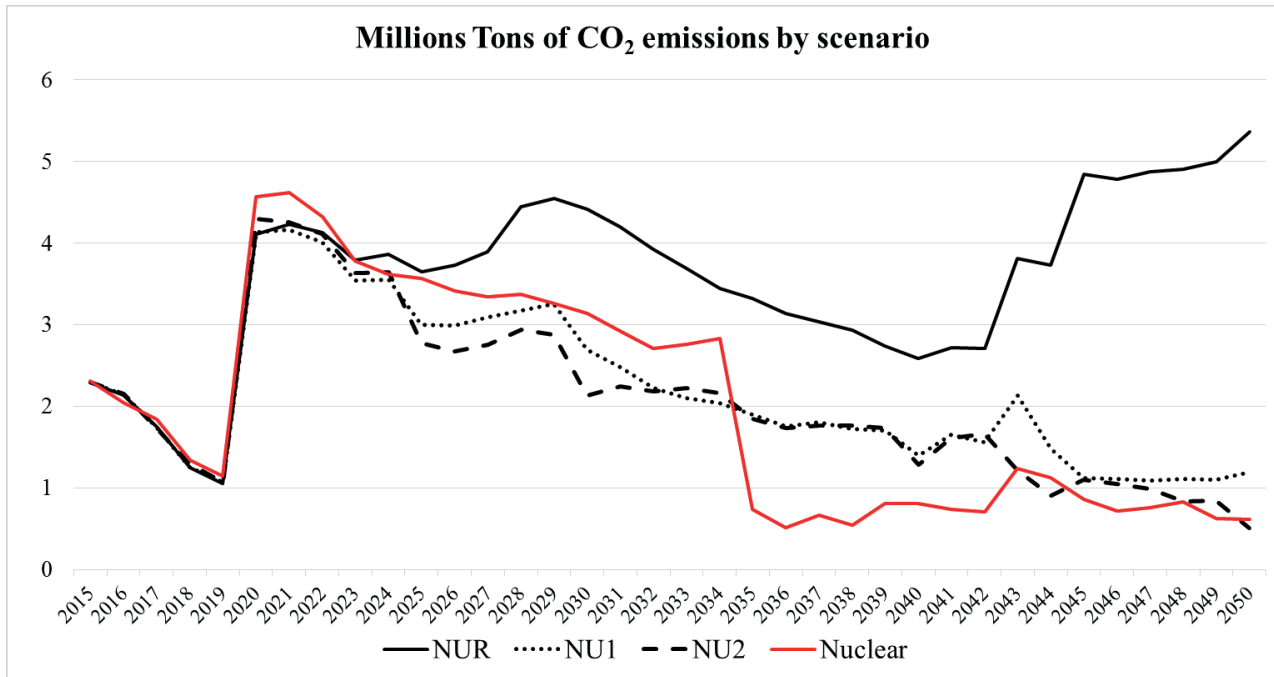


Figure 8 Greenhouse gasses emissions in Nuclear scenario

It is evident that Nuclear scenario provides approximately same CO<sub>2</sub> emissions decrease as scenarios NU1 and NU2 with significant drop in year 2035 when NPP is built.

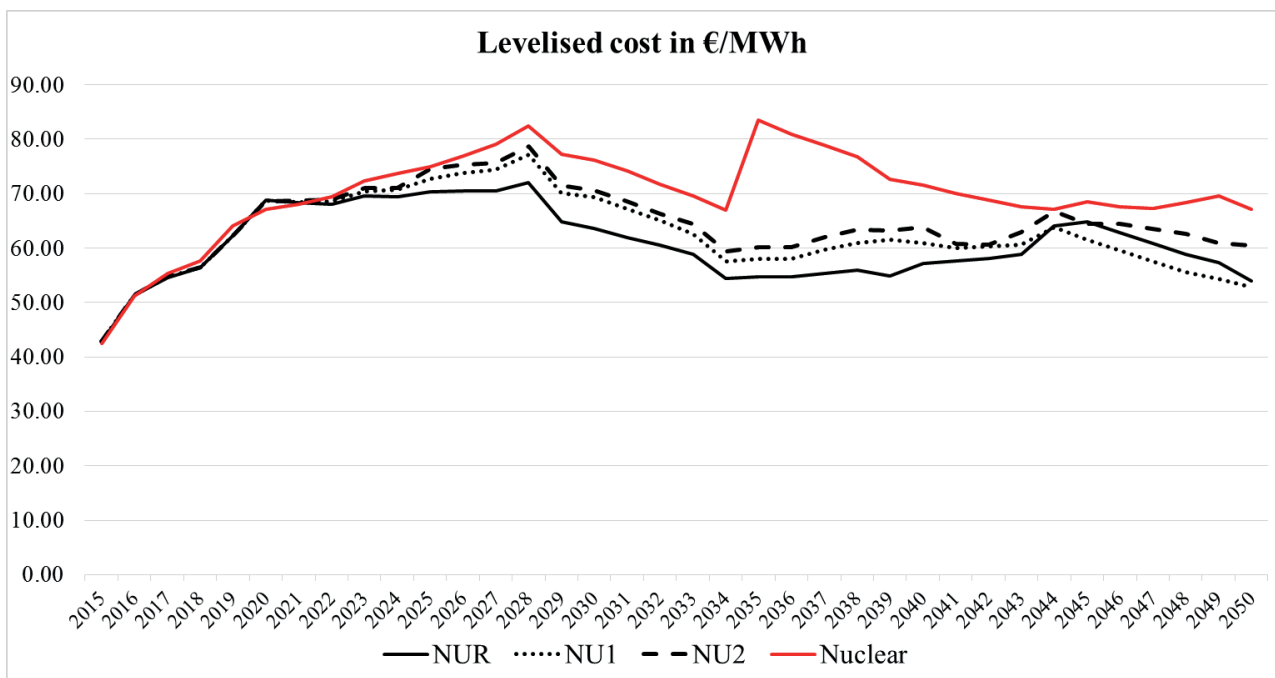


Figure 9 Levelized Energy Cost for each scenario

Now question can arise: Why Nuclear scenario isn't optimal one? Answer is given by Figure 9 where levelized cost between all scenarios are compared. Now it is evident that NUR scenario is the cheapest one and that at the same time Nuclear scenario is by far the most expensive one.

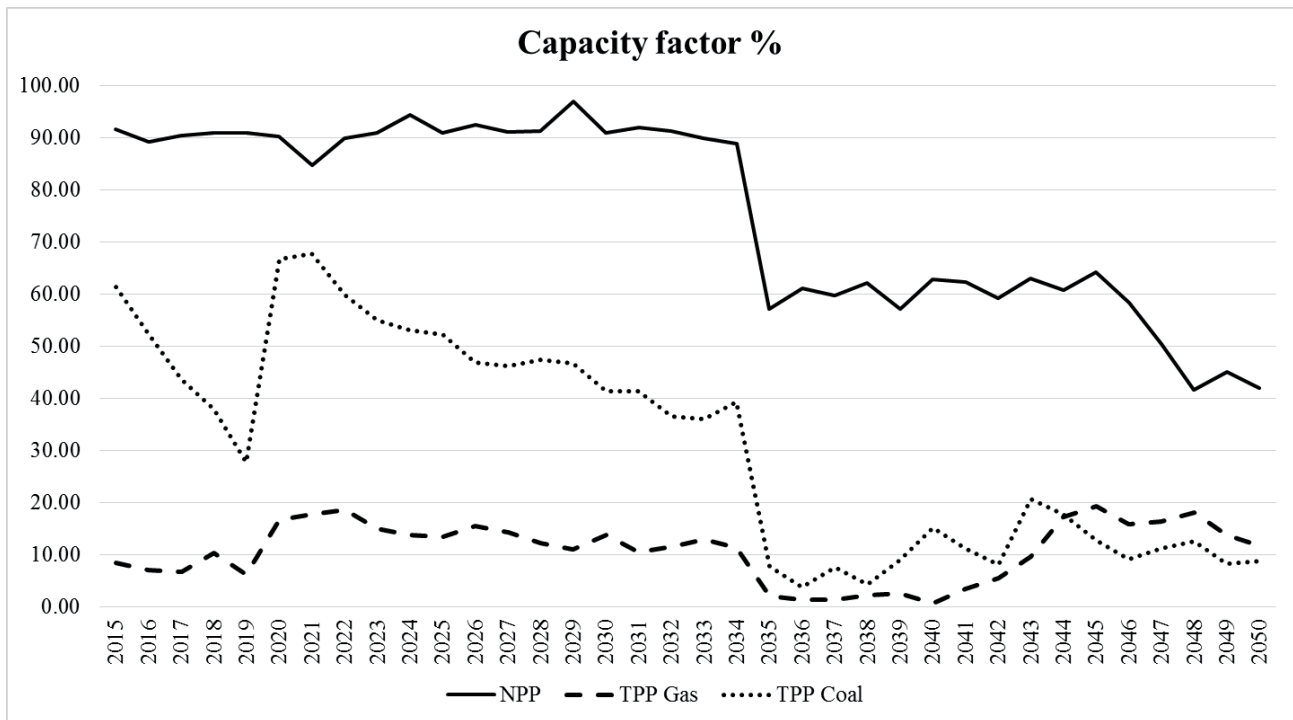


Figure 10 Capacity factors of power plant technologies

Another reason why Nuclear scenario is sub optimal is shown in Figure 10. By the year 2035, capacity factor of nuclear power plants was around stable level of 90%, as is usual for NPP. With addition of new 1000 MW of nuclear capacity, capacity factor decreased to approximately 60%. Meanwhile, it is obvious that coal power plants (usually treated as base units) become peak units after year 2035, with capacity factor between 10 and 20%. This situation is not economically nor technically sustainable from perspective of both NPPs and coal fired thermal power plants. Even gas fired power thermal power plants suffer greatly for first few years after NPP commission, but their capacity factor recovers to expected levels after that period.

## 6 CONCLUSION

Croatian LEDS is based on analysis of three scenarios: NUR – business as usual scenario; NU1 – huge energy efficiency measures implementations and consequently lowered electricity demand and NU2 – large scale electricity usage implementation, especially in transport sector and consequently increased electricity demand. This paper focuses on power system effects regarding LEDS. Long term planning horizon from 2015 to 2050 was analysed using model in PLEXOS. Based on assumptions and performed analysis it can be concluded that CO<sub>2</sub> in 2050 emission are expected to be significantly lower in NU1 and NU2 in comparison to NUR scenario.

In all three final scenarios: NUR – business as usual scenario; NU1 – huge energy efficiency measures implementations and consequently lowered electricity demand and NU2 – large scale electricity usage implementation, especially in transport sector, nuclear power plants were expansion candidates but have not become part of optimal solution. From that reason Nuclear scenario was created. In this case nuclear power plant entry was forced and results are compared with other scenarios.

Comparison shows that situation of these two cases shows that even nuclear case indicates some benefits, but also certain disadvantages. Analysis has shown that Nuclear scenario is viable and that it can provide about the same greenhouse gases decrease as scenarios NU1 and NU2. Further, main barrier for nuclear power plant is low growth of demand because of strong energy

efficiency policy. Therefore, NPP would operate with low capacity factor of around 60% and would also negatively affect other thermal power plants which is not economically nor technically sustainable. Comparison based on levelized cost levels also indicates that Nuclear scenario is more expensive than scenarios analysed in Croatian LEDS.

## 7 BIBLIOGRAPHY

- [1] OECC, The NAMA Guidebook (Manual for practitioners working mitigation actions), Japan, 2015.
- [2] International climate agreements: <http://www.consilium.europa.eu/hr/policies/climate-change/international-agreements-climate-action/>, 22. April 2015.
- [3] Croatian Ministry of Environmental Protection, Physical Planning and Construction: „Okvir za izradu strategije niskougljičnog razvoja Republike Hrvatske – Sažetak“, Croatia, 2013.
- [4] Clapp, C. et al: „Low-Emission Development Strategies (LEDS): Technical, Institutional and Policy Lessons“, OECD, November, 2010.
- [5] Low Carbon Growth Plans: Advancing Good Practice, Project catalyst, August 2009.
- [6] Levin, K. et al: „Recommendations for Effective Low Emissions Development Strategies“, 02. April, 2012.
- [7] Grgasović, V. et al: „Tranzicija prema niskougljičnom razvoju Republike Hrvatske“, Croatian Ministry of Environmental Protection, Physical Planning and Construction, Croatia, 2013
- [8] United Nations Framework Convention on Climate Change: [http://unfccc.int/meetings/cancun\\_nov\\_2010/meeting/6266.php](http://unfccc.int/meetings/cancun_nov_2010/meeting/6266.php), Cancun climate Change Conference, November, 2010.
- [9] The NAMA Guidebook. 2nd. Edition, OECC, Japan, 2015.
- [10] European Commission: „2030 climate and energy goals for a competitive, secure and low-carbon EU economy“, Bruxelles, 22. January 2014.
- [11] European Commission: „A Roadmap for moving to a competitive low carbon economy in 2050.“, Bruxelles, 8. March 2011.
- [12] Croatian Ministry of Environmental Protection, Physical Planning and Construction: „Strategija niskougljičnog razvoja Hrvatske“, <http://www.mzoip.hr/hr/klima/strategije-planovi-i-programixxxx.html>, 18. May 2015
- [13] Croatian Ministry of Environmental Protection, Physical Planning and Construction: „Stručne podloge za izradu strategije niskougljičnog razvoja Republike Hrvatske za razdoblje do 2030. s pogledom na 2050. godinu, Zelena knjiga“. Zagreb, Croatia, 2015.
- [14] Jelavić, V: „Mogućnosti smanjenja emisije iz energetike i industrije“: [http://mzoip.hr/doc/dr\\_vladimir\\_jelavic\\_mogucnosti\\_smanjenja\\_emisije\\_iz\\_energetike\\_i\\_industrije.pdf](http://mzoip.hr/doc/dr_vladimir_jelavic_mogucnosti_smanjenja_emisije_iz_energetike_i_industrije.pdf), 8. March 2016.
- [15] Croatian Environment Agency. „Izvješće o provedbi politike i mjera za smanjenje emisija i povećanje odliva stakleničkih plinova“. Zagreb, Croatia, 2015.
- [16] Croatian Parliament, Croatian Energy Strategy (NN 130/09), [http://narodne-novine.nn.hr/clanci/sluzbeni/2009\\_10\\_130\\_3192.html](http://narodne-novine.nn.hr/clanci/sluzbeni/2009_10_130_3192.html), October, 2009.

## I<sup>2</sup>S-LWR Top-Down Differential Economics Evaluation Approach

**Giovanni Maronati, Bojan Petrović**

Nuclear and Radiological Engineering, Georgia Institute of Technology  
770 State St., Atlanta, GA 30332, USA  
[gmaronati@gatech.edu](mailto:gmaronati@gatech.edu), [bojan.petrovic@gatech.edu](mailto:bojan.petrovic@gatech.edu)

**Nikola Čavlina**

University of Zagreb, Faculty of Electrical Engineering and Computing  
Unska 3, 10000 Zagreb, Croatia  
[Nikola.Cavlina@fer.hr](mailto:Nikola.Cavlina@fer.hr)

### ABSTRACT

The Integral Inherently Safe Light Water Reactor (I<sup>2</sup>S-LWR) is a design concept of a large (~1000 MWe) light water reactor with integral primary circuit configuration. One of the key design features promoting inherent safety is implementation of an integral primary circuit configuration, which in turn requires a compact design of the core and primary circuit components.

Assessments of the cost of I<sup>2</sup>S-LWR is an important aspect of the overall evaluation of the new reactor concept. There are several approaches to cost estimation and economics evaluation of the new nuclear power technologies. Frequently used guidelines rely on the Code of Accounts, originally developed in the U.S. Department of Energy (DOE) Energy Economics Data Base (EEDB) Program Code of Accounts, proposed as evaluation tool by C.R. Hudson, and further popularized in the guidelines for economic evaluation of bids, by The International Atomic Energy Agency (IAEA). The code of accounts allows to break down main costs (Total Capital Investment Cost, Fuel Cycle Cost, Operation and Maintenance) to individual systems and items.

This work aims to implement and apply a top-down differential economics evaluation approach to the Code of Accounts based guidelines, to assess the costs of the I<sup>2</sup>S-LWR relative to a representative “standard” PWR. In this methodology, a representative PWR design was taken as a reference and the differential cost was estimated for each individual account based on the design difference (or similarity). Cost estimating techniques were applied to the accounts representing systems that differ from the ones of the reference PWR. In this manner, the cost of the common components cancels out, and the uncertainty in the estimate is reduced.

While this preliminary evaluation yet needs to be completed, the indications so far are that the I<sup>2</sup>S-LWR LCOE will be economically competitive with a standard PWR.

**Keywords:** PWR, I<sup>2</sup>S-LWR, NPP Cost Assessment, Differential Economics, Code of Accounts

## 1 INTRODUCTION

The Integral Inherently Safe Light Water Reactor (I<sup>2</sup>S-LWR) concept [1,2] is being developed by a multi-disciplinary multi-organization team led by the Georgia Institute of Technology. The reactor concept aims to advance the performance and safety beyond that of current Gen-III+ reactors while maintaining economic competitiveness, through a simplified and low maintenance operation. In particular, the reactor is characterized by an innovative fuel/clad system, passive Decay Heat

Removal System (DHRS), and in-vessel microchannel heat exchangers combined with flashing drums into a Steam Generation System.

Assessments of the cost of I<sup>2</sup>S-LWR is an important aspect of the overall evaluation of the new reactor concept and its viability for commercialization. There are several approaches to cost estimation and economics evaluation of the new nuclear power technologies. Frequently used guidelines rely on the Code of Accounts, originally developed in the U.S. Department of Energy (DOE) Energy Economics Data Base (EEDB) Program Code of Accounts [3], proposed as evaluation tool by Hudson [4], and further popularized in the guidelines for economic evaluation of bids, by The International Atomic Energy Agency (IAEA) [5]. The code of accounts allows to break down main costs (Total Capital Investment Cost, Fuel Cycle Cost, Operation and Maintenance) to individual systems and items.

In this paper we implemented and applied a top-down differential economics evaluation approach to the Code of Accounts based guidelines, to assess the costs of the I<sup>2</sup>S-LWR relative to a representative “mainstream” PWR. In this methodology, a representative PWR design was taken as a reference and the differential cost was estimated for each individual account based on the design difference (or similarity). Cost estimating techniques were applied to the accounts representing systems that differ to the ones of the reference PWR. In this manner, the cost of common components cancels out, and the uncertainty in the estimate is reduced. A similar approach was used in [6] to estimate the cost of a Fluoride-salt High-temperature Reactor (FHR).

Cost definitions are summarized in Section 2. Techniques to estimate the Total Capital Investment Cost (TCIC) are discussed in Section 3. The differential economics approach is presented in Section 4. Uncertainties are briefly addressed in Section 5. While this preliminary evaluation yet needs to be completed, the indications so far are that the I<sup>2</sup>S-LWR LCOE will be economically competitive with a standard PWR.

## 2 COST DEFINITIONS

The main parameter that is used to compare the cost of electricity produced through different sources, methods and designs is the Levelized Cost of Electricity (LCOE). LCOE represents the cost (in present-value dollars, or other selected currency) per-kWh produced of building and operating a generating plant over an assumed financial life and duty cycle. The factors that affect the LCOE are the following:

- Total capital investment (including interest during construction);
- Operation and Maintenance;
- Fuel;
- Decommissioning.

The predicted LCOE for a given Nuclear Power Plant (NPP) at a time  $t$  can be evaluated calculating the present value of all the costs items through the following equation [7]:

$$LCOE = \frac{\sum_t \frac{investment_t + OM_t + Fuel_t + Decom_t}{(1+r)^t}}{\sum_t \frac{Electricity_t}{(1+r)^t}} \quad (1)$$

Where  $r$  denotes the discount rate, corrected for inflation. This relation is based on two assumptions:

1. The discount rate is stable and does not vary during lifetime of the project under consideration;
2. The price of electricity,  $P_{el}$ , is considered to be stable and not to change during the lifetime of the project. All the electricity, once produced, is sold at this price.

To systematically cover these factors for I<sup>2</sup>S-LWR, the IAEA code of accounts was used. The IAEA account system is in principle capable of describing in detail the cost of a NPP of any size and design, down to individual systems and components. The breakdown of the IAEA accounts system according to the factors that contribute to LCOE is described in this section.

## 2.1 Total Capital Investment Cost

Total Capital Investment Cost (TCIC) is the parameter that represents the cost of design, construction and testing of the NPP up to commercial operation. TCIC is broken down into the factors shown in Fig. 1. The ‘base costs’ include costs associated with the equipment, structures, installation and materials (direct costs, allocated to accounts 21-29), as well as the engineering, construction and management services (indirect costs, allocated to accounts 30-41). Supplementary costs include spare parts, contingencies and insurance and are allocated to accounts 50-54. Owner’s costs include the owner’s capital investment and services costs, escalation and related financing costs and are described by account 70. The ‘fore costs’ or ‘overnight costs’ consist of the base costs, the supplementary costs and the owner’s capital investment and service costs. Financial costs include escalation (accounts 60, 71), interest during construction (IDC) and fees (accounts 61, 62, 72). Fore costs, escalation costs and IDC and fees define TCIC.

$$\begin{aligned}
 \text{Base costs} &= \left\{ \begin{array}{c} \text{Direct costs (Account nos 21-29)} \\ + \\ \text{Indirect costs (Account nos 30-41)} \end{array} \right\} \\
 \text{Fore costs (overnight costs)} &= \text{Base costs} + \left\{ \begin{array}{c} \text{Supplementary costs (Account nos 50-54)} \\ + \\ \text{Owner's capital investment and services costs (Account no. 70)} \end{array} \right\} \\
 \text{Total capital investment costs} &= \text{Fore costs} + \left\{ \begin{array}{c} \text{Escalation costs (Account nos 60, 71)} \\ + \\ \text{Interest during construction and fees (Account nos 61, 62, 72)} \end{array} \right\}
 \end{aligned}$$

Figure 1: TCIC breakdown [5]

## 2.2 Fuel Cycle Cost

Fuel cycle cost is described by the series of accounts presented in Table 1. Fuel cycle cost consists of the cost of the uranium mining, conversion and enrichment; fuel assembly fabrication and transport; spent fuel storage and disposal or reprocessing.

Table 1 – Fuel Cycle code of accounts

100	Fuel assembly, supply, <i>first core</i>
101	Uranium supply
102	Conversion
103	Enrichment
104	Fuel assembly fabrication
105	Supply of other fissionable materials
110	Services, <i>first core</i>

111	Fuel management (U, Pu, Th)
112	Fuel management schedule
113	Licensing assistance
114	Preparation of computer programs
115	Quality assurance
116	Fuel assembly inspection
117	Fuel assembly intermediate storage
118	Information for the use of third party fuel
120	Fuel assembly, supply, <i>reloads</i>
121	Uranium supply
122	Conversion
123	Enrichment
124	Fuel Assembly Fabrication
125	Supply of other fissionable materials
130	Services, <i>reloads</i>
131	Fuel management
132	Fuel management schedule
133	Licensing assistance
134	Preparation of computer programs
135	Quality assurance
136	Fuel assembly inspection
137	Fuel assembly intermediate storage
138	Information for the use of third party fuel
140	Reprocessing of irradiated fuel assemblies
141	Credits for uranium, plutonium and other materials
142	Final disposal of fuel assemblies (in the case of no reprocessing)
143	Final waste disposal
170	Financial cost of the nuclear fuel cycle

### 2.3 O&M

Operation and maintenance costs include all non-fuel related costs needed to operate the plant, as well as maintenance costs. The outline for the IAEA O&M costs account system is presented in Table 2.

Table 2 – O&M code of accounts

800	Wages and salaries for engineering and technical support staff, and O&M and administration staff
810	Consumable operating materials and equipment 820 Repair costs, including interim replacements 830 Charges on working capital
840	Purchased services
850	Insurance and taxes
860	Fees, inspections and review expenses
870	Decommissioning allowances, if not included in capital costs (account 54) 880 Radioactive waste management costs
890	Miscellaneous costs

### 3 TCIC COST ESTIMATING TECHNIQUES

Total Capital Investment Cost is estimated to contribute about 50-70% to the LCOE for a NPP, followed by O&M and fuel cost [7]. From this consideration arises the importance of studying and analyzing this particular factor above the others. In this section TCIC estimating techniques are presented, with a particular focus on direct cost estimating.

#### 3.1 Bottom-Up Cost Estimating

Bottom-up cost estimating consists of collecting very detailed data on components and activities involved in the NPP construction, such as equipment, materials and labor quantities. Labor-hour rates, installation rates, commodities and unit prices are then applied to calculate costs of activities and components. This approach requires having available a detailed design and construction documents and is applicable to relatively mature designs.

#### 3.2 Top-Down Cost Estimating

For projects early in the development process, bottom-up cost estimates are often not practical (or viable) to use, as information on manufacturing and installation techniques of these systems is not available. For these projects, top-down cost estimating techniques are preferable. The first step consists of identifying a reference design to which estimating techniques can be applied. The estimating part consists of scaling up or down the costs of systems and components used in similar projects.

### 4 I<sup>2</sup>S-LWR DIFFERENTIAL ECONOMICS APPROACH

The I<sup>2</sup>S-LWR is a reactor at an early stage of development with a small design/development/estimating staff and limited financial resources. The project objective is to assess the difference in TCIC between the I<sup>2</sup>S-LWR and an idealized representative of current PWRs, to evaluate whether the reactor can be competitive to a standard PWR. For these reasons, a top-down differential approach was used, which consists of evaluating the accounts containing I<sup>2</sup>S-LWR systems and components that differ from that of the reference design. The approach is illustrated in this section.

#### 4.1 Baseline cost estimate

The reference design was obtained starting from public data [6,7,8], itemized with a great level of detail according to the Code of Accounts. Nuclear Power Plant Cost Data for PWR12BE (best estimate cost for a 1,200 MWe, loop PWR) from [6] were used as the most recent publicly available data. This report provides, for each account, the cost of equipment, site labor and site material. A representative sample of cost data for accounts 22X is shown in Table 3. Summary of costs per high-level accounts is given in Table 4.

The total cost shown in Table 4 is \$3.49B. The costs were reviewed by industry experts, and several corrections and adjustments were made. First, as already shown in Table 4, previously used accounts 91-93 have been replaced with accounts 31-37. Second, detailed review of each subaccount revealed the need to increase the estimates for several items, including the NSSS equipment, reactor I&C, and construction supervision. The combined effect is that the estimated total cost increased to \$3.92B. Moreover, this amount was escalated to 2016\$, giving an updated estimate of \$4.26B. This amount is consistent with the actual current NPP construction costs in the US. For comparison, the cost of the ongoing project constructing two new PWRs is estimated to ~\$16B, or ~\$8B per one PWR.

However, this project cost includes financing costs (interest during construction), grid upgrade costs, and reflects essentially a FOAK construction. The overnight cost of the NOAK NPP alone could then be estimated to be in the \$4B-\$5B range.

Table 3 – Sample of PWR12BE cost data, per account, in 2011\$

Account	Description	Equipment	Site Labor	Site Material	Total
220A	Nuclear Steam Supply (NSSS)				
221	Reactor Equipment	174,178,627	9,032,621	14,195,662	197,406,910
222	Main Heat transfer transport system	136,086,550	15,282,276	1,512,180	152,881,006
223	Safeguards systems	79,582,610	13,153,848	1,624,966	94,361,424
224	Radwaste Processing	38,785,262	9,630,929	1,845,586	50,261,777
225	Fuel Handling and storage	26,809,188	2,058,938	253,858	29,121,984
226	Other Reactor Plant Equipment	66,528,996	39,681,605	5,933,026	112,143,627
227	Reactor Instrumentation and Control	53,138,621	18,497,230	1,617,598	73,253,449
228	Reactor Plant Miscellaneous items	-	10,255,392	7,630,068	17,885,460
22	Reactor Plant Equipment	575,109,854	117,592,839	34,612,944	727,315,637

Table 4 – Summary of PWR12BE costs (high-level accounts), in 2011\$

Account	Description	Equipment	Site Labor	Site Material	Total
21	Structures and Improvements Subtotal	\$ 54,070,351	\$ 272,431,859	\$ 155,283,624	\$ 481,785,834
22	Reactor Plant Equipment	\$ 575,109,854	\$ 117,592,839	\$ 34,612,944	\$ 727,315,637
23	Turbine Plant Equipment	\$ 416,437,613	\$ 100,710,443	\$ 19,920,021	\$ 537,068,077
24	Electric Plant equipment	\$ 78,512,203	\$ 83,340,216	\$ 33,322,119	\$ 195,174,538
25	Miscellaneous plant equipment subtotal	\$ 44,773,942	\$ 54,413,727	\$ 12,896,887	\$ 112,084,556
26	Main Condenser heat rejection system	\$ 73,541,933	\$ 36,672,240	\$ 7,340,144	\$ 117,554,317
	<b>Total Direct Costs</b>	\$1,242,445,896	\$ 665,161,324	\$ 263,375,739	\$ 2,170,982,959
		Home Office	Site Labor	Site Matl	Total
31	Home Office Design services	\$ 482,090,400	\$ -	\$ -	\$ 482,090,400
32	PM/CM at home office	\$ 28,490,400	\$ -	\$ -	\$ 28,490,400
33	Design services at site	\$ -	\$ -	\$ -	\$ -
34	PM/CM at site	\$ -	\$ 14,625,600	\$ 5,320,800	\$ 19,946,400
35	Construction Supervision	\$ -	\$ 175,005,600	\$ 16,281,600	\$ 191,287,200
36	Field Indirect	\$ 149,260,800	\$ 217,833,600	\$ 206,587,200	\$ 573,681,600
37	Plant Commissioning	\$ 27,040,800	\$ -	\$ -	\$ 27,040,800
	<b>Total Indirect Costs</b>	\$ 686,882,400	\$ 407,464,800	\$ 228,189,600	\$ 1,322,536,800
	<b>TOTAL</b>	\$1,929,328,296	\$ 1,072,626,124	\$ 491,565,339	\$ 3,493,519,759

## 4.2 Differential Economics

Since the purpose of this work is not to establish the absolute cost of I<sup>2</sup>S-LWR, but to evaluate the cost of electricity produced by the I<sup>2</sup>S-LWR as compared to that of current PWRs, a differential approach is used. Under this approach, only the cost of components that differ from the standard design are evaluated, through cost estimating techniques. For example, applying differential economics, it is reasonable to assume that both I<sup>2</sup>S-LWR and a loop PWR of same power level would use essentially identical switchyards, at essentially identical cost, whatever that cost may be. On the other hand, when the design is different, the cost difference will be estimated. Three examples are given to further illustrate this point:

- Due to its cladding material selection, and other safety features, I<sup>2</sup>S-LWR does not require hydrogen recombiners. Thus, its equipment cost is reduced by the estimated typical cost of this equipment.

- On the other hand, I<sup>2</sup>S-LWR will have a larger reactor pressure vessel, due to its integral configuration. Thus, we need to estimate the cost increase of its vessel.
- As a trade-off example, instead of primary loops with steam generators, I<sup>2</sup>S-LWR will have primary heat exchangers combined with flash drums to generate steam. In this case, cost of both systems needs to be estimated. However, the relevant outcome of our analysis is the difference, not the individual numbers. The uncertainties in some assumptions needed for analyses (e.g., cost of material, needed in both cases) may partly or almost completely cancel out thus reducing the uncertainty in differential economics.

The accounts describing components that are different than that of the PWR12-BE were identified first. For these accounts, the percentage of the total direct investment cost was calculated. A higher priority was assigned to those components with a higher cost percentage of the total cost and the cost estimating process started from the accounts having a higher priority. The accounts cost and their relative weights (percent contributions to the total cost) are shown in Table 5.

Table 5 – Accounts with differing cost basis and their percent contributions to the total cost

<b>Account</b>	<b>Cost</b>	<b>% Cost</b>
211 Yardwork	59,982,046	2.56%
212 Reactor Containment Building	121,358,642	5.17%
217 Fuel Storage Building	23,709,846	1.01%
218A Control and Diesel Generator Building	43,436,753	1.85%
218J Main steam and FW pipe enclosure	18,881,193	0.80%
218T Ultimate heat sink structure	11,031,771	0.47%
221 Reactor Equipment	197,406,910	8.41%
222 Main Heat transfer transport system	252,881,006	10.78%
223 Safety systems	94,361,424	4.02%
226 Other Reactor Plant Equipment	112,143,627	4.78%
227 Reactor Instrumentation and Control	148,253,449	6.32%
228 Reactor Plant Miscellaneous items	17,885,460	0.76%
231 Turbine Generator	321,562,255	13.71%
233 Condensing Systems	69,556,766	2.96%
234 Feedwater Heating system	56,613,122	2.41%
235 Other turbine plant equipment	53,575,665	2.28%
236 Instrumentation and control	16,450,109	0.70%
237 Turbine plant miscellaneous items	19,310,160	0.82%
241 Switchgear	28,671,080	1.22%
242 Station service equipment	48,392,131	2.06%
243 Switchboards	4,917,355	0.21%
244 Protective equipment	10,227,327	0.44%
245 Electric structure and wiring	53,524,039	2.28%
246 Power and Control wiring	49,442,606	2.11%
251 Transportation and Lifting equipment	14,385,192	0.61%
252 Air, water and steam service systems	68,941,569	2.94%
253 Communication equipment	15,396,111	0.66%
254 Furnishing and Fixtures	6,566,362	0.28%
255 Waste water treatment equipment	6,795,322	0.29%
261 Structures	10,398,528	0.44%
262 Mechanical Equipment	107,155,789	4.57%

The main component contributing to direct cost is the main heat transfer system (Account 222). The system includes main coolant pumps, pressurizer and steam generation system (primary heat exchangers, intermediate piping). The steam generation system is different from that of a standard PWR as it is made of innovative components (microchannel heat exchanger).

The integral configuration has another implication on Account 221, which includes the Reactor Pressure Vessel (RPV), which has a larger diameter and height, control rods and internals. On the cost reduction side, the reactor coolant piping (in Account 222) is not present and the pressurizer is integrated in the hemispherical head of the vessel.

Safety systems are allocated to Account 223. The passive DHRS of the I<sup>2</sup>S-LWR consists of a helical coil intermediate heat exchanger placed in the RPV, a water intermediate loop, and a tower water to air heat exchanger. A careful cost analysis of the items included in this account is needed.

Turbine generator equipment (Accounts 23x) is believed to be not much different than that of the reference design. Factors will be applied to scale the cost of these components to the power level of the I<sup>2</sup>S-LWR.

I<sup>2</sup>S-LWR structures (Accounts 21x) mainly differ from that of a standard LWR in yardwork for the reactor containment vessel, which is partially below grade. The cost associated to this account will depend on the excavation depth that will be chosen. The seismic protection relies on seismic isolators installed on the nuclear building sub-foundation, which are also included in these accounts.

## 5 TREATMENT OF UNCERTAINTIES

In the cost estimation stage, costs data is collected from historically built plants, manufacturing techniques and expert knowledge on fabrication of innovative components. These costs are then analyzed and manipulated through cost estimating techniques. The cost that will be used for each account is a “most likely” estimate based on industry experts experience and historical data [9]. However, an amount of uncertainty is associated to both the cost analysis process and the cost estimating techniques, with a resulting uncertainty level associated to each account. Uncertainties are inherent to the cost estimating process and are not possible to eliminate, in particular at an early stage of the project. As the development of the I<sup>2</sup>S-LWR proceeds and the components sizing, life performance and manufacturing techniques get more well-defined, the level of uncertainty of each account will be reduced. The combination of uncertainties of different accounts might result in a large uncertainty in the value of TCIC and LCOE that needs to be assessed. Therefore, in the cost estimating process, both the best estimate and the appropriate probability distribution function need to be identified for each cost item and account.

In our future work, stochastic methods will be applied to the cost estimating process, associating each cost with a probability distribution. In project management, triangular distributions are often used to describe the stochastic nature of the cost of activities and components [10]. A triangular distribution is defined by three values: the best estimate, the minimum value and the maximum value. Multiple triangular distributed random variables result in a non-triangular distributed combined random variable whose probability distribution can be estimated analytically [11] or through stochastic simulations. The TCIC probability distribution and level of uncertainty, which is a result of the uncertainties of all accounts, can also be assessed through Monte Carlo calculations. Through this method, costs of components and accounts are repetitively sampled according to their probability distribution to estimate the dispersion on the value of TCIC.

## 6 CONCLUSION

Because of its innovative design, a top-down differential economics methodology was adopted for the evaluation of I<sup>2</sup>S-LWR economic. This methodology relies on the Code of Accounts and aims to evaluate the cost difference with respect to a representative conventional reactor. A 1,200 MWe standard PWR was taken as a design reference and cost estimating techniques were applied to assess

the cost difference between the reference reactor and the I<sup>2</sup>S-LWR. The process and methodology are based on an open methodology and on publicly available data, and in principle can be applied to NPPs of any size and design.

While this preliminary evaluation yet needs to be completed, the indications so far are that the I<sup>2</sup>S-LWR LCOE will be economically competitive with a standard PWR.

## ACKNOWLEDGMENTS

Funding to perform research for the first two authors was received from the DOE Office of Nuclear Energy's Nuclear Energy University Programs (NEUP). The authors would like to acknowledge the support of B. Mack of Westinghouse Electric Company LLC on estimating the cost of a representative PWR (PWR12BE in the text).

## REFERENCES

- [1] B. Petrovic, "Integral Inherently Safe Light Water Reactor (I<sup>2</sup>S-LWR) Concept: Extending SMR Safety Features to Large Power Output", *Proc. International Congress on Advances in Nuclear Power Plants (ICAPP'2014)*, April 6-9, 2014, American Nuclear Society (2014).
- [2] B. Petrovic, "The Integral Inherently Safe Light Water Reactor", *Nuclear Engineering International*, 26-30 (2014).
- [3] Phase IX Update Report for the Energy Economic Data Base Program EEDB-IX, *DOE/NE-0091*, U.S. Department of Energy (1987).
- [4] C.R. Hudson, Cost Estimate Guidelines for Advanced Nuclear Power Technologies, *ORNL/TM-10071*, Oak Ridge National Laboratory (July 1986).
- [5] "Economic Evaluation of Bids for Nuclear Power Plants: 1999 Edition", *IAEA Technical Report Series No. 396*, International Atomic Energy Agency, Vienna, Austria (1999).
- [6] D. E. Holcomb, F. J. Peretz, and A. L. Qualls, "Advanced High Temperature Reactor Systems and Economics Analysis", *ORNL/TM-2011/364*, Oak Ridge National Laboratory, Oak Ridge, TN (2011).
- [7] Projected Cost of Generating Electricity", IEA/NEA technical document (2010).
- [8] S. Boarin, M. Mancini, M. Ricotti, G. Locatelli, "Economics and financing of small modular reactors (SMRs)", in *Handbook of Small Modular Reactors*, Woodhead Publishing (2014).
- [9] D. Feretic, N. Cavlina, and D. Grgic, "Analysis of future nuclear power plants competitive investment costs with stochastic methods," *Kerntechnik*, Vol. **70**, No. 4, pp. 213-217 (2005).
- [10] J. C. Goodpasture, *Quantitative Methods in Project Management*, J. Ross Publishing Inc. (2003).
- [11] M. Garg, S. Choudhary, S. L. Kalla, "On the sum of two triangular random variables", *International Journal of Optimization: Theory, Methods and Applications*, **1(3)**: 279-290 (2009)

## Medium and Low Voltage Cable Measurements - TD, PD, LIRA

**Josip Čeović**

Elmont d.o.o Krško  
Cesta Krških Žrtev 135e, 8270 Krško, Slovenia  
[josip.ceovic@elmont-kk.si](mailto:josip.ceovic@elmont-kk.si)

**Matko Širola**

Elmont d.o.o Krško  
Cesta Krških Žrtev 135e, 8270 Krško, Slovenia  
[matko.sirola@elmont-kk.si](mailto:matko.sirola@elmont-kk.si)

### ABSTRACT

Elmont d.o.o. Krško – We have spread our main scope of the services from electrical maintenance, modifications implementations and quality control to cable testing area. The main reason for expanding our scope was to support Nuclear Power Plant Krško Cable Aging Management program and the world trend of LTE (Life Time Extension) in power plants.

Scope of work – We are identifying potential downgraded conditions for safety and operational important cables in special areas (heat, water, radiation). Our main scope is visual control, and testing with analysis.

For **low voltage** cables the main testing method is Line Resonance Analysis (LIRA). LIRA technology is based on the transmission line theory, through the estimation and analysis of the complex line impedance as a function of the applied signal frequency. We can monitor the global, progressive degradation of the cable insulation due to harsh environment conditions (high temperature, humidity, radiation) and detect local degradation of the insulation material due to mechanical impacts or local abnormal environmental conditions.

For **medium voltage** cables we are using new methods with a power generator that uses Very Low Frequency – 0,1Hz (VLF). The main reason for this is that the measurement unit needs 500 times less energy than the unit which uses 50Hz frequency ( $50/0,1=500$ ). With this power source we are performing dielectric loss measurements – Tan delta (TD) and Partial discharge measurements (PD).

TD measurements show the severity of Water treeing in the measured cable. Water trees mainly come from moisture and are therefore present in cables that lie in manholes filled with water or they submerged in any other way.

PD measurements show the severity of voids or other types of defects in cable insulation. These defects can arise during the manufacturing of the cable or they can arise during the installation of the cable or from an accident with the cable during the operational time.

**Keywords:** *Line Resonance Analysis, Tan Delta, Partial Discharge, Water Treeing*

# 1 INTRODUCTION

Cable integrity is vital to the safe and efficient operation of a nuclear power plant or facility, especially as a plant enters into long-term operation of 40 years or more. Despite their importance, cables typically receive little attention – they are considered passive, long-lived components that are very reliable. However, cable failures have caused plant shutdowns, safety concerns and loss of revenue. Performance and safety concerns demand proactive and preventative approaches to cable integrity and reliability. A cable health and aging management program anticipates and addresses cable aging issues, helps reduce maintenance costs, avoids unscheduled shutdowns and repairs, incorporates industry best practices and addresses regulatory requirements.

Field testing (such as tan delta, partial discharge, LIRA) provide a basis for establishing appropriate maintenance.

For low voltage cables our main testing method is Line Resonance Analysis (LIRA). The LIRA technology was developed by the Institute for energy Technology (IFE) in Halden, Norway in the early 2000's. It was initiated by the need of non-destructive test and condition assessment methods for cables in nuclear power plants. Many cable condition assessment technologies in the market today are potential destructive, and cannot be regarded as an alternative test method for cables where cable destruction leads to time consuming and cost driving maintenance operations. Other technologies are non-destructive, but provide too little information and security related to the continued operation of the relevant cable.

AC power frequency test sets are relatively large, heavy, and expensive and they require large impractical amounts of power in the field to energize cables. The reason why cables require so much power to energize at power frequency is because they are essentially seen as “capacitors” to an AC power source. The longer the cable, the larger the capacitance becomes. The cable capacitance is mainly dependent upon the geometry and dielectric constant of the insulation. For most cables, a rough guide for a cable capacitance is 300pF per meter of cable. The power required to energize, even relatively short sections of cable, at relatively low test voltages, will soon overload a standard AC power supply. The only practical component that can be adjusted to reduce the power requirement is that of the applied frequency. The reactive power required by an applied test voltage level at 0.1Hz is 500 times lower than that at 50Hz. This was originally the main driving force behind the development and use of VLF for testing capacitive loads such as cables, generators etc.

For medium voltage cables we are using high voltage system HVA28 from *b2 electronic GmbH* company with a power generator that uses Very Low Frequency (VLF) – 0,01- 0,1Hz .

## 2 LINE RESONANCE ANALYSIS PROCEDURE

### 2.1 LIRA basic

The LIRA (Line Resonance Analysis) Technology is a cable condition assessment, cable fault location and cable aging management system that works in frequency domain through advanced proprietary algorithms. LIRA is based on the transmission line theory, and calculates and analyze the complex line impedance as a function of the applied signal for a wide frequency band. It detects and locate changes in the cable impedance and makes it possible to perform fault location and cable condition monitoring on I&C, low, medium and high voltage cables even in inaccessible challenging environments. The applied frequency band is a 5V signal, and is harmless to the cable. LIRA will detect and locate local degradations in the cable, which is specific to certain sections of the cable and caused by mechanical stress and damages, or by heat-induced oxidation and radiation. It will also detect global degradation in the cable, which is applicable for the entire cable, and is caused by general aging, influenced by external and internal environmental conditions.

LIRA relies on the correlation between insulation's condition and its dielectric constant (mainly capacitance) and calculates the impedance spectrum (amplitude and phase) as a function of the applied signal over a wide frequency band. The capacitance of a cable changes as a function of changes in the cables permittivity and changes in the cable's radius, as shown in Figure 1.

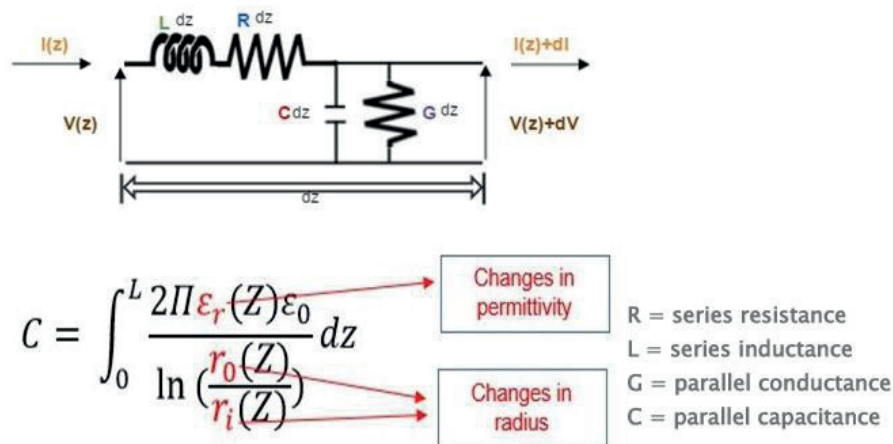


Figure 1: Schematic representation of transmission line model

## 2.2 LIRA Measurements

For a complete cable analysis, LIRA provides the following tools:

- *Input impedance spectrum check (Imp)* - The spectrum is used to adjust the used bandwidth so that the high frequency part of the spectrum still contains useful information, or, in other words, it does not completely fade out because of the cable attenuation. Figure 2. represents impedance spectrum of 47 m long EPR insulation based test cable.

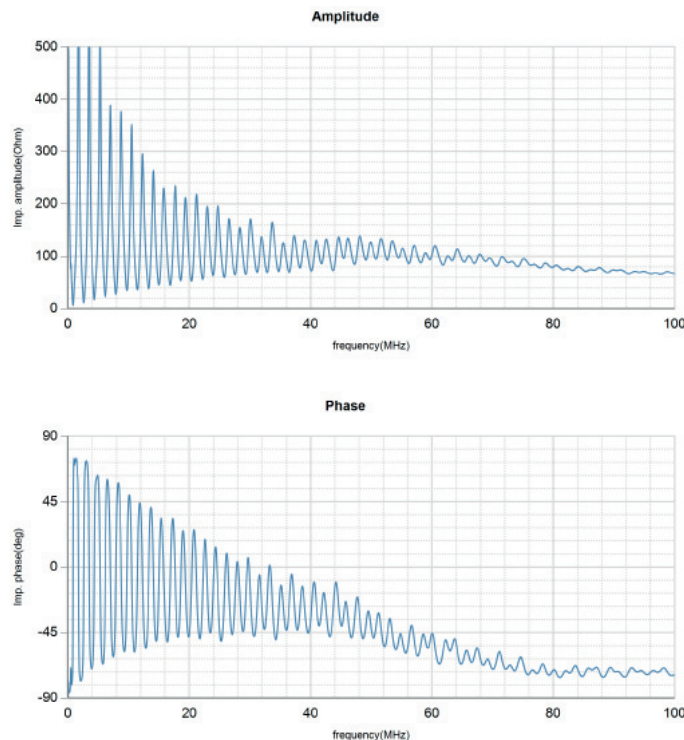
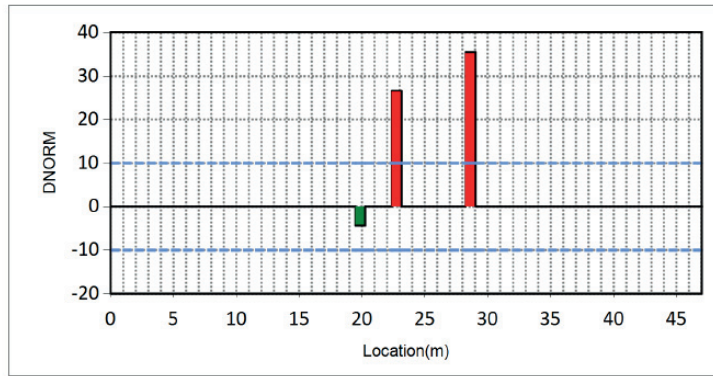


Figure 2: EPR insulation based test cable impedance spectrum

- *DNORM view (DNORM)* - This is the severity assessment tool in LIRA. Any feature, visible in the signature, is tagged as green, orange or red, according to the estimated severity. The DNORM tab shows a normalized graphical interpretation of the finding along the measured cables length, without the start and end terminations shown. Bars are shown in red when they exceed the double of the threshold (default: 10), orange from 80% of the threshold to the red threshold, otherwise in green. Our test cable isolation was cut at approximately 20m, what is visible as green bar ( Figure 3.). Cable also had two splices (22m and 28m ) visible as red bars in Figure 3.



Event	Loc(m)	Peak(dB)	Direction	DNorm	Severity
Event 1	19.5	1.46	↓	4.38	●
Event 2	22.4	8.89	↑	26.65	●
Event 3	28.2	11.85	↑	35.52	●

Figure 3: DNORM view of test cable

- *Global parameters* - The estimated cable parameters (Figure 4.) C (dielectric capacitance), L (cable inductance), att (cable attenuation), Z0 (characteristic impedance) and VR (phase velocity ratio) can be compared to the expected values to increase the measurement reliability.

Test results & key parameters	
Max frequency band(MHz)	99.99
Bandwidth utilization(%)	100
Cable length(m)	47.05
Velocity ratio	0.563
Calculating frequency(Hz)	1301068
Attenuation(db/Km)	19.3
Capacitance(pF/m)	55.6
Char.Impedance(O)	107.3
BTS	0.0
DeltaG	0.0

Figure 4: Test cable global parameters

- *Cable trend graphs* - The frequency trends (Figure 5.) are provided for the following parameters: Characteristic impedance (Z0), Velocity Ratio (VR), Attenuation Resistance, Dielectric capacitance, Cable inductance.

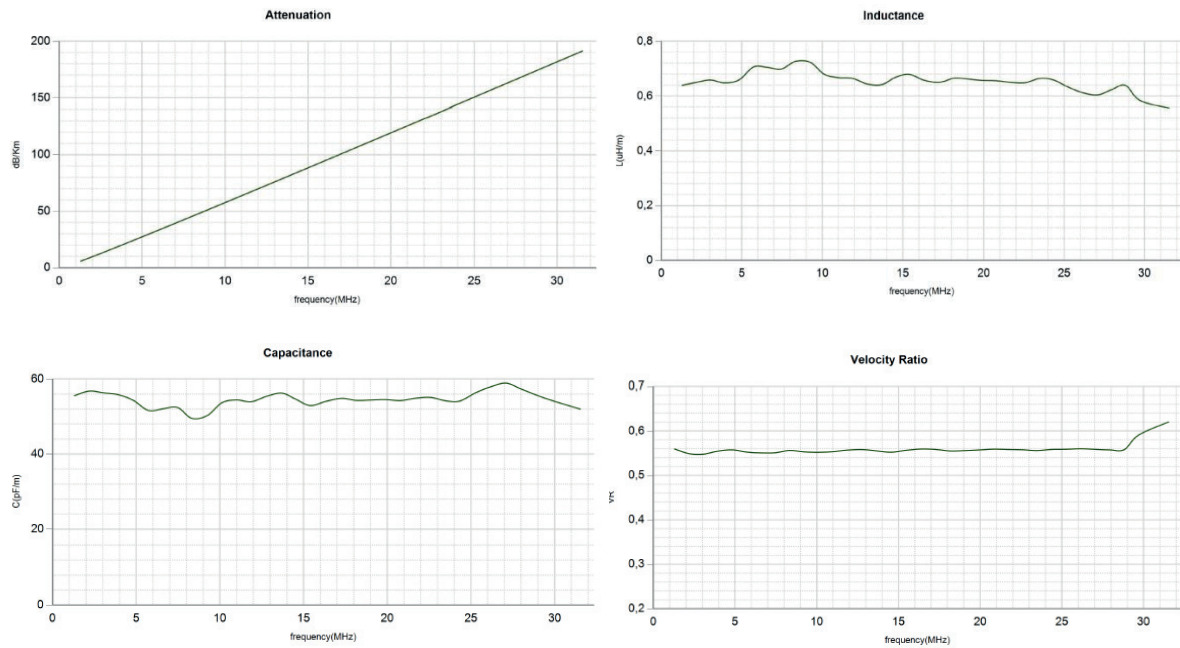


Figure 5: Test Cable trend graphs

- Termination assessment (BTS)* - is based on the Fourier transform of the cable impedance spectrum, at the maximum bandwidth allowed by the applied maximum frequency. While the output of the Fourier analysis for the LIRA signature is a power spectrum, for the BTS analysis the complex output is preserved. The ratio between the difference of the imaginary and real component of the transformation function (also called the BTS signature function) has a significant diagnostic value and it is bounded between  $+\sqrt{2}$  and  $-\sqrt{2}$ . Figure 6a. shows resulting BTS graph of our test cable with a good termination. The largest peak in Figure 6a. is the cable termination. Any change in the insulation properties at or near the termination (inside the shadow area), would cause an undershoot below zero. In another measurement test cable had bad termination (moisture). Figure 6b. shows degraded cable termination with characteristic undershoot.

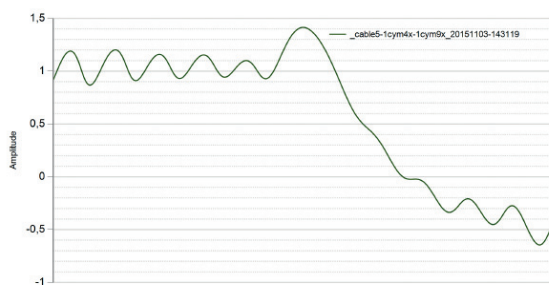


Figure 6a: BTS graph for a normal termination condition



Figure 6b: BTS graph for degraded termination condition

### 3 VLF MEASUREMENTS

### 3.1 Tan Delta (TD) Basic

Tan Delta ( Loss Angle or Dissipation Factor) testing, is a diagnostic method of testing cables to determine the quality of the cable insulation. This is done to try to predict the remaining life expectancy and in order to prioritize cable replacement. If the insulation of a cable is free from defects, like water trees, electrical trees, moisture and air pockets, etc., the cable approaches the properties of a perfect capacitor. It is very similar to a parallel plate capacitor with the conductor and the neutral being the two plates separated by the insulation material.

In a perfect capacitor, the voltage and current are phase shifted 90 degrees and the current through the insulation is capacitive. If there are impurities in the insulation, like those mentioned above, the resistance of the insulation decreases, resulting in an increase in resistive current through the insulation. The current and voltage will no longer be shifted 90 degrees. The extent to which the phase shift is less than 90 degrees is indicative of the level of insulation contamination, hence quality/reliability. This “Loss Angle” is measured and analyzed.

Tangent delta can be calculated according to:

$$\tan\delta = \frac{I_R}{I_c} = \frac{\frac{V}{R}}{V \times 2\pi f C} = \frac{1}{2\pi f C R} \quad (1)$$

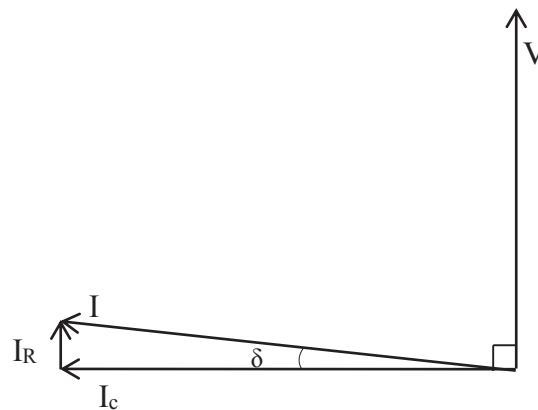


Figure 7: Tan Delta

Dielectric losses are mainly dominated by the conductive losses that occur in the insulation material. In simple terms, the insulation resistance is inversely proportional to Tan Delta.

### 3.2 TD Measurements

For our measurements we have selected a powerful unit – high voltage (HV) source with integrated TD measuring equipment. The unit has following specifications:

- Output voltage 28kVpeak, 20kVrms;
- Pure sinusoidal output voltage(load-independent);
- Output current 20mA max;
- Highest test capacity of 10μF;
- Internal TD measurement with high accuracy ( $1 \times 10^{-4}$ );
- Tan Delta measurement with various frequencies (0,01 – 0,1 Hz);
- Cable testing according to the standards:  
CENELEC HD 620/621, IEEE 400.2-2004, IEEE 400-2001, etc.



Figure 8: Measurement of TD

On each phase-line of cable we perform a measurement in four steps according to Table 1. Each step has five measurements or takes two minutes. For the test to start we need additional info from the cable manufacturer and/or user so that we can determine the appropriate voltage levels and acceptance criteria.

For acceptance criteria we use standard IEEE 400.2 – IEEE Guide for Field Testing of Shielded Power Cable Systems Using Very Low Frequency (VLF).

All results can be displayed on-line on a personal computer or on the instrument.

Calculating the appropriate voltage levels:

$$U_0 = \frac{U_N}{\sqrt{3}} \quad (2)$$

$U_0$  – Output voltage

$U_N$  – Nominal voltage of one phase

Table 1: Course of steps

step	voltage
1	0,5 $U_0$
2	$U_0$
3	1,5 $U_0$
4	2 $U_0$

### 3.3 Partial Discharge Basic

Partial Discharge (PD) is a localized dielectric breakdown of a small portion of a solid or fluid electrical insulation system under high voltage stress, which does not bridge the space between two conductors. PD affect the surrounding isolating material through heat, chemical reaction, light emission. Damaged isolation material leads often to the formation of electrical trees with the subsequence of breakdown.

A long high voltage cable behaves as a wave guide. The cable has a conductor, a dielectric and a coaxial neutral (Screen copper tape or lead) which forms an ideal wave guide. The dielectric creates a large capacitor. The longer the cable, the more of these capacitors are in parallel. These PD waves travel down the wave guide – one PD wave to the one end of the cable and the other PD pulse to the opposite end. If we now place a capturing device – a coupling capacitor and a Digital Storage Oscilloscope at the one end, it is possible to view the “time of flight” of these PD pulses.

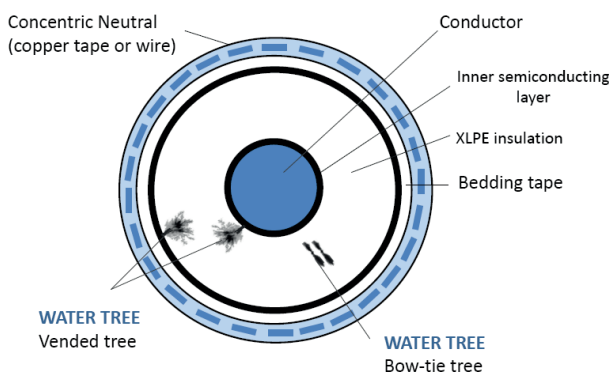


Figure 9: Typical XLPE cable

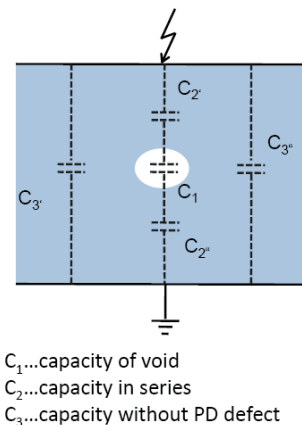


Figure 10: PD schematic representation

The 1st PD pulse in the echogram below (emanating from the PD source) arrives first at the coupling unit (see Figure 11. blue pulse ) whilst the 2nd pulse travels to the far end, travels the full length of the cable and arrives at the coupling unit (see green pulse). The 1st pulse reflects out of the coupling unit and travels to the far end and reflects back hence 3rd pulse.  $\Delta t_2$  is therefore the time differences between these two incoming pulses and the time to the PD source from the far end. If we now know the velocity of propagation of the PD pulse in the cable we can calculate the distance to the PD source (Dist = Velocity x time)

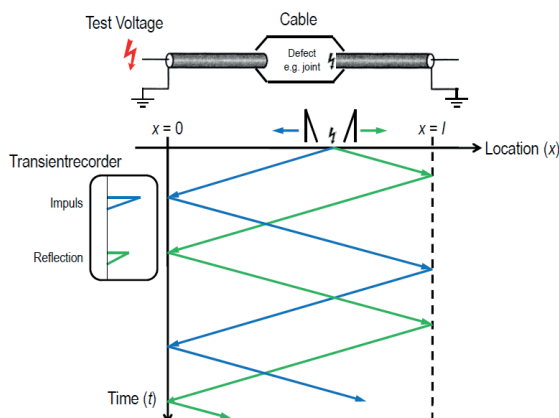


Figure 11: PD pulse travel diagram

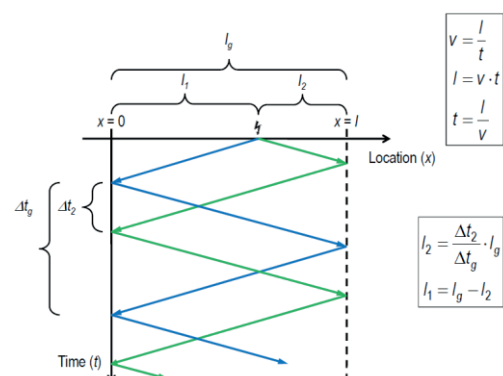


Figure 12: Distance to PD calculation

Unfortunately on very long cables the subsequent reflections may be attenuated to such an extent that they are not visible. Joint/splices also attenuate these pulses. PILC cables have a greater attenuation on these traveling PD waves than that of a similar XLPE cable. If the returning pulse (2nd) is not visible it is not possible to do a location. The 1st pulse only indicates that there is a discharge on the cable. By examining the rise times of the calibration pulse and this PD pulse it is possible to determine if it is from the near end termination or not.

### 3.4 PD Measurements

For measurement we need a high voltage power supply, for that we use the unit used for TD measurements. Additionally we need a PD detector to detect the partial discharges and calibrator to get the accurate cable length so that we can determine the location of the fault.

During the measurement all results are transmitted directly to the PC. There we can define the noise level, filters, calibrate the cable set - length, measure the PD events and analyze the results. PD measurements take more time and results are much more complex to analyze. The definition of the voltage steps is the same as used in TD measurements.

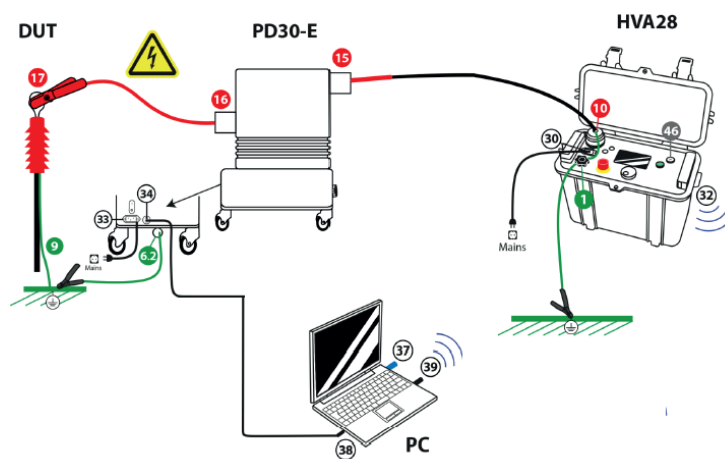


Figure 13: PD Measurement setup

There is not yet any standard from where we can get the acceptance criteria. There are only *b2 electronic GmbH* standards shown in Figure 14. The best practice is to monitor the cables and look at the trending – sudden changes in the cable insulation. Therefore we actively participate in international conferences and courses related to this topic where we can exchange knowledge and experience.

XLPE Cables	0 pC - 50 pC	Discharge within acceptable limits
	50 pc -150 pC	Some concern, monitoring recommended
	150 pC - 500 pC	Some concern, regular monitoring recommended
	> 500 pC	Major concern, repair or replace
EPR Cables Joint & termination XLPE	< 500 pC	Discharge within acceptable limits
	500 pC - 1 nC	Some concern, monitoring recommended
	1 nC - 2.5 nC	Some concern, regular monitoring recommended
	> 2.5 nC	Major concern, repair or replace

Figure 14: b2 standard for PD Tolerance Levels for MV Cables

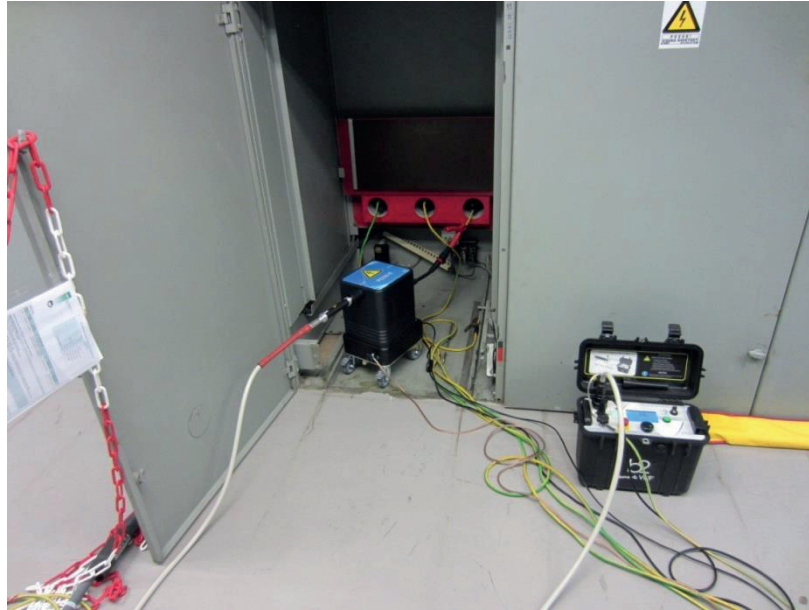


Figure 15: Measurement of PD

#### 4 RESULTS ANALYSIS

The analysis of the results for TD is done according to standard IEEE 400.2 – IEEE Guide for Field Testing of Shielded Power Cable Systems Using Very Low Frequency (VLF). We are also cooperating with other companies and utilities with whom we compare the results.

The results of the measurements depend on the type of the insulation that is used in a cable. TD assessment criteria for different cable insulations can be seen in tables 2 and 3.

Table 2: IEEE 400.2 -2013a ranges in the TD assessment criteria for XPLE insulation cables

Condition assessment	TD stability (measured by standard deviation) at $U_0$ [ $10^{-3}$ ]		Differential TD (difference in mean TD) between $2U_0$ and $U_0$ [ $10^{-3}$ ]		Mean TD at $2U_0$ [ $10^{-3}$ ]
No Action Required	< 0.1	and	< 0.6	and	< 1.2
Further Study Advised	0.1 to 0.5	or	0.6 to 1	or	1.2 to 2
Action Required	> 0.5	or	> 1	or	> 2

Table 3: IEEE 400.2 -2013a ranges in the TD assessment criteria for EPR insulation cables

Condition assessment	TD stability (measured by standard deviation) at $U_0$ [ $10^{-3}$ ]		Differential TD (difference in mean TD) between $2U_0$ and $U_0$ [ $10^{-3}$ ]		Mean TD at $2U_0$ [ $10^{-3}$ ]
No Action Required	< 0.5	and	< 4	and	< 10
Further Study Advised	0.5 to 1	or	4 to 10	or	10 to 80
Action Required	> 1	or	> 10	or	> 80

In Figure 16. we see a constant rise in the measured TD values. This indicates good insulation that does not change when the voltage increases. Also all the measured values are in the acceptance criteria for EPR insulation.

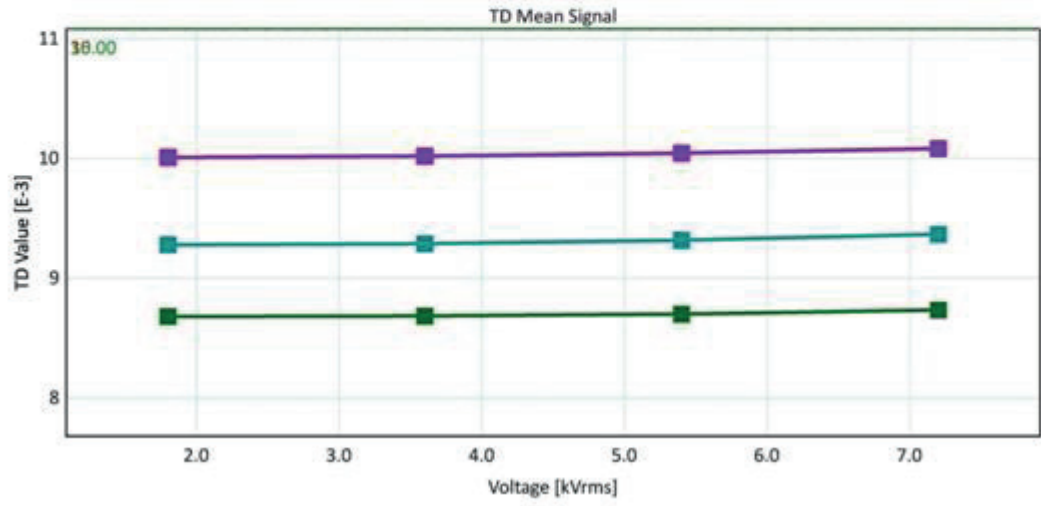


Figure 16: Example report of TD measurement

Analysis of the PD events is a completely different matter. There is no standard for the acceptance criteria for Field Testing of Shielded Power Cable Systems Using Very Low Frequency (VLF). Mainly look at the peak values that occur repeatedly at the same place and then we summarize and analyze them. We have to watch for joints and splices which are usually the main source of the

PD events. When we define them and define the location of the event we have to do a visual inspection of the localized event.

Additional info matter can be found when we are measuring the Inception and Extinction voltage, Impulse rate  $n$ , PD level :

- $U_i$  Inception voltage - the first PD occur at Inception voltage
- $U_e$  Extinction voltage - Test voltage slowly decreased – PD stops at extinction voltage
- Impulse rate  $n$  - Number of PD impulses / time range
- PD level - Strength of the PD signal measured.

With analysis of the parameters above we can predict the severity of the PD event.

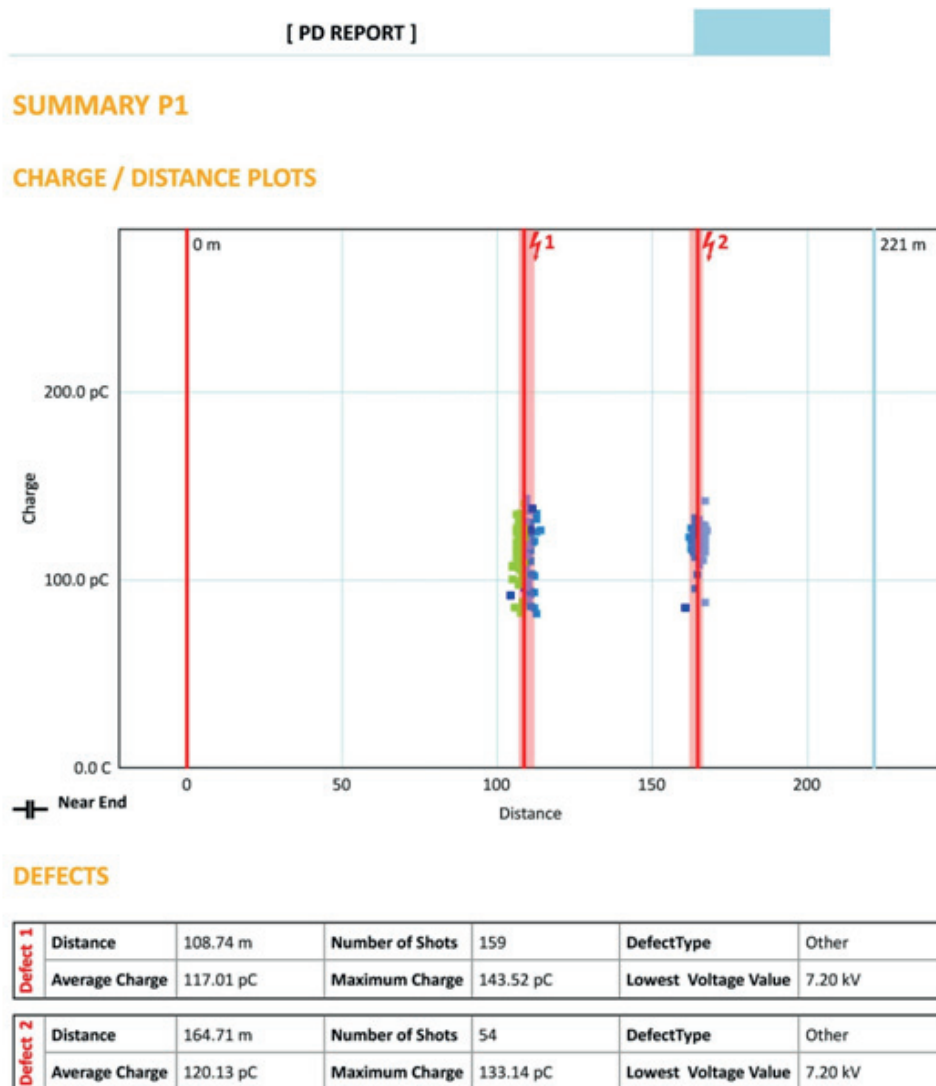


Figure 17: Example report of PD measurement

In Figure 17. we can see a cable set that has 2 locations with many PD events. After the visual inspection we determined that location 2 is a splice location in a manhole. The other one is a dilatation conduit that has moved slightly during the years of operation of the power plant. All measured results had a very low peak value, therefore it was advised to look at the trending if the cable is degrading with years.

## 5 CONCLUSION

LIRA is a frequency domain system for condition monitoring of electrical cables. This paper shows some laboratory and field cases where LIRA was used to successfully detect locations where the cable insulation was degraded because of thermal, electrical or mechanical stress. The system is used for assessing the conditions of installed signal, medium and high voltage cables.

Tan Delta ( Loss Angle or Dissipation Factor) testing, is a diagnostic method of testing cables to determine the quality of the cable insulation. The analysis of the results for TD presented in this paper is done according to standard IEEE 400.2.

Analysis of the PD events is a complex matter. The best practice that other utilities are performing is to do as many measurements as possible and to compare the results and also repeat them periodically. This way we can look at the trending of the results. The best way would be if first we could take a fingerprint of new cable before installation in field and then taking periodic measurements and comparing results.

Nevertheless there are new fields of cable measurements that should be explored and standardized in an attempt to ensure better maintenance and tracking of cable lifetime.

## REFERENCES

- [1] IEEE 400.2-2013, IEEE Guide for Field Testing of Shielded Power Cable Systems Using Very Low Frequency (VLF)(less than 1 Hz), STANDARD IEEE, 6 September 2013
- [2] Wirescan AS, Norway CS R1 LIRA User Manual, July 2015
- [3] P.F. Fantoni, Cable Ageing Management and Condition Monitoring Using Line Impedance Resonance Analysis (LIRA), PLIM&PLEX Europe, Budapest, 15 April 2015
- [4] International Atomic Energy Agency, Assessing and Managing Cable Ageing in Nuclear Power Plants No. NP-T-3.6 , 2012
- [5] b2 Suite User manual DHV0048 Rev02, 2015

## High-Temperature Ultrasound NDE Systems for Continuous Monitoring of Critical Points in Nuclear Power Plants Structures

**Petar Mateljak, Marko Budimir**

INETEC - Institute for nuclear technology Ltd.

Dolenica 28, 10250 Lučko, Croatia

[petar.mateljak@inetec.hr](mailto:petar.mateljak@inetec.hr), [marko.budimir@inetec.hr](mailto:marko.budimir@inetec.hr)

**Mario Koštan, Abbas Mohimi**

Brunel Innovation Centre, Brunel University

Granta Park, Great Abington, Cambridge CB21 6AL, United Kingdom

[mario.kostan@brunel.ac.uk](mailto:mario.kostan@brunel.ac.uk), [abbas.mohimi@brunel.ac.uk](mailto:abbas.mohimi@brunel.ac.uk)

### ABSTRACT

High temperature pipe cracks are the root of a steam power failure in the EU typically every 4 years, resulting in loss of human life, serious accidents and massive financial losses. According to IAEA's Reference Technology Database, such an event on a nuclear power plant has an average cost of €120 million, including outage costs, emergency repair costs, insurance and legal costs. Since only one growing crack is needed to cause a major failure, they have to be inspected and monitored thoroughly.

Breakdowns at extreme conditions (e.g. 580°C, 400 bar) are a result of two major weld failure modes: a) creep cracks near pipe welds; b) fatigue cracks on pipe welds. Current maintenance practice is to proceed with repairs on a detected crack according to its severity. For cost reasons, cracks that are not judged as severe enough will not be repaired. Crack severity judgement is based on its probability to cause a failure and this probability is derived taking into account the crack size and operational lifetime. More variables such as operating temperature and vibrations may rarely be found in other studies. Recent data from fracture mechanics statistical studies shows this connection between the size of a crack on a nuclear power plant pipe and its probability to lead to a failure.

To deal with the above problems two Structural Health Monitoring (SHM) systems have been developed and they are presented in this work. These systems are able to achieve continuous operation for an extended time period at operating temperatures of nuclear power plants. The developed systems employ novel phased array (PA) ultrasonic and ultrasound guided wave (UGW) probes able to withstand and continuously operate even up to 580 °C. The systems are designed to be permanently mounted on superheated steam pipes, at locations of known defects and to continuously monitor their size. However, this supposes that defects will have already been detected by a traditional method during an outage. The PA transducers are placed according to the Time-of-Flight Diffraction (TOFD) technique's topology, thus creating a novel configuration, while the UGW transducers are placed on a stainless steel ring in a circular array configuration. These configurations can enable continuous tracking of cracks growth with high accuracy, enabling maintenance crews to estimate the severity directly and not through statistics.

**Keywords:** *nuclear power plants, high temperature ultrasound, phased array, guided waves, signal analysis*

# 1 INTRODUCTION

The recent accident in the Fukushima nuclear power plant has made governments all over the world re-discuss and re-evaluate the safety procedures and regulations for their nuclear power plants. The outcome of those re-evaluations is not yet precisely defined – nevertheless the final solution should not neglect that there is a non-negligible amount of data showing that failures and accidents in NPPs become more probable as the plants age. A large portion of active NPPs in the world are close to the end of their operating license, which is generally 40 years. The economically sound solution seems to be granting the license extensions and increasing the safety levels by additional inspection and repair activities. A continuous online monitoring of the structural health monitoring of such facilities and incorporated logic for prediction (modelling) of transient failures/cracks behaviour turns out to be one of the most prospect tools [1]. For such a solution one has to have systems that are functional and resistant to harsh working environment of NPPs. For ultrasound monitoring systems of that kind, the high operating temperatures are one of the key obstacles to overcome, due to generally low Curie temperatures of commercially available piezoelectrics and to weak ultrasound reception capability of piezoelectrics at high temperatures.

Outages in the power plants (both nuclear and classic fuel) involve shutdowns of the power plant, erecting of scaffolding and removal of insulation to gain access which is a significant part of the inspection cost. Generally, the higher the pressure and the temperature of the steam entering the turbine, the greater the efficiency of the electrical generator; thus the goal of both manufacturers and operators is to carry as hot and more pressurized steam as possible from the boilers to the steam turbines. As a result, a typical thermal power plant (0.5 GW) has approximately 4km of pipes operating at temperatures of 580°C and pressures of 400bar, while the steam generators in typical nuclear power plants operate at temperatures up to 345°C and pressures of 155 bar.

If defects are identified during the outage the plant operators need to make a decision to either replace the defective pipeline or decide that the defect is not severe and monitor it closely at the next outage. However, uncertainties in the calculation of the lifetime of these superheated steam pipes that contain a minor defect may potentially have catastrophic consequences.

This paper presents the developing work on two different and partly complementary high temperature Structural Health Monitoring (SHM) systems that utilize high temperature Phased Array (PA) probes in Time of Flight Diffraction (TOFD) configuration to continuously monitor the defect growth over time (and thus inform the plant operator if the defect reaches a critical size so that the plant can be shut down and maintenance can take place before failure) and a long range ultrasound testing (LRUT) system for NDE of NPP piping at operating temperatures. The systems can provide early warning mechanisms. The first system consists of high temperature PA probes, ruggedized PA pulser-receiver unit, and signal processing & visualisation software, the other (LRUT) system is similar, the only difference being that there is an array of high temperature single element shear-wave ultrasound probes aligned in a stainless steel ring (collar) that can be wrapped around a hot pipe.

## 2 HIGH-TEMPERATURE UGW PROPAGATION MODELLING

The behaviour of the ultrasonic guided waves (UGW) for the LRUT at room temperature, 260°C and 595°C was modelled for this work. Frequencies varying between 10-200 kHz were investigated. Steel pipes are ideal for application of guided ultrasonic waves as they require an elongated medium to propagate – the wave propagation is not dependent only on the material from which the pipe has been manufactured but also on the size and thickness of the pipe. The pipe studied was 8 inches, ANSI Schedule 40. Calculation of dispersion curves for three temperatures (room temperature, 260°C and 595°C) has been carried by using literature available material data for steel. Three wave modes have been selected: L(0,1), identified as a candidate during the preliminary investigation, L(0,2) and the torsional vibration mode T(0,1) (Figure 1). The transient analysis simulations were performed using the same pipe material and geometry as for the

dispersion curves calculation. The crack was selected to be 1mm wide and for practical reasons covering 90 degrees of the circumference. Different frequencies have been investigated (60kHz, 100kHz, 150kHz, 200kHz). The excitation was applied axially on 32 points equally distributed in the circumference of the pipe (the real configuration of transducers in the UT collar).

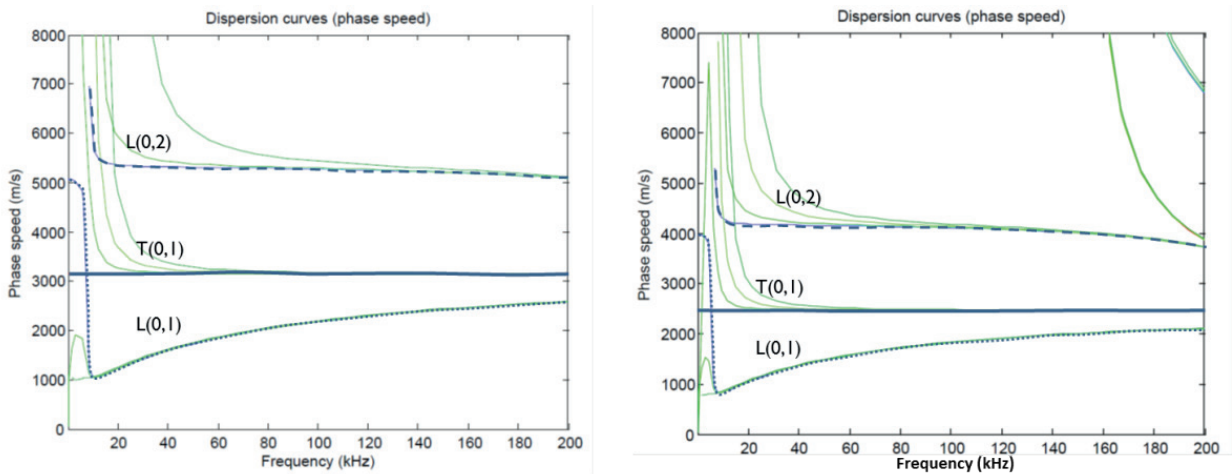


Figure 1: Dispersion curves generated for 8 inches pipe at 260°C and 595°C. Further material data for different Poisson’s ratio was also calculated to investigate impact of Poisson’s ratio to the dispersion curves

The torsional (shear) mode T(0,1) was finally selected to be exploited in the transducers design due to its non-dispersive behaviour throughout the frequency range of interest.

### 3 PA-TOFD PROBES

PA-TOFD is the combination of the pitch-catch technique with the generation of a range of angle beams. The transmission and the reception of the sound are separated by two transducers positioned on either side of the weld. It has been shown that the focused ultrasonic phased array was capable of detecting diffraction signal from crack like flaws, enabling detection and through wall sizing [2]. Therefore the PA technology combined with the TOFD principle allows coverage of a large weld volume and the heat-affected zone (HAZ) with a single probe set and reduces the need to use several probe sets and mechanical scanning. This presents the advantage of simplifying the inspection implementation.

Figure 2 presents the PA-TOFD concept, where one linear PA probe operates as a transmitter focusing the sound and the other as a focused receiver.

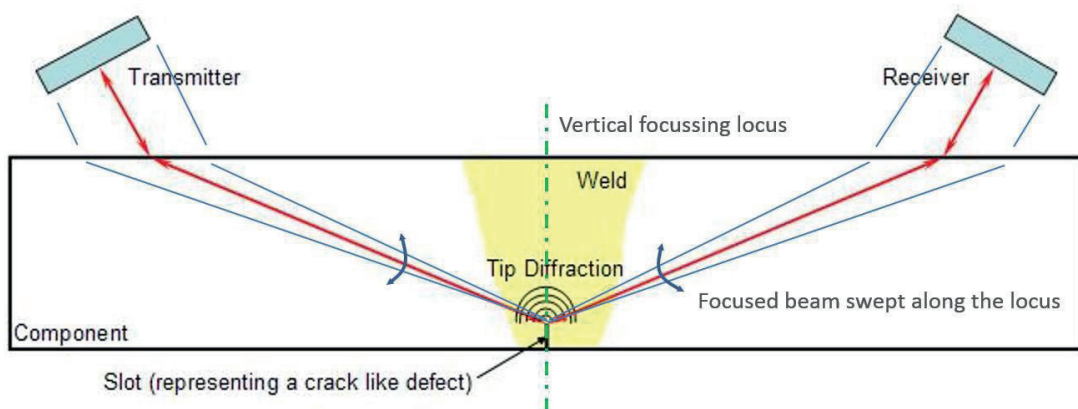


Figure 2: PA-TOFD concept

The inspection of the weld is to be performed while the pipe is in service. During the operating condition, the worst-case temperature at the surface of testing is around 580°C.

Unfortunately, commercial PA probes that can operate at these high temperatures (580°C for thermal and 345°C for nuclear power plants) are rare or non-existent. For example, PZT5A piezoelectric materials can operate on maximum temperatures between 242°C and 350°C, which makes them unsuitable for constant monitoring of pipes in nuclear and thermal power plants. Hence, it was vital to develop high-temperature probes by selecting suitable piezoelectric materials and other components that can withstand temperatures approximately up to 580°C, and design, build and test prototype probes under laboratory conditions.

The PA probes use piezoelectric elements for generation and reception of ultrasound needed for inspection and monitoring. Several high temperature piezoelectric materials were considered [3,4], taking into account their respective Curie temperature, piezoelectric charge constant  $d_{33}$ , piezoelectric voltage constant  $g_{33}$  and electromechanical coupling factor  $k_t$ . Gallium orthophosphate (GaPO<sub>4</sub>) has been selected for further investigation via high temperature impedance measurements, with results given in Figure 3.

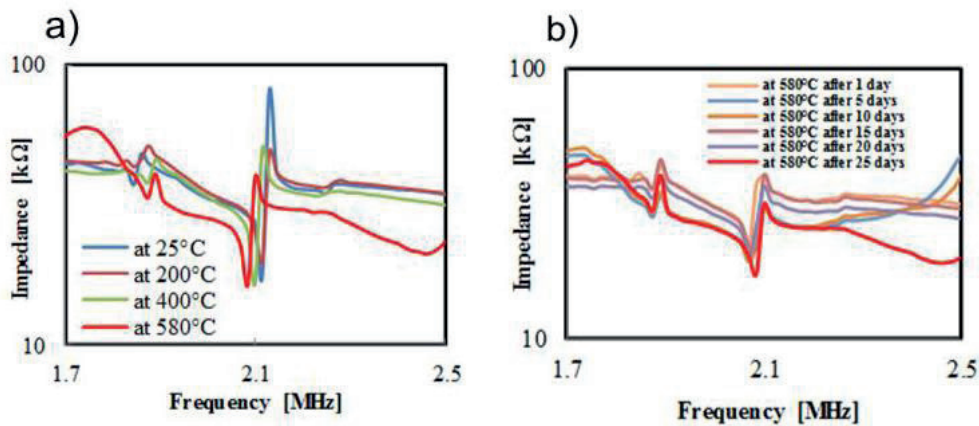


Figure 3: Frequency dependent electrical impedance of the tested GaPO<sub>4</sub> array element with the respect to: a) the temperature, in the temperature range from 25 °C up to 580 °C; b) elapsed time on constant temperature of 580 °C, ranging from 1 to 25 days. Five elements were used for the characterization, with the following dimensions: 1 mm thickness, 3 mm width and 12 mm length

It can be seen that the impedance values at resonant and anti-resonant frequencies vary with temperature, i.e. the impedance at resonance decreases with increase in temperature. There are no significant changes in the resonant and anti-resonant frequencies or their corresponding impedances before and after the exposure to temperatures up to 580°C. Exposing the GaPO<sub>4</sub> elements to high temperatures for extended periods of time (up to 25 days) has shown that the resonant and anti-resonant frequencies remain stable, while the impedances at these frequencies exhibit a decrease in value. However, the difference between the impedance values at critical frequencies remains constant over large exposure times, and any decrease in absolute values can be mitigated by varying the gain of pulser-receiver electronics.

The final PA probe CAD design is shown in Figure 4, with specifications given in Table 1.

Table 1. HotPhasedArray probe parameter specifications

<b>Type of transducer</b>	Linear phased array
<b>Number of elements</b>	16
<b>Element width</b>	0.9 mm
<b>Gap between elements</b>	0.1 mm
<b>Element pitch</b>	1 mm
<b>Center frequency</b>	5 MHz

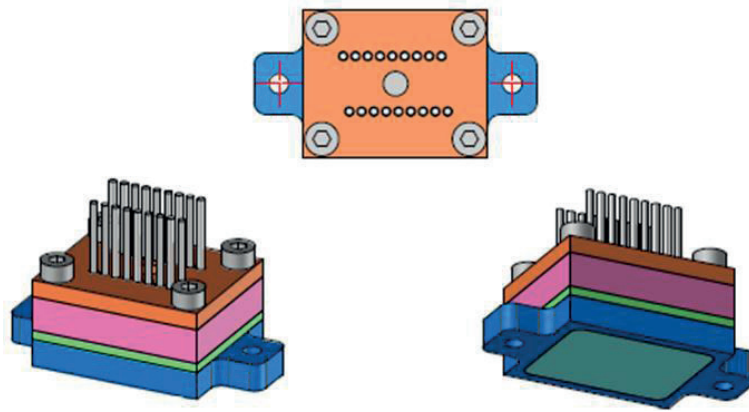


Figure 4. CAD design of the prototype high temperature phased array ultrasound probe

Two prototype PA probes (Figure 5) were then manufactured using GaPO<sub>4</sub> single crystal elements according to the design presented above.



Figure 5: Two manufactured high temperature PA ultrasound probes using piezoelectric GaPO<sub>4</sub>

The two PA probes were mounted to two wedges made in stainless steel, placed onto a pipe section (P91 steel) representing the pipe from a power plant and tested (Figure 6).

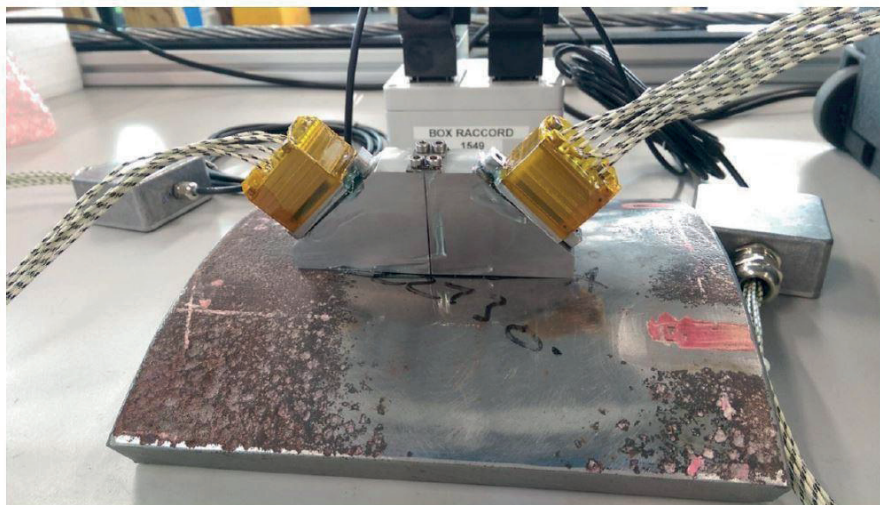


Figure 6: Two GaPO<sub>4</sub> high temperature PA ultrasound probes mounted on two stainless steel wedges and placed on a P91 steel pipe for PA-TOFD configuration measurements

#### 4 HIGH-TEMPERATURE ULTRASOUND SHEAR WAVE TRANSDUCERS

For the other, UGW LRUT SHM system, piezoelectric lithium niobate in single crystal form was selected for development of high temperature transducers. The high temperature piezoelectric properties of the  $\text{LiNbO}_3$  were studied previously – it was observed that the samples retained its piezoelectric properties at up to  $600^\circ\text{C}$  [5,6]. The performance of the transducer made for this work was examined by pitch-catch experiments taken at ambient ( $20^\circ\text{C}$ ) and high temperatures (up to  $600^\circ\text{C}$ ). The  $\text{LiNbO}_3$  samples were used with dimensions of  $13\text{mm} \times 3\text{mm} \times 0.5\text{mm}$ , and gold coated on both sides of the length-width plane. The samples were placed in a specially designed sample holder inside a furnace. The high temperature impedance measurements were sequentially performed in  $50^\circ\text{C}$  intervals beginning at  $50^\circ\text{C}$  up to  $600^\circ\text{C}$ . The characteristic frequencies, capacitance, density and dimensions of samples were used to calculate the dielectric, elastic and piezoelectric coefficients. Subsequently, complete high-temperature prototype transducers were manufactured and tested ultrasonically up to  $600^\circ\text{C}$ . This was carried out on a steel rod at  $70\text{ kHz}$ . Figure 7a shows the temperature dependence of the piezoelectric coefficient  $d_{15}$ . The increase of  $d_{15}$  from  $350^\circ\text{C}$  to  $600^\circ\text{C}$  means that the transmission quality of the material should improve. Figure 7b shows the temperature dependence of the piezoelectric coefficient  $g_{15}$ . The decrease of  $g_{15}$  from  $350^\circ\text{C}$  to  $600^\circ\text{C}$  means that the reception quality of the material should deteriorate.

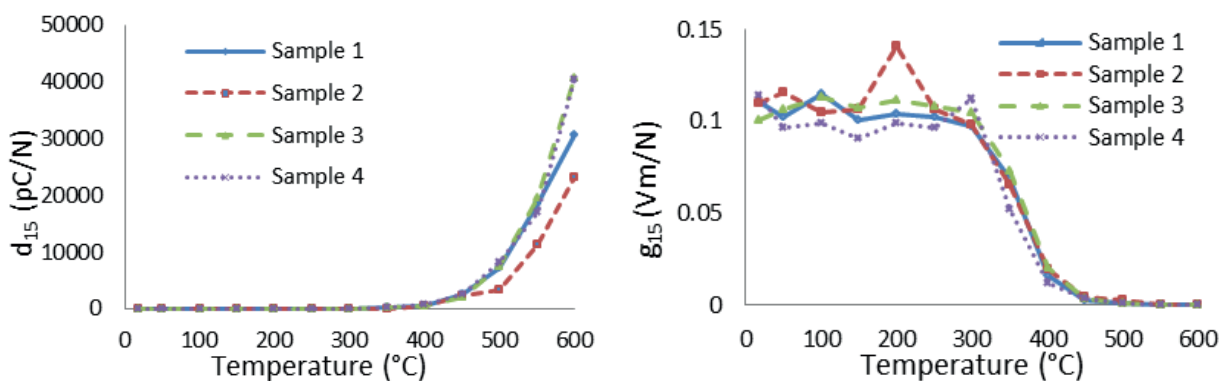


Figure 7: The temperature dependence of the lithium niobate samples piezoelectric coefficients a)  $d_{15}$ ; b)  $g_{15}$ .

The transmission and reception quality of the transducer up to  $600^\circ\text{C}$  was measured using a pitch-catch set-up. A  $1.5\text{m}$  long square steel bar ( $12\text{mm}^2$ ) was used as the wave guide. On one end a PZT element was permanently fixed on to bar, and the other end was placed inside the furnace. The peak-to-peak amplitude value of the fastest arriving wave mode was used as an indication of transducer's performance. Measurements were taken from room temperature ( $20^\circ\text{C}$ ) up to  $600^\circ\text{C}$ , at  $50^\circ\text{C}$  intervals (Figure 8).

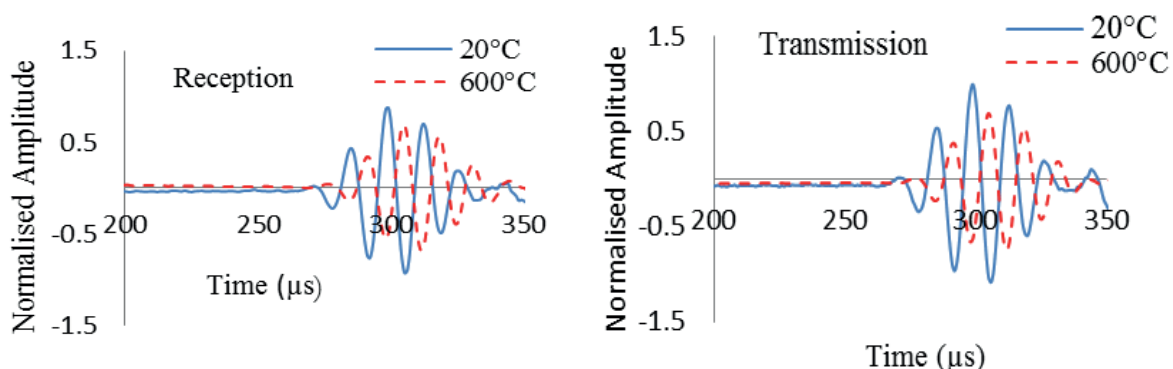


Figure 8: The measured reception and transmission transducer signals at  $20^\circ\text{C}$  and  $600^\circ\text{C}$  – the transducer is operational at  $600^\circ\text{C}$ , with an observable decrease in peak-to-peak amplitude

Figure 9 shows the manufactured transducer picture and average transmission and reception quality of lithium niobate LRUT transducer at up to 600°C. In the reception mode, a significant decrease can be observed between 200°C to 400°C, but from 450°C it starts to improve and at 600°C it reaches a similar performance in the reception quality as was observed at ambient temperatures. This behaviour could be due to the assembly procedure. The transmission quality is lower than the reception quality at ambient temperature, but between 250°C and 450°C the reception quality is lower than transmission quality. In the transmission mode the transducer is relatively stable between 20°C and 600°C.

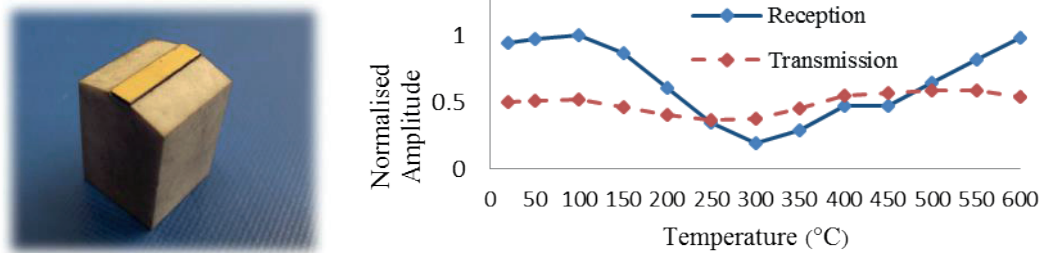


Figure 9: The lithium niobate shear-wave ultrasound transducer (left) and average transmission and reception quality of lithium niobate LRUT transducer at up to 600°C (right)

## 5 PULSER-RECEIVER ELECTRONICS FOR HIGH TEMPERATURE PA-TOFD

Each of the channels of the PA probe would have to be independently powered up by the pulser unit to control the direction of the wave front and define the focal point through high voltage signals time delays controlled by the microcontroller unit ( $\mu P$ ). Switching of the transmit/receive mode (T/R) is also governed by the microcontroller, with the need of exhibiting high clock speed capabilities, especially considering the number of elements and frequency specifications of the probe. The reflected signals have to be amplified and filtered after being transmitted through the material in order to increase their signal-to-noise ratio (SNR). Finally, the function of the receiver is to employ the analogue-to-digital conversion (ADC) for microcontroller input.

The high-level block diagram of the pulser-receiver unit is being shown in Figure 10.

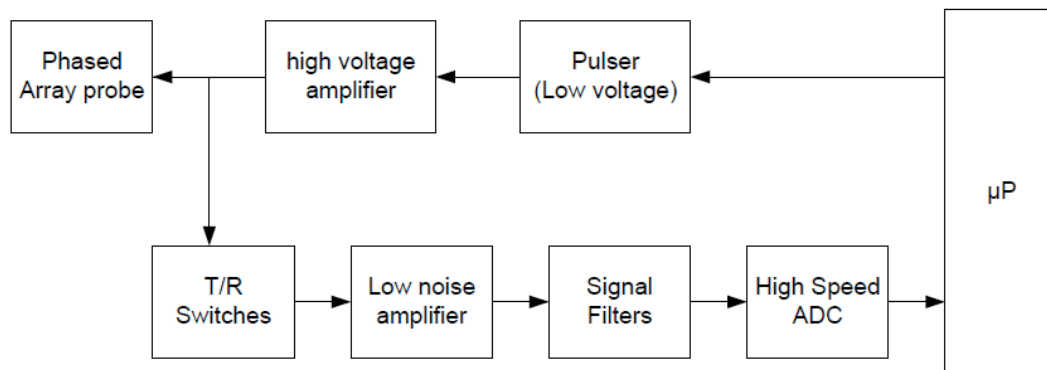


Figure 10: High level block diagram of the pulser-receiver unit.

The functions of the pulser-receiver unit were evaluated by powering a 5 MHz test probe in order to test the dimensions of an aluminium block, with known thickness of 38.5 mm. The results are demonstrated in Figure 11, with the time between the echo and the original pulse being 12.17  $\mu s$ . As the sound propagation speed in aluminium is equal to 6320 m/s, it can be estimated that the thickness of the inspected material is equal to 38.45 mm.

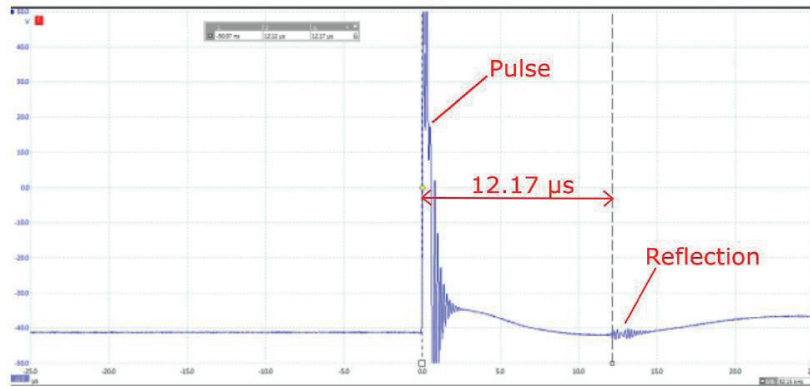


Figure 11: Aluminium block testing with the pulser-receiver unit and the test probe.

## 6 STRUCTURAL HEALTH MONITORING SYSTEMS

Plant operators are under increasing pressure to minimize the life cycle costs whilst maintaining availability targets and safety compliance. By defining the Probability of Failure (POF), the component with high risk level can be identified and it is possible through Risk- Based Inspection (RBI) assessment to set inspection and maintenance plans in order to obtain maximum value from the associated budgets.

The material properties of P91 steel had to be reviewed in order to generate a numerical model for: 1) prediction of the remaining life of each weld, 2) establishing POF curves for each weld, and 3) detection of the effectiveness of each risk factors and mitigation actions. RBI methodology can be used to manage the overall risk of a plant by focusing inspection efforts on the process equipment with the highest risk. In general, a large percent of the total unit risk is concentrated in a relatively small percent of the equipment items.

The calculation of risk involves the determination of a probability of failure combined with the consequence of failure. Failure in task is defined as loss of the capability of service of a component. SHM system analysis flowchart made for this work is given in Figure 12, with an example of POF calculation results done for this work are demonstrated in Figure 13.

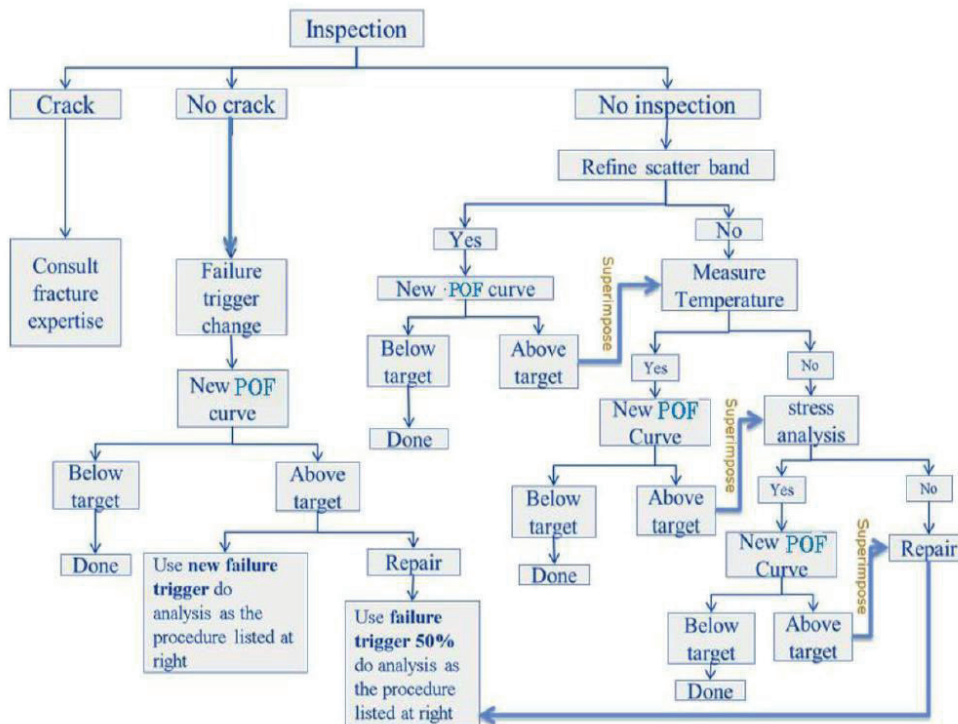


Figure 12: Structural Health Monitoring system analysis flowchart

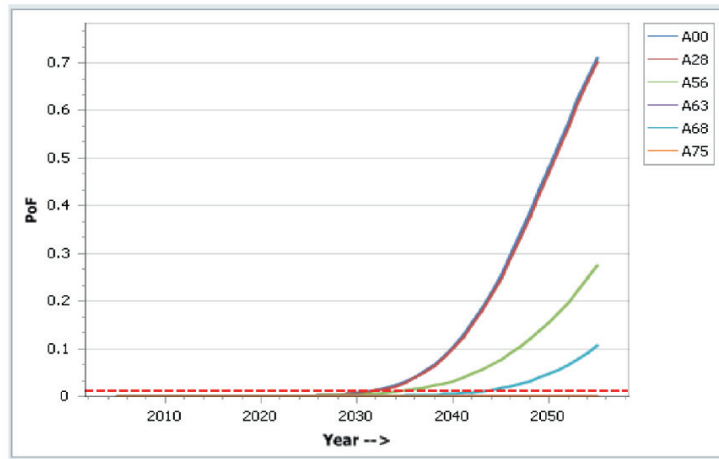


Figure 13: Example of POF-time curves for different welds

For the purposes of the demanding flaw detection task in the case of the UGW LRUT monitoring system, advanced signal processing techniques were developed and integrated within this work, using normalization, signal smoothing, correlation, baseline subtraction, feature extraction, selection and classification based on Support Vector Machines. For the training and validation of the UGW LRUT system, an extensive experimental investigation was carried out on different experimental setups. The results (Figure 14) show that the proposed method is able to effectively detect flaws under various temperature conditions and experimental scenarios.

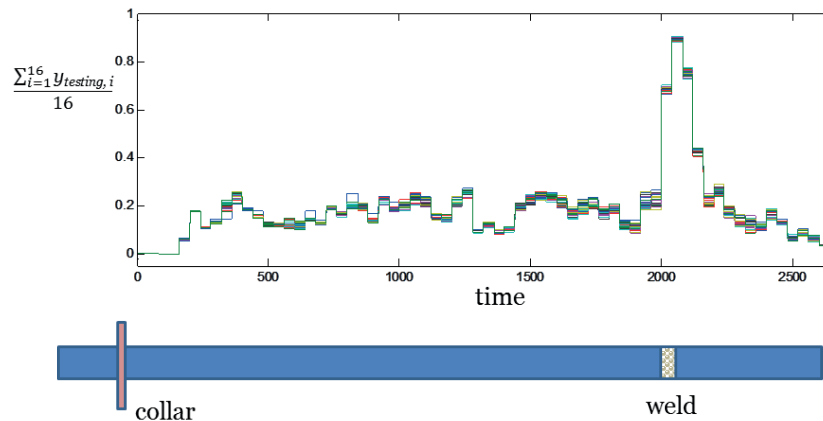


Figure 14: The output of the proposed signal processing module for a pipe at 250°C with a 9% Cross Section Area (CSA) weld defect and a graph indicating the weld defect location in the pipe

The design of the high temperature stainless steel ring (collar) that carries the transducers is shown in Figure 15, together with a manufactured collar installed on a pipe.

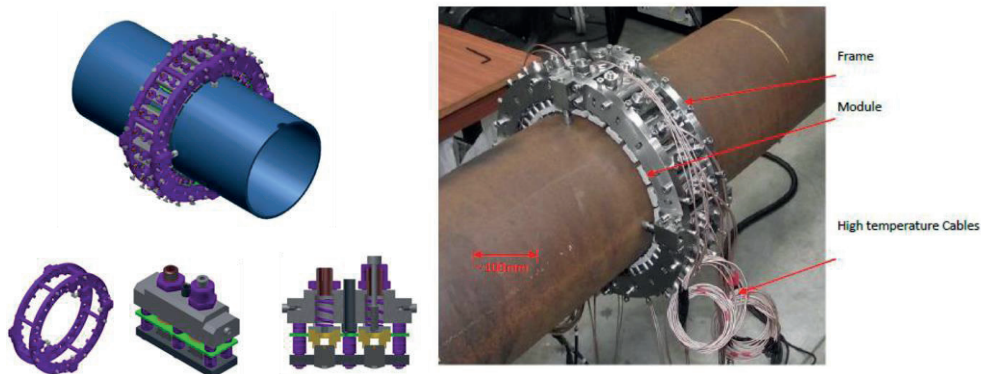


Figure 15: High temperature UGW LRUT monitoring system collar array

The integrated high temperature phased array TOFD system can be seen in Figure 16. The system consists of following key components: (a) high temperature PA probes using GaPO<sub>4</sub>; (b) ruggedized PA pulser-receiver unit; (c) signal processing and visualisation software.

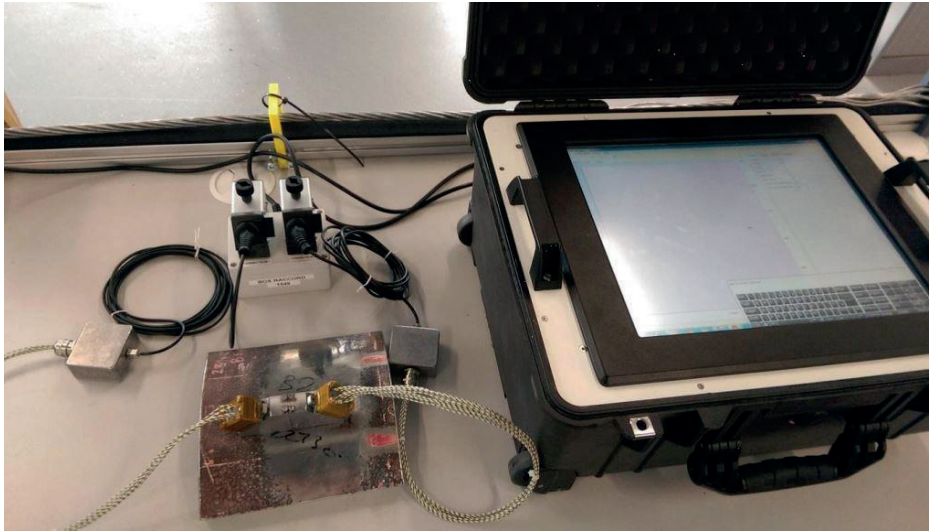


Figure 16: Integrated high temperature phased array TOFD SHM system

The PA probe using GaPO<sub>4</sub> was tested up to the target temperature of 580°C. For the coupling solution, SONO 1100 high temperature couplant was used. In Figure 17 one can see the manufactured PA probe using GaPO<sub>4</sub> coupled to a 25 mm thick P91 steel pipe section using the SONO 1100 high temperature couplant and placed in an oven. A thermocouple leading to a PC was used to ensure that the achieved temperature at the surface of the pipe test section is the correct one needed for measurement (580°C). After the pipe section was heated to the temperature of 580°C, the ultrasonic measurements with the manufactured PA probe were carried out to validate its performance at the target temperature of 580°C.



Figure 17: Phased array probe using GaPO<sub>4</sub> placed in an oven for characterisation at the target temperature of 580°C

In Figure 18 it is possible to see A-scans with multiple echoes from the back-wall of the pipe test section recorded at 580°C. The three echoes in the A-scan at 580°C are delayed compared to the echoes recorded at 25°C due to the change in velocity of P91 steel with rise in temperature.

Exposure to the temperature of 580°C was fatal for the elements 2 and 3 which responded with very much deteriorated ultrasonic signals.

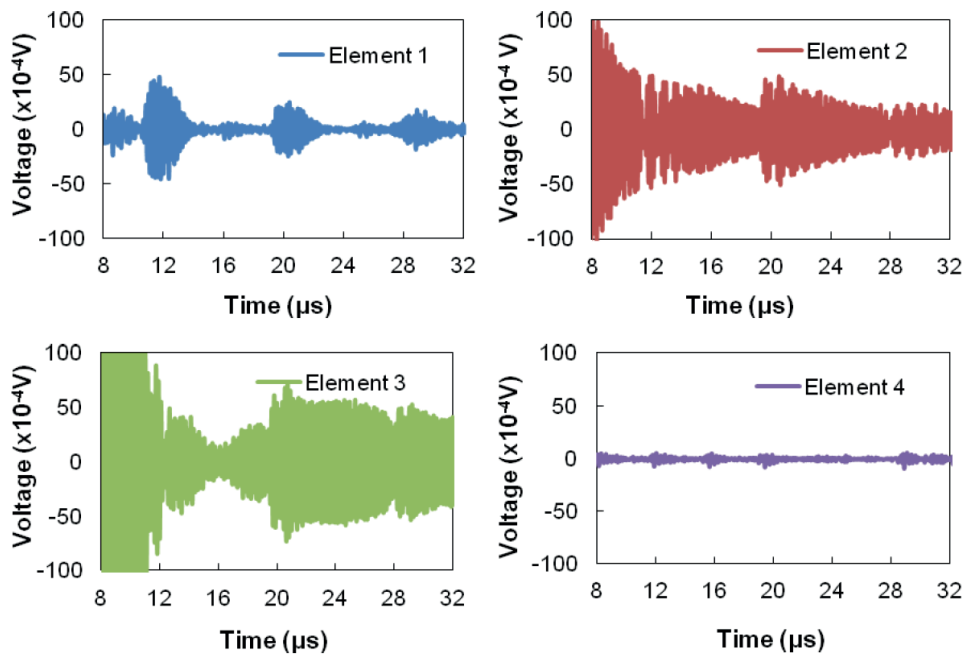


Figure 18: Multiple ultrasonic echoes at 580°C received on the 4-element GaPO<sub>4</sub> PA probe coupled to P91 steel pipe section using SONO 1100 high temperature couplant

On the other hand, the element 1 has survived the high temperature exposure and only a minor decrease in the amplitude value was observed from 25°C up to 580°C (Figure 19). This is more likely to be due to the adhesive rather than the element.

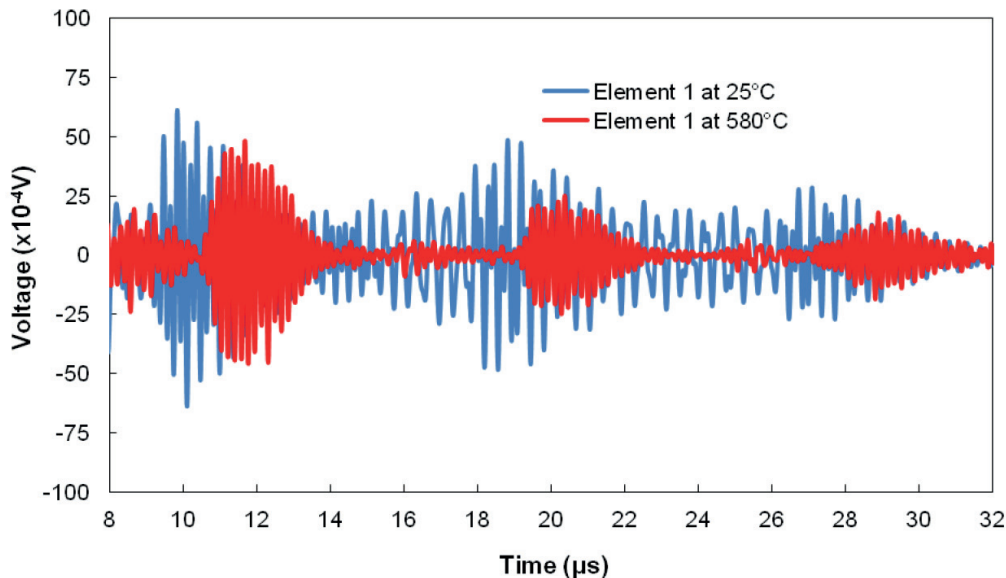


Figure 19: Compared multiple ultrasonic echoes at 25°C and 580°C received on the element 1 of the manufactured PA probe using GaPO<sub>4</sub> coupled to P91 steel pipe section using SONO 1100 high temperature couplant

## 7 CONCLUSIONS

Non-destructive testing of high temperature pipes and other critical components, as well as the estimation of their lifetime, is crucial for prevention of potentially catastrophic scenarios in power plants. This paper presents concepts and components of monitoring systems that will be

permanently mounted on superheated pipes at the locations of known defects. The overall systems incorporate the use of ultrasonic phased array probes in time-of flight diffraction configuration, or an array of single element shear-wave ultrasound transducers, for the inspection of pipe welds. The usual problems with the acoustically active commercial piezoelectric materials (PZT ceramics) at high temperatures have been tried to be solved by using gallium orthophosphate and lithium niobate single crystals, which have been demonstrated as promising solutions even at temperatures up to 580 °C, at least for a reasonable period of monitoring time.

A pulser-receiver unit for the excitation of 16-element phased array probe has been shown, with functions validated through an example of the calculation of aluminium block depth. This unit also includes sensors for the monitoring of pipe temperature and calibration of pulsing/receiving signal parameters. The algorithm for the calculation of the Probability of Failure parameter, highly important in pipe lifetime estimation, has been developed and presented in this paper as well.

The expected benefits of such systems for high temperature pipe monitoring are:

- Increased safety in electrical production power plants;
- Elimination of catastrophic accidents from superheated steam pipe failures;
- Decrease of the required shut-down time for inspection purposes;
- Increase in confidence in the safety of thermal power and nuclear energy plants.

## ACKNOWLEDGMENTS

This research has received funding from the European Commission through the FP7 Programme under the grant agreements no. 262574 and no. 605267, as parts of collaborative projects “HotPhasedArray” and “HotScan”. See projects websites <http://www.hotphasedarray.eu> <http://www.hotscan.eu> for more information.

## REFERENCES

- [1] L. J. Bond, IEEE Spectrum Inside Technology, pp 25-29, August (2012)
- [2] C. Nageswaran, C. Bird, "Evaluation of the phased array transmit-receive longitudinal and time-of-flight diffraction techniques for inspection of a dissimilar weld", Insight, 50, 2008, pp. 678 – 684.
- [3] K. J. Kirk, A. McNab, S. Cochran, I. Hall, G. Hayward, "Ultrasonic arrays for monitoring cracks in an industrial plant at high temperatures", IEEE T. Ultrason. Ferr., 46, 1999, pp. 311-319.
- [4] S. Zhang and F. Yu, "Piezoelectric materials for high temperature sensors", J. Am. Ceram. Soc., 94, 2011, pp. 3153 – 3170.
- [5] A. McNab, K. J. Kirk and A. Cochran, IEEE Proceedings-Science, Measurement and Technology, 145, 5, pp. 229 (1998)
- [6] A. Baba, C.T. Searfass and B.R. Tittmann., Appl. Phys. Lett. 97, 232901 (2010)

## Cable Aging Management Program Implementation in Krško NPP-NEK

**Marko Pirc**

NEK d.o.o.

Vrbina 12, 8270 Krško, Slovenia

[marko.pirc@nek.si](mailto:marko.pirc@nek.si)

### ABSTRACT

As a requirement for plant life extension for more than 40 years some additional Aging Management Programs (AMP) for passive equipment have to be implemented. The article presents overview of Cable Aging Management Program (CAMP) implementation. Program defines basic rules and initial activities for identification of adverse operation environment parameters that could lead to accelerated aging of specific materials. Samples of cables are selected based on nuclear safety and electrical equipment criticality for inspection and testing, to check functionality and prevent unexpected failure during normal operation. Acceptance criteria for environment parameters and diagnostic testing have been set. Initial visual inspection of cables condition in adverse environment and testing of sampled cables and environment are giving results for in time preventive measures. First cable aging management program is implemented since 2010 and its experience could be accommodated to other companies with cables recognized as key components.

### 1 INTRODUCTION

The purpose of Cable Ageing Management Program (CAMP) [1] is to provide reasonable assurance of functionality of the electrical cables with connections exposed to localized adverse environments. Identification of potential adverse localized environments or adverse service conditions and management of cable insulation and connections are its main concern. Main goal is to confirm functionality of cables for planed extended life operation more than 40 years.

CAMP defines activities on low voltage power, control, instrument and medium voltage cables with associate connections to safety related equipment (1E), critical equipment and cables identified in operating experience of plant as exposed to adverse localized environment.

Aging Management Program for cables uses two approaches. First is visual inspection of cable areas to search for potential local adverse environment so called harsh environment or “hot spot” such as high temperature, humidity or submergence, chemical or mechanical wear. Second approach is to do additional diagnostic testing of selected cables in specific local adverse environment. In NPP Krško (NEK) there are more than 1000 km installed cables in more than 21000 circuits of different type, material and manufacturer. It is obvious, all cables could not be inspected nether tested, though scoping of most critical cables are sampled in adverse environment. Sampling approach is shown on Figure 1. CAMP is continuing process with conclusion made, if all inspected and tested cables in harsh environment are meeting acceptance criteria, whole population of cables is functional for at least next period of inspection.

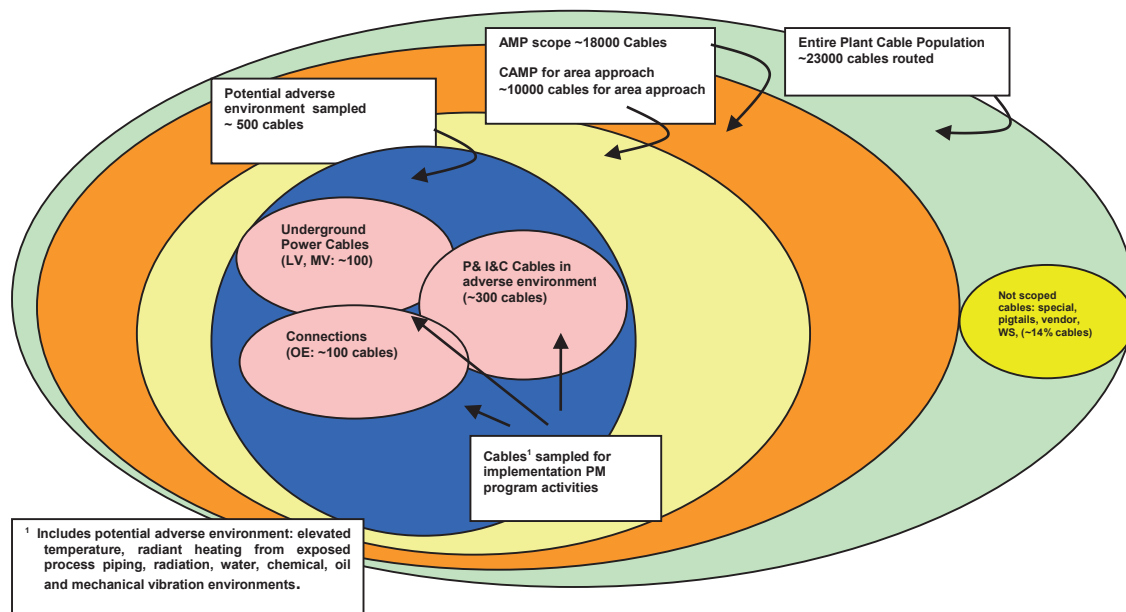


Figure 1: Cable scoping and sampling process [1]

Most of cables sampled in program scope are recognized as qualified safety related class SR (1E). LOCA qualified cables could be considered by spaces approach assuming all cables are installed in environmentally benign areas having all five of the following characteristics will remain operational for 40 years. If these environment conditions are met, there is no appreciable aging of cables during 60 years:

- room ambient temperature never exceeds 40°C,
- no close hot process lines,
- no radiation sources,
- no connections frequently manipulated,
- area is always dry.

Program applies to different cable groups in adverse environment: qualified safety related cables (1E) purchased in accordance with technical specifications, operationally important cables (N1E), critical equipment and Operating Experience.

Different cable types are grouped based on voltage or type:

- Medium Voltage (MV) Power Cables (5 bill of material-BOM types, ~1%)
- Low Voltage (LV) Power Cables (42 BOM types, ~10% of cable)
- Control Cables (23 BOM types, 70% of cables)
- Instrumentation Cables (45 BOM, 19% of cables)

Several different manufacturers were identified. Three of them are recognized during construction time as main producers of installed cables for SR (1E) circuits: Okonite for MV, Boston Insulated Wire (BIW) and Rockbestos for LV. Most of cable materials identified for insulation used in safety related 1E qualified cables are Ethylene propylene rubber (EPR) and cross linked polyethylene (XLPE) with CSPE (Hypalone®) for jacket. All materials have good thermal, radiation and moisture resistance for long-term operation lasting more than 40 years in normal designed temperature and radiation. Jacket material, Hypalone® as most susceptible material, used for mechanical and fire protection, is a good indicating material for adverse environment effects.

## 2 LICENSING REQUIREMENTS AND PROGRAM OVERVIEW

NUREG-1801 Generic Aging Lessons Learned (GALL) [1] requires aging management program to detect possible aging effects on electrical cables with appropriate consideration for low voltage power, control, instrument and medium voltage cables with connections in period of plant life time. Other licensing sources were considered: Maintenance Rule (10 CFR 50.65), License Renewal Rule (10 CFR 54) and Critical Components-reliability (INPO AP-913). Their additional requirements to be in scope are cables used to mitigate accidents or transients or support emergency operating procedures, cables whose failure could cause a reactor scram or actuation of a safety-related system, Station Blackout, Fire Protection, and reliability - cables supporting the function of critical components. The CAMP is conservative and specific in activities to identify adverse environment and do the assessment on exposed and sampled cables by:

- Identification of locations and parameters where environments are more severe than the plant design environment for those areas and could cause premature aging effects.
- Visual inspection of sampled accessible cables on located adverse environment.
- Evaluation of calibration and surveillance testing results to identify deviations leading to direct testing of the circuits with involved cables and connections
- Inspection for water collection in power cable manholes and draining water.
- Electrical test samples of inaccessible cables in identified adverse environment.
- Testing samples of power cable connections (i.e. IR camera, resistance testing, or other).
- If an unacceptable condition is identified at inspection or testing, a determination is made as to whether the same condition or situation is applicable to other (in) accessible cables.
- Estimating life prediction for exposed cables with site testing, theoretical calculations or laboratory testing to predict residual life of cable insulation.
- Corrective actions with repair and replace cables are planned to eliminate and prevent aging effects on cables (rerouting, thermal insulation, shielding, water pumping, ...).

CAMP is a coordinated effort between different existing programs and organization departments of Technical Operation (TO), Engineering Support Division (ESD), QA, and Training. Responsibilities are defined with roles of personnel on specific department. The following figure 2 represents organizational chart for implementing CAMP activities.

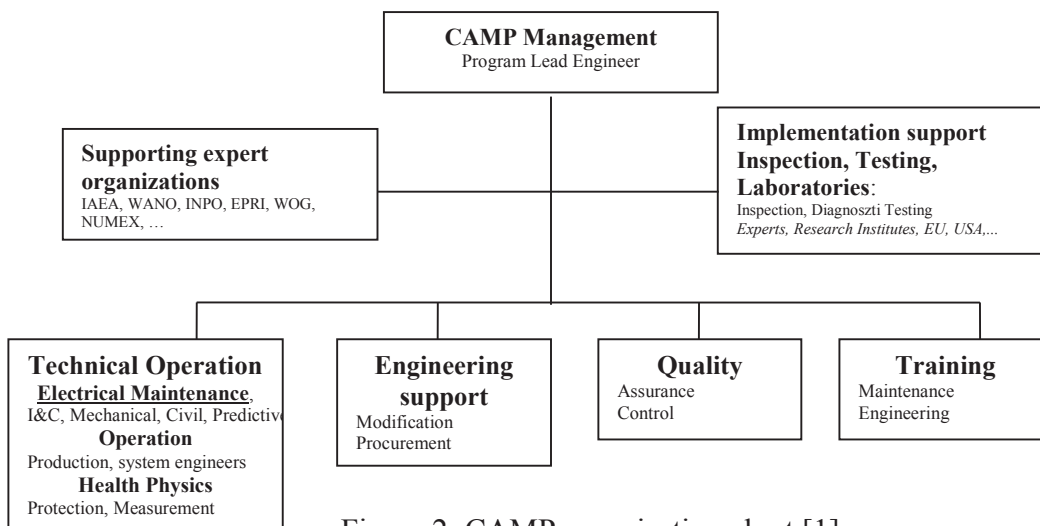


Figure 2: CAMP organisation chart [1]

## 3 DIAGNOSTIC TESTING METHODS AND CRITERIA

The focus of Cable Aging Management Program is to implement the best inspection approach and testing methods with acceptance criteria to detect possible cable aging on time and take

appropriate action based on risk ranking model or remaining life prediction. Overview of concept is shown on Figure 3.

In the first phase, at aerial approach focus is to determine adverse environment parameters with visual inspection and environment monitors to find hot spots and deficiencies.

In second phase, onsite diagnostic testing methods are used with acceptance criteria to evaluate basic electrical and mechanical properties to check functionality and risk ranking of cables.

In the third phase, aged samples are taken for laboratory test to determine the actual scale of different properties change. Laboratories testing are used for detailed remaining life prediction.

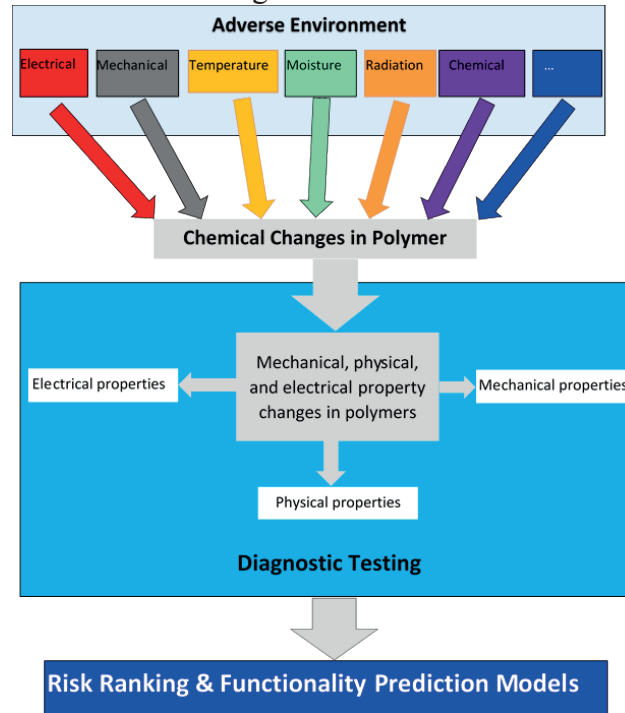


Figure 3: Cable Aging Detection and Remaining Life Prediction [4]

### 3.1 Visual inspection

Visual inspection is started with area approach to look for adverse environment and service conditions looking for hot spots observable on cable surface (colour change, hardening, cracking...).

Basic adverse environment conditions are defined as initial “hot spot”:

- High Local Temperature:  $T_{\text{ambient}} > 50^{\circ}\text{C}$ .
- High Radiation:  $> 200 \text{ mSv/h}$ .
- Long-term wetting: 75%-100% RH.
- Mechanical: no hardening, cracking, no indentations, no cuts.
- Chemical: no softening, swallowing, swelling, no oil, acid, or base contamination.

Adverse service conditions for power cables are:

- High conductor temperature from ohmic heating.
- High resistance connections.

### 3.2 Temperature monitoring

Elevated temperature is the most common cause of long-term aging of cable insulations and jackets in dry areas. For most insulation types and jackets identified in NEK, thermal aging causes the materials to harden, lose elongation properties, and eventually tensile properties. For low voltage power cables, operational ratings are based on a maximum conductor temperature in an assumed  $40^{\circ}\text{C}$  ambient environment. Power cables have  $90^{\circ}\text{C}$  conductor temperature ratings. Accordingly, power cable in areas with high ambient temperature ( $> 40^{\circ}\text{C}$ ) will tend to thermally age more rapidly

if operated close to ampacity if the elevated ambient temperature was not considered in the derating process. As ambient temperature increases above 50°C, the jacket materials of some power cables will begin to thermally age. Finding a hardened cable jacket would indicate that assessment of the aging of the cable is desirable to determine if the insulation has hardened and may be susceptible to cracking and failure. Table 1 provides approximate time to the point, where jacket aging would be detectable via tactile assessment for various ambient temperatures. The values are given to show that elevated temperatures greatly reduce life. The table gives a rough indication of temperature sensitivity for identifying areas where cable condition should be assessed.

Table 1: Approximate Time When Jacket Aging Would Be Detectable (hardened) [1]

Jacket Material <sup>1</sup> \ Temperature	50°C	60°C	70°C
Neoprene	16 – 20 years	2 – 3 years	Very short
CSPE (Hypalon)	Very long life	25 – 30 years	9 – 11 years
PVC	14 – 22 years	5 – 8 years	2 – 3 years

<sup>1</sup>Generic material data used (not NEK specific)

Appropriate tools for local temperature harsh environment finding are Infrared Camera, Data logger and Memory sticker for one time use showed with some results in Figure 4.

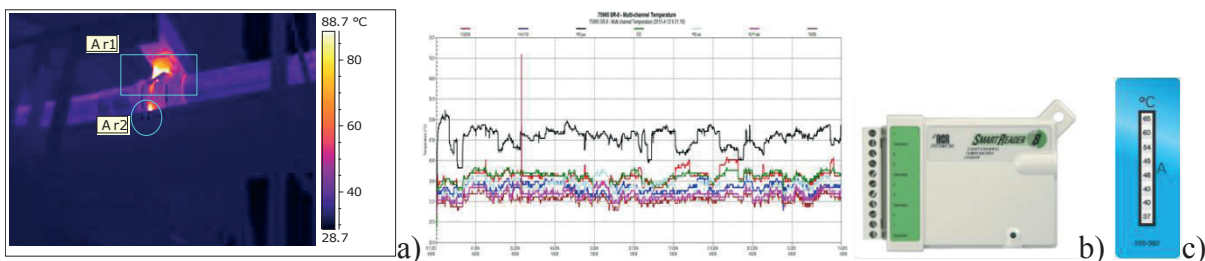


Figure 4: Different temperature monitors: a) IR camera, b) data logger, c) irreversible label [9]

### 3.3 Radiation Monitoring

With respect to radiation effects, most cables will be in low dose areas of the plant. However, some cables may be located in areas with appreciable doses. Some early Sandia research, showed that effects on physical properties are not observable at 1-5 Mrad (10-50 kGy). The effects of radiation and temperature are to change the physical properties (loss of elongation and tensile properties) of the insulation and after very severe aging eventually affect the electrical properties.

Radiation zone maps and environmental reports were reviewed and dose rates >200mSv/h was set for hot spot evaluation in scope of CAMP. To determine if there are any additional zones where high radiation may exist addition alanine pellets were set on 50 locations for gamma radiation and 5 neutron detectors. Conservative estimation was done, that maximum radiation that cables would “see” in 60 years at selected hot spots would not reach more than 60-80 Mrad. Cables are qualified for 200 Mrad. In general, high radiation conditions are expected to be accompanied by elevated thermal conditions and few additional areas needing assessment should be identified by additional research about simultaneous effects of radiation and actual temperatures.

### 3.4 Humidity

There are two concerns associated with wet conditions. One is moisture in the vicinity of connections where conditions for corrosion of terminations is possible. Damp terminal blocks may also be subject to surface tracking that can lead to failure connections in damp areas. The second concern is long-term wetting of cable as could occur in underground applications. The duct/manhole system containing low and medium voltage power cable were reviewed and determine long-term wetting of cable in adverse condition. A conservative approach was assumed underground cables are wet. Underground systems have been designed to be dry or drained automatically. “Rain and drain” applications where a duct or manhole may be wet for a short period until natural draining systems

where ducts slope towards manholes or other structures that are drained such that cables neither sit in nor are submerged in water for any significant period may be treated as dry with respect to cable longevity. Cables mounted on the walls of trenches and not subject to wetting along their length are considered dry. Main holes are checked monthly and water is pumped as needed to prevent wetting of cables. Periodic exposures to moisture lasting less than a few days (i.e., normal rain and drain) are not significant. Significant voltage exposure is defined as being subjected to system voltage for more than twenty-five percent of the time. Potentially wet cables not energized more than 25% of the time have a low likelihood of sustaining water related degradation. As long as the continuously energized cables remain healthy, there is little concern that the normally de-energized cables have degraded. The second half of the quote refers to impervious cable that has a metallic barrier that precludes ingress of water and 75%-100% relative humidity is considered as too high and calculated in risk ranking contribution.

### 3.5 Chemical

Most cables are not subject to contamination with oil or chemicals. Areas containing borates or other chemicals should be identified and evaluated for having cables. With respect to borates, deterioration of exposed terminations is more of a concern than jacket/insulation deterioration.

In general, contamination with oil is more related to a spill. Cables subjected to oil contamination should be cleaned and evaluated for any effects on longevity around turbine and large oiled pumps. Some traces of mineral oils were found in special sealants on tray to conduit that might effect Hypalone jacket with softening and swallowing effect. Tests were conducted at different laboratories with no evidence on primary insulation confirmed. Visual inspection is planned on specific location with repair and replace as needed.

### 3.6 Ohmic heating

Current in the conductor of power cable causes temperature rise due to ohmic heating in cables, mainly at connections. The review of the power circuits load currents with respect to the ampacities of the cables. If the normal conservatisms were applied during design, cables were applied with no more than 80 percent of ampacity. Given temperature rise is proportional to the square of the current, 80 percent of ampacity should result in 64% of the allowed temperature rise. In the case of a 90°C cable in a 40°C environment, the rise at 80% ampacity should be approximately 32°C such that the conductor temperature would be 72°C.

Ohmic heating should be considered in conjunction with identified adverse thermal conditions in rooms especially if ambient temperature coupled with the conductor rise result in temperatures approaching the rated temperature of the cable.

There are more approaches to evaluate ohmic heating induced aging of polymers or connections:

- Tests were conducted for different materials and resulting in realistic calculated addition 14°C to 17°C temperature rise due to ohmic heating depending of material type [9].
- MV cables high electrical fields could impact impurities and voids in insulation resulting in partial discharge as microscopic arcs leading to electrical trees resulting in dielectric failure or insulation break down. We start to use partial discharge testing.
- Infrared camera - Any temperature difference above reference (dT) is a concern. Table 2 provides suggested severity ranges for evaluating electrical power connections.

Table 2: Suggested Severity Ranges for Indoor Electrical Power Connections [1]

Status	Range
Advisory	0.5°C to 8°C Rise Above Reference
Intermediate	9°C to 28°C Rise Above Reference
Serious	29°C to 56°C Rise Above Reference
Critical	> 56°C Rise Above Reference

### 3.7 On site mechanical test of tensile strength - Indenter Modulus

For onsite mechanical test, evaluation of tensile strength (hardness), Indenter Modulus (IM) testing method was implemented and acceptance criteria developed. This method, shown graphically in Figure 6, uses a small-diameter probe to press against a cable. The force needed to compress the EPR jacket to a limited, defined extent is measured. The force  $F$  used and the displacement  $X$  are plotted against each other as shown in Figure 6. The indenter modulus  $\sigma$  of the material is the slope of the line relating the change in force  $\Delta F$  to the change in displacement  $\Delta X$ .

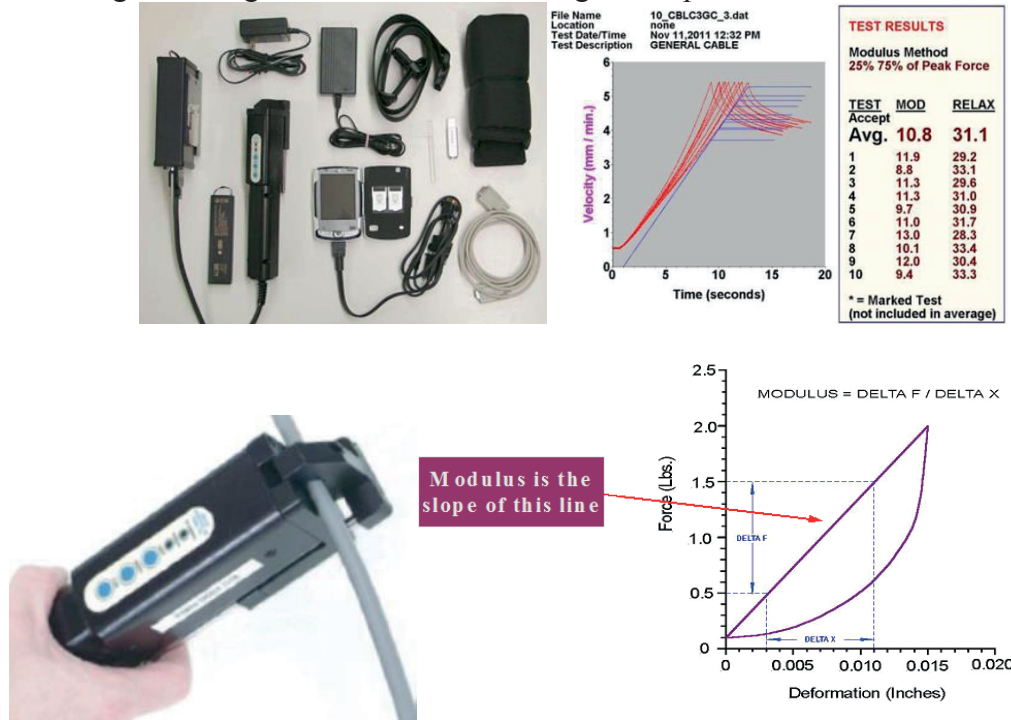


Figure 5: Concept and Equipment for Indenter Modulus Test

Criteria was developed on 21 samples of cables from warehouse and aged in oven at 120°C for 9 different time stages and results shown on Figure 6 [6]:

- Sample #1 new cable: from 10 to 13 N/mm NEW
- Sample #A (72 h) and #B (144 h): 10-13 N/mm OK
- Sample #C (240 h) and #D (360 h): 11-17 N/mm and 14-20 N/mm TRENDING
- Sample #2 (528 h): 85-118N/mm and #3 (1032 h): 151-206 /mm End of Life (EOL)-Replace
- Sample #4 (1872 h): 170-250N/mm and #5 (3264 h): 227-283N/mm EOL- Replace

Samples are used for training for visual inspection and acceptance criterial development for IM of different materials. For jacket material CSPE (in all SR cables) three stages: up to 15 N/mm NEW material; from 16-80 N/mm initial degradation of jacket, insulation OK; 3 year – TRENDING; more than 80 N/mm End Of Life reached: Replace Cable Jacket hardened and can crack; insulation possible damaged.

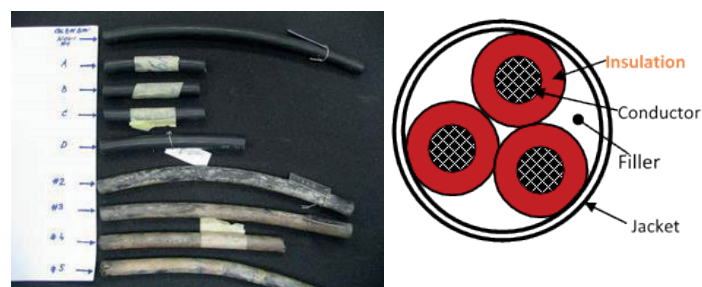


Figure 6: Samples of 9 stages Owen Aged Control Cable (BIW 7C#14 AWG) [6] and description of jacket and insulation

### 3.8 On site electrical tests

Evaluation of electrical properties is done by different testing methods depending on cable type and voltage (LV/MV). Some of most useful techniques with comparison in Table 3:

- Insulation resistance ( $R_{iz} > 2-100 \text{ M}\Omega$ ) and polarisation index ( $PI=R_{10}/R_1 < 1,5$ )
- Connection Resistance ( $R < 0,1 \Omega$ ); voltage drop at 100A ( $dU > 0,1V$  deviation, asymmetry)
- Capacity (nF-pF)
- Dielectric Losses  $\tan \delta$  (EPR:  $\tan \delta < 0,015$  in XLPE:  $\tan \delta < 0,0015$ ; Constant With Volt Rise)
- Partial Discharges (PD as low as possible PD LAB  $< 5pC$  and PD industry  $< 500 pC$ )
- Time/Frequency Domain Reflectometry (TDR/FDR)
- Impedance, line impedance resonance analyse (LIRA)

Table 3: Comparison of available cable inspection techniques [4]

Inspection Method	Advantages	Disadvantages
Time-Frequency Domain Reflectometry (TDR and FDR)	Commonly used for the condition of inaccessible instrumentation, control and power cables.	Currently intrusive, requires disconnecting the cables to install instrumentation.
Insulation Resistance	Commonly performed in industry to determine the condition of the cable insulation.	Currently intrusive, requires disconnecting the cables to install instrumentation.
Inductance/Capacitance/Resistance (LCR)	Good for detecting changes in cable and terminations by trending changes in inductance, capacitance and resistance.	Currently intrusive, requires disconnecting the cable at one end. Does not indicate location or cause of change in measurement.
Tan Delta ( $\tan \delta$ )	Determines changes in insulation (dielectric) properties by measuring change in dielectric loss angle. Can measure aging effects over entire cable length.	Intrusive, requires disconnecting the cables at both ends. Single number from long cable makes isolating location of aging section difficult. Loss angle may be trended but single test insufficient to estimate remaining life.
Partial Discharge	Good in determining voids and defects in insulators of medium voltage cables.	Test can damage insulator with localized heating that causes degradation.
Line Impedance Resonance Analyse (LIRA)	Indicate location of change in measurement.	A lot of data setup and interpretation knowledge.



Figure 7: a)  $\tan \delta$  testing equipment with 50Hz and b) 0,1Hz and c) LIRA

### 3.9 Laboratory testing

For additionally laboratory testing different sizes of samples are needed (large/small-mg):

- **Elongation At Break (EaB):** is the ratio between changed length and initial length after breakage of the test specimen. The elongation at break defined by the EN ISO 527 standardized method for tensile mechanical properties of the polymer, used for End of Life (EoL) prediction, with known and predefined acceptance criteria for different materials (i.e. 300% for new cable and 50% for EoL). Testing equipment is presented on Figure 8.



Figure 8: Testing equipment for EaB

Other testing methods for testing chemical properties:

- **FTIR Fourier Transform Infrared Spectroscopy:** Oxidation and crosslinking of cable insulation polymers such as EPR and XLPE inherently introduce new chemical bonds within the material, including C=O carbonyl and C=C carbon bonds that have unique vibrational frequencies. A convenient method, therefore, for characterization of related polymer degradation is FTIR spectroscopy. An example FTIR spectrum of EPR is provided in Figure 9.

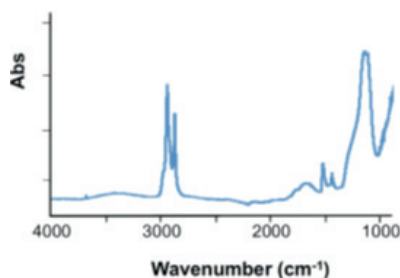


Figure 9: FTIR Spectrum for EPR [3]

- **DSC Differential Scanning Calorimetry** Differential scanning calorimetry (DSC) is a technique that is especially useful for characterization of semi-crystalline polymer systems. DSC measures the flow of heat in and out of test samples over time as a function of sample temperature. Features in a DSC curve include phase change transitions. As illustrated in the DSC curve of EPDM and Oxidation Induction Time (OIT) in Figure 10, heat flows into a sample with rising temperature to effect endothermic transitions including transition from solid to a glassy state, the glass transition, and from a glassy solid to a melted liquid. Heat is also consumed in the evaporation of volatile compounds such as added processing aids. In a semi-crystalline polymer, it is the material in the crystalline regions that undergoes a distinct melting transition. The integral of the melting peak in the DSC curve is thus a direct measure of the crystalline content of the system. The shape of the DSC curve, including the location of glass transition, is also related to chain scission and cross-linking that the polymer may have experienced.

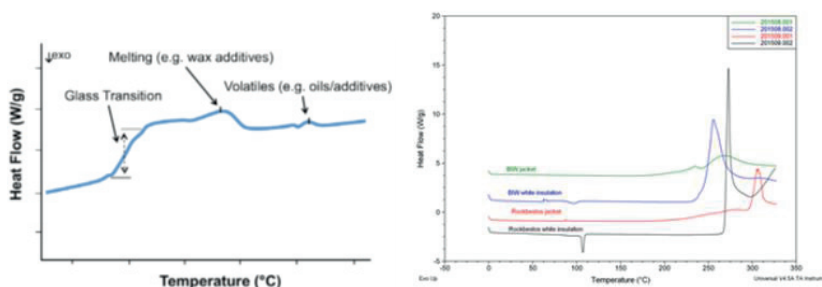


Figure 10: Description of DSC Curve of EPDM Showing Glass Transition, Melting Point and Evaporation of Processing Additives [3], [9]

- **TGA - Thermogravimetric Analysis** – In thermogravimetric analysis (TGA), the mass of a sample is monitored as a function of temperature and time. The experiment may be performed under inert, reactive, or oxidizing atmosphere and the TGA may be combined with a mass spectrometer to detect mass fragments of species volatilized during sample heating. Mass loss with heating can reveal copolymer ratio, moisture content, volatile additive content, and inorganic filler content. The decomposition behaviour of polymer samples at higher temperatures can also reveal information regarding the extent of chain scission and cross-linking in the polymer. Thermal decomposition in the TGA experiment may be a useful measure of relative degradation and history of polymer samples. The thermogram curve in Figure 11 illustrates transitions with 1) onsets of mass loss of distinct constituents, 2) inflections of mass loss curve, and 3) conclusion of mass loss.

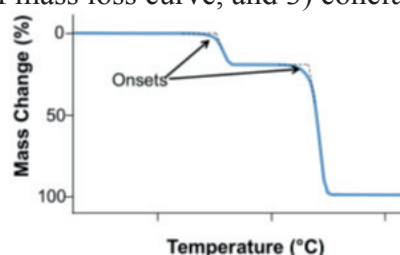


Figure 11: Illustrative TGA Showing Mass Loss due to Decomposition of Distinct Components [1]

#### 4 DIAGNOSTIC TESTING RESULTS

Using all of described onsite diagnostic methods, different tests were conducted and a lot of results collected. After 6 years of CAMP implementation we can summarize results in table 4 as follows [5], [7], [8], [9]. We can summarize as most valuable technics in visual inspection with temperature monitoring and IM hardness test. Between electrical tests  $\tan\delta$  and new LIRA are giving best results with most deficiencies found.

Table 4: Number of tests/findings/deficiencies (red) by diagnostic method

Diagnostic method	Insulation resistance (IR)	Dielectric loss ( $\tan \delta$ )	LIRA	Partial discharge (PD)	Visual inspection	Humidity	Temperature (T)	Radiation	Indenter (IM)
Cable type									
MV(10 kV)	55/2	55/5	2/2	30/3	55/7	55/25mhe/5	55/3	8/4/2	8/0
LV-P,C,I (<1000 V)	130/4	0	6/6	0	240/60/15	120/25mhe/2	240/45/12	120/15/4	45/12

- All 30 cable areas were revivied by buildings and more than 45 temperature hot spots were considered and action taken. Actions with rerouting cable from hot spot and repair or replace as needed. More than 60 cables were rerouted and not in single one insulation failed but only outer jacket. 12 cables were replaced due to jacket hardening/cracking.
- In outage 2015: 37 cable routes detailed inspection and 2 buildings walk down in/out, 25 LV cables tested, 12 MV cables tested (1 trending – underground tape splice, 10 cables rerouted from hot spots T – 4 replaced due JCKT cracks, RB hot spot identification (>50 location for RAD /T)
- Insulation resistance (IR) or Megger test as standardized test is not giving very useful results finding mainly severely damaged, failed cables: 3 LV power cables failure found due mechanical damage in tray (all triplex power cables without jacket) shown on Figure 12 and one N1E underground failure c), in splice .



Figure 12: Failures due of LV power cables found with IR test

- 55 MV cables were tested with 5 findings in trending criteria for  $\tan \delta$  results (all with accessories – connections and splices). The only qualified cable trending results for last three tests conducted in 2012, 2013 and 2015 on Figure 13 does not show significant changes from lower trending limit (in both testing methods – power frequency and VLF).

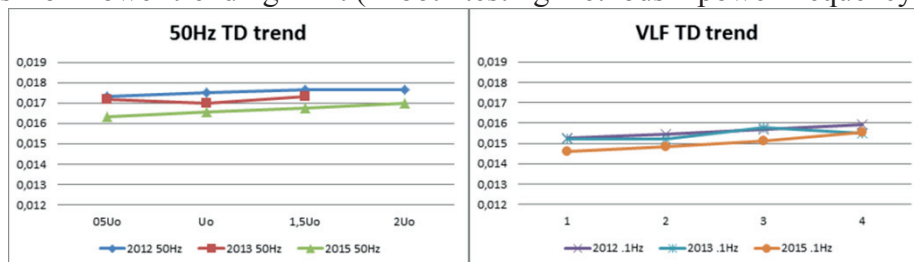


Figure 13: Trending results for  $\tan \delta$

- MV cable N1E with XLPE insulation and splice improved trending results significantly after corrections in field Figure 14.

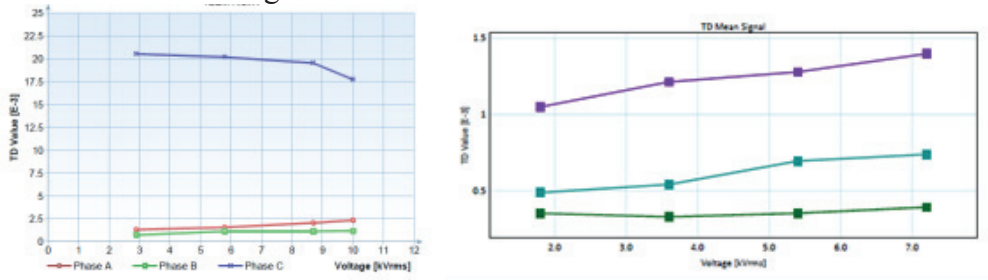


Figure 14:  $\tan \delta$  results for XLPE after corrections

- MV cable N1E with XLPE insulation found bad connection

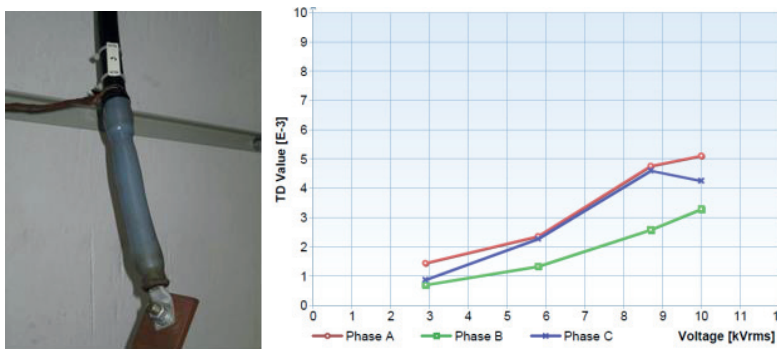


Figure 15: Found deficiency on XLPE cable connection with diagnostic test

- TDR results of RTD cables after modification on Figure 16

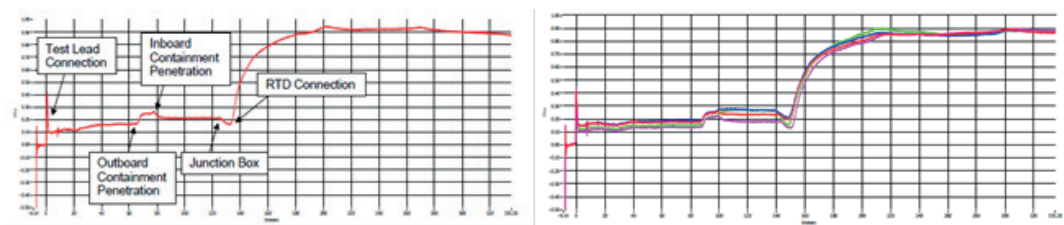


Figure 16: TDR test plot for comparison

- MV cable Partial Discharge test results on Figure 17.

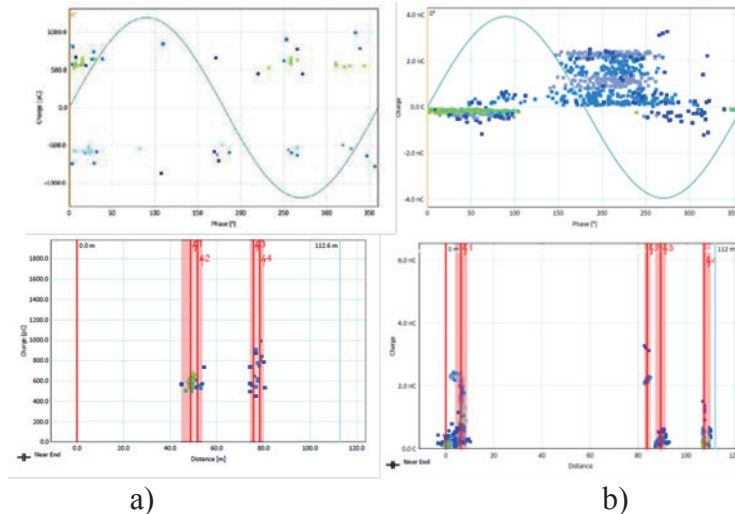


Figure 17: a) Nonsignificant PD events at 50m and 80m of cable end; no action taken  
 b) Significant PD events: XLPE cable failure at 5 m from cable near end-replacement

- LIRA 8 testing done 8 findings and deviations: 3 on field cables and 5 at beginning LIRA instrument testing with known location of cable damage (short circuit, bad connection, cut in insulation, local burned insulation). In figure 18 Spot Signature (dB) is shown with LV cable failure at two locations. Short circuit on Figure 12 was found on 30m from cable end (at load) is visible as left marked pick on Figure 18 b) and c).

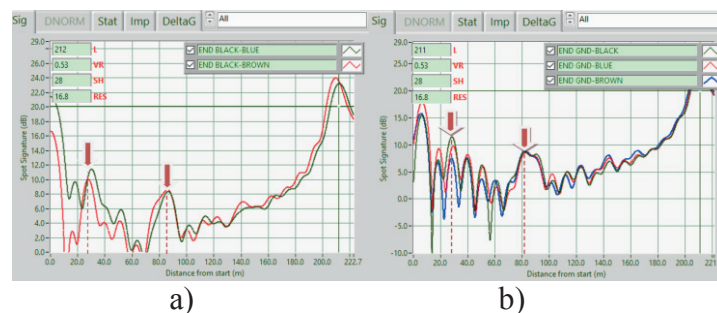


Figure 18: a) Location of two failures on LV cable between phases from cable end (at load) and b) between phase and ground

## 5 CONCLUSION

CAMP is in implementation phase for the last 6 years. Diagnostic testing results are promising and trending with immediate actions taken as needed. Most useful and promising on site testing methods are infrared camera, hardness test-Indenter Modulus, dielectric Losses-  $\tan \delta$  and LIRA.

Laboratory test has not been required nether implemented in larger scale. It will be used only in some special examples for additional evaluation of specific effects that might be found in future.

Additional diagnostic on site and laboratory tests will help for residual life time prediction and risk ranking according to deviations between qualification test methods and real environmental conditions including simultaneous aging effects of radiation, temperature, humidity, chemicals environment and mechanical load, vibrations,... Addition testing would also help to control functionality and possible new failure mechanisms such as LOCA testing condition with lo oxygen atmosphere or inverse temperature effect including Arrhenius calculation for temperature calculation with activation energy ( $E_a$ ) as temperature dependant, where small difference in material constant is giving big result change ( $\pm 10\% E_a$  resulting double/half residual life time) [3].

Program health report and risk ranking tool are in development phase and are planned to be implemented after testing period in 2016.

## REFERENCES

- [1] M. Pirc, Cable Aging Management Program, TD-2D, rev.1 Nuklearna elektrarna Krško, 2011
- [2] Generic Aging Lessons Learned (GALL), NUREG-1801 rev.2
- [3] International Atomic Energy Agency, “Assessing and Managing Cable Ageing in Nuclear Power Plants”, IAEA-Nuclear Energy Series NP-T-3.6, 2012
- [4] K.L. Simmons, , Determining Remaining Useful Life of Aging Cables in Nuclear Power Plants – Interim Study FY13, PNNL for US DOE, September 2013
- [5] M.Pirc, Vzpostavljjanje programa nadzora staranja električnih kablov v NEK, CIGRE Ljubljana, 2011
- [6] M. Pirc, HS-2011-02-T-IM: Development of acceptance criteria for Indenter Modulus, NEK, 2011
- [7] M.Pirc, Diagnostična testiranja električnih kablov v Nuklearni elektrarni krško, CIGRE Laško, 2013
- [8] M.Pirc, Rezultati diagnostičnih testiranj kablov v NEK, CIGRE Portorož, 2015
- [9] Testing reports in scope of work orders and internal NEK database

## The Efficiency of Nuclear Ion Exchange Resins Applied in the Primary Circuit Demineralizers of NPP Krško

Violeta Čalić

Krško Nuclear Power Plant  
Vrbina 12, 8270 Krško, Slovenia  
[violeta.calic@nek.si](mailto:violeta.calic@nek.si)

### ABSTRACT

Chemistry can influence dose rates by two aspects: chemistry conditions applied in the primary circuit and removal of (in)soluble particles. Since the primary coolant activity can have a significant impact on area dose rates and personnel doses, the main objective of purifying the primary coolant is to act on the radioactive source and keep it as low as reasonably achievable. Reduction of occupational exposure maintains confidence among workers and the public. Other factors, such as fuel duty, cycle operation, length and history, materials, steam generator (SG) surface area and particulate redeposition, also have significant contribution to the doses.

Ion exchange (IEX) is one of the most common and effective liquid effluents treatment methods in nuclear fuel cycle operations. IEX technology encompasses the sciences of thermodynamics, kinetics, ion chemistry, fluid mechanics, and economics. In the industrial water treatment, cation exchangers are used in combination with downstream anion exchangers or as a mixed bed demineralizer (combination of both cation and anion) for full demineralization. IEX is also an effective treatment method for liquid radioactive waste. In spite of its advanced stage of development, various aspects of ion exchange technology are being studied to improve its efficiency and economy in its application to radioactive waste management and coolant cleaning processes.

Over the years desire to improve the efficiency of fine colloidal particles removal and corrosion particulate removal in the primary systems has increased. There is a need for more and more efficient purification in order to decrease worker's dose during maintenance but also to decrease volumes of radioactive resin waste. Homogenization of products and usage on primary coolant treatment take into account the compromise between source term reductions, liquid and solid waste, and buying and disposal cost. As the disposal costs are much greater than the buying costs, optimization of the lifetime of the purification media, along with an increasing efficiency of pollutant removal is a major goal.

One of the effective purification methods for particulate removal is layering of macroporous (MP) resin in clean-up beds, spent fuel pit (SFP) and radwaste beds.

Lately, MP resins were also implemented in the primary circuit demineralizers of NPP Krško. The paper evaluates resin purification efficiency of different primary media, and assesses performance of gel and macroporous resin types.

**Keywords:** *ion exchange, resin, macroporous, gel, primary water purification, demineralizer, dose rate*

### 1 INTRODUCTION

The most important parameter in controlling and reducing source term in the reactor coolant system (RC) and associated systems is the control of pH. A principal contributor to source term is

large inventory of components containing nickel and cobalt in the reactor primary systems wear during plant operation, resulting in activation when transported to the reactor core. This process contributes to elevated concentrations of the major contributors to radiation fields  $^{58}\text{Co}$  and  $^{60}\text{Co}$  nuclides in the reactor coolant and the subsequent incorporation into the oxide layers of primary system piping and components. Shutdown plan (chemistry, operations and radiological protection), proper water chemistry and media clean-up must be correct for maximum reduction in source term and critical path reduction opportunities.

Generally, purification of the various circuits in nuclear facilities is ensured by a chain of filters and demineralizers. A combination of cation, anion and/or mixed bed resins is used to remove the undesired ionic species dissolved in the fluid such as those which can induce corrosion or radioactive elements that affect local dose rate. A fine filter upstream of the demineralizers traps solid particulate matter and a filter downstream protects the circuit from resin fines.

For decades, limited number of different resins has been applied in the nuclear industry since there are very few producers of the nuclear grade resins. NPP Krško ion exchange resin practice is very similar as worldwide. Resin efficiency is constantly controlled and very good resin operability is attained.

There is a desire for more improvements of the fine colloidal particles and corrosion particulate removal in the primary systems. CVCS configuration does not provide efficient removal of colloids and extremely fine corrosive particulates which are present in RC, especially in phase of shutdown and cooldown of the plant. One of possibilities for improved efficiency of a particulate removal in the primary system is usage of a MP ionic exchange resins.

MP resins are currently used in more than 50% of the US PWR units (many comprehensive studies were performed, e.g. Duke Energy NPPs) and EPRI strongly supports such a practice. EDF also has a long-time experience with application of MP resins and uses them to a certain extent.

MP resins are one option to mitigate the effect of radiation source term; greater dose is being retained on clean up beds during outage activity and lower activity is remaining in systems and being released to radwaste treatment. The larger surface pore geometry of MP resin is more conducive to physically absorbing colloidal materials as they pass through the demineralizer bed. Matrix composition (polystyrene crosslinked with divinylbenzene, DVB) and chemical functionality (anion with quaternary ammonium as functional group and cation resin with sulfonic acid as functional group) are identical in gel and macroporous resins; they are different in internal physical structure and that gives MP resins advantage in colloidal removal. MP IE resins have pores of a considerably larger size than those of the gel type resins (resin beads are about 300 to 500  $\mu\text{m}$  in diameter). The theory behind MP resins is that they can remove particles more effectively than gel resin. Gel resin is a smooth gel bead that allows water to diffuse into the bead for ion exchange. MP resin beads are a conglomeration of much smaller beads that allows water to diffuse into the “macropores” allowing ion exchange on the surface. The pores allow for more surface area and “nooks and crannies” to capture the particles. Their surface area may reach 500  $\text{m}^2/\text{g}$  or higher. Cation MP resins have higher cross-linkage in the matrix and are more resistant to the oxidation decomposition from the hydrogen peroxide than the gel resins. This property is extremely useful for usage in SFP demineralizer. Industrial experience also showed that a let-down filter change outs during the shutdown decreased with MP resin usage.

## **2 RESIN OPERATION EVALUATION**

### **2.1 NPP Krško primary ion exchange operational practice**

More or less since the beginning of operation, gel type IEX resins are used in all primary demineralizers of NPP Krško.

From 2014 MP resins have been introduced in some systems. SFP and WS (refueling water storage tank) demineralizer were loaded completely with MP resins (mixed bed with 300L of strong acidic cation - SAC and 500L of strong base anion - SBA resins).

During refueling outage RFO2015, for the first time, overlayer of MP mixed bed was implemented in CVCS or CS (chemical and volume control system) shutdown demineralizer. Mixed bed contained: 500 L of gel type resin (200 L of anion + 300 L of cation) and 300 L of MP overlay (100 L of anion + 200 L of cation).

Detailed information about the primary resins applied in Krško is presented in Table 1.

Table 1 Current resin practice in primary circuit of NPP Krško

System	CVCS			SFP & (RWST)	BR	WP
<b>Resin type</b>	Mixed gel / MP 1. SAC + SBA 2. SAC- <sup>7</sup> Li + SBA	Cation gel SAC	Anion gel SBA	Mixed gel / MP SAC +SBA	Mixed gel SAC +SBA	Mixed gel SAC +SBA
<b>Number of beds</b>	2	1	3	1 (1)	2	1
<b>Resin design volume* [L]</b>	850	850	2100	850 (1100)	850	850
<b>Mixed bed vol. ratio* [C:A]</b>	3 : 1	-	-	3 : 5	3 : 1	5 : 1
<b>Resin capacity [min. eq/L]</b>	2.1 / 1.2	2.1	1.1	2.1 / 1.2	2.1 / 1.2	1.8 / 1.1
<b>Mean bead size [mm]</b>	0.60(0.64) ± 0.05			0.064 ± 0.05	0.60(0.64) ± 0.05	0.57(0.064) ± 0.05

\* Resin volumes and volume ratios are variable depending on actual conditions in a treated media

## 2.2 Data evaluation

The effectiveness of the resins is evaluated by measuring different parameters in the RC/CS/SFP/WS media (pressure drop, decontamination factor drop, chemical and radiochemical leakages from the resin, resin lifetime, etc.).

Figure 1 shows SFP resin lifetimes in the last cycles. Replacements of mixed bed were made due to high pressure drop over demineralizer and/or reduced flow through the demineralizer.

For now one obvious benefit of MP resins is longer operational time but it should be confirmed in future.

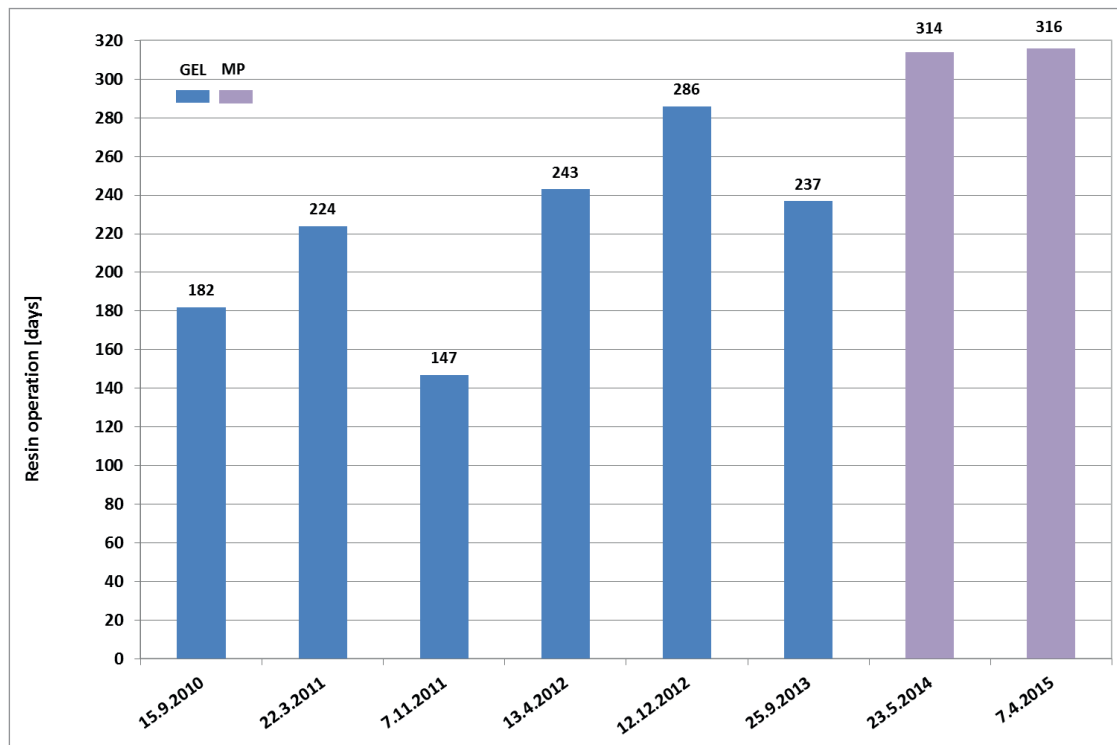


Figure 1. SFP resin operation lifetimes for the last cycles

Concentrations of aggressive ions, fluorides, chlorides and sulfates, in WS and SFP media at power operation are shown on Figures 2 and 3. Macroporous resin is efficiently purifying the media from sulfates and seems like the resin itself is more resistant to oxidizing media than gel type. For clear opinion on this we should wait for at least three complete MP resin operations.

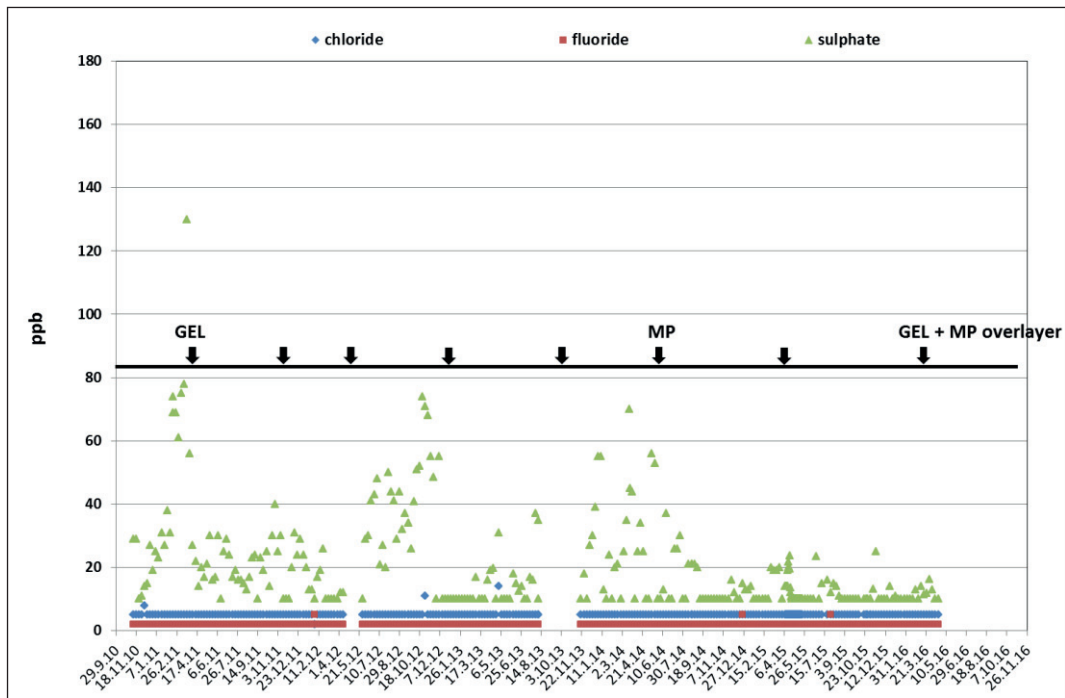


Figure 2. Impurity ion concentrations in SFP (arrows represent resin replacements)

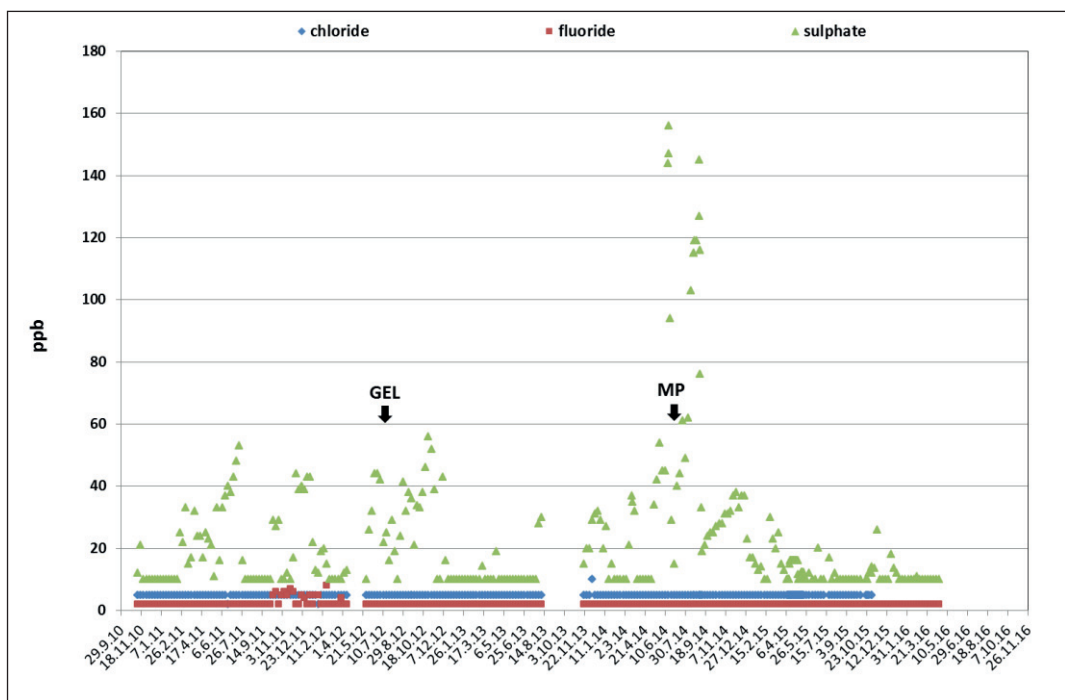


Figure 3. Impurity ion concentrations in RWST

Resin efficiency of WS demineralizer for radionuclide purification during online operation was not evaluated because of inconstant data. Operating time of demineralizer is non-continuous, variable and generally too short.

Specific activities of several radionuclides in SFP media during on line operation are shown on Figures 4 and 5 (OL25 - OL28). Good removal of soluble fraction of Ag-110m, Cs-137 and Co-58 is observed with both resins, gel and MP (Figure 6).

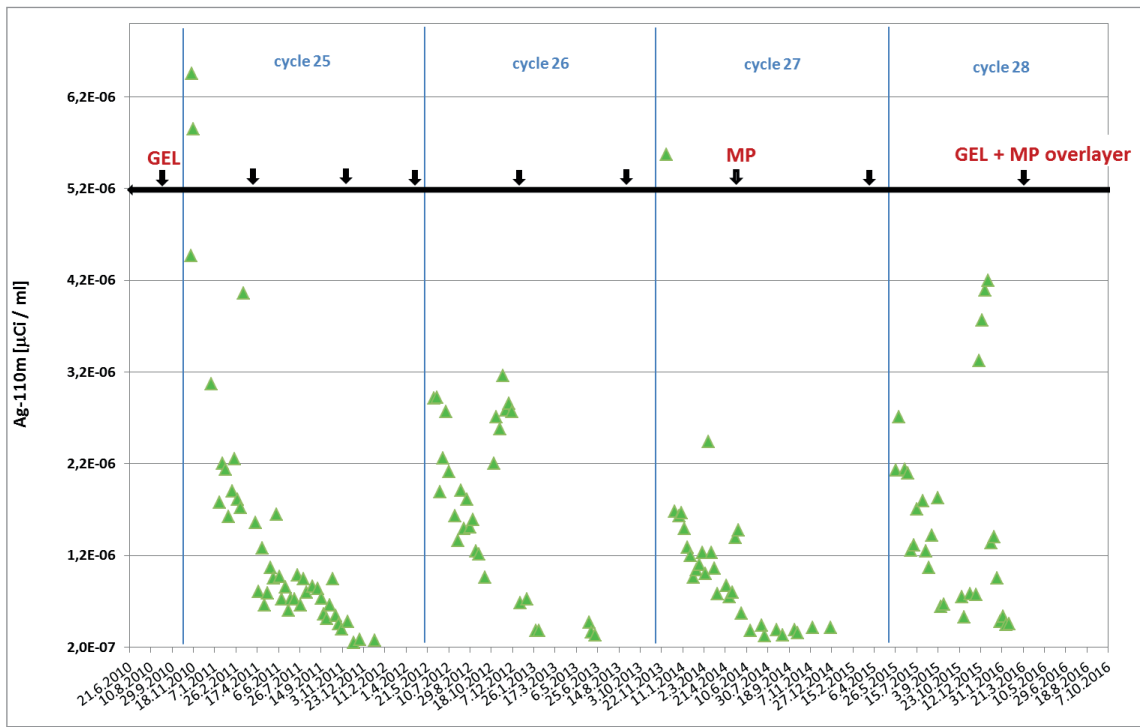


Figure 4. Specific activities of silver-110m in SFP (RFO data excluded)

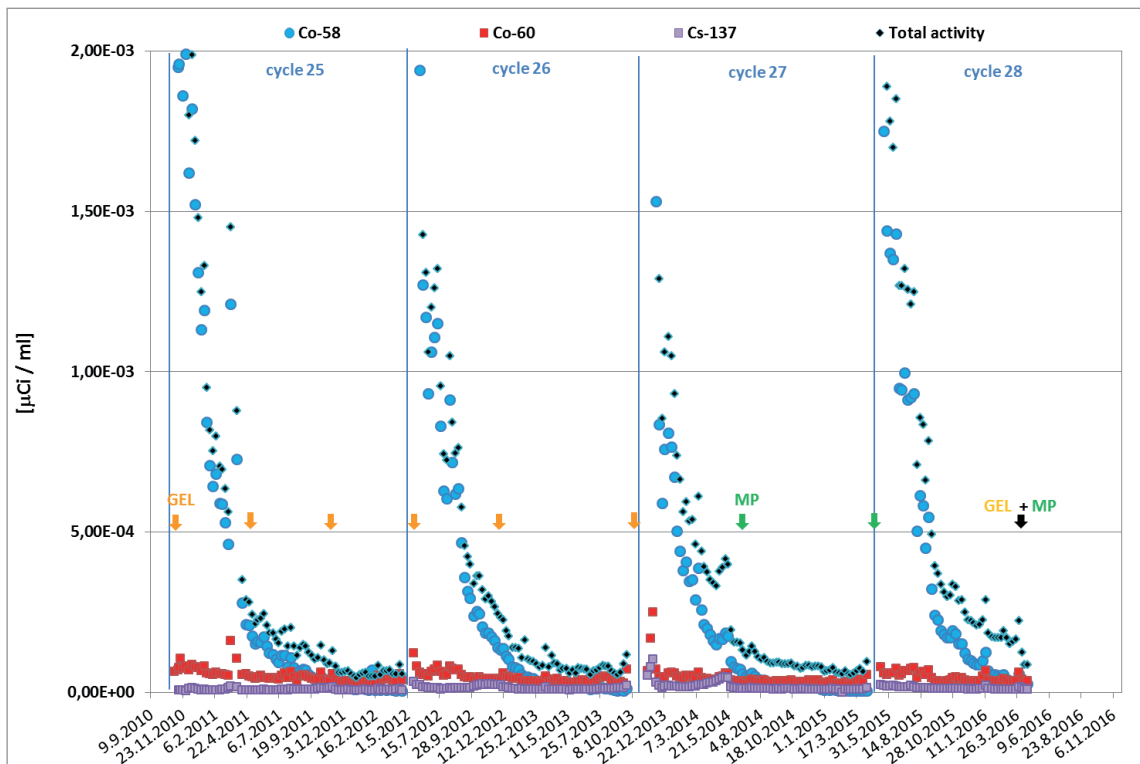


Figure 5. Specific activities of cobalt-58, cobalt-60, cesium-137 and total activity in SFP (RFO data excluded)

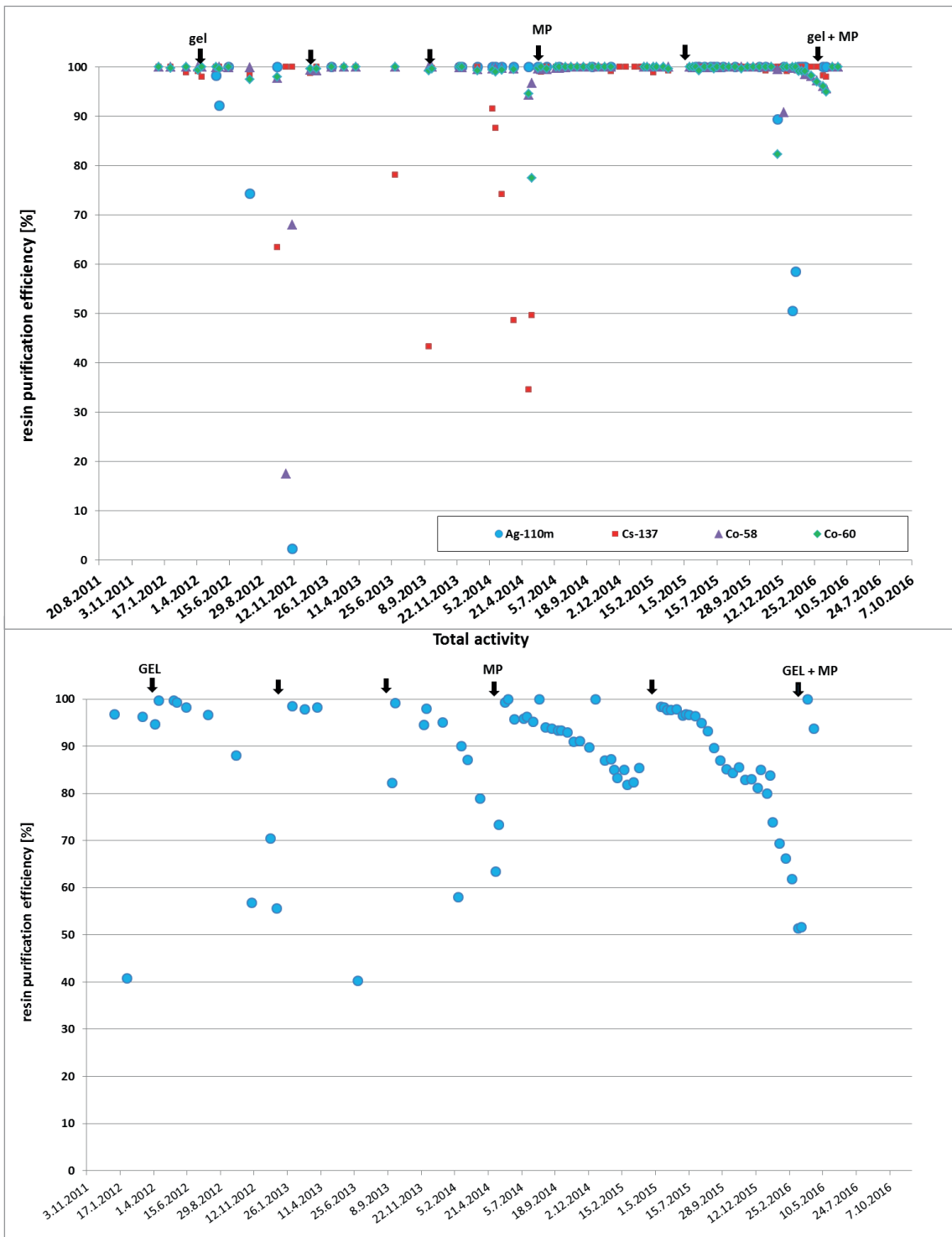


Figure 6. Purification efficiency of SFP demineralizer during on line operation (OL25-28)

Figure 7 presents comparison of the two resins, gel and macroporous, applied in SFP demineralizer (the last four replacements i.e. the last two operational cycles). Specific activities of several radionuclides (Co-58, Cs-137, Ag-110m and total activity) are observed during resin online operation. No significant differences in performance are observed from cycle to cycle or from resin to resin operation time. At the beginning of cycles radioactivities are generally higher and they decrease towards the end.

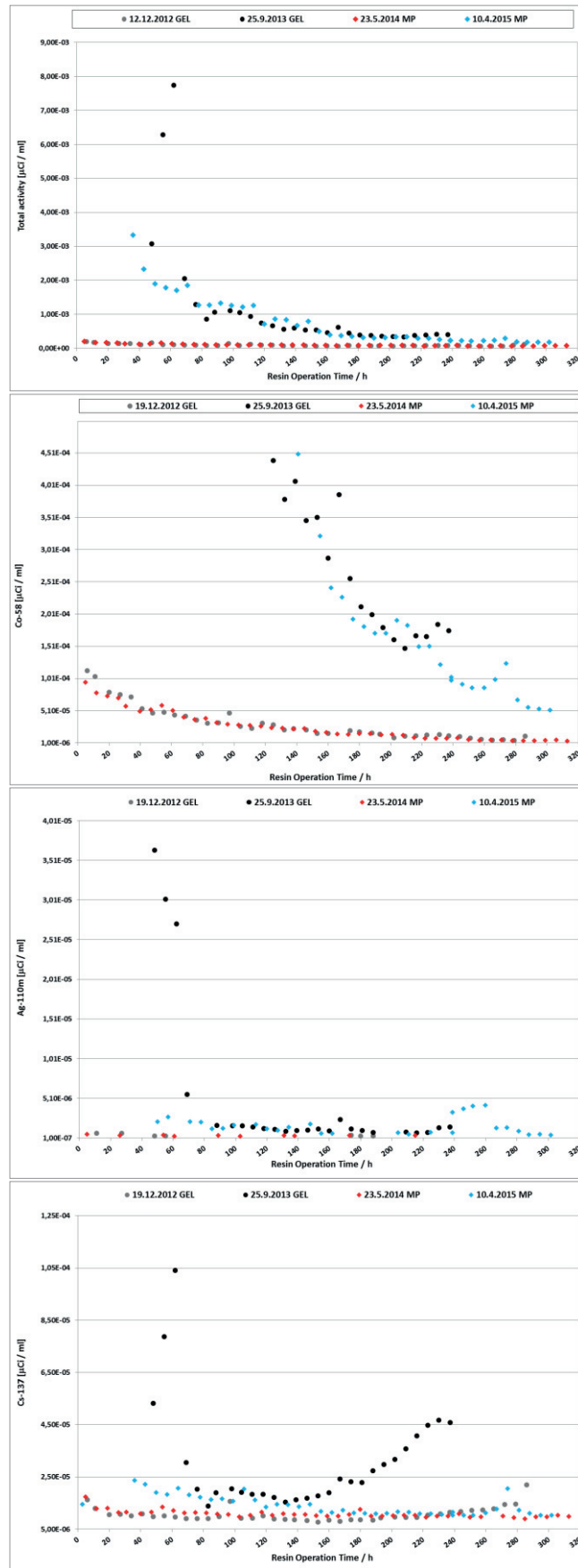


Figure 7. Comparison of specific activities in SFP media during operation time of resins, gel and macroporous: total activity, cobalt-58, silver-110m and cesium-137

Shutdown CSMB resin purification efficiencies during RFO2012, 2013 and 2015 are presented in Figures 8 - 10. It is too early to make any reliable conclusions (few more cycles and resin change outs should pass) but CVCS shutdown purification seems more stable and more efficient with MP resin overlay in comparison with gel type resins; efficiency factors are generally higher and less scattered. Removal of Ag-110m from primary coolant is performed much better with MP resins. Unfortunately no matter what resin type is used, a slight decrease of removal efficiency is observed for some radionuclides at start up (Cr-51, Mn-54, Co-60, Cs-137). It looks like non-continuous operation, temperature and flow changes, have effect on shutdown CSMB performance.

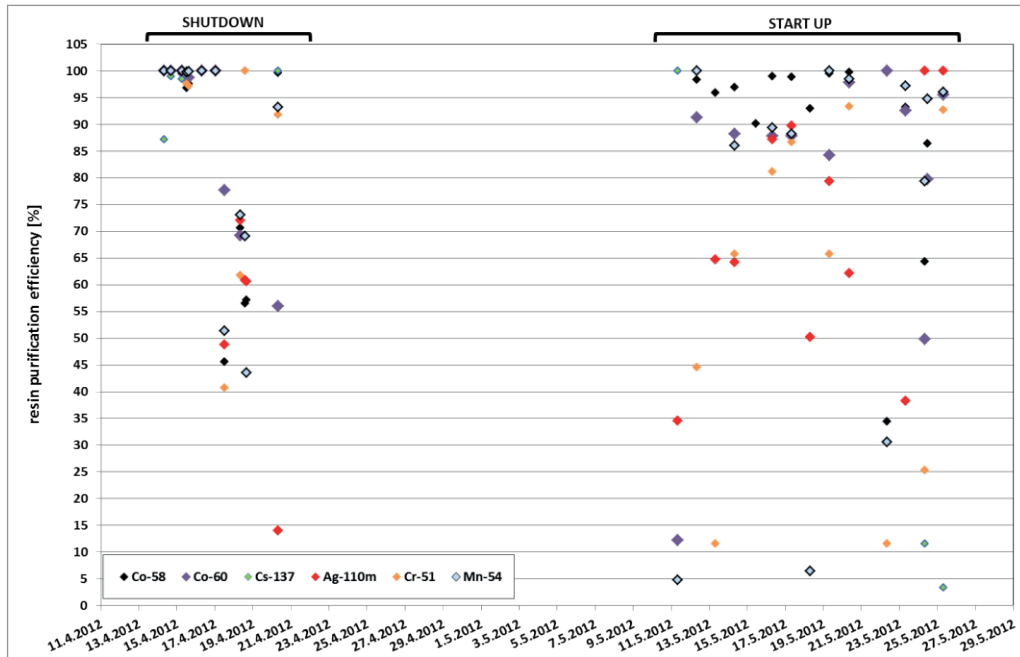


Figure 8. CVCS shutdown mixed bed resin efficiency during refueling outage 2012

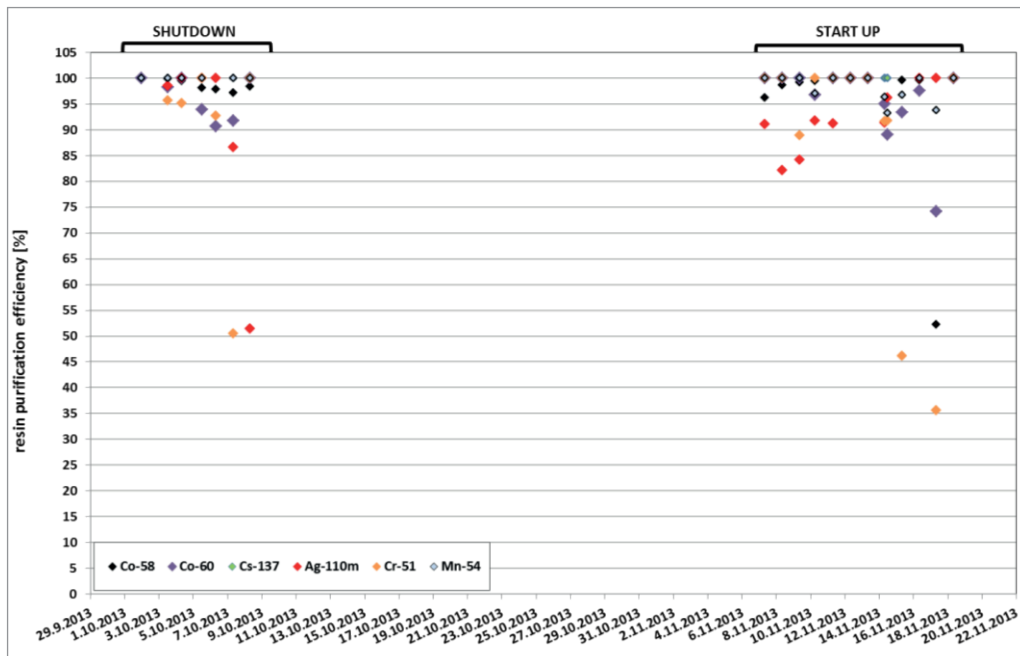


Figure 9. CVCS shutdown mixed bed resin efficiency during refueling outage 2013

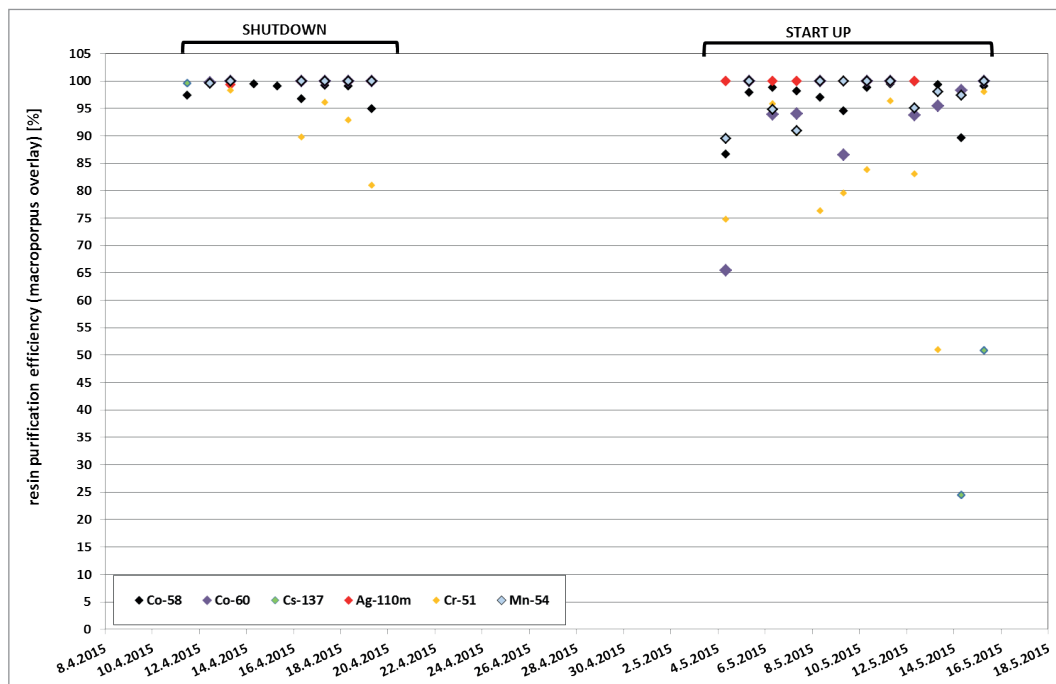


Figure 10. CVCS shutdown mixed bed resin efficiency during refueling outage 2015

### 3 CONCLUSION

Some NPPs use specialty resins which have more effective means of particulate removal. Layering of macroporous resin in clean up beds and in spent fuel and radwaste has become common practice. Macroporous (MP) resins were implemented in the primary circuit demineralizers of NPP Krško during OL27 and RFO2015. It is too early to make any reliable conclusions (few more cycles and resin change outs should pass) but some observations about macroporous resins could be indicated:

- MP resins are fulfilling their function and are efficiently purifying the primary media. Similar performance is observed for removal of radionuclides in SF media with both, gel and MP resins.
- Removal of sulfates is good and seems like the resin itself is more resistant to peroxide than gel type. SFP MP resin mixed bed has longer lifetime than average (over 300 days).
- During outage periods purification with MP resins seems more stable with macroporous resin in comparison with gel type resins; resin efficiency factors for different radionuclides are generally higher and less scattered.
- Generally, certain stability is noted in behaviour of Ag-110m after the MP resin implementation.

Unfortunately no matter what resin type is used, a slight decrease of removal efficiency is observed for some radionuclides at start up: non-continuous operation, temperature and flow changes effect shutdown CSMB performance.

Additionally, price of MP resin is similar to gel type resins previously used in SF/WS/CS demineralizers and better removal efficiency of MP resins would be certain cost benefit.

In the future an additional evaluation of operation of the primary ion exchangers (SF, WS and CS) is planned (approximately at a beginning of the 30th cycle) and final conclusions about the (further) use of macroporous resin will be drawn.

Lately, development of new resins is in progress. Improvements of the performance and selection characteristics of the ion exchange resins lead to the increased resin bed life, higher

superior capacity, and increased selectivity (removal of target ions with a good efficiency in the presence of other ions or under harsh operating conditions) and high crush strength.

## REFERENCES

- [1] F Nordmann, D Rochester, J Kysela, S Odar. Operational issues and practices; Chapter 3.4 Use of macroporous resins in NPP for corrosion products removal in PWR. ANT International 2011
- [2] Radioactive Colloid Removal by Optimizing Chemical Parameters. Palo Alto: EPRI 2003. 1003232
- [3] DP Rochester, Duke Power Company, Oct 06 2012, pers. comm.
- [4] F Gressier, EDF, October 05 2012, pers. comm.
- [5] NEK ESD-TR-20/12 (rev. 0) “The Ion Exchange Resins in PWRs: Applications, Operational Practice and New Trends”, Technical report (2013)
- [6] NEK ESD-TR-09/13 (rev. 0) “Introduction and Application of Macroporous Resins in the Primary Circuit Demineralizers”, Technical report (2013)
- [7] NEK ESD-TR-15/15 (rev. 0) “Evaluation of the Efficiency of Macroporous Resins Applied in the Primary Circuit Demineralizers during OL27 and RFO2015”, Technical report (2015)

## Sludge Deposit Mapping for Steam Generators

Ivan Rep, Tomislav Tomašić, Darko Barilar

INETEC – Institute for Nuclear Technology

Dolenica 28, Lučko, Croatia

[ivan.rep@inetec.hr](mailto:ivan.rep@inetec.hr), [tomislav.tomasic@inetec.hr](mailto:tomislav.tomasic@inetec.hr), [darko.barilar@inetec.hr](mailto:darko.barilar@inetec.hr)

### ABSTRACT

During plant operation, corrosion products from feedwater, drain and condensate system accumulate on the secondary side of steam generator in form of scaled deposits around the tubes and sludge piles on top of the tubesheet. These deposits increase potential for corrosion, affect fluid flow and reduce heat transfer efficiency of the steam generator.

Using data obtained during periodical eddy current examination of steam generator tubing, information on sludge deposit location and thickness is extracted from low frequency absolute channels. Sludge deposits can be detected over the whole length of the inspected tube. Using automatic analysis deposit results are provided within 36 hours after the inspection. Results are imported in Sludge Mapping software and presented in 3D visualization of steam generator. Both PWR and VVER steam generator visualization is supported.

Sludge mapping software provides visual information on sludge deposit thickness using color code and by calculation position of sludge indication, software draws the indication on the location within the steam generator where indication was found. Sludge mapping software provides information on heavy sludge loading areas of steam generator and can help with tracking of sludge build-up over time that can be used for optimizing steam generator maintenance.

This paper presents INETEC's Sludge Mapping solution, its functionality and features for visualization of sludge deposit location and thickness within the steam generator.

**Keywords:** *steam generator, NDE, sludge deposit, sludge mapping*

### 1 INTRODUCTION

Steam generators are primary circuit components that are used for transfer of thermal energy from primary circuit water to secondary circuit water and steam. Thermal energy transferred to secondary side is further transformed into electrical energy in the steam turbine. Due to its vital role and the fact that complex water flows occur within steam generator primary and secondary side, it is critical that the maximum efficiency of heat transfer is realized.

As the level of control for the secondary side water is somewhat lower compared to the primary side water, secondary side water includes various deposits, like corrosion products from feedwater, drain and condensate system that can accumulate on the outside surface of the tubes. Such deposits on the secondary side of the tube can reduce the heat transfer capability which has two major effects: firstly, lowered heat transfer capability lessens the efficiency of the entire heat transfer process and therefore reduces efficiency of the entire plant operation and secondly, reduced capability of tube to remove heat generated on primary side creates an environment susceptible to development of degradation on the secondary side of the heat exchanger tubes. Tubes with large accumulation of sludge on the secondary side are ideal location for development of degradation and various operational experience has verified initiation of such degradation. [1]

Nuclear industry has developed number of different methods that can be utilized for removal of sludge deposits from the secondary side. Earlier solutions were based on chemical methods but such approach can affect chemical balance of the secondary side water and despite short term benefits can create long-term consequences and instability. As an answer to sludge removal challenge, mechanical methods of sludge removal were developed that are based on application of water spray under pressure that breaks down sludge deposits in smaller, free particles.

However, one of the main issues when applying any sludge deposit removal process is to determine whether the total amount of the sludge in the steam generator is so large that removal actions are necessary or not. And once it is determined that sludge removal is necessary, it is important to identify what are the areas most affected by the sludge depositions and where majority of the removal efforts should be directed.

In recent years sludge deposit mapping tools have proven to be a very valuable tool for nuclear power plant system engineers in determining the total amount of sludge deposits in the steam generator and the distribution of the deposits in the steam generator. Sludge deposit mapping is based on use of data obtained through standard eddy current inspection of steam generator heat exchanger tubes. From this data, through sludge mapping process, information is obtained about the amount and distribution of sludge deposits.

## **2 SLUDGE MEASUREMENT CONCEPT AND MODEL**

Sludge deposit mapping uses data collected during the standard periodic eddy current inspections of steam generator tubes that are scheduled to be performed during regular outages of the power plant. One of the strongest and most important advantages for sludge mapping process is that mapping is performed on the same data that is collected during regular eddy current inspection. No additional activities or additional data collection is necessary and no additional inspection time is required and such concept results in same outage time, whether the sludge mapping is performed or not.

In modern applications, eddy current inspections are performed by multi-frequency technique and usually responses on higher frequencies are used for defect detection, confirmation and sizing while and responses on lowest frequency are used for determination of locations of support structures on the steam generator tube and lowest frequency is often referred as “locator frequency”. Response on absolute channel on “locator frequency” is the only information of interest that is used for sludge location determination and sludge length and thickness measurements as shown in Figure 1.

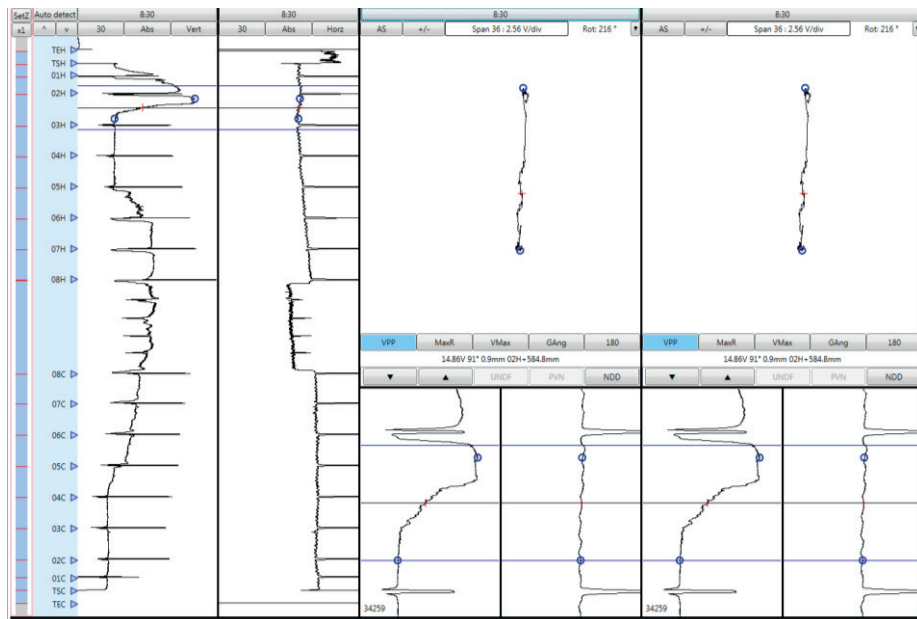


Figure 1 Example of sludge signals on “locator frequency”

Eddy current data of the “locator frequency” absolute channel are examined for the existence of sludge signals and in case that such signals are observed, location and sludge length and thickness are reported. Earliest sludge mapping activities were performed as manual analysis of certain regions of the steam generator where largest accumulations of the deposits were existent, usually areas above top-of-tube sheet of the hot leg of the steam generator.

With the advent of computer technology and development of automatized eddy current analysis that applies computer algorithms for evaluation of the eddy current data more complex arrangements for sludge detection and measurement became available. Such solutions are based on selection of the appropriate measurement model that offer representable measurement of sludge dimensions and once the measurement model is selected it can be applied through measurement algorithm for the entire length of the tube, for larger number of the tubes.

## 2.1 Sludge measurement model

For achieving adequate measurement capability of the sludge mapping system careful selection of the parameters for the measurement must be done. Measurement of the sludge deposits provides information about the following deposit dimensions:

- Deposit location along the axis of the tube
- Deposit length (or height on vertical steam generators)
- Deposit thickness

Deposit location along the axis of the tube is determined by same method that is applied in standard eddy current inspections, where location is calculated from the speed of the probe and the sample rate of the eddy current instrumentation. Deposit length is determined in similar fashion. By using the locations where amplitude of sludge deposit signal exceeds certain threshold values, start and end location for sludge deposit are calculated. However, accumulations are usually related to the support structures in the steam generators and are deposits are adjacent to the structures.

Deposit thickness is the parameter of sludge deposit that is most challenging and requires most experiments and testing to achieve adequate measurement capability. For deposit thickness measurement amplitude dependant curve is used that correlates amplitude of the sludge deposit

signal with thickness of the sludge deposit. Such measurement curves are common in eddy current software and higher amplitude of the measured signal will result with higher thickness of the deposit. Real challenge is to develop a curve that will provide realistic measurement of deposit thickness and such task is usually done in an experimental way.

Experiments are performed on tests specimens with different thickness of sludge layers around the tube. Common approach is that imitation of sludge is created based on the results of the sludge chemical analysis from the actual steam generators. Data with chemical composition of the sludge is available, as analysis is frequently performed in nuclear power plants. Based on such chemical composition, mixtures with similar characteristics are created and used as simulation of sludge. In recent times, efforts have been made to acquire clean sludge from the secondary side of steam generators and such sludge can also be used for preparation of sludge mapping calibration standards.

Figure 2 shows examples of dry sludge retrieved from actual steam generator secondary side. Such clean sludge is packed in rings of various thickness and compactness and put around defect free steam generator tube.

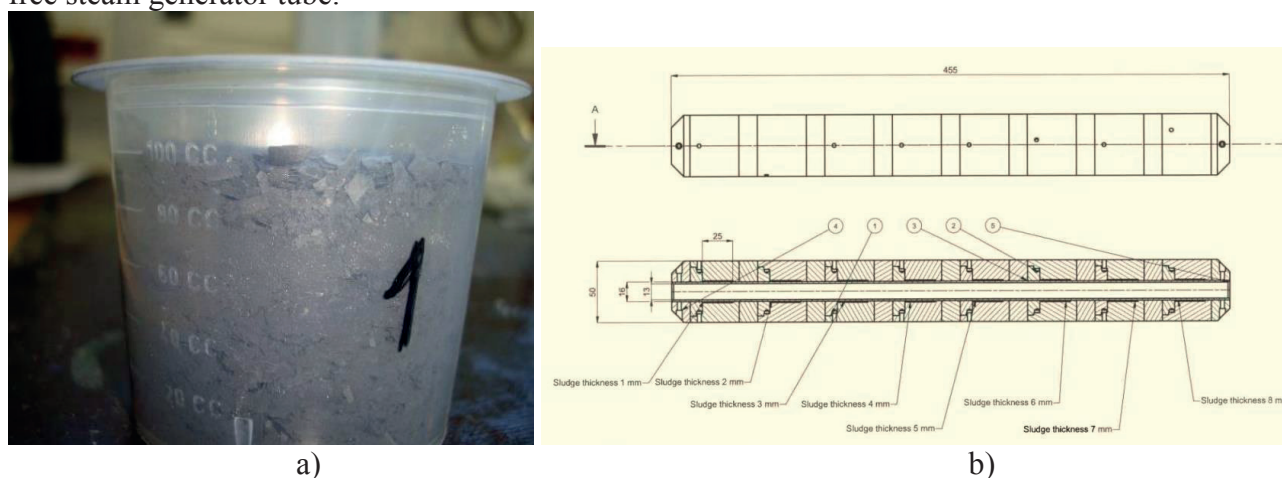


Figure 2 Sludge calibration standard: a) dry sludge retrieved from secondary side, b) example of calibration standard for sludge thickness measurement

Once all the parameters of the measurement model are selected, the analysis of sludge can be performed. As number of tubes and support structures in steam generator is very large, manual analysis approach to sludge mapping has proven to be a laborious effort. Initially, only areas above top-of-tubesheet on the hot legs of the steam generators, often referred in the industry as "sludge pile" were examined for sludge and only the height of sludge accumulations from the tubesheet was measured. Automatic analysis enabled more options and capabilities for sludge mapping, and such algorithms can be applied on the entire length of the tube with possibility of different measurement grids and settings.

## 2.2 Automatic measurement algorithm

Automatic analysis of eddy current data refers to application of computer algorithms that are applied on eddy current data with purpose of evaluating the data. Usually application is such that algorithms are developed and set in such way that degradation existing on the tube and recorded in the eddy current data will be detected and reported. As sludge signals are clearly distinguishable on the eddy current data, automatic analysis algorithms can also be set so that all signals meeting sludge reporting criteria are detected and reported.

When automatic algorithm is applied on the eddy current data, such evaluation results with significant amount of data and reported sludge occurrences. Most common approaches are to divide

steam generator tube into sections and in each one of them perform measurement or to perform measurements and evaluation only on segments of the tube adjacent to each support structure. Table 1 presents average numbers of reported sludge occurrences in steam generator for different settings of the automatic sludge mapping algorithm.

Table 1 Average number of reported sludge occurrences for different measurement algorithm

Type of sludge measurement algorithm	Number of results per SG
Axial grid with 64 divisions per tube	~ 350 000
Axial grid with 128 divisions per tube	~ 700 000
Axial grid with 256 divisions per tube	~ 1 400 000
Axial grid with measurement only adjacent to support structures	~ 40 000

As it can be seen in table above, automatic algorithms with strict division of the tube in sections results in significantly larger number of measurements and larger amount of data to process. For each section measurement will be performed and values will be created. Algorithm setting where evaluation and measurement is performed only on sections adjacent to support structures usually results with a lower amount of data and such application is especially convenient in applications for horizontal steam generators.

Normally during steam generator eddy current inspections acquired data is organized in calibration groups, where the data from certain number of tubes is recorded and each tube is recorded and archived as separate file. For each calibration group usually single textual report file is created that consists of all report entries for all tubes inside that specific calibration group. Each report entry (sludge measurement result) is one line in group report textual file.

Once the process of sludge measurement is completed for the entire steam generator, from obtained results database with results can be created and various processing of results can be performed as well as preparation of sludge distributions in different modes.

### 3 3D VISUAL MAPPING OF DEPOSITS

After the data has been processed it is imported into the sludge mapping visualization software. This software provides visual information on sludge deposit thickness using the color code which by default shows thicker deposits in red and thinner deposits in blue. The actual color scale can be selected from a set of predefined color scales.

The user interface displays a 3D model of the steam generator, showing all the tubes, supports and the sludge data. It provides a set of standard controls for 3D space navigation (rotate, zoom, pan) and specific controls for slicing and data display. The position of each sludge point is calculated from the imported data and drawn on the location in steam generator where the indication was found.

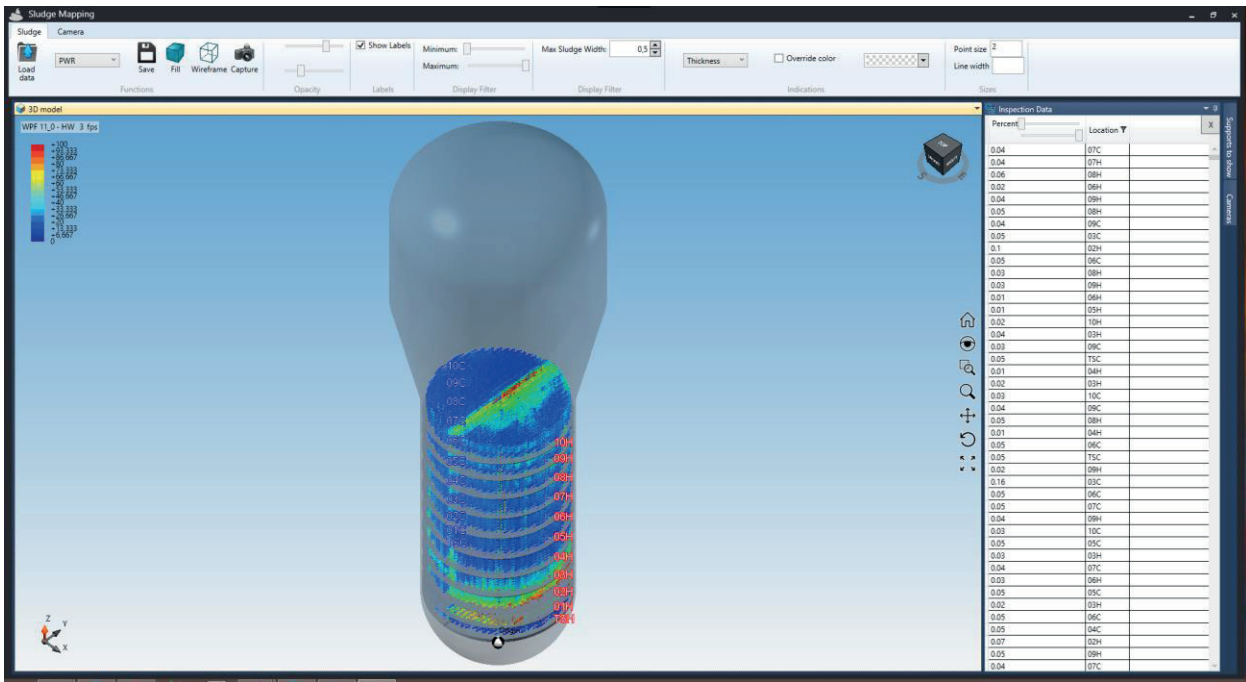


Figure 3 Sludge mapping user interface

The software supports two major SG types, the PWR and VVER and their subtypes. Steam generator configuration data is saved in a configuration file which enables the user to simply add a new custom steam generator type. The configuration file contains all the information about the generator geometry, tube positions and the positions and names of each support.

The sludge points shown in the visualization can be filtered on the fly by using the filters available in the header of each column of the data table. User can filter the data by position (row, column or section), sludge thickness, the support on which the measurement was made and the distance from it.

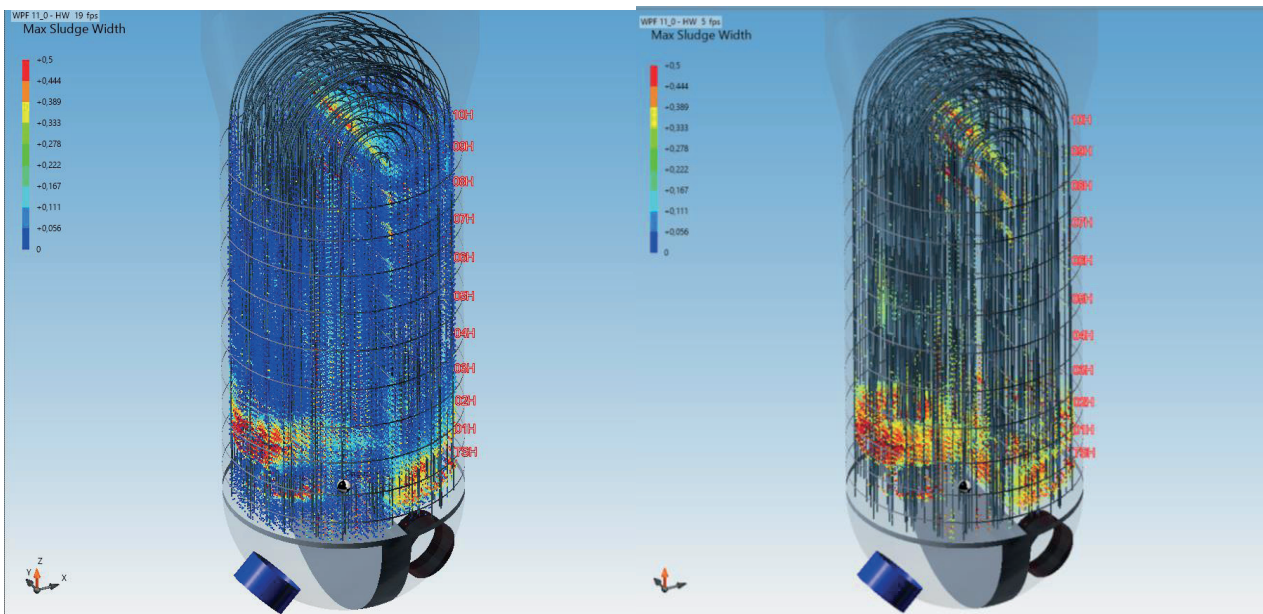


Figure 4 Example of filtering the data by sludge thickness

The SG model can be sliced by one or multiple arbitrary planes to show the sections of interest. By using two slicing planes, a cutout between the two supports can easily be made. These

features allow for an easy estimation of the heavy sludge deposit areas in the steam generator and can also help with tracking of sludge build-up over time that can be used for optimizing steam generator maintenance.

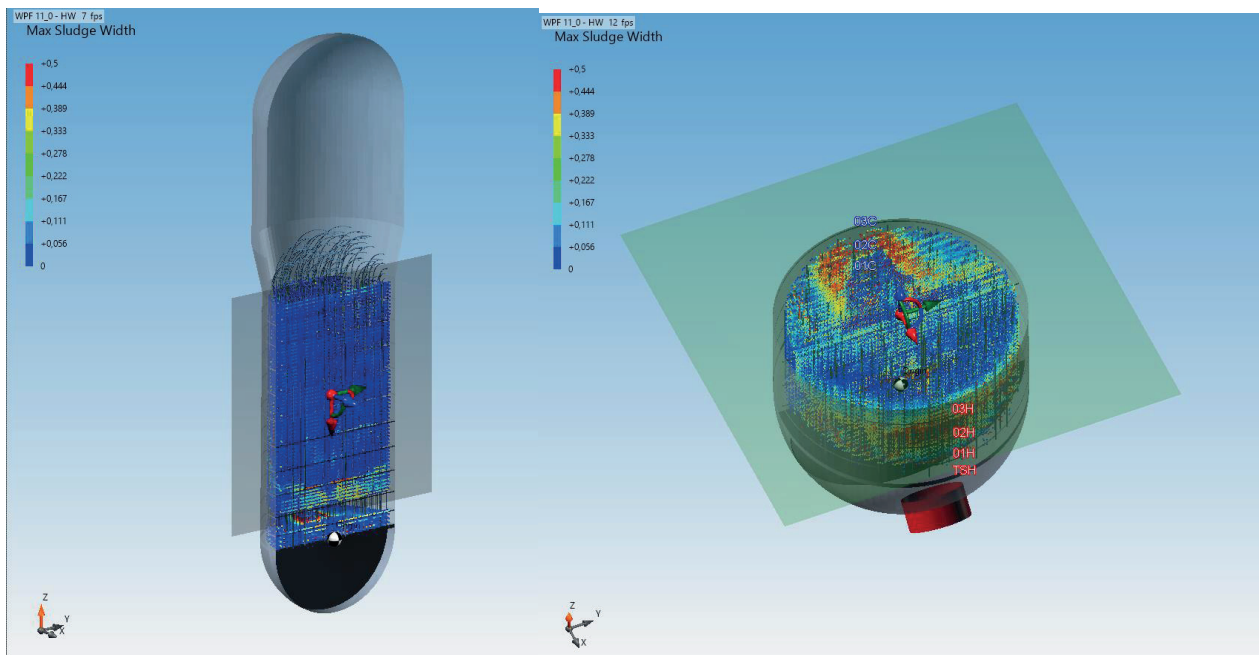


Figure 5 Examples of slicing the generator model by different planes

Automatic generation of a sludge deposit mapping report is supported. The generated report contains all the statistics about the sludge position relative to the supports and the estimates of the sludge mass. User can also predefine multiple 3D viewpoint positions which can later be automatically integrated into the report. This greatly speeds up and simplifies the process of generating of quality reports.

#### 4 CONCLUSION

Sludge deposit mapping of steam generator tubes is an activity that can significantly enhance operational capability of nuclear power plants. Accumulations of sludge on the secondary side of steam generator tubes can have significant impact on the functionality of steam generators as sludge deposits reduce the heat transfer capability and overall efficiency of the power plant, and additionally sludge accumulations create environment susceptible to development of tube degradation. Recent operational experience has also emphasized mechanisms like tube support clogging [4] that can also have impact on steam generator tubes. System engineers in nuclear power plants require more information about the amount and distribution of sludge on secondary side of steam generators and sludge deposit mapping is solution for obtaining such information.

Modern computer technology has enabled use of automatic eddy current data analysis and such solution offers quick method of evaluating large volumes of eddy current data for existence of sludge. Sludge measurement algorithms can perform evaluation of eddy current data in parallel with standard eddy current inspection of steam generators and such capabilities result in possibility that sludge mapping of steam generator can be finalized in very short time after the removal of equipment for standard eddy current inspection. Such features allow system engineers to have information about sludge deposits and make decisions even during outage period in which eddy current inspection was performed. Large amount of available data and three-dimensional

presentations of distributions of sludge deposits throughout secondary side of steam generators offer possibility of better understanding sludge creation and other related phenomena. Sludge deposit mapping is an activity that augments operation of nuclear power plant and ensures necessary background for activities that can further improve the efficiency and safety of nuclear power plants.

## REFERENCES

- [1] Seong Sik Hwang, Man Kyo Jung, Dong Jin Kim, Jangyul Park, Hong Pyo Kim “Relationship between SCC of Alloy 600 Tubes and Sludge Pile in a Retired Steam Generator”, Transactions of the Korean Nuclear Society Spring Meeting Jeju, Korea, May 10-11, 2007
- [2] Kim, M., Yim, C., Um, K., Kim, J., Kim, C. & Lee, S. “Development of Scaled Deposit Measurement Technologies for Steam Generator Tubing”, Singapore International NDT Conference & Exhibition. 4th April. 2011.
- [3] Jäppinen, T., Lahdenperä, K, Ala-Kleme, S. “Locating Magnetite on the Steam Generator Tubes with Eddy Current”, WCNDT. Durban, South Africa, 16th-20th April. 2012
- [4] Bodineau H and Sollier T, “Tube support plate clogging of french PWR steam generators”, Eurosafe Forum, Paris, 3-4 November, 2008

## Increasing Needs and Solutions for Non-Base-load Operation of Nuclear Power Plants

**Arif N. Kilic**

International Atomic Energy Agency, Department of Nuclear Energy  
Vienna International Centre, PO Box 100, 1400 Vienna, Austria  
[a.n.kilic@iaea.org](mailto:a.n.kilic@iaea.org)

**David M. Ward**

Consultant, Grid Technologies  
Cedar Lodge, 2A Stoke Park Road, Stoke Bishop, Bristol, BS9 1LF, UK  
[dmward@theiet.org](mailto:dmward@theiet.org)

**Philippe H. Lebreton**

Consultant, Energy Technologies  
Sterrenlaan 17, 3360 Bierbeek, Belgium  
[lebretonphr@gmail.com](mailto:lebretonphr@gmail.com)

### ABSTRACT

Operation at steady full power, i.e. baseload operation, of nuclear power plants (NPPs) is usually considered to be the most efficient use of capital investment. Therefore, design and operation of most existing nuclear power plants (NPPs) are optimised to operate in baseload mode. Recently, there is an increasing need to operate NPPs in non-baseload mode, specifically performing frequency control and load following. These needs are typically due to a large nuclear generating capacity, increasing share of renewable generation, deregulation or evolution of the electricity supply systems and markets. Re-optimization of NPP design and operation for non-baseload (flexible) mode of operation necessitates operational, economic and financial rearrangements to maintain the capital investment, in addition the adaptation of technical and regulatory changes. This paper discusses the aspects of design or operation of NPPs in flexible mode based on the existing knowledge and experience and it is primarily based on the recent study that was prepared by the International Atomic Energy Agency (IAEA).

**Keywords:** *non-baseload, load following, frequency control, flexible operation*

### 1 INTRODUCTION

In absence of a direct and economical storage of electrical energy on a large scale, the electrical generation is currently adjusted to closely match electrical demand continuously. The main reason for this balancing is to maintain a stable system frequency since a mismatch between the generation and demand will increase or decrease the system frequency. Although this balancing may be partially achieved by several methods on the demand side, i.e. to encourage electricity consumers to alter their electrical usage from periods of high electrical demand to periods of low electrical demand, balancing of the electrical system mainly controlled by the management of generation. This is achieved by changing the electrical output of some individual generating units to stabilize system frequency, as well as to control power flows on the transmission system. Usually,

the grid system operator manages the balancing of demand and generation and requests electrical output adjustments from the individual generation units. Need and performance of increasing or decreasing the electrical generation by individual generation units varies depending on the grid needs, demand variations, generation mix and commercial or regulatory arrangements. Changing the electrical output may be needed and to be performed rapidly, i.e. within seconds, or slowly, within timescales of minutes or hours. This output change can occur several times a day or a few times in several years. Furthermore, the generating units utilizing various fuel sources are requested to change output, customarily, in a commercial/financial merit order to minimize overall operating costs while providing the benefit of grid system stability. As such, the generating units with lower marginal cost are operated at full power as much as possible, i.e. in baseload mode, while higher marginal cost (typically corresponding to higher fuel costs) units reduce or cease output, e.g. at times of low electrical demand, or operated at partial load to be able to change output when requested by the grid system operator, i.e. operate flexibly.

Herein, the term ‘flexible operation’ (or ‘operating flexibly’) is used interchangeably with ‘non-baseload operation’ to describe any mode of operation of a generating unit that is not ‘baseload’ as defined by the IAEA publication [1] and the specific focus in the following discussions are on changing electrical output to match generation with electrical demand on the electricity grid system (Fig. 1) in NPPs.

Since NPPs have relatively low fuel cost (low marginal cost), nuclear generating units are preferred to operate as baseload generation units except when it is necessary to reduce power or shutdown due to the plant specific needs, i.e. for maintenance, refuelling or for other operational or safety reasons. In the early years, a number of countries/utilities considered and requested NPPs with flexible operation capabilities. Some also carried out some flexible operations such as a limited amount of load following [2–6]. Nevertheless, since that time, the majority of NPPs have been baseload generation units and their plant systems, procedures and equipment have been optimized for operation in that mode. However, due to several reasons, there is an increasing need to operate nuclear units in non-baseload mode. More specifically, NPPs are being considered to perform frequency control and load following. These needs are typically due to (or as a result of combined impact of) a large nuclear generating capacity, increasing share of renewable generation, deregulation or evolution of the electricity supply system and the market. This increased the consideration for operating NPPs in flexible mode.

The decision on whether — all or some of — the NPPs should operate in a flexible or baseload mode requires an understanding of the grid system needs. Subsequently, thorough investigation of several factors which would impact all stakeholders who should agree on the feasibility of flexible operations of particular NPPs should be evaluated. Within the electricity market framework, the impact from flexible operation of NPPs and associated needs have to be well understood with respect to the efficient use of capital investment and the impacts need to be minimized, eliminated or compensated for serving the overall energy structure needs while preserving the nuclear safety.

Technically, the planning and design of a new built NPP should have usually had flexible operations in mind and these capabilities need to be validated during commissioning with any limitations should be determined at the beginning of operations. The NPPs that have previously operated only in a baseload mode, and are now converting to non-baseload mode, similar considerations should be given and solution for design and operational changes should be developed. Substantial plant modifications may be needed to support flexible operations, depending on the existing design capabilities and the extent of flexibility requirements. In either case, the operating license application (safety case) would be developed to support flexible operations and existing operation and maintenance strategies may need adjustments.

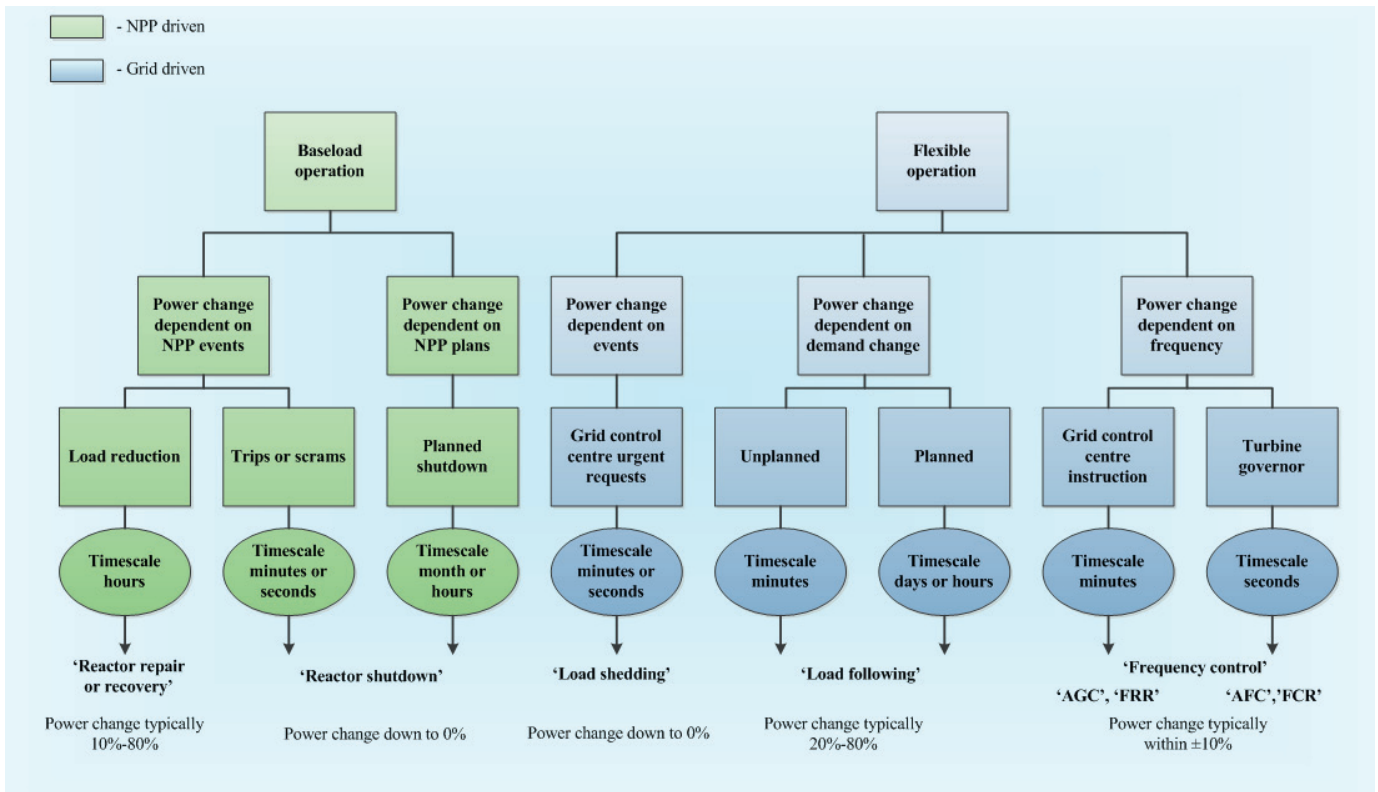


Figure 1: Definition of Load Changes under Baseload and Flexible Operations [1].

## 2 REASONS FOR FLEXIBLE OPERATION OF A NPP

If the total electrical generation capacity of the NPPs in a grid system is a small percentage of total capacity; and, it is significantly less than the minimum residual demand, there would be little or no need for NPPs to operate flexibly. It should be noted, however, that this is a general rule and particular grid systems may have some other specific needs and requirements to balance generation with demand. “The definition of ‘small fraction’ and ‘significantly less’ depends on the structure, conditions and control methods of the grid system” [1].

Moreover, it will become necessary for NPPs to operate flexibly in order to control system frequency and power flows, if:

- Nuclear share in the total electric generation capacity is large;
- NPP generation is too large on a small grid system;
- There is a significant share of intermittent or non-dispatchable generation;
- Transmission system has constraints;
- There are limitations and constraints on non-nuclear generators legislatively and/or within market regulations.

The reason for NPPs to consider and implement flexible operations can be based on one or more of these conditions.

### 2.1 Nuclear share in the total generation/nuclear output scale on a grid size

If the total capacity of nuclear generation is near or above the minimum electricity demand in a grid system, it will challenge the grid system operator in matching generation with demand — or maintain adequate reserves utilizing only the non-nuclear generation. This will not be particularly possible during periods of low electricity demand. In such cases, flexible operation of NPPs will be needed and they would be requested to reduce output to contribute to frequency control at times of the minimum demand. This condition is not necessarily limited to overall percentage of generation in a country scale and it may be applicable in regional networks or may extend to networks international level. For example, NPP(s) may contribute a large percentage of generation in one region of a country, even though the nuclear generation is a small percentage in the whole country. This may be particularly applicable and significant if grid connection of that particular region with large nuclear generation to the rest of the country is weak. On the other way around, there may be no need for NPPs to operate flexibly if a country (or region) is connected strongly to a large network, although the share of nuclear generation is very large.

Also, NPPs are typically large, if not the largest, generators unit on many grid systems. This is especially the case in the countries connecting their first NPP to the grid (newcomer countries) considering the available NPP designs currently. For such cases, the effect of an unplanned trip of large NPP on the system frequency can be problematic in order to avoid a system blackout, if the output of that generating unit is more than about 10 per cent of the system demand at the time [5]. Therefore, operating the new NPP flexibly may be needed, e.g. reducing electrical output and/or thermal power whenever demand on the electricity system is low.

It should be noted here, as stated in Reference [1], that: “system frequency is generally more variable on small electricity systems than on large interconnected networks. Therefore, for a country that is installing its first NPP on a relatively small system, the NPP can greatly improve the stability of system frequency while it is operating if it is able to provide good AFC”.

### 2.2 Share of intermittent or non-dispatchable generation

Lately, a significant growth in renewable generation, particularly from wind and solar energy sources, has been observed in many countries, specifically due to the carbon emissions strategies in



during its operational lifetime, due to aforementioned commercial or grid operational reasons. Framework of energy policies and technical, economical and legal regulations or market incentives also have to be considered in preparation of the business case.

A typical feasibility study by the NPP owner/operator organization on identification of technical, financial or operational impacts is illustrated in Fig. 2.

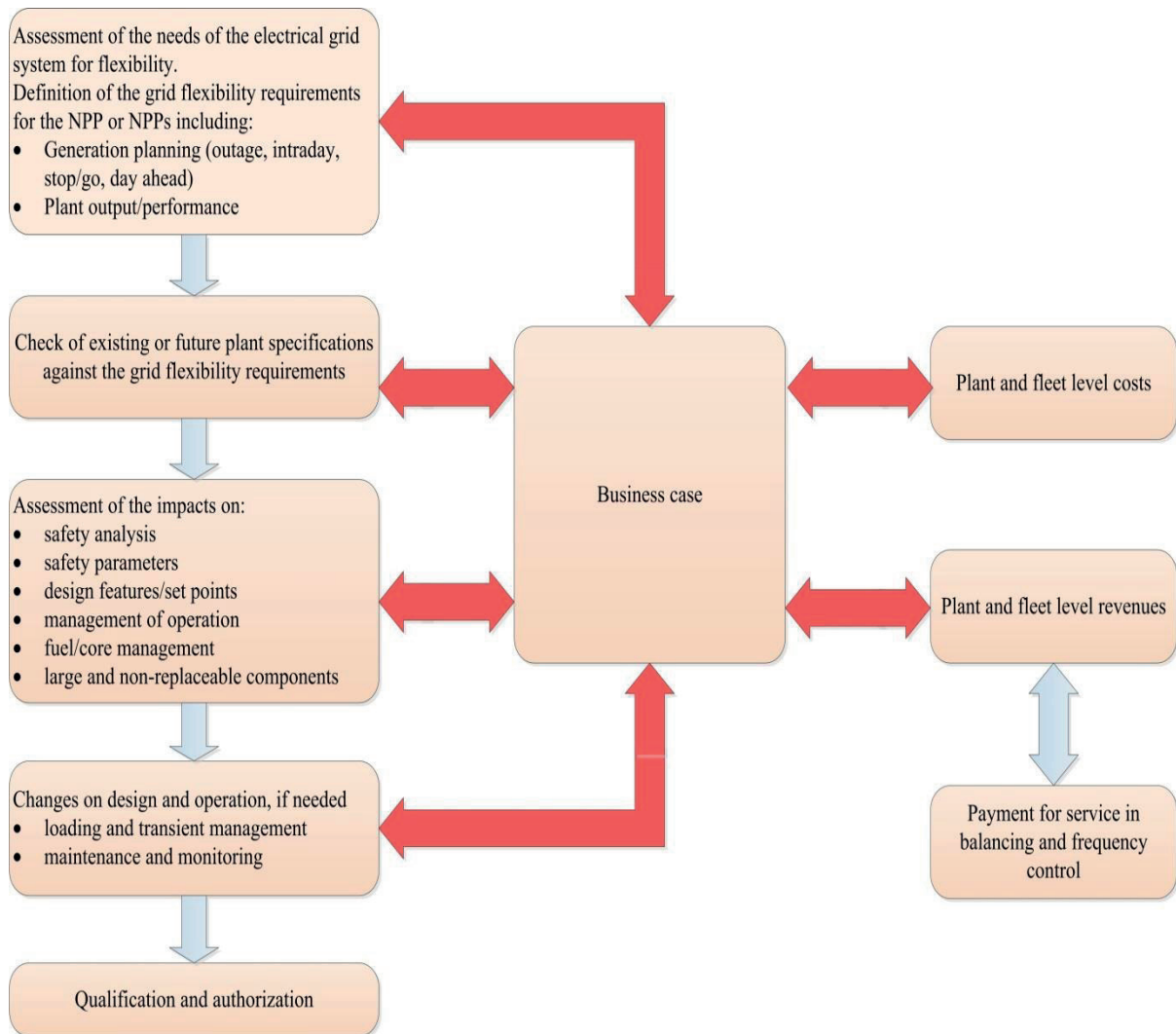


Figure 2: A Simplified Process by NPP Owner/Operating Organization in Making Flexible Operation Decision [1].

Such study is part of a decision making by integrating the impacts, associated costs-benefits including the potential payments for providing balancing services, overall energy policy and legal and regulatory aspects, etc. This fundamental process by the NPP owner/operator organization for deciding on whether to operate flexibly should cover the key aspects in deciding on the desired extent and form of NPP flexible operations. It should also be noted that the decision has many stake holders in addition to the NPP owner/operating organization (Fig. 3).

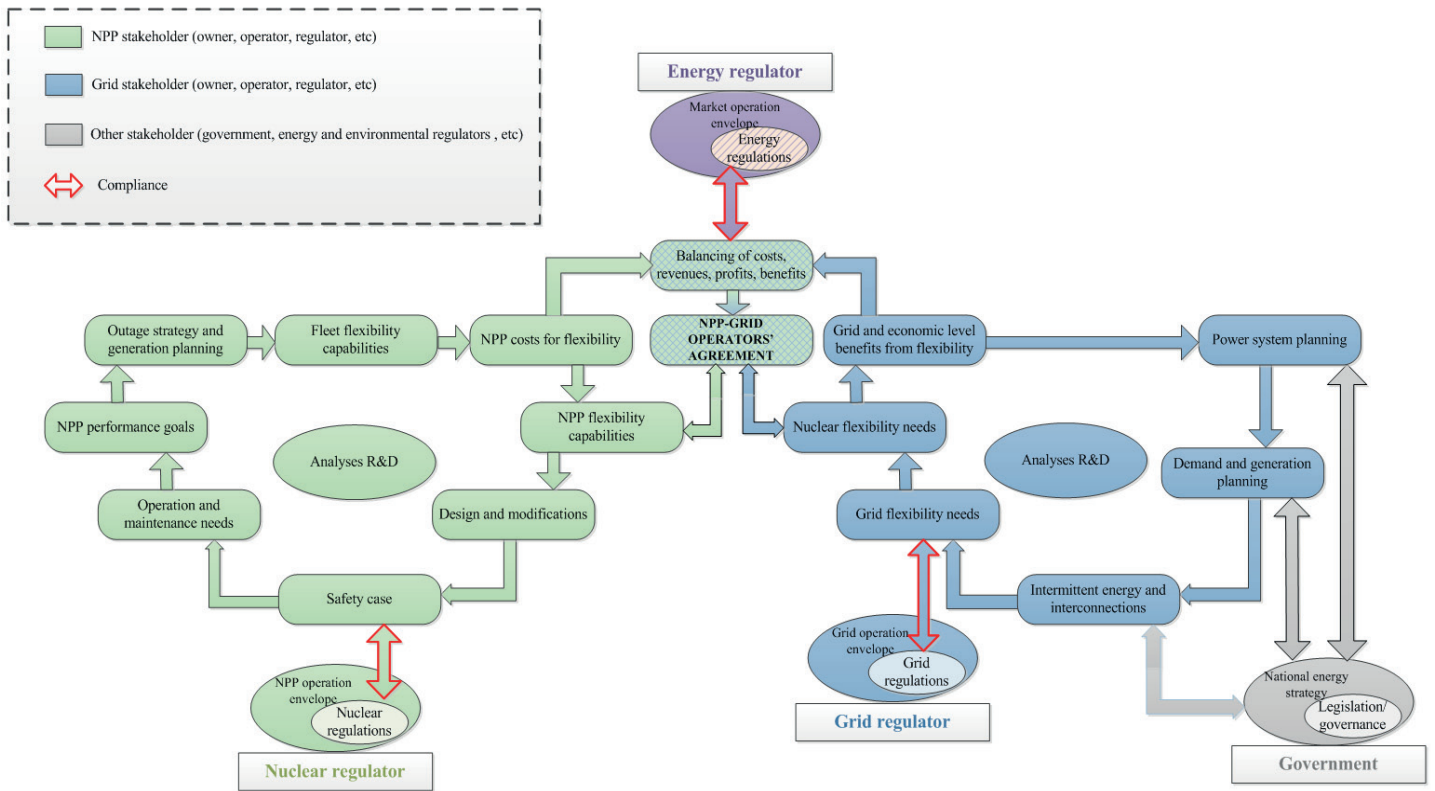


Figure 3: Interfaces in Flexible Operation Decision Making Activities [1].

## 4 ASPECTS OF FLEXIBLE OPERATION IMPLEMENTATION

A complete understanding and evaluation of a NPP's existing design and licensing basis and operational strategies, as well as the future state of those during the flexible operations, is necessary for making an informed and effective decision on the need for, and extent of, flexible operations. Knowing the current plant capabilities and operational strategies will confirm the capacity and capability for flexible operations and will support planning and implementation of new design features or modifications to achieve future capabilities. More importantly, it will ensure that the NPP will perform flexible operations safely, reliably and efficiently. Therefore, this evaluation includes a complete review of not only the design, operation and maintenance specification of NPP's system, structures and components (SSCs), but also the design and safety analyses, operational limits and conditions (OLCs), applicable regulations, codes and standards, operating procedures, training and qualification of personnel. The scope and extent of this evaluation varies for each individual NPP since it depends on many variables such as technology, design, operating experience, regulatory conditions, and of course, the magnitude, rate and periodicity of flexibility required.

Some countries, such as France and Germany have already designed (or modified) and have operated their NPPs flexibly collecting many reactor-years of experience and knowledge of flexible operation. This experience and knowledge provide a valuable resource in understanding the requirements, needs, challenges, solutions, and lessons learned. In addition to the French and German operational experience, various studies [7–13] investigated the feasibility of NPP flexible operation. The IAEA study [1], which collected this information in order to disseminate to IAEA Member States, organized impacts and solutions into four areas based on the aspects of impacts:

- Analysis based aspects;
- Phenomenon based aspects;
- Component based aspects;
- Human performance based aspects.

Table 1 illustrates a subset of impacts discussed in the IAEA study, namely the interface of the phenomenon and component based aspects on the reactor core and associated systems.

Table 1: Flexible Operations Impact on Reactor Core and Associated Systems [1].

Phenomenon	Component					
	Fuel rod	Fuel assembly (and fuel channel for BWR)	Control rods	Control rod drive mechanism	Core detectors	Core shroud
Fatigue	X	X	X	X		X
Erosion/corrosion	X					
Wear and tear			X	X		
Core power redistribution	X				X	
Pellet-to-clad interaction	X					
Creep induced channel distortion	X	X				
Extended operating cycle	X	X	X	X		
Chemical impurities	X	X				
Ageing			X	X		

## 5 CONCLUSIONS

In several countries, flexible operations have been a daily operational reality for many years with full compliance and conformance with safety, quality and reliability requirements while managing the efficiency and financial impacts of such operation. Additionally, in many countries who have not had their NPPs operating flexibly, assessment and evaluations of the electricity system and associated energy plans and strategies have been performed and decision have been made for the current or future NPPs to operate flexibly. Therefore, it has been feasible to design a new NPP, or convert an existing NPP, for flexible operation with safety, reliability and quality.

Primary consideration for flexible operation is matching the flexibility needs of the grid system and the capabilities of NPPs for flexible operations. Therefore, the owner/operators of the NPP and the grid have to understand and agree to a feasible solution that would satisfy needs and capabilities.

As the nuclear safety is overriding priority, it is also necessary to communicate with nuclear regulatory body (and the grid regulators) during the process to inform and obtain guidance for an effective regulatory and operational decision making framework for safety.

## REFERENCES

- [1] INTERNATIONAL ATOMIC ENERGY AGENCY, Non-Baseload Operations in Nuclear Power Plants: Load Following and Frequency Control Modes of Flexible Operations, IAEA Nuclear Energy Series No. NG-T-3.23, IAEA, Vienna (in print).
- [2] INTERNATIONAL ATOMIC ENERGY AGENCY, Interaction of Grid Characteristics with Design and Performance of Nuclear Power Plants: A Guidebook, IAEA Technical Reports Series No. 224, IAEA, Vienna (1983).
- [3] INTERNATIONAL ATOMIC ENERGY AGENCY, Expansion Planning for Electrical Generating Systems — A Guidebook, IAEA Technical Reports Series No. 241, IAEA, Vienna (1984).
- [4] INTERNATIONAL ATOMIC ENERGY AGENCY, Introducing Nuclear Power Plants into Electrical Power Systems of Limited Capacity, IAEA Technical Reports Series No. 271, IAEA, Vienna (1987).
- [5] INTERNATIONAL ATOMIC ENERGY AGENCY, Electric Grid Reliability and Interface with Nuclear Power Plants, IAEA Nuclear Energy Series No. NG-T-3.8, IAEA, Vienna (2012).
- [6] INTERNATIONAL COUNCIL ON LARGE ELECTRIC SYSTEMS (CIGRE), Nuclear Power Plant Performance in Power System Control – A Review of International Practice, CIGRE Working Group: 39–04, CIGRE Publication No. 31 (1985).
- [7] LUDWIG, H., SALNIKOVA, T., STOCKMAN, A., WAAS, A., Load Cycling Capabilities of German Nuclear Power Plants (NPP), International Journal of Nuclear Power, 55 8/9 (2010). Available from:
- [8] HUPOND, H., Load following and Frequency Control Transients vs. Loading and Design: EDF Experience and Practice, presented at the IAEA Technical Meeting on Flexible (Non-Baseload) Operation Approaches for Nuclear Power Plants, Paris (2013).

- [9] FEUTRY, S., Load Following EDF Experience Feedback, presented at the IAEA Technical Meeting on Flexible (Non-Base-load) Operation Approaches for Nuclear Power Plants, Paris, 2013.
- [10] LEFTON, S., KUMAR, N., HILLEMANN, D., AGAN, D., A New Paradigm: Cycling Operations at Nuclear Power Plants in the United States, American Society of Mechanical Engineers (ASME) Paper No. 2013-98079, paper presented at the ASME 2013 Power Conference, Boston, MA, 2013.
- [11] FLACHET, F., BALASSONE, S., Flexibility in Belgium, presented at the IAEA Technical Meeting on Flexible (Non-Base-load) Operation Approaches for Nuclear Power Plants, Paris, 2013.
- [12] NUCLEAR ENERGY AGENCY OF THE ORGANISATION FOR ECONOMIC CO-OPERATION AND DEVELOPMENT (OECD-NEA), Technical and Economic Aspects of Load Following with Nuclear Power Plants, OECD/NEA, Paris (2011).
- [13] ELECTRIC POWER RESEARCH INSTITUTE (EPRI), Technical Report — Program on Technology Innovation: Approach to Transition Nuclear Power Plants to Flexible Operations, Palo Alto, CA (2014).

## NPP Krško Post-UFC Transient Response during MSLB

Štefica Vlahović, Davor Grgić, Vesna Benčik

Faculty of Electrical Engineering and Computing

Unska 3, 10000 Zagreb, Croatia

stefica.vlahovic@fer.hr, davor.grgic@fer.hr, vesna.bencik@fer.hr

### ABSTRACT

UpFlow Conversion (UFC) was implemented in NPP Krško during the last outage in order to reduce the pressure differential across baffle plates and the possibility of the fuel damage caused by flow induced vibration. The paper describes the coupled code calculation (RELAP5 and PARCS) of MSLB accident at power for pre and post-UFC configuration of reactor vessel. In the calculation, the split model of the reactor vessel was used to better describe asymmetric conditions in loops. It has been demonstrated that the basic parameters (pressure, temperatures) stayed unchanged and there was little change in the flow rates except in baffle-barrel region of the vessel where both flow direction and amount of flow were changed.

*Keywords: upflow conversion, MSLB, coupled code, reactor vessel model*

### 1 INTRODUCTION

During NPP Krško refuelling outage in May 2015, a modification in reactor vessel internals was made [1]. Bypass flow in the baffle-barrel region, which was previously a downward flow, was converted to an upward flow. This modification reduced the pressure differential across baffle joints and therefore decreased the possibility of the fuel damage. On the other hand, it increased the bypass flow and thereby slightly decreased the core mass flow. Based on the safety review, the greatest influence should be related to LOCA (Loss Of Coolant Accident) and all other accidents should be unaffected. In this paper, the coupled code calculation of MSLB (Main Steam Line Break) accident for pre and post UFC modification was performed. Cycle 27 was used for pre and Cycle 28 for post UFC calculation of NPP Krško. The split reactor vessel model was taken into account because it better describes the asymmetric character of MSLB.

### 2 UPFLOW MODIFICATION

Damaged fuel assemblies have been identified in NPP Krško during 2013. outage refuelling activities. According to Westinghouse, the main reason for those fuel rod failures was flow-induced vibration. This phenomenon, known as “baffle jetting” is common among fuel assemblies in the periphery of core, depending on orientation and condition of baffle plate joints. Baffle jetting is a hydraulically induced vibration of fuel rods caused by a high velocity lateral jet of water. This jet is created by high-pressure water, forced through gaps between baffle plates near upper core plate. In that area, pressure differential across the baffle joints is the largest, and it becomes smaller downward to the lower core plate. Baffle-barrel bypass flow direction is responsible for this significant pressure differential.

Figure 1 shows modification required in reactor vessel discretization to take into account changes in vessel bypass flows. Primary flow passes down through the downcomer region, enters

the lower plenum, then upward into the core region, into the upper plenum and out through the outlet nozzle. The portion of the primary coolant does not participate in removing core heat and it is called bypass flow. Following streams belong to bypass flow:

- head cooling spray nozzle – the portion of the flow that flows from the vessel inlet nozzle into the vessel head region,
- outlet nozzle – the portion of the flow that leaks through the gaps between the core barrel outlet nozzles and reactor vessel outlet nozzles and merge with the vessel hot leg outlet nozzle,
- core cavity gap – the flow between peripheral fuel assemblies and baffle plates, which has the same direction as the flow through the core,
- thimble tubes – the flow through thimble tubes, which has the same direction as the flow through the core,
- baffle-barrel region – the flow between baffle and barrel, which had the opposite direction to the flow through the core (for the nodalization before UFC).

Most affected part of bypass flow is baffle-barrel bypass. Before UFC modification, it had the opposite direction to the flow through the core. As the primary coolant entered the downcomer, a portion of the flow diverted and passed through the holes in the core barrel between the top first and second former plate. The pressure in this region is higher than pressure in the core at the same elevation. This pressure differential caused baffle jetting by high pressure water, which passed through gaps between the baffle plates. Through the time, baffle jetting had been causing damage of the fuel rods, which could lead to cladding failure and the dispersal of the fuel pellets into the coolant. To solve this problem, Westinghouse developed an approach where downward flow in the baffle-barrel region was reversed to the upward flow.

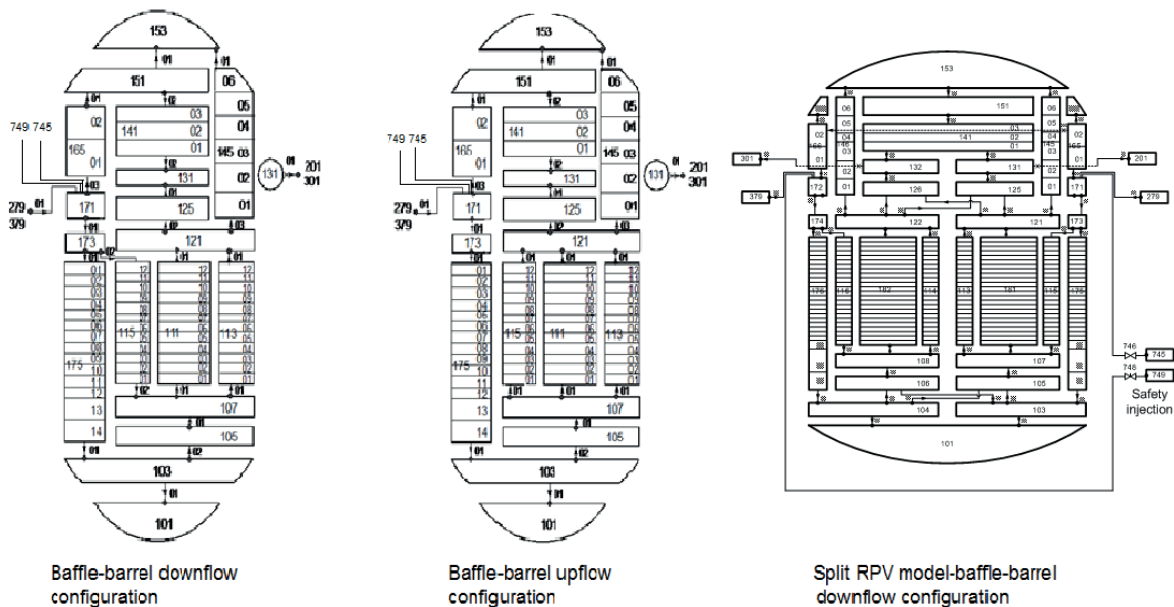


Figure 1: RELAP5/mod 3.3 nodalization of NPP Krško reactor vessel: a) baffle-barrel downflow and b) upflow for one coolant channel, c) split RPV model

The left side of the Figure 1 shows RELAP5 nodalization (single core channel) of NPP Krško reactor vessel before and after UFC modification. The same type of change apply for split vessel nodalization (two downcomers, two bypass channels, two or more core channels) on the right side of the figure. As part of the modification, 16 core barrel flow holes between top first and second former plate were plugged, and 8 new holes, each having nominal diameter of 2.5 inches, were machined in the top former plate.

The analysis of the UFC modification has proved the decrease in the pressure differential across the baffle joints. Figure 2 shows the difference between pre and post UFC modification. Gray color shows pressure differential before UFC modification, and it is clear, as previously said, that the greatest pressure differential is near the upper core plate and is continuously decreasing towards the lower core plate. After modification, pressure differential is lower, and it alternates from positive values (yellow) to negative values (red).

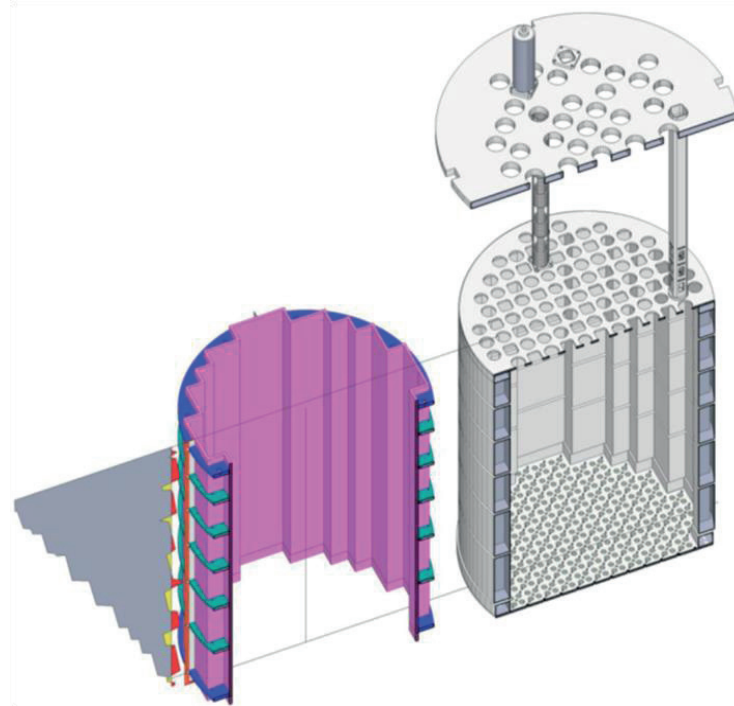


Figure 2: Pressure differential along baffle plates for pre and post UFC configuration

### 3 COUPLED RELAP5 AND PARCS PROGRAM

Code coupling is a standard methodology used to describe transients having spatial reactivity dependence in the core and thermal-hydraulic influence from rest of the system [7]. The coupled code RELAP5/mod3.3-PARCS v2.5 (R5PA) has been developed at FER. RELAP5/mod3.3 [2] is a code for modeling complex thermal-hydraulic systems and PARCS [3] is a three-dimensional (3D) reactor core simulator. Therefore RELAP5/mod3.3 calculates system thermal-hydraulics, average core channel thermal-hydraulics and heat conduction whereas the code PARCS calculates 3D neutron kinetics. Within R5PA it is possible to use COBRA code to perform core channels thermal-hydraulics calculation within PARCS code.

Taking into account asymmetric character of MSLB accident [6], the split model of the reactor vessel was used (Figure 1). The main difference, compared to the standard nodalization, is that all reactor vessel parts below hot and cold nozzles (downcomer, core inlet plenum, active core, guide tubes, core bypass and core outlet plenum) have been subdivided in two main parts, each corresponding to the one plant loop. The mixing was modeled in inlet and outlet plenum with coefficients 0.4 and 0.5, demonstrating that 70% of the cold leg flow is delivered to the closer region of the core and 75% of the hot leg flow is from the half of the core closer to the loop. There are 18 thermal-hydraulic channels in the core, 9 for each part of the core (loop), and 24 equidistant axial subdivisions for the active core region. The lower plenum is divided into seven CVs: 101, 103 and 104 connected to downcomer parts from the two halves of the vessel (before mixing), 105 and 106 describing the middle parts after mixing and the volumes 107 and 108 representing upper parts of the lower plenum before entering the reactor core. The active core is modeled with 18 channels (181 to 198) that are divided in two halves of the core (volumes 184, 185, 186, 190, 191, 192, 196, 197 and 198 for the loop 1 and volumes 181, 182, 183, 187, 188, 189, 193, 194 and 195 for the loop

2). The core channels are modeled as PIPE components each consisting of 24 volumes. RCCA guide tubes inside core are represented with volume 113 for 1<sup>st</sup> half and volume 114 for 2<sup>nd</sup> half of the core. The region between baffle and barrel is also represented with two volumes (CV 115 and CV 116 for each half). The region above the active core is represented with CV 121 and 122 before mixing and with CV 125 and 126 after mixing. Upper downcomer is also subdivided in two halves with corresponding volumes 165 and 166 with which the bypass flow path to the upper head is introduced. Another bypass is modeled in the reactor inlet volume (CV 171) connecting core outlet (CV 125) for the 1<sup>st</sup> half of the core and volume 172 connecting core outlet 126 for 2<sup>nd</sup> half.

The detailed description of the NPP Krško RELAP5/mod3.3 nodalization before UFC modification is reported in [4], [5]. Cycle 27 is representative for pre UFC condition of NPP Krško. On the other hand, Cycle 28 is representative of condition after UFC modification. Those two nodalization are very similar except for small UFC related change and usual small variation in the point kinetics and distribution of the power in the core. To take into account change in the direction of the flow path in the baffle-barrel region the junction 02 in branches 106 and 107 is directed upward. The junction 02 in branches 173 and 174 is deleted because no coolant flow is directed downward the baffle-barrel region after core barrel flow hole plugs are installed in the former plates. The new flow path is introduced to model the flow in the barrel baffle region from the upper plate to the outlet plenum of the reactor vessel. The same modifications are done to the 2<sup>nd</sup> part of the reactor vessel in split model. In addition to reactor split vessel model used till now, alternative model was developed with additional lateral connections between two downcomer halves. The model showed benefits for LOCA modeling and we wanted to see what is its influence for other asymmetric accidents.

Used NPP Krško nodalization, Figure 3, has 1054 control volumes, 1146 junctions, 1157 heat structures (with 10159 mesh points), 733 control variables, with 197 variable and 221 logical trips.

The coupled code steady state calculation was performed for 1000 s at full power nominal conditions.

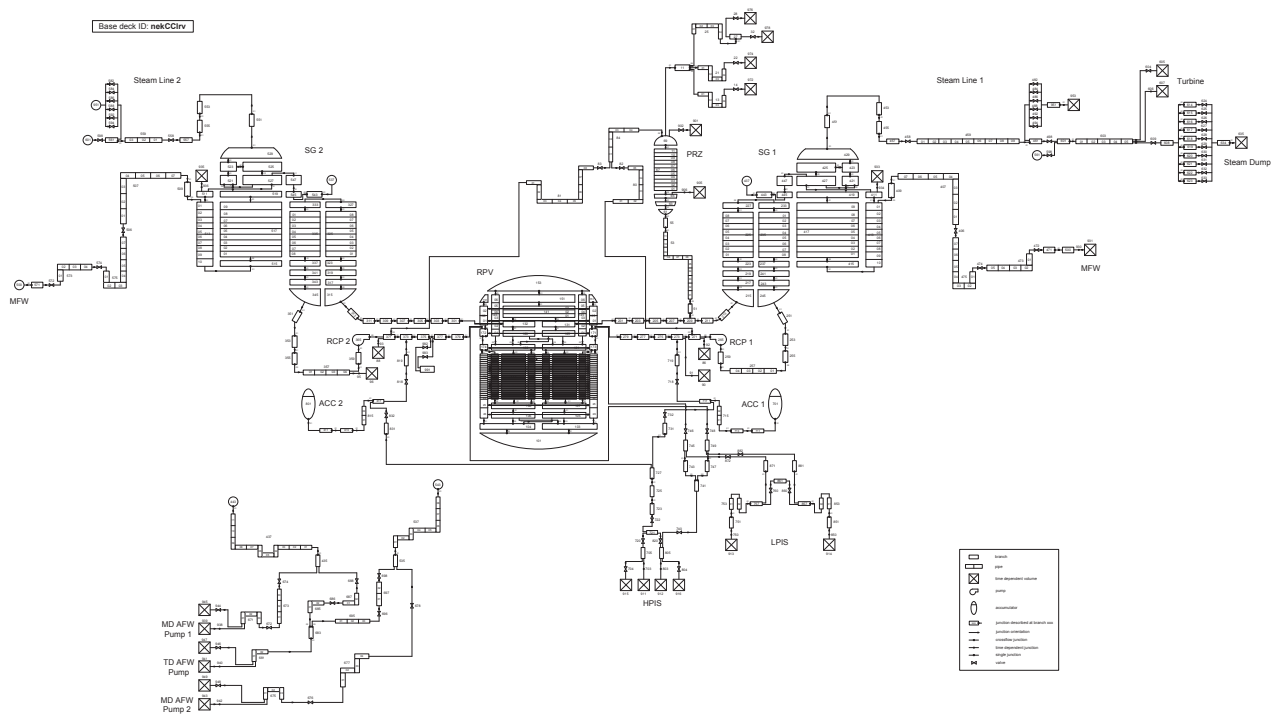


Figure 3: NEK nodalization for RELAP5/mod3.3 code calculation, split vessel

## 4 RESULTS OF THE CALCULATION

### 4.1 Accident Description

The analyzed transient was the main steam line break which is classified as ANS Condition IV event. It belongs to accidents which cause increased energy removal from the Reactor Coolant System (RCS) consequently leading to the reduction of coolant temperature and pressure. Main assumptions for the accident are:

- double ended (guillotine) break,
- end of core life,
- hot full power - normally, NPP is at the zero power for MSLB accident because the coolant flow through the break is at the higher rate and the core locally reaches higher power, but it is noticed, that for the UFC modification, the full power has bigger impact on the limiting faults,
- reactor trip occurs on the low pressure signal in the steam line,
- most negative rod cluster control assembly is assumed to be stuck in its fully withdrawn position after reactor trip,
- core boron concentration is 0 ppm
- 0% SGTP
- main feedwater system supplies both steam generators whereas auxiliary feedwater system supplies only broken steam generator,
- reactor coolant pumps trip 60 s after reactor trip.

The transient calculation was performed for 1000 s, yet all the important cooldown related changes happened in first 200 s.

The analysis has shown that there was no return on the power after MSLB accident and that the integrity of the cladding was conserved. Steam generator 1 was assumed to be broken and the steam generator 2 stayed intact during the accident. The steam release arising from the rupture of the main steam line resulted in an initial increase in steam flow. This rupture in the steam line rapidly decreased broken steam generator pressure, Figure 4. As the pressure in the broken steam generator was falling, the steam flow started decreasing during the accident. The increase in the energy removal from the reactor coolant system caused a reduction of the coolant temperature and pressure, Figure 5. The SG 1 pressure was constantly falling until it reached the containment pressure. Pressurizer pressure was also falling, and after approximately 100 s started increasing, shortly after the initiation of the safety injection system and isolation of the broken steam generator. The similar pressure behavior was presented in the unbroken steam generator, firstly the pressure decreased, and then it increased after heat transfer reversal. Due to the cooldown accident and sink in the secondary system, temperatures, both hot and cold legs, decreased. With the split model of the reactor vessel, better asymmetric character of MSLB accident is described, therefore different distribution of cold and hot legs temperature was presented in comparison with standard 1 channel model of the reactor vessel, Figure 6. The reverse heat removal started in the intact steam generator, approximately 5 s after reactor trip. That means that the steam generator became heat sink in oppose to his standard function. This change is noticeable in the intact cold leg temperature which increased and intact steam generator power which became negative after reversal. Mass flow in both loops increased little due to reduction of temperature, Figure 8, and then decreased rapidly after reactor coolant pumps trip.

## 4.2 Comparison of conditions before and after UFC modification

Figure 4 and Figure 5 show that basic parameters (pressure and temperatures) stayed unchanged after modification. Very small difference in the basic accident behaviour is visible among two nodalizations/core cycles. As expected, due to asymmetric nature of accident, there is difference between coupled code split vessel model and RELAP5 calculation using point kinetics (PK) and one-channel vessel model, Figure 4 and Figure 6. The differences are mostly related to different cold leg temperatures. Differences between old and new model of split vessel (lateral connections) are shown in coolant temperature response in Figure 7. The influence is rather small and it is more significant for pre than for post UFC conditions.

UFC modification has direct influence to core bypass flow, mostly to baffle-barrel region flow. Overall influence is small increase in loop flows (lower hydraulics resistance of the vessel), and decrease in core flow, Figure 8. Total bypass flow is increased with baffle-barrel region flow being larger, Figure 9, and guide-tubes bypass flow being lower than before UFC modification. Figure 9 and Figure 10 show mass flow in the baffle-barrel region in both parts of the reactor vessel, before and after UFC. Mass flow changed direction (sign), as expected, and now has positive value because the direction is the same as in the active core. Furthermore, mass flow rate increased, approximately 20 kg/s in each part of the core, leading to approx 40 kg/s increase for the whole core. Small influence of change in vessel model and change in vessel downcomer model can be seen in Figure 9 and Figure 10, respectively.

As a consequence of small changes in thermal-hydraulics variables the changes in nuclear variables are not expected. Pre and post UFC reactivity components are shown Figure 11, and differences are very small. Nuclear peaking factor is shown in Figure 12. Reference coupled calculation is without stuck rod to be more similar to PK response. When stuck rod is assumed, increase in peaking factor is present during core cooldown. In addition there is small Fq difference due to different mixing in downcomer when lateral connections are used. Taking into account that core power is reduced immediately after break initiation due to reactor trip, the difference in peaking factors has no practical value. Pin power distribution in case of stuck rod is shown in Figure 13. The location of the rod is usually in more affected (cooled) part of the core.

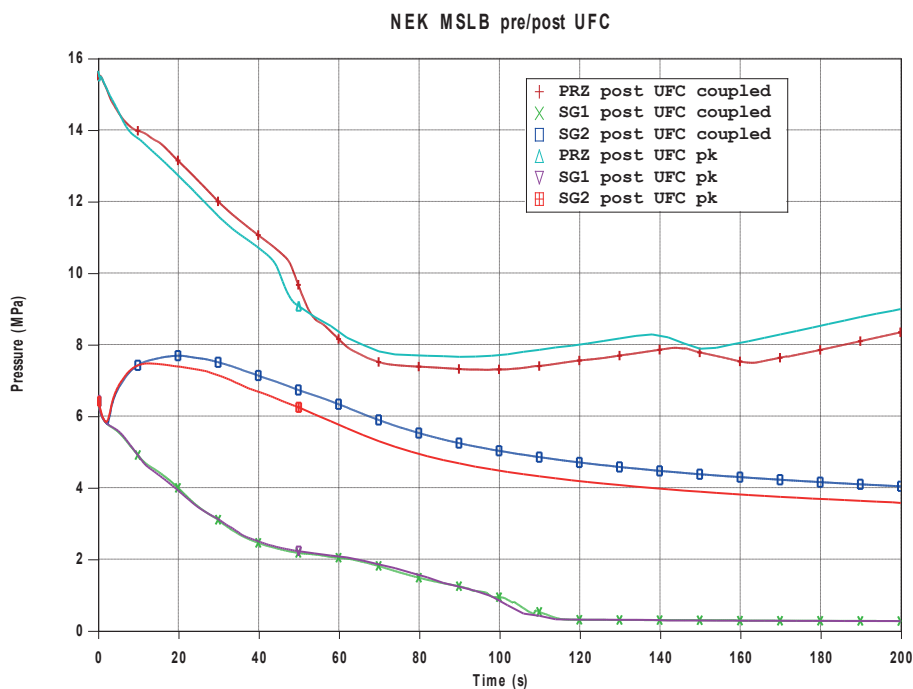


Figure 4: Pressurizer, Steam generator 1 and 2 pressure

NEK MSLB pre/post UFC coupled

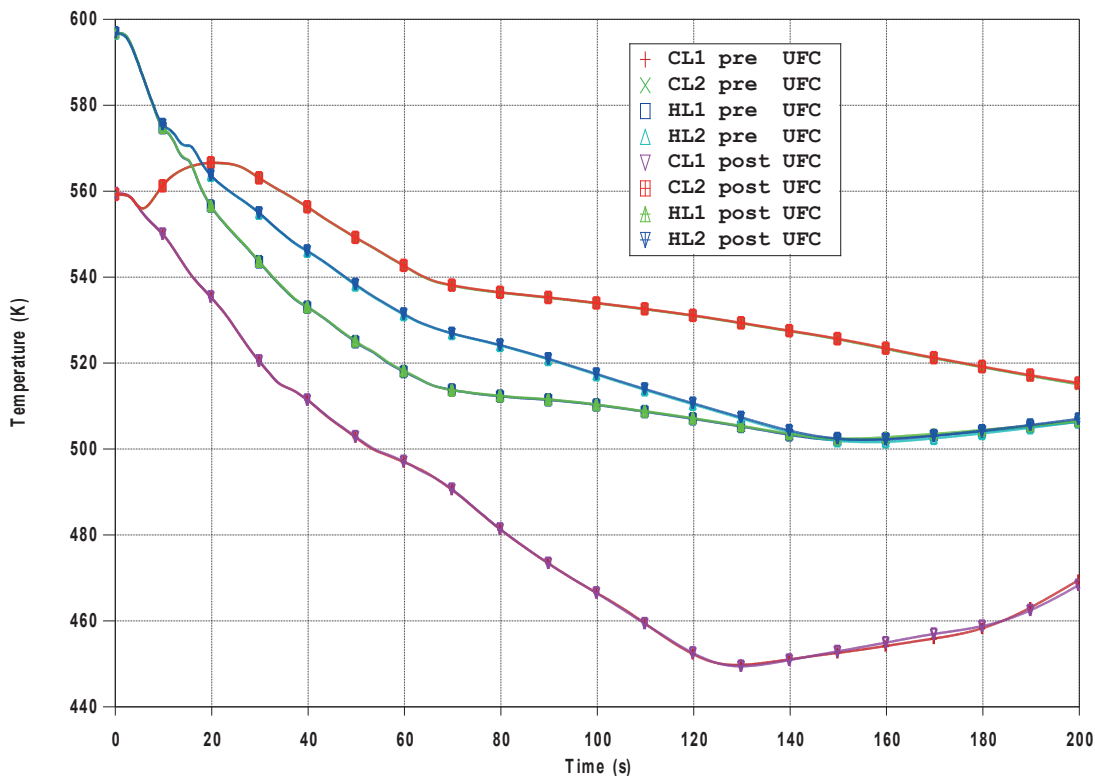


Figure 5: Cold and hot leg temperatures, pre vs. post UFC

NEK MSLB post UFC coupled/pk

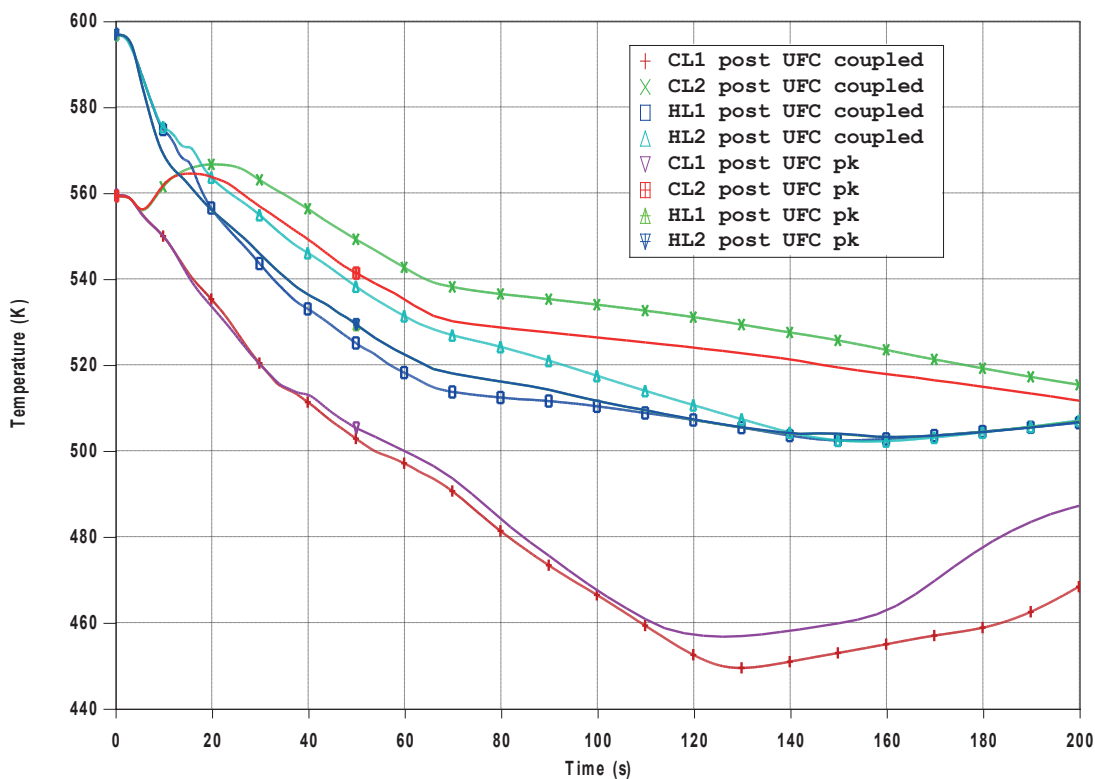


Figure 6: Cold and hot leg temperatures, coupled vs. PK

NEK MSLB post UFC new/old DC

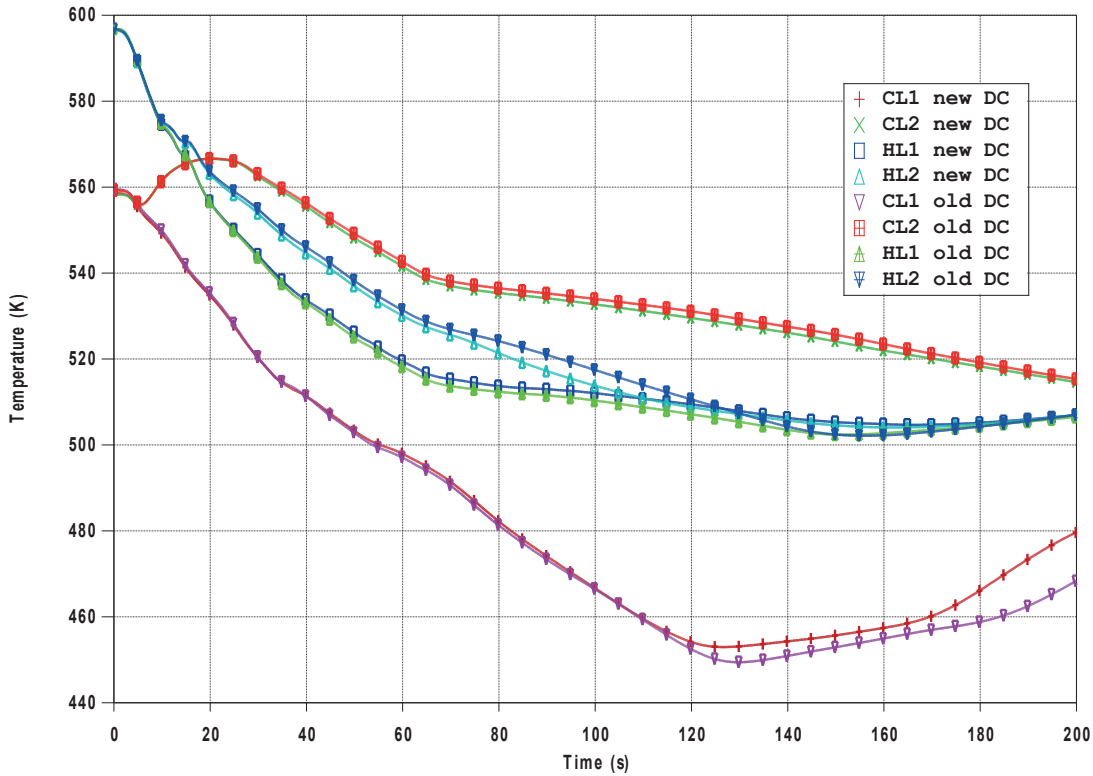


Figure 7: Cold and hot leg temperatures, new vs. old downcomer

NEK MSLB pre/post UFC

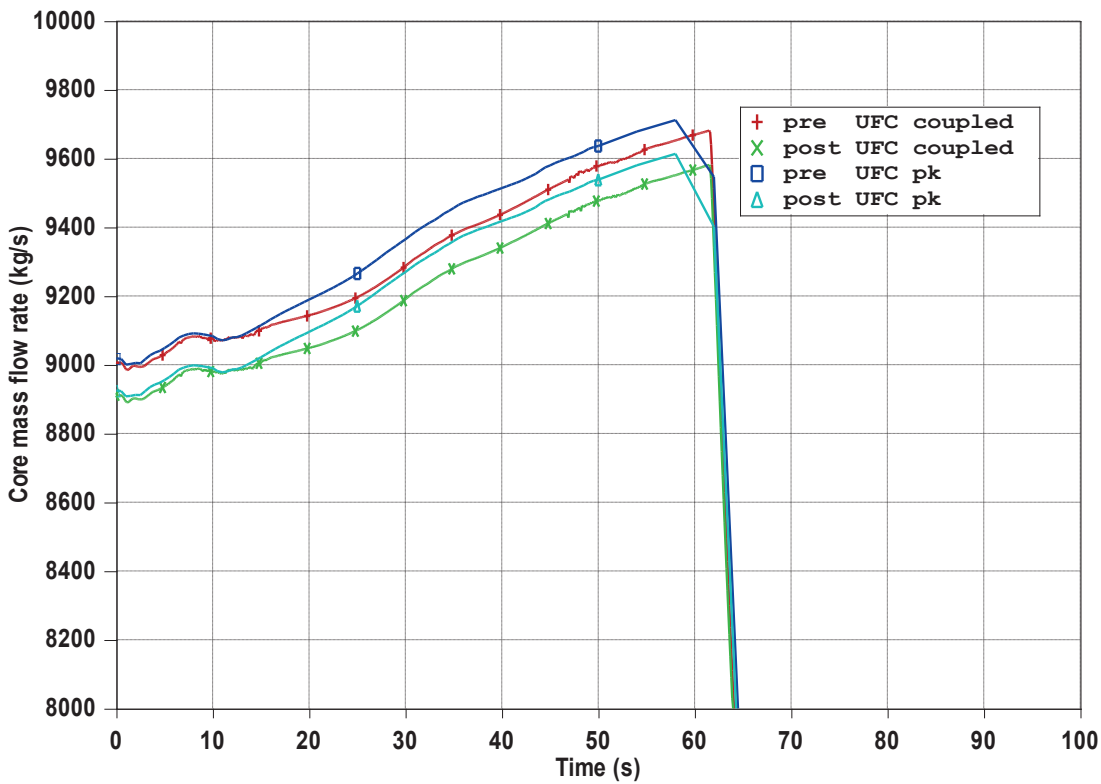


Figure 8: Core mass flow rate, pre vs. post UFC

### NEK MSLB pre/post UFC

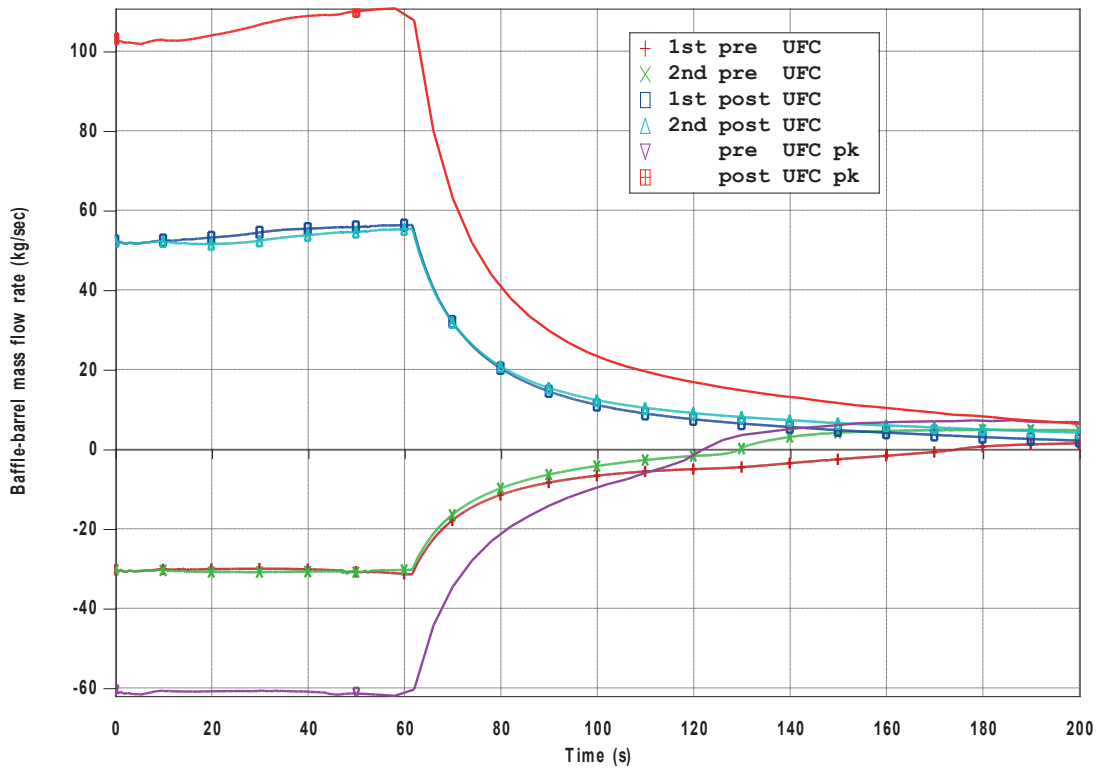


Figure 9: Baffle-barrel mass flow rates, pre vs. post UFC

### NEK MSLB post UFC new/old DC

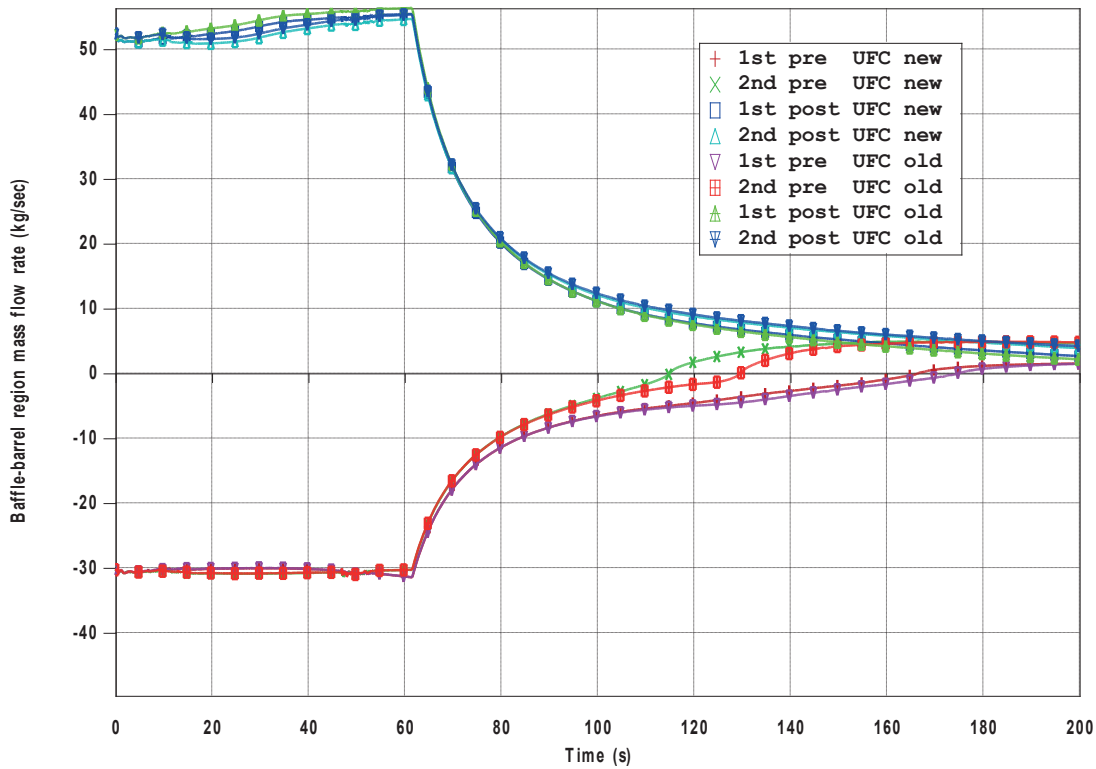


Figure 10: Baffle-barrel mass flow rates, new vs. old downcomer

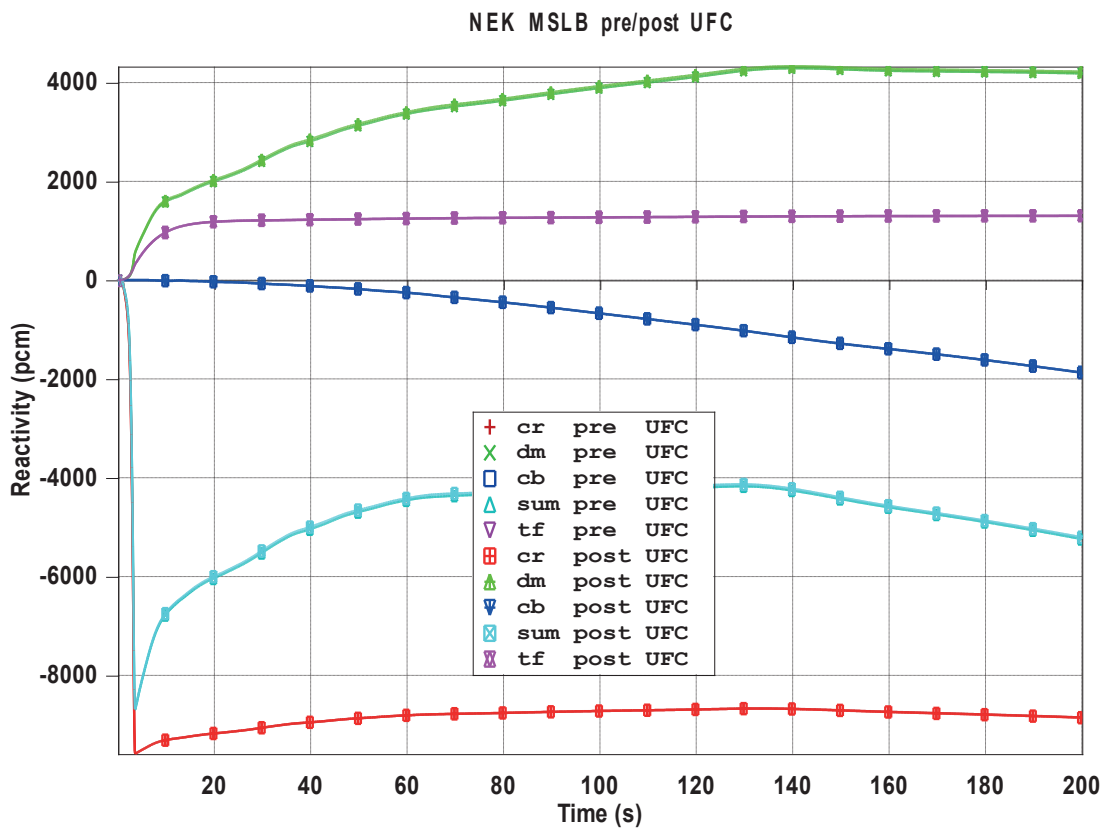


Figure 11: Reactivity components, pre vs. post UFC

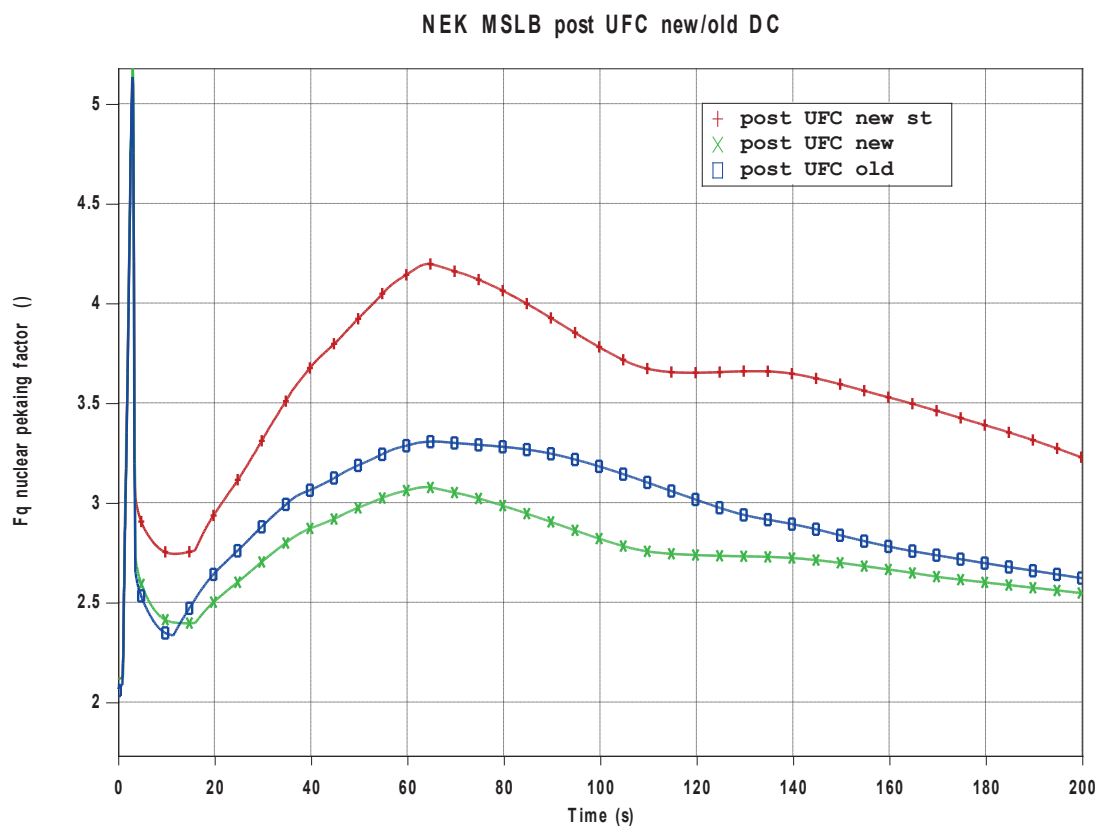


Figure 12: Fq nuclear peaking factor, post UFC, influence of stuck rod

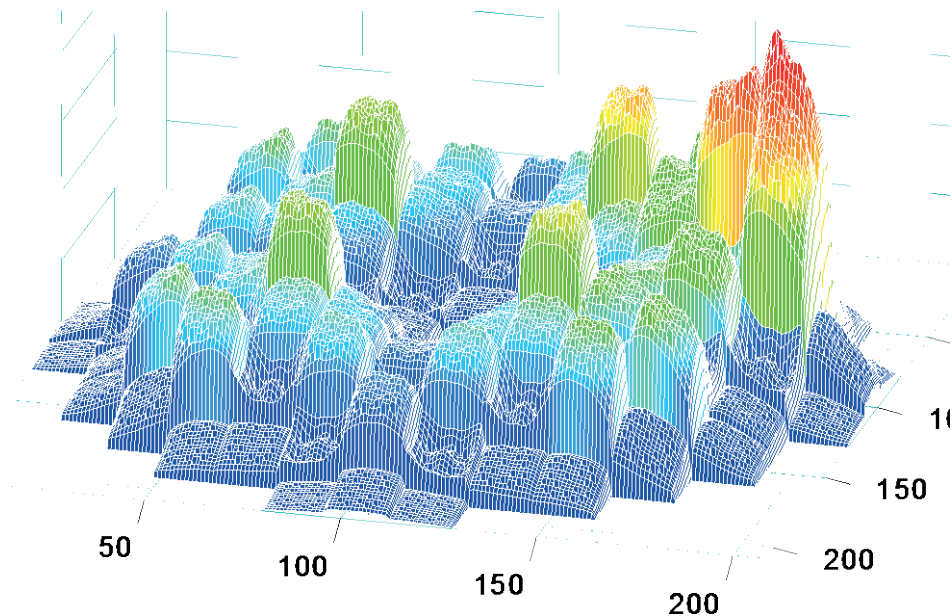


Figure 13: Pin powers at 200 s, post UFC case with stuck rod

## 5 CONCLUSION

No significant difference was found between the standard 1 channel model of the reactor vessel and split model of the reactor vessel, only a slightly different behaviour of the temperature in loops due to the different mixing. Furthermore, the comparison of the accident behaviour before and after UFC modification did not show difference as it was expected from screening analyses performed before the modification was implemented in the NPP Krško. The results only showed difference in the reactor vessel flows. After UFC modification, the bypass flow increased from 0.5 to 1% of the total coolant flow value, and stayed within design project calculations of the total 6.5% bypass flow. The baffle-barrel flow increased for approximately 40 kg/s and changed sign due to the opposite direction of the flow paths after modification. The guide tubes flow decreased a little bit, less than the baffle-barrel flow increased, therefore the active core flow decreased. The coolant flow toward the upper head stayed practically the same and the mass flow in loops slightly increased. The reactor vessel split model with additional lateral connections between downcomer parts showed similar results as original split vessel model (fully separated downcomer halves).

## REFERENCES

- [1] Reactor Internals Upflow Conversion Program - Engineering Report, Krško Nuclear Power Plant, WCAP-17932-P, Revision 1, March 2015
- [2] RELAP5/MOD3.3 User's Manual, The RELAP5 Code Development Team, NUREG/CR-5535/Rev 1, Information Systems Laboratories, Inc., Rockville - Maryland, Idaho Falls - Idaho, January 2002.
- [3] US NRC, PARCS v2.6, US NRC Core Neutronics Simulator, Draft, November 2004
- [4] NEK RELAP5/mod3.3 Post-RTDBE Nodalization Notebook, NEK ESD TR 02/13, Revision 1, Krško 2014.

- [5] NEK RELAP5/MOD3.3 Post-RTDBE Steady State Qualification Report, NEK ESD-TR-03/13, Revision 1, Krško 2014.
- [6] RELAP5/MOD3.3 Post-RTDBE Steam Line Break Analysis (Cycle 26), NEK ESD-TR-04/13, Revision 0, Krško 2013.
- [7] Grgić D., Benčik V., Šadek S., Coupled code calculation of rod withdrawal at power accident, Nuclear engineering and design, 261 (2013), 285-305

## Validation of the CORD-2 System for the NPP Krško Nuclear Core Design Calculations

**Marjan Kromar**

“Jožef Stefan” Institute  
Reactor Physics Division  
Jamova 39, 1001 Ljubljana, Slovenia  
[Marjan.Kromar@ijs.si](mailto:Marjan.Kromar@ijs.si)

**Bojan Kurinčič**

Nuclear Power Plant Krško  
Engineering Division - Nuclear Fuel & Reactor Core  
Vrbina 12, 8270 Krško, Slovenia  
[Bojan.Kurincic@nek.si](mailto:Bojan.Kurincic@nek.si)

### ABSTRACT

The CORD-2 package intended for core design calculations of PWRs has been recently updated with some improved models. Since the modifications could substantially influence the obtained results, a technical validation process is required. This paper presents comparison of some calculated and measured parameters of the NPP Krško core needed to qualify the package. Critical boron concentrations at hot full power for selected cycle burnup points and several parameters obtained during the start-up testing at the beginning of each cycle (hot zero power critical concentration, isothermal temperature coefficient and rods worth) for all 27 finished cycles of operation are considered. In addition, assembly-wise power distribution for some selected cycles is checked. Comparison has shown very good agreement of the CORD-2 calculated values with the selected measured parameter of the NPP Krško core.

*Keywords:* PWR, nuclear core design calculations, core simulator

### 1 INTRODUCTION

The CORD-2 system [1], developed by the Reactor Physics Department of the Jožef Stefan Institute, is intended for core design calculations of PWRs. The main goal in assembling the computational tools was to provide a package that could be used for simple very fast calculations (such as those frequently required for fuel management) as well as for accurate calculations (for example, reload core design) needed to be executed in acceptable time. The CORD-2 system consists of two basic reactor physics codes: WIMS-D [2], and GNOMER [3]. WIMS-D is a well-known and widely used lattice code. Version WIMS-D5 is available from the NEA data bank in Paris. A 69-group neutron cross-section library based on the ENDFB-VII.0 neutron data files has been used. GNOMER solves the neutron diffusion equation in three-dimensional Cartesian geometry by using Green's function nodal method [4]. It also includes advanced features for cross-section homogenization and a simple thermal-hydraulic module so that thermal feedback can be taken into account. The CORD-2 system enables determination of the core reactivity and power distribution. While average assembly powers come directly from the diffusion equation, a reconstruction procedure is needed, which couples heterogeneous pin by pin distribution with the homogenous nodal solution, to obtain final full core pin by pin distributions. The package has been

validated for the nuclear design calculations of PWR cores and has been used for the verification of the NPP Krško reload cores since 1990.

The CORD-2 package has been recently updated with some improved models:

- more elaborate calculation of Dancoff factor in the lattice cell calculations,
- expanded set of nuclides considered explicitly during the fuel cooling period,
- improved neutron reflector cross section determination,
- improved model of burnable poison inserts containing Pyrex glass,
- implementation of the neutron cross-section library based on the ENDFB-VII.0 neutron data files.

Since the modifications substantially influence the obtained results, a validation process is required. This paper presents comparison of some calculated and measured parameters of the NPP Krško core needed to qualify the package.

## 2 BRIEF NPP KRŠKO CORE DESCRIPTION

The Krško plant is a 2-loop Westinghouse PWR that began electricity production in 1981. The start-up core had a rated thermal capacity of 1,876 MWt, and a 626 MWe gross electric power. Currently, the thermal rating is 1,994 MWt with 727 MWe gross electric power. The core consists of 121 fuel assemblies. Each assembly has 235 fuel rods arranged in a 16×16 array. The remaining 21 positions contain guide tubes and are intended for control rods, neutron source and in-core instrumentation. The core features 33 Reactivity Control Cluster Assemblies (RCCA) arranged in 6 banks (D, C, B and A with the shut-down banks SA and SB). The RCCA locations and bank assignment are shown in Fig. 1.

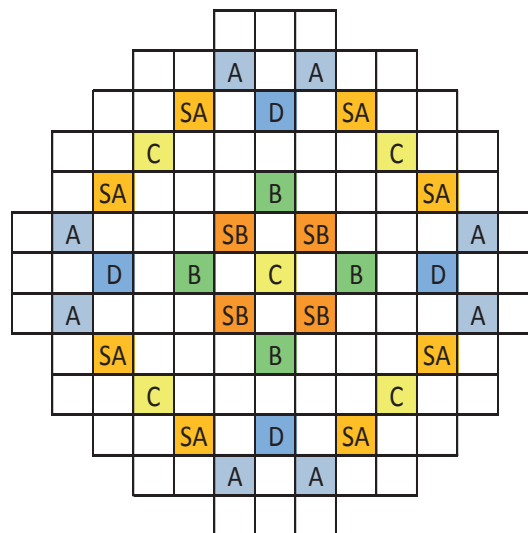


Figure 1: Krško RCCA locations (control bank ID shown)

## 3 RESULTS AND DISCUSSION

Validation of the CORD-2 system has been accomplished by the comparison of the most important calculated reactor parameters to the available measurement values. All 27 finished plant cycles of operation are considered.

### 3.1 Critical boron concentration

Comparison of the critical boron concentration is shown in Figure 2. Differences from measurements (C-M) are presented for some selected statepoints:

- Hot Zero Power (HZP) at Beginning Of Cycle (BOC)
- Hot Full Power (HFP) at burnup:
  - 150 MWd/tU
  - 500 MWd/tU
  - End Of Cycle (EOC)

Results are showing consistent CORD-2 behaviour. Differences from measurements are within  $\pm 50$  ppm band, which is usually taken as an acceptable tolerance level at start-up tests. Only in cycle 17 the HZP value of 62 ppm exceeds the imposed limit. Furthermore, for each cycle, the error critical boron concentration spread from BOC to EOC is almost everywhere within 50 ppm.

Averaged differences and standard deviation are presented in Table 1. A slight tilt smaller than 18 ppm from the BOC to EOC critical boron concentration can be observed confirming good CORD-2 burnout prediction capabilities. Standard deviation of results is within 25 ppm, therefore there is the 95% confidence that predicted critical boron concentrations are within  $\pm 50$  ppm band.

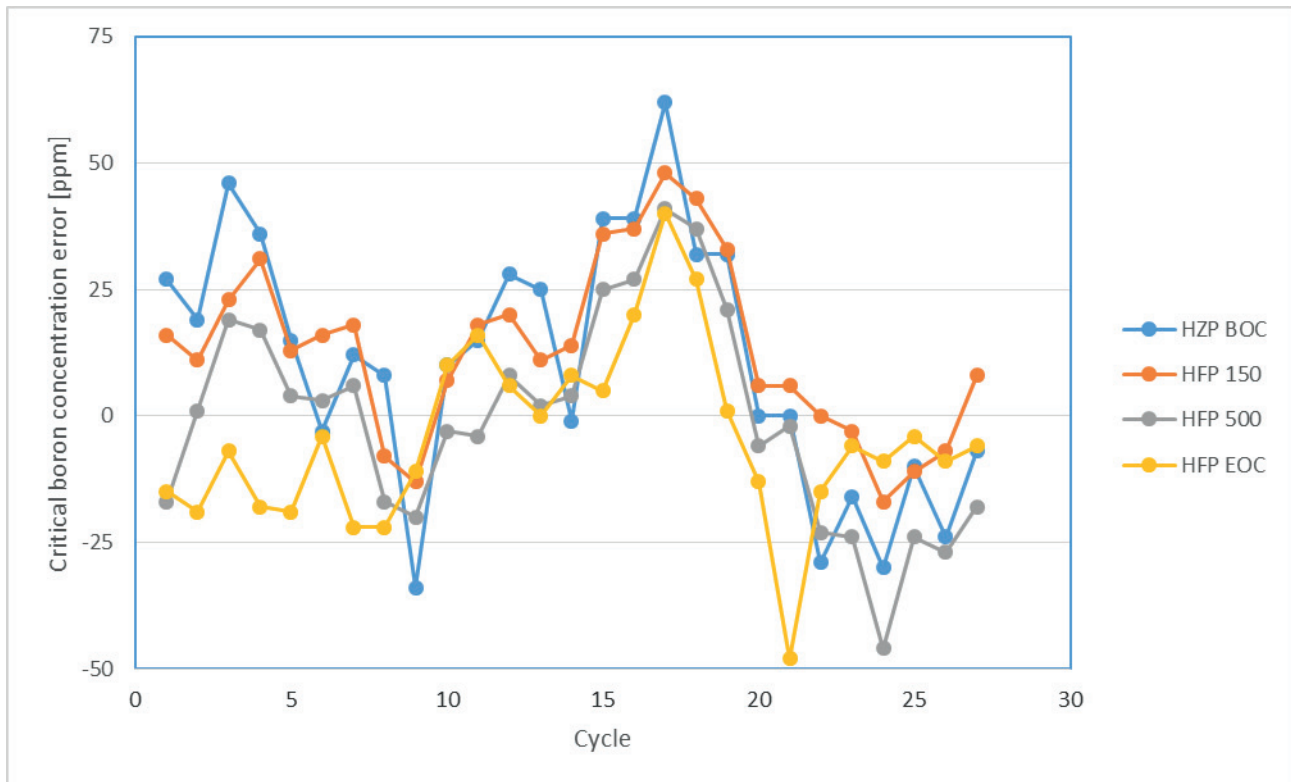


Figure 2: Critical boron concentration differences (C-M)

Table 1: Statistical data of critical boron concentration differences

	HZP BOC [ppm]	HFP 150 [ppm]	HFP 500 [ppm]	HFP EOC [ppm]
<b>Average</b>	10.8	13.2	-0.6	-4.2
<b>St. Dev.</b>	24.6	16.9	20.7	17.3

### 3.2 Isothermal temperature coefficient and control rods worth

Isothermal temperature coefficient (ITC) and control rods worth at HZP are measured during the start-up test at the beginning of plant operation following each fuel reload. Comparison of the CORD-2 results is presented in Table 2. Since the ITC is very sensitive to the boron concentration, the coefficients are calculated at the measured critical boron concentration.

ITC is almost everywhere lower than the 1.8 pcm/K value, which is usually considered as a measurement uncertainty. Larger difference is found only in Cycle 7. However, all values are well inside the  $\pm 5.4$  pcm/K tolerance band, which is usually imposed at start-up tests. Average value of 0.72 pcm/K is showing small overprediction of the CORD-2 system. Standard deviation of all 27 values is less than 1 pcm/K.

Control rods worth differences are mostly below 10%. Somewhat larger differences are observed in cycle 7, where rod swap technique with significant higher measurement uncertainty was applied. In other cycles boron dilution and rod insertion methods were applied. Average values of all control rods worths are below 10%, with standard deviation lower than 6%. However, the average value of the differences for the sum of all control rods worths is -2.6%, which is significantly lower than 10% acceptance criteria usually taken at start-up tests.

Table 2: ITC and control rods worth differences

Cycle	ITC [pcm/K]	D	C	B	A	Sum
1	1.17	0.1%	2.4%	-1.4%	-2.2%	-0.5%
2	-0.67	-11.0%	-3.9%	0.9%	-7.5%	-5.7%
3	-1.10	-3.5%	6.0%	4.3%	-1.7%	0.8%
4	-0.06	-2.8%	-2.6%	6.5%	-6.0%	-2.5%
5	0.70	1.2%	3.7%	5.1%	3.9%	3.6%
6	1.81	6.8%	6.8%	20.1%	0.2%	5.7%
7	4.47	-1.6%	-19.8%	-14.5%	-22.0%	-16.5%
8	1.12	4.6%	0.0%	9.4%	-11.3%	-1.3%
9	1.05	0.3%	-0.6%	5.0%	-8.0%	-2.7%
10	0.00	-2.6%	-1.7%	5.4%	-9.3%	-3.8%
11	-0.51	3.1%	-4.9%	10.5%	-11.5%	-2.8%
12	0.21	-2.0%	0.4%	5.3%	-12.9%	-2.2%
13	1.02	1.3%	1.4%	3.5%	-10.2%	-1.8%
14	1.45	-0.5%	-1.5%	6.0%	-14.7%	-4.2%
15	0.46	-0.8%	0.4%	5.9%	-8.0%	-1.7%
16	0.53	2.7%	-3.4%	1.8%	-8.8%	-3.1%
17	0.10	4.8%	-2.4%	5.7%	-9.2%	-2.1%
18	0.75	6.1%	-3.1%	8.8%	-10.7%	-1.1%
19	0.48	0.3%	-1.1%	8.8%	-4.9%	-1.0%
20	0.85	3.8%	-0.2%	12.7%	-9.5%	-1.1%
21	0.91	-8.4%	-1.7%	1.6%	-7.1%	-3.5%
22	0.45	-4.8%	-4.4%	2.6%	-6.0%	-3.5%
23	0.25	-1.5%	-4.6%	3.3%	-3.9%	-2.0%
24	1.11	-4.0%	-5.1%	2.5%	-4.9%	-3.0%
25	0.69	-3.1%	-8.5%	-0.8%	-9.2%	-5.8%
26	1.02	-3.1%	-3.5%	-0.4%	-5.1%	-3.0%
27	1.26	-7.7%	-5.5%	-0.4%	-8.7%	-5.5%
Average	0.72	-0.8%	-2.1%	4.4%	-7.7%	-2.6%
St. Dev.	0.98	4.3%	4.9%	5.9%	4.9%	3.7%

### 3.3 Power distributions

HFP radial power distribution comparison with assembly powers derived from measured in-core flux distributions (C-M) at several burnup points are provided in Tables 3-7. Burnup steps and maximal differences are listed in the lower right corner. The first cycle and a few last cycles are presented. Cyclic quadrant symmetry was respected in all calculations.

Differences are showing pretty consistent behaviour. CORD-2 is mostly underpredicting power in the core centre and at some specific assemblies bordering the reactor baffle. The zone in between experiences higher power compared to measurements. Maximal differences are inside  $\pm 0.05$  band.

Table 3: Assembly-wise power differences (C-M) for the cycle 1

-0.041	-0.027	-0.017	-0.002	0.003	-0.005	0.015
-0.038	-0.022	-0.011	0.006	-0.004	-0.007	0.011
-0.032	-0.016	-0.008	0.006	0.003	-0.007	0.010
-0.029	-0.017	-0.007	0.007	-0.001	-0.011	0.005
-0.025	-0.015	-0.005	0.006	-0.005	-0.010	0.005
-0.024	-0.009	-0.005	0.009	-0.006	-0.011	0.002
-0.022	-0.008	-0.003	0.010	0.003	-0.009	0.004
-0.018	-0.004	0.000	0.008	0.001	-0.013	0.002
-0.024	-0.015	-0.007	0.006	0.005	-0.004	0.007
-0.028	-0.029	-0.015	-0.003	0.000	-0.002	0.010
-0.022	-0.019	-0.005	0.003	-0.001	-0.008	0.005
-0.016	-0.018	-0.005	0.006	0.000	-0.006	0.004
-0.017	-0.021	-0.007	0.001	0.003	-0.005	0.004
-0.016	-0.018	-0.007	0.003	0.003	-0.005	0.004
-0.010	-0.016	-0.002	0.007	0.005	-0.007	0.001
-0.009	-0.012	-0.001	0.006	0.004	-0.006	0.001
-0.005	-0.009	-0.002	0.006	-0.002	-0.009	-0.001
-0.015	-0.019	-0.009	0.004	0.004	-0.006	0.001
-0.014	-0.012	-0.006	0.006	0.006	0.002	
-0.009	-0.004	0.001	0.006	-0.001	-0.006	
-0.005	-0.004	-0.001	0.006	0.003	-0.004	
-0.005	-0.004	-0.003	0.004	0.009	0.000	
-0.003	-0.005	0.000	0.005	0.010	0.001	
-0.003	0.000	0.002	0.006	0.007	-0.004	
-0.001	0.000	0.001	0.007	0.005	-0.005	
0.002	0.000	0.003	0.007	0.005	-0.005	
-0.005	-0.007	-0.002	0.002	0.008	-0.004	
-0.002	-0.006	0.005	0.008	0.004	0.007	
0.006	0.001	0.005	0.007	0.002	0.003	
0.006	0.001	0.001	0.004	0.000	0.002	
0.007	0.000	0.005	0.010	0.006	0.004	
0.006	0.001	0.004	0.009	0.006	0.003	
0.009	0.005	0.006	0.009	0.004	0.000	
0.009	0.004	0.005	0.004	0.002	-0.003	
0.007	0.005	0.010	0.004	0.002	-0.003	
0.006	0.003	0.005	0.003	0.007	-0.003	
0.003	0.003	0.013	0.014	0.005		
-0.005	0.001	0.009	0.012	0.006		
0.002	0.001	0.008	0.007	0.000		
-0.002	0.001	0.010	0.013	0.003		
-0.006	0.001	0.009	0.012	0.000		
-0.008	0.001	0.009	0.011	-0.002		
0.001	0.001	0.007	0.009	-0.003		
0.000	-0.001	0.010	0.013	-0.002		
0.004	0.003	0.011	0.014	-0.002		
-0.005	0.000	0.009	0.010			
-0.007	-0.004	0.005	0.009			
-0.007	-0.004	0.004	0.006			
-0.011	-0.010	0.000	0.006			
-0.009	-0.010	-0.001	0.002			
-0.011	-0.012	-0.004	0.000			
-0.009	-0.010	-0.005	-0.002			
-0.013	-0.013	-0.005	-0.002			
-0.004	-0.005	0.002	-0.001			
0.016	0.014					
0.012	0.010					
0.011	0.008					
0.006	0.003					
					<b>Burnup</b>	<b>Maximal</b>
					<b>[MWd/tU]</b>	<b>diff.</b>
					4099	-0.041
					5249	-0.038
					6427	-0.032
					7781	-0.029

0.006	0.002
0.002	0.000
0.004	0.000
0.002	-0.001
0.008	0.003

8988	-0.025
9727	-0.024
11689	-0.022
12996	-0.018
13320	-0.024

Table 4: Assembly-wise power differences (C-M) for the cycle 24

0.010	0.010	0.016	0.005	-0.007	0.000	-0.004
-0.012	-0.002	0.007	-0.004	0.001	0.006	-0.004
-0.033	-0.020	-0.005	-0.007	0.017	0.020	0.000
-0.042	-0.026	-0.014	-0.012	0.020	0.026	0.002
-0.043	-0.026	-0.013	-0.009	0.023	0.025	0.003
-0.041	-0.024	-0.011	-0.007	0.023	0.023	0.001
0.010	0.011	0.008	0.007	-0.001	-0.003	-0.016
-0.002	-0.001	-0.003	-0.001	0.003	0.002	-0.016
-0.020	-0.015	-0.013	-0.008	0.015	0.011	-0.014
-0.026	-0.022	-0.019	-0.013	0.015	0.015	-0.013
-0.026	-0.022	-0.016	-0.011	0.017	0.015	-0.013
-0.024	-0.023	-0.015	-0.011	0.015	0.012	-0.013
0.016	0.010	0.007	0.007	0.004	-0.008	
0.007	0.000	0.002	0.004	0.011	-0.005	
-0.005	-0.012	-0.005	0.002	0.016	-0.002	
-0.014	-0.018	-0.008	0.000	0.018	0.002	
-0.013	-0.016	-0.008	0.001	0.016	0.001	
-0.011	-0.014	-0.009	0.000	0.014	0.003	
0.005	0.006	0.006	0.015	0.007	-0.011	
-0.004	0.000	0.005	0.024	0.015	-0.008	
-0.007	-0.008	0.001	0.027	0.016	-0.008	
-0.012	-0.012	0.001	0.028	0.018	-0.006	
-0.009	-0.011	0.002	0.024	0.014	-0.008	
-0.007	-0.010	0.003	0.023	0.013	-0.007	
-0.007	0.000	-0.005	-0.001	-0.017		
0.001	0.006	0.003	0.008	-0.013		
0.017	0.016	0.009	0.010	-0.012		
0.020	0.018	0.015	0.014	-0.012		
0.023	0.020	0.014	0.012	-0.013		
0.023	0.022	0.016	0.011	-0.013		
0.000	-0.004	-0.013	-0.015			
0.006	0.002	-0.010	-0.011			
0.020	0.012	-0.007	-0.011			
0.026	0.016	-0.002	-0.010			
0.025	0.016	-0.002	-0.011			
0.023	0.014	0.000	-0.011			
-0.004	-0.018					
-0.004	-0.018					
0.000	-0.015					
0.002	-0.014					
0.003	-0.014					
0.001	-0.013					
					<b>Burnup</b>	<b>Maximal</b>
					<b>[Mwd/tU]</b>	<b>diff.</b>
					164	-0.018
					3148	0.024
					6555	-0.033
					10177	-0.042
					13570	-0.043
					17010	-0.041



Table 6: Assembly-wise power differences (C–M) for the cycle 26

-0.009	-0.005	-0.009	-0.006	-0.012	-0.004	-0.004
-0.041	-0.027	-0.017	-0.011	0.003	0.011	-0.002
-0.046	-0.033	-0.020	-0.012	0.017	0.019	-0.002
-0.050	-0.035	-0.024	-0.015	0.023	0.025	0.002
-0.050	-0.029	-0.021	-0.014	0.023	0.026	0.003
-0.048	-0.026	-0.017	-0.013	0.023	0.024	0.003
-0.005	0.002	0.003	0.000	0.003	-0.003	-0.015
-0.027	-0.019	-0.011	-0.007	0.014	0.008	-0.013
-0.033	-0.026	-0.017	-0.010	0.019	0.014	-0.012
-0.035	-0.028	-0.022	-0.012	0.018	0.017	-0.011
-0.029	-0.023	-0.022	-0.012	0.016	0.019	-0.010
-0.026	-0.021	-0.020	-0.012	0.012	0.018	-0.009
-0.009	0.007	0.008	0.017	0.011	-0.009	
-0.017	-0.007	0.003	0.013	0.019	-0.008	
-0.020	-0.015	-0.002	0.006	0.020	-0.004	
-0.024	-0.018	-0.005	0.003	0.019	-0.002	
-0.021	-0.016	-0.002	0.003	0.016	-0.002	
-0.017	-0.016	-0.005	-0.002	0.012	-0.002	
-0.006	0.003	0.015	0.033	0.018	-0.008	
-0.011	-0.004	0.007	0.043	0.025	-0.009	
-0.012	-0.006	0.005	0.039	0.022	-0.009	
-0.015	-0.010	0.004	0.035	0.021	-0.008	
-0.014	-0.009	0.004	0.032	0.018	-0.009	
-0.013	-0.008	0.003	0.029	0.016	-0.009	
-0.012	-0.007	0.002	0.017	-0.012		
0.003	0.003	0.007	0.028	-0.010		
0.017	0.014	0.014	0.022	-0.010		
0.023	0.017	0.016	0.021	-0.010		
0.023	0.016	0.015	0.016	-0.012		
0.023	0.017	0.015	0.017	-0.009		
-0.004	-0.008	-0.011	-0.008			
0.011	0.001	-0.007	-0.006			
0.019	0.008	-0.008	-0.008			
0.025	0.014	-0.003	-0.008			
0.026	0.014	-0.004	-0.010			
0.024	0.015	0.000	-0.009			
-0.004	-0.018					
-0.002	-0.017					
-0.002	-0.016					
0.002	-0.013					
0.003	-0.013					
0.003	-0.011					
					<b>Burnup</b>	<b>Maximal</b>
					<b>[Mwd/tU]</b>	<b>diff.</b>
					259	0.033
					3421	0.043
					6740	-0.046
					10435	-0.050
					13012	-0.050
					16710	-0.048

Table 7: Assembly-wise power differences (C–M) for the cycle 27

0.032	0.008	0.001	0.002	0.022	0.006	-0.003
0.020	0.003	0.001	-0.008	-0.001	0.003	-0.005
-0.006	-0.017	-0.013	-0.015	0.012	0.016	-0.002
-0.013	-0.019	-0.017	-0.016	0.017	0.019	-0.002
-0.016	-0.019	-0.017	-0.016	0.018	0.022	0.000
-0.016	-0.016	-0.014	-0.016	0.014	0.021	-0.001
0.008	0.010	0.006	0.016	0.007	0.000	-0.013
0.003	0.009	0.002	0.005	0.005	-0.001	-0.015
-0.017	-0.010	-0.013	-0.003	0.014	0.008	-0.012
-0.019	-0.014	-0.017	-0.009	0.017	0.008	-0.014
-0.019	-0.015	-0.018	-0.009	0.017	0.013	-0.011
-0.016	-0.012	-0.015	-0.009	0.015	0.012	-0.010
0.001	0.005	0.015	0.011	0.011	0.006	-0.011
0.001	0.003	0.020	0.013	0.010	-0.011	
-0.013	-0.011	0.009	0.010	0.018	-0.005	
-0.017	-0.015	0.003	0.004	0.023	-0.002	
-0.017	-0.015	0.001	0.005	0.017	-0.002	
-0.014	-0.012	0.001	0.005	0.014	-0.001	
0.002	0.014	0.008	-0.004	-0.003	-0.012	
-0.008	0.006	0.015	0.011	0.006	-0.010	
-0.015	-0.003	0.010	0.018	0.013	-0.007	
-0.016	-0.006	0.007	0.017	0.016	-0.003	
-0.016	-0.007	0.006	0.017	0.013	-0.005	
-0.016	-0.007	0.007	0.016	0.011	-0.003	
0.022	0.002	-0.007	-0.014	-0.028		
-0.001	0.003	0.004	0.000	-0.023		
0.012	0.013	0.013	0.009	-0.019		
0.017	0.017	0.015	0.010	-0.017		
0.018	0.018	0.015	0.011	-0.017		
0.014	0.015	0.014	0.011	-0.016		
0.006	-0.003	-0.017	-0.019			
0.003	-0.002	-0.015	-0.016			
0.016	0.007	-0.010	-0.013			
0.019	0.013	-0.007	-0.012			
0.022	0.012	-0.007	-0.011			
0.021	0.011	-0.006	-0.011			
-0.003	-0.016					
-0.005	-0.017					
-0.002	-0.015					
-0.002	-0.013					
0.000	-0.013					
-0.001	-0.012					

Burnup [MWd/tU]	Maximal diff.
210	0.032
2610	-0.023
6060	-0.019
9750	0.023
13160	0.022
16854	0.021

## 4 CONCLUSION

All 27 completed operational cycles of the NPP Krško plant have been reanalysed using the most recent core simulator package CORD-2 of the Jožef Stefan Institute. The package has been recently updated with some improved models. The key core parameters, such as critical boron concentrations, control rods worth, isothermal temperature coefficient and assembly power distributions are compared to the measured values. Differences in critical boron concentration are less than 50 ppm. The predicted isothermal temperature coefficient is within the  $\pm 1.8$  pcm/K review criteria. The individual bank worths are mostly inside  $\pm 10\%$  criteria, while the sum of all control rods worths is inside 6%. Assembly-wise power differences are within the  $\pm 0.05$  band.

The results confirm satisfactory performance of the CORD-2 code system and its adequacy to support the core design and fuel loading optimization for the Krško NPP.

## REFERENCES

- [1] M. Kromar, A. Trkov, "Nuclear Design Calculations of the NPP Krško core", *Journal of Energy Technology*, Volume 2, Issue 4, 2009, pp. 41-50.
- [2] J. R. Askew, F. J. Fayers, P. B. Kemshell, "A General Description of the Code WIMS", *J. Br. Nucl. Energy Soc.*, 5, 1966, p. 564.
- [3] A. Trkov, "GNOMER - Multigroup 3-Dimensional Neutron Diffusion Nodal Code", Institute Jožef Stefan, Ljubljana, Slovenia, IJS-DP-6688, March 1993.
- [4] A. Trkov, M. Najžer, L. Škerget, "Variant of Green's Function Nodal Method for Neutron Diffusion", *J. Nucl. Sci. Technol.*, 27, 8, 1990, pp. 766-777.

## Peculiarities of Neutronics Characteristics of Integral Reactor WWER of Small Capacity

Grigory Leonidovitch Ponomarenko

OKB "Gidropress"

Ordzhonikidze Street, 21, Moscow region, 142103 Podolsk, Russian Federation

[g\\_ponomarenko@mail.ru](mailto:g_ponomarenko@mail.ru)

### ABSTRACT

In the present paper are analyzed the neutronic characteristics of the stationary fuel loading of the core of integral reactor WWER with a small power 600 MW (th.) and about 200 MW (el.) calculated with Russian code BIPR-7. The core and the FAs, and also the technological parameters are basically analogous to serial reactor WWER-1000; however, there are essential differences in comparison with the WWER-1000:

- in the core are placed 85 FAs (163 in WWER-1000) with an active length 250 cm (355 cm in WWER-1000);

- it is used the reactor campaign of 24 months length and the fuel campaign of 48 months (in WWER -1000 is used 12-18 months the reactor campaign and 36-48 months the fuel campaign);

- for reduction in the neutron leakage on the core periphery are placed burnt out FAs with the smallest multiplication properties, and also FAs have axial blankets with the smaller enrichment (in WWER-1000 they are used to a lesser degree or they are not used);

- there are 18 Guiding Tubes placed in FAs for reactor control and EP provision for the arrangement in them the Black and Grey CRs CPS (in WWER-1000 they are used only Black CRs CPS for EP provision);

- for compensating of the reactivity margin for fuel burn-up and for subcriticality provision of reactor in shut-down conditions are widely used the IFBA in FAs – 18-30 FRs with 8% of natural Gd (tvegs), and also Grey and Black CRs CPS and is not used the dissolved boron in the coolant (in WWER-1000 in essence it is used dissolved boron in the coolant and to a lesser degree the tvegs);

- under the conditions for boron-free control, for guaranteeing the minimum power peaking factors in the core it is fitted the optimum axial enrichment profiling of FAs and axial profiling of concentration of BA in tvegs, and also the axial profiling of concentration of absorber in CRs CPS (in WWER-1000 it is not used).

The neutronic characteristics were investigated in the process of burning out of fuel in the base operating mode at the nominal power for variant of boron-free control. They are compared with analogous characteristics for usual variant of boron control.

The mode of the daily manoeuvring in a wide range of power change 100-30-100% of nominal power is also analyzed for variant of boron-free control and with use of additional regulation by various primary coolant temperatures (modes " $P_2=\text{const}$ ", " $t_{in}=\text{const}$ ", " $t_{av}=\text{const}$ ").

The positive results were obtained, which make it possible to make a conclusion about the relatively simple feasibility of WWER technology in the neutronic aspect in the integral small-power reactor.

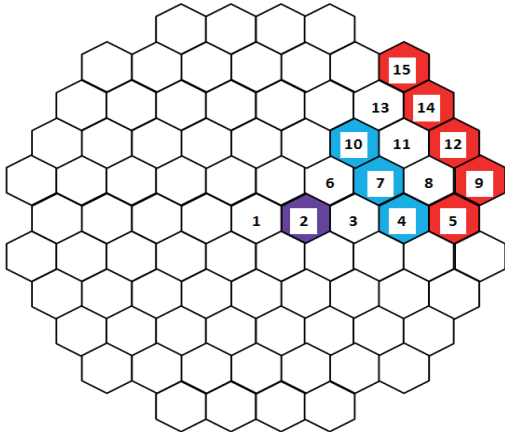
**Keywords:** *Neutronics, Boron-free control, WWER technology for small capacity, Base and maneuvering modes*

### 1 INTRODUCTION

Unit of small power with reactor WWER-I of integral arrangement supposes the usage of innovative solutions and acquisition of advantageous effects from their realization.

**In the part of shortening volumes and periods of construction of NPP:**

- decrease of sizes of the reactor compartment building;
- reduction of a quantity of units of basic RP's equipment;
- reduction of equipment and pipelines of safety system;
- decrease of specific quantity of metal of RP (tons/MW);
- shortening the periods of building and assembly of equipment.



Cartogram of the core of 85 cells of FAs. Cells of the symmetry sector  $60^\circ$  are numbered (if CR CPS presences in the cell, the number of the CR CPS group coincides with the number of cell).  $1+9\cdot6=55$  CRs CPS are in all cells of FAs, except of  $5\cdot6=30$  of peripheral cells (5, 9, 12, 14, 15 and symmetrical to them). From them  $1+5\cdot6=31$  "black" CRs CPS in the cells 1, 3, 6, 8, 11, 13 and symmetrical cells.  $3\cdot6=18$  "grey" CRs (with less absorption of neutrons than "black" CRs) in the cells 4, 7, 10 and symmetrical cells.  $1\cdot6=6$  composite "black & grey" CRs CPS in the cell 2 and symmetrical cells.

Figure 1: Cartogram of the core of 85 cells of FAs

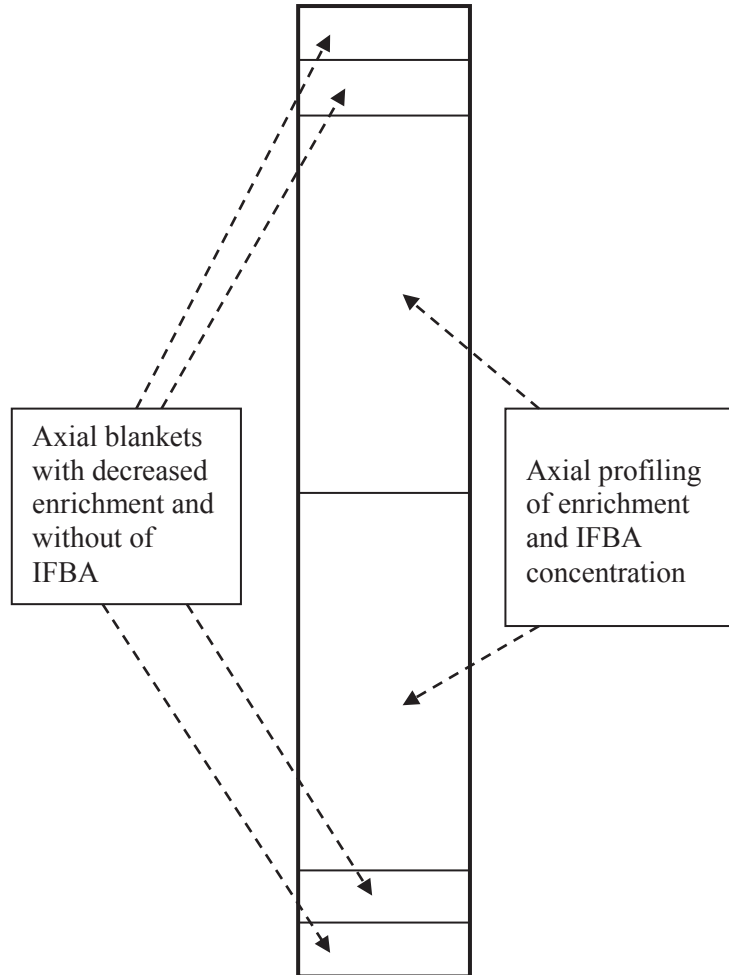


Figure 2: Typical scheme of FA's axial profiling

**In the part of the readiness of production and construction:**

- complete factory readiness of RP;
- the small duration of arrangement and commissioning;
- high operational reliability.

**In the part of the electro-generation:**

- the possibility of incorporation into the low capacity power system;
- the possibility of construction near the consumer.

**In the part of the safety support:**

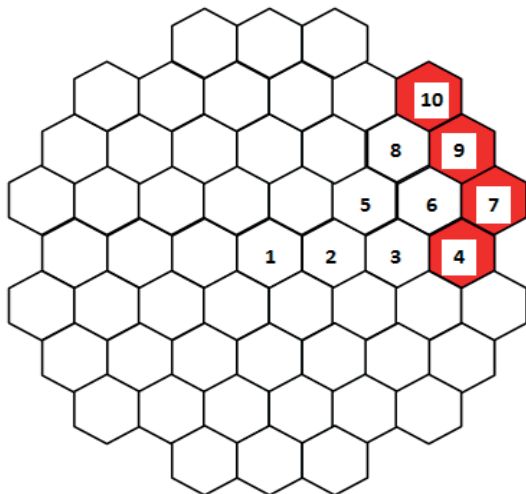
- the possibility of different placement of radioactive waste (ground-based, deepened, underground);
- the exception of LBLOCA emergency;
- the possibility of more widely use of passive safety systems.

FA's geometrical parameters in plan are the same as FAs of WWER-1000. In all cells of FAs, except the peripheral cells adjoining with the baffler, are located black and grey CRs CPS (see

Figure 1). Force framework of FA consists of 18 guiding tubes and welding to them spacing grids. Channel of in-reactor diagnostics is placed in the one of guiding tubes. There are 313 FRs with diameter of fuel pellets 7.6 mm in FA. Part of these FRs (up to 30-42 pcs.) are so called tvegs in each FA. Tvegs contain IFBA in the form of Gadolinium Oxide ( $Gd_2O_3$ ) with concentration up to 8-12 weight %. Axial profiling of fuel enrichment and IFBA concentration are used in FAs (see Figure 2).

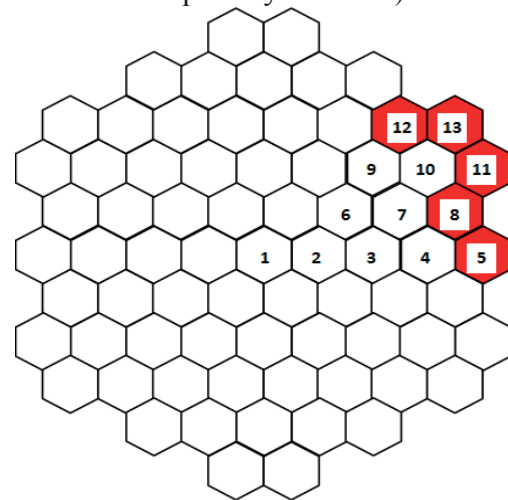
In principle there are different possible combinations of the following variations and diapasons of parameters of integral reactor of WWER type of low or middle power:

- Reactor power: (300-900) MW(th.);
- Number of FAs in the core: 55, 73 or 85 pcs. (see Figures 1, 3, 4);
- The height of the fuel column in the core: (140-270) cm;
- Average fuel enrichment: (3.5-5)%  $^{235}U$ ;
- Duration of reactor operation between the refueling: (500-1000) eff.days;
- Duration of fuel operation before unloading from the core: (1000-2000) eff.days;
- Variants of reactor control: usual for WWER and PWR "high" boron control or recommended by EUR option of low boron control (with increased quantity of IFBA) or supposed in this paper boron-free control (with use of CRs CPS and increased quantity of IFBA).



Cells of the symmetry sector  $60^\circ$  are numbered.  $1+5 \cdot 6=31$  CRs CPS are in all cells of FAs, except of  $4 \cdot 6=24$  of peripheral cells (4, 7, 9, 10 and symmetrical to them)

Figure 3: Cartogram of the core of 55 cells of FAs



Cells of the symmetry sector  $60^\circ$  are numbered.  $1+7 \cdot 6=43$  CRs CPS are in all cells of FAs, except of  $5 \cdot 6=30$  of peripheral cells (5, 8, 11, 12, 13 and symmetrical to them)

Figure 4: Cartogram of the core of 73 cells of FAs

This paper presents the description and characteristics of the specific combination of parameters:

- Reactor power: 600 MW(th.) and  $\sim 200$  MW(el.);
- Number of FAs in the core: 85 pcs. (see Figure 1);
- The height of the fuel column in the core: 250 cm;
- Average fuel enrichment: 3.5%  $^{235}U$ ;
- Duration of reactor work between the refueling: 700 eff.days;
- Duration of fuel work before unloading: 1400 eff.days;
- Two variants of reactor control – usual boron control and boron free control are compared for this combination of parameters.

The main aim of this paper is the checking and demonstration of the principle ability of realization and achievement of advantages of boron-free control in the basic and maneuvering operational modes with the use of the different methods of additional temperature control.

## 2 RESULTS OF RESEARCHES

**Basic operational mode.** The neutron characteristics were analyzed and compared for two variants of reactor control – the compensation of the reactivity margin for fuel burn-up and also for heating-up and reactor power raise.

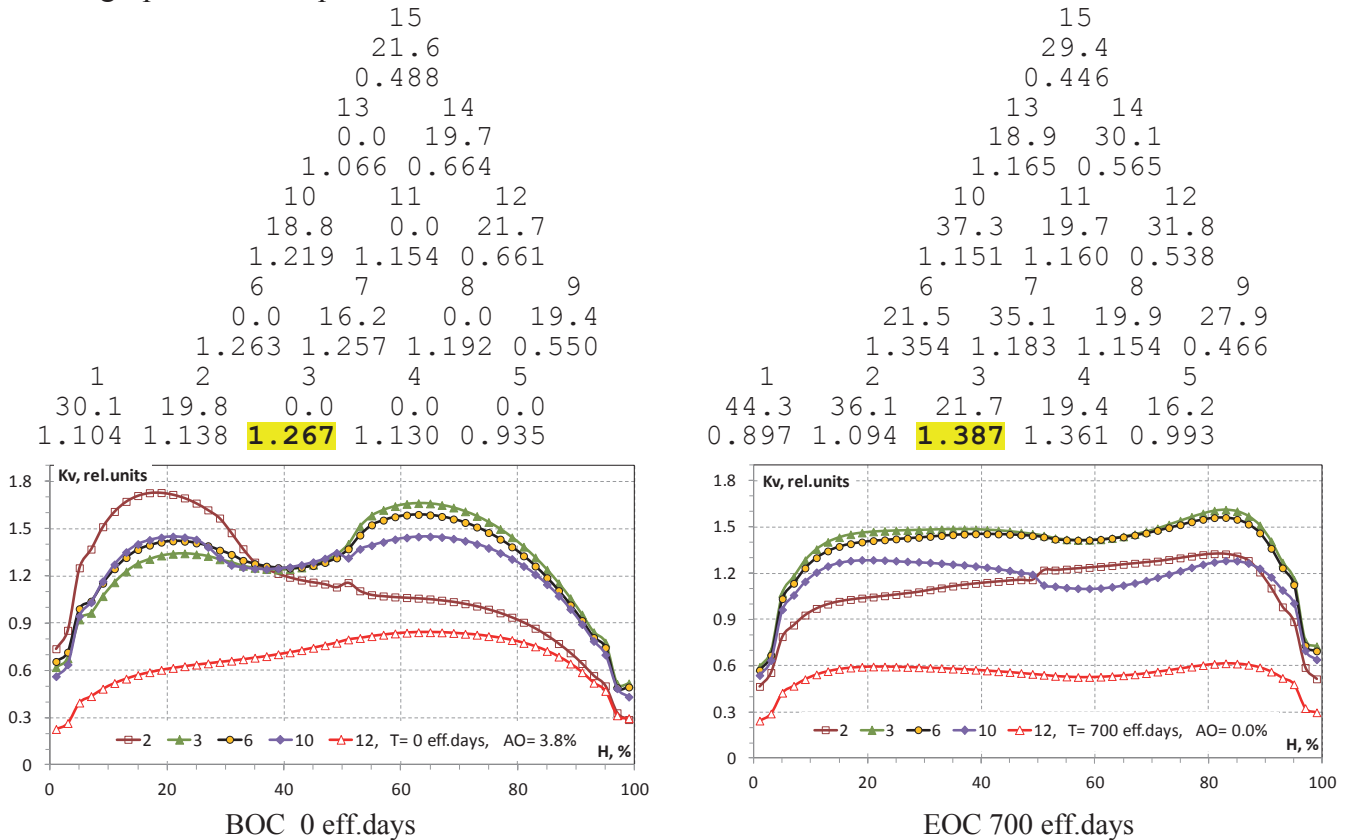


Figure 5: Typical radial and axial power (burn-up) distributions in the core for variant of the **boron-free** control

The **first variant**, the so-called variant of boron-free control is characterized by the application of the increased IFBA quantity, integrated with the fuel in the separate FRs with  $Gd_2O_3$  (so called tvegs), by introduction/withdrawing of CRs CPS in/from the core, and also by a change in the coolant temperature at the core entrance. This makes it possible to manage without the use of a boric acid in the coolant both in the base operating mode at the nominal power and in the mode of power maneuvering.

However the complete exclusion of boron system from WWER technology is technically hardly feasible and contradicts with safety requirements. The variant of completely boron-free control can be realized not in all states and modes. Reason is that safety provision and normative regulation document require the presence of the second shut-down system (besides mechanical EP system), based on other operating principle. Furthermore, the rule of WWER technology and operation during the PPR and the fuel reloading is the provision of subcriticality only with boron in the water without the account of inserted mechanical CRs CPS.

Therefore in the first variant the boron system is simplified and is used only for guaranteeing the subcriticality with the failures of mechanical EP system, and also in the cold (less than  $200^\circ C$ ) depoisoning state of reactor, which is realized during the PPRs and fuel reloadings. During start-up of reactor, up to the moment of reaching MCL (at a temperature more than  $200^\circ C$ ) boron is completely removed from the coolant. Similar variants of boron-free control are assumed also in the designs of integral type foreign reactors, for example in IMR (Mitsubishi Heavy Industries, Japan 350 MW(e) and 1000 MW(th)). European Utility Requirements EUR [1] recommends considering the option of so called *low boron* control capability for PWRs in the basic operational mode and

notes its advantages above the usual "high" boron control. EUR [1] also recommends the regulation without adjusting soluble boron concentration for load following and maneuvering.

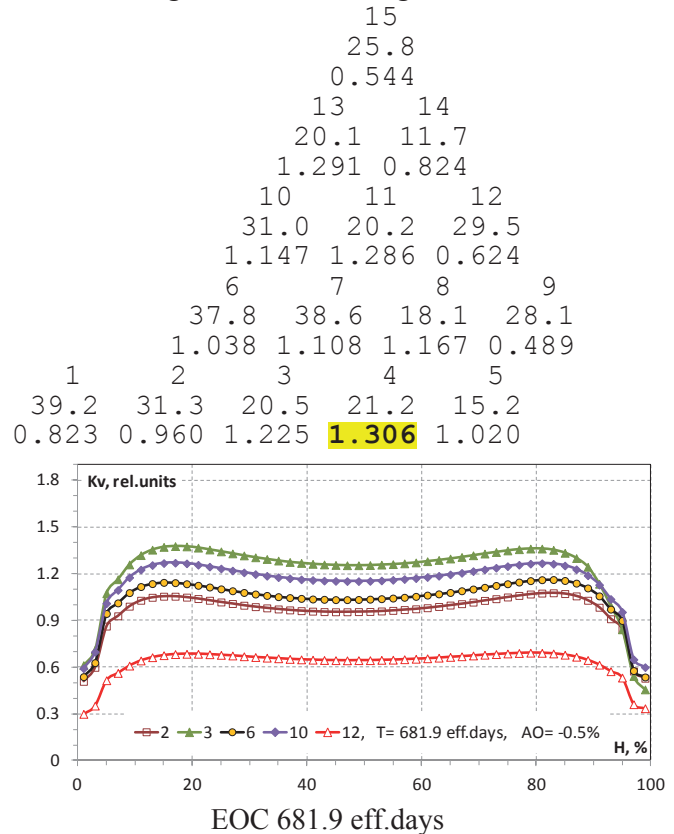
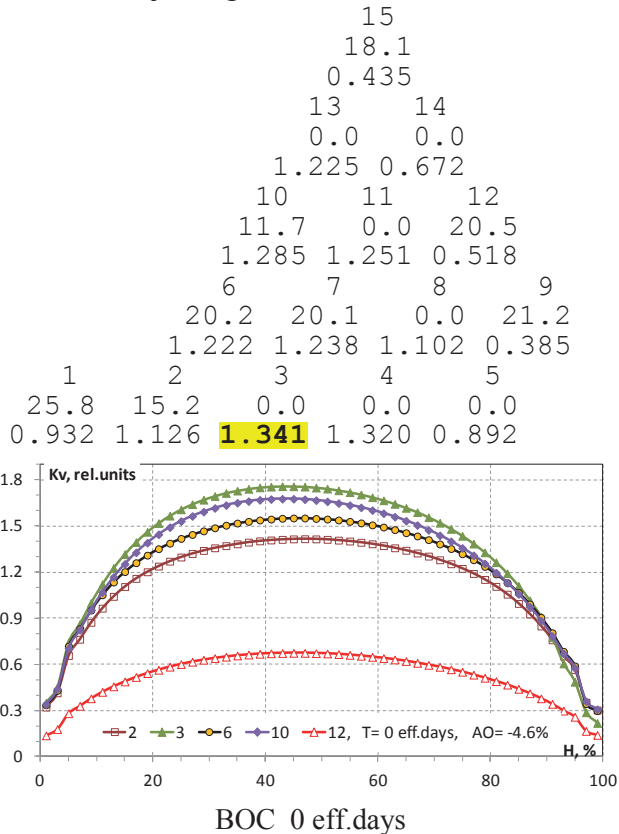


Figure 6: Typical radial and axial power (burn-up) distributions in the core for variant of the **boron** control

The **second variant** relates to the traditional for WWERs and PWRs boron control and is characterized by the compensation for temperature, power and burning-out effects mainly due to the boric acid in the coolant and partially due to IFBA (in less extent than in the first variant).

As it is demonstrated further, there are following **advantages** on safety and economy of the taken variant of boron-free control as compared to the variant with the boron control:

- the course of ATWS modes (with EP failure) is more safe since TCR is strongly negative during the entire reactor operating period and in any power level. On the contrary, in the boron control variant the TCR is near to zero at the beginning of operating period in the low power conditions;
- TCR remains negative at the criticality accident in the cold depoisoning condition, in contrast to the boron control variant. On this reason the complete removal (dilution) of boron from the coolant introduces substantially smaller positive reactivity. Thus, the course of DEC modes is also safer;
- the absence of boron in the coolant at the power operation removes the radioactive tritium generation and improves the radiological index ALARA;
- the smaller boron concentration in the reactor and in the HAs the less probability of dangerous boron crystallizing during the LOCA;
- strongly negative TCR provides the possibility of the safe early achievement of MCL power (at 200°C) and further reactor heating-up due to the nuclear reaction instead of heating-up due to pumps (economic effect);
- simplification of the boric system and reduction in liquid radioactive wastes (economic effect);
- the possibility of the more effective fuel utilization due to the more flexible regulation by CRs and the smaller radial neutron leakage from the core (economic effect).

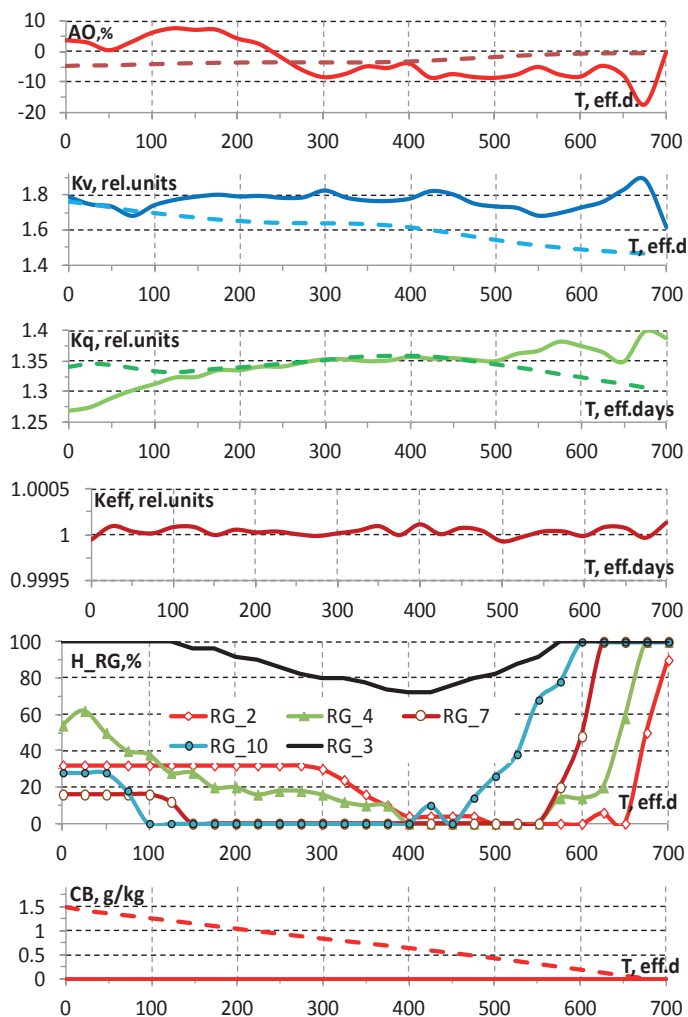


Figure 7: Change of characteristics vs. burn-out time in stationary fuel loading for variants of boron (dashed lines) and boron-free (solid lines) control

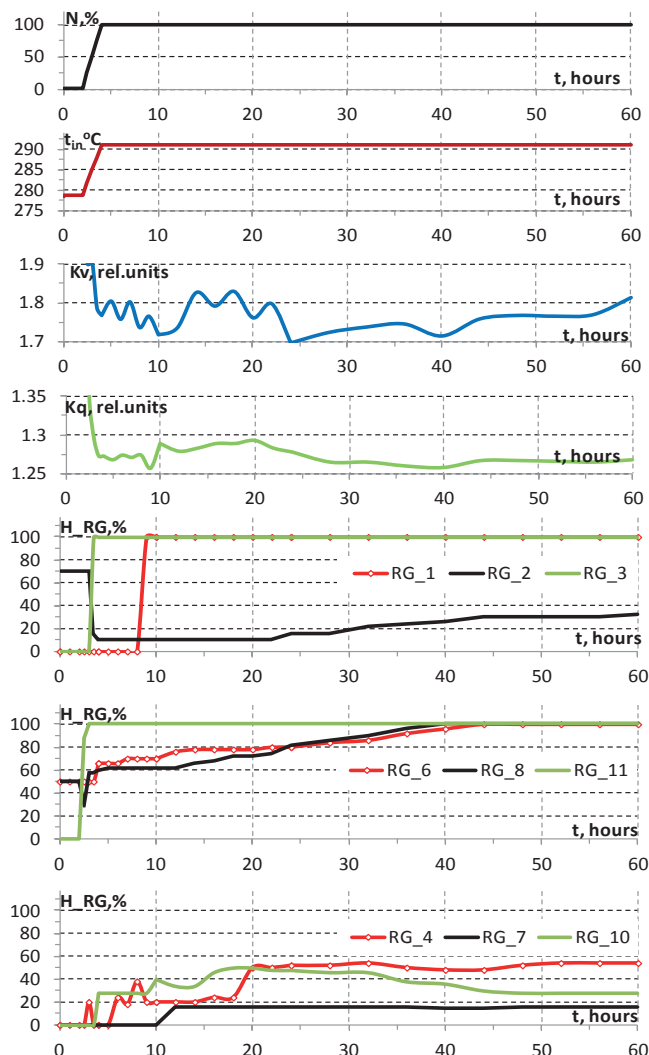


Figure 8: Change of characteristics vs. time at power increase by the CRs moving from MCL till nominal power for the BOC of stationary fuel loading for variant of boron-free control

A **deficiency** of the variant of boron-free control as compared to the variant with boron control is more complicated regulation by the control rods moving and caused by it certain (not very large) increase of power peaking factors  $Kq$  and  $Kv$  in the core. However just this deficiency makes it possible to obtain some benefit in fuel utilization. And this deficiency itself is not principal thing, since the power peaking factors are within the permissible limits. Taking into account remaining advantages (see above) the variant of boron-free control seems as more preferable. Therefore mainly this variant is analyzed in this paper. At the same time, both variants have right to be realized and in principle can be used as the options taking into account the customer's desire.

Typical power and burn-up distributions in the core at the beginning (BOC) and the end (EOC) of the stationary fuel loadings for variants of boron-free and boron control respectively are presented on Figures 5, 6. These are the relative power and burn-up distributions by FAs in the core symmetry sector  $60^\circ$  and axial relative power distributions on separate typical FAs.

Change of main characteristics ( $AO$ ,  $Kv$ ,  $Kq$ ,  $H_{RG}$ ,  $CB$ ) vs. burn-out time in stationary fuel loading for variants of boron (dashed lines) and boron-free (solid lines) control is shown on the Figure 7. One can see rather small increase of power peaking factors (about 3 % by maximal  $Kq$  and 7 % by maximal  $Kv$ ) in the core for variant of boron-free control as compared to the variant with boron control. It was achieved by means of the grey CRs usage ( $RG_4$ ,  $RG_7$ ,  $RG_{10}$ ) and

proper algorithm of CRs moving for compensation of different burn-up rate of fuel and BA. During first 400 eff. days the BA's burn-up rate is more intensive than for the fuel. It requires insertion of several RGs. After 400 eff. days the BA is burnt out almost entirely and fuel burn-up requires the step-by-step withdrawn of all inserted CRs CPS until EOC.

Figure 8 shows the change of characteristics vs. time at power increase by CRs moving from MCL till nominal power for the BOC of stationary fuel loading for variant of boron-free control.

**Power maneuvering.** Figures 9-13 present the characteristics vs. time at daily power maneuvering in wide diapason (100-30-100% of nominal power) in the modes " $P_2=const$ " and " $t_{av}=const$ " for the BOC, near middle (450 eff.days) and EOC of stationary fuel loading for variant of boron-free control.

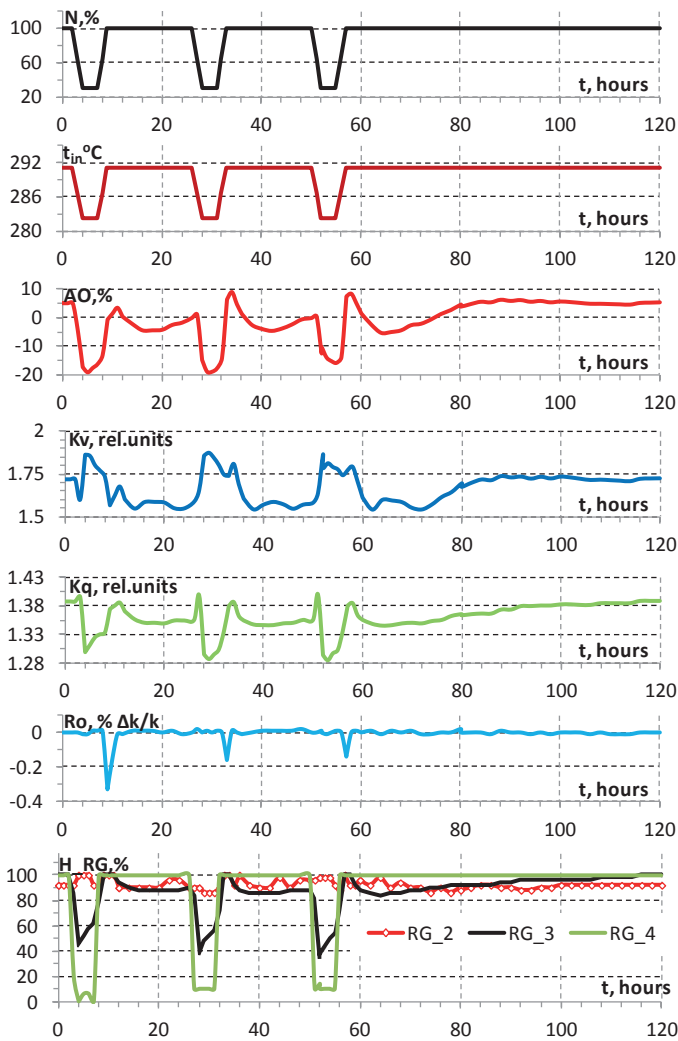


Figure 9: Power maneuvering at EOC.  
Mode " $P_2=const$ "

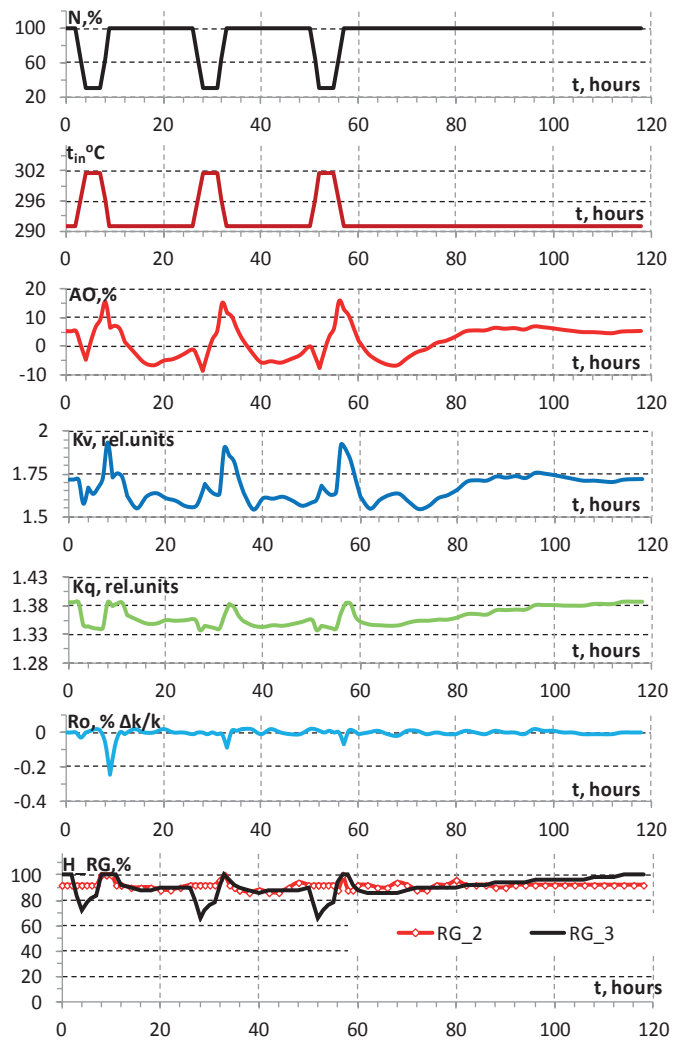


Figure 10: Power maneuvering at EOC.  
Mode " $t_{av}=const$ "

Daily work at power level 30% is continued during 3 hours and at power level 100% is continued during 17 hours. Decrease down to 30% and increase up to 100% power levels are continued during two hours. Three daily cycles of power maneuvering from 0 till 72 hours were modeled, last of them may be considered as stationary daily cycle. Further from 72 till 120 hours modeling was continued with the constant nominal power. The analysis of period from 72 till 120 hours is intended for the test whether the axial Xenon instability occur in the core. Such instability may occur as a result of previous deep change of power and CRs movement and is typical for big core of WWER-1000 type. However it was obtained that similar instability does not occur in the considered rather small and short core. I.e. there is big negative stability index, because of all

significant characteristics, presented on Figures 9-13 are smoothly returned to their initial (at zero hours) values in 16-18 hours (at the moment 88-90 hours).

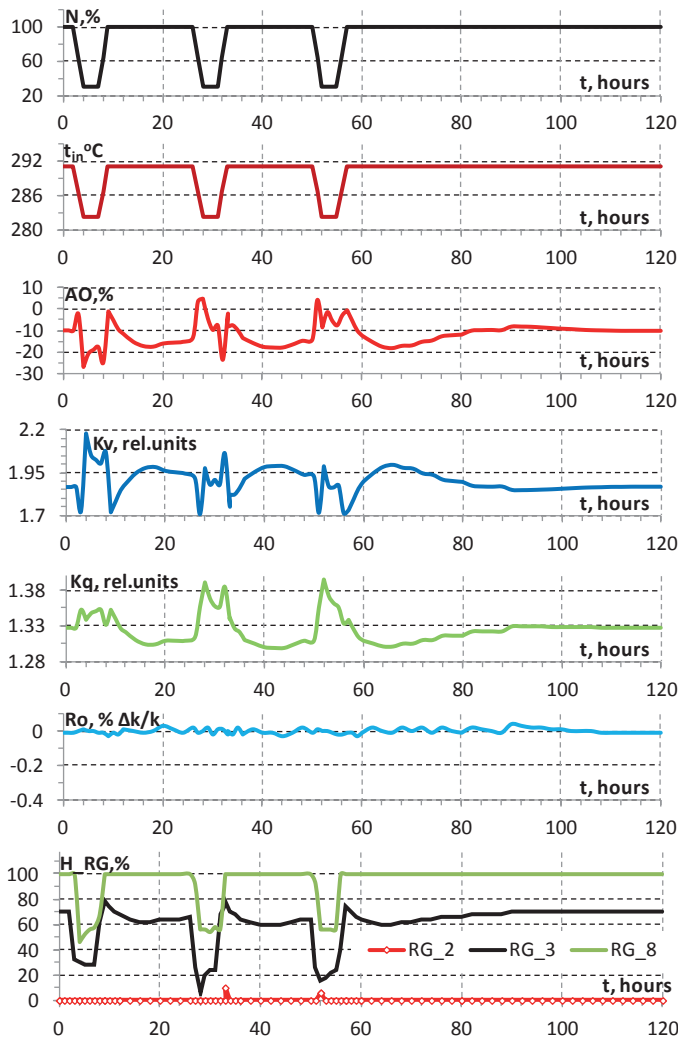


Figure 11: Power maneuvering at burn-up time 450 eff.d. Mode "P<sub>2</sub>=const"

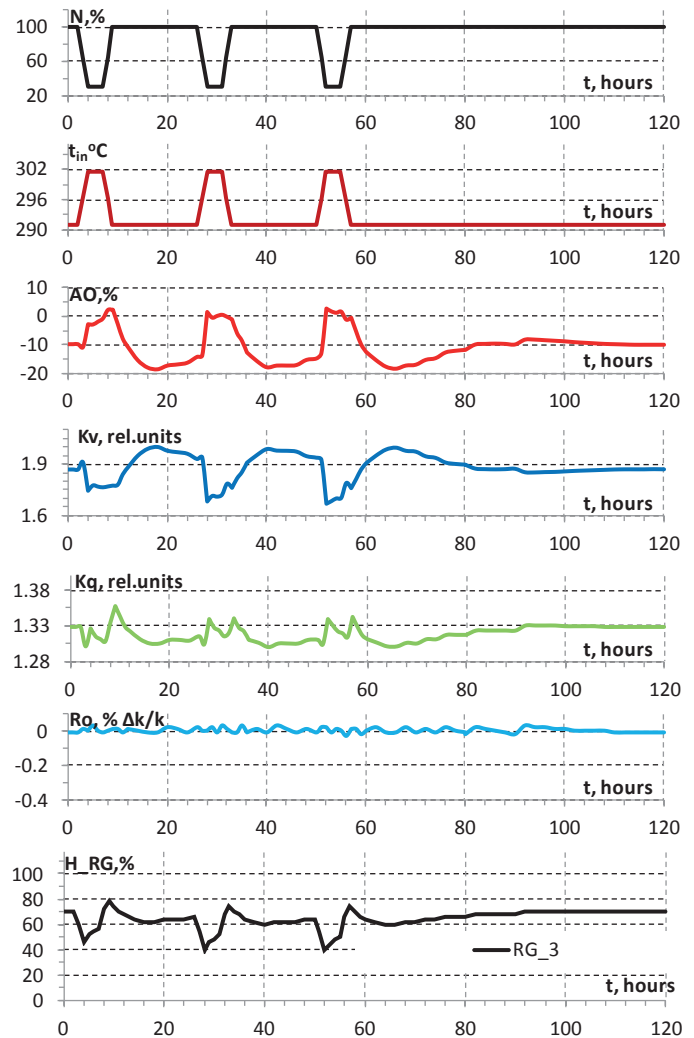


Figure 12: Power maneuvering at burn-up time 450 eff.d. Mode "t<sub>av</sub>=const"

The mode of regulation "t<sub>av</sub>=const" is differed from the mode "P<sub>2</sub>=const" by less diapasons of CRs moving that one can see from the comparison of Figure 9 with Figure 10 and Figure 11 with Figure 12. Explanation is that in the mode "t<sub>av</sub>=const" the change of t<sub>in</sub> inserts the same sign of reactivity as CRs, but in the mode "P<sub>2</sub>=const" – on the contrary – reactivity inserted by the change of t<sub>in</sub> has the opposite sign. The mode "t<sub>in</sub>=const" was considered also and it is placed in an intermediate position between two above-mentioned modes "P<sub>2</sub>=const" and "t<sub>av</sub>=const".

On the Figure 9 is presented the mode "P<sub>2</sub>=const" for the EOC. In contrast to other moments of reactor campaign, presented on Figures 11-13, the power rise up to 100% at the very end of campaign may require more time approximately by one hour due to the so called effect of *iodine pit* and exhausting of possibility to insert the positive reactivity by the CRs withdrawal. This effect is presented in the form of small short-term peaks of negative reactivity Ro(t) on the Figures 9 and 10. This additional one hour should be enough for burning-out of excessive <sup>135</sup>Xe at power level near 90% and gradual power rise up to 100%.

**Reactivity effects and coefficients.** The following values of TCR are realized during the Hot Full Power, t<sub>in</sub>=279 °C and the stationary <sup>135</sup>Xe and <sup>149</sup>Sm poisoning:

- for variant of the boron-free control: -61.2·10<sup>-5</sup>, -58.2·10<sup>-5</sup>, -60.6·10<sup>-5</sup> 1/°C for the BOC (0 eff.d), 450 eff.d and EOC (700 eff.d) respectively;

- for variant of the boron control:  $-24.9 \cdot 10^{-5}$ ,  $-49.4 \cdot 10^{-5}$ ,  $-64.5 \cdot 10^{-5}$   $1/^\circ\text{C}$  for the BOC (0 of eff.s), 450 eff.s and EOC (681.9 of eff.s) respectively.

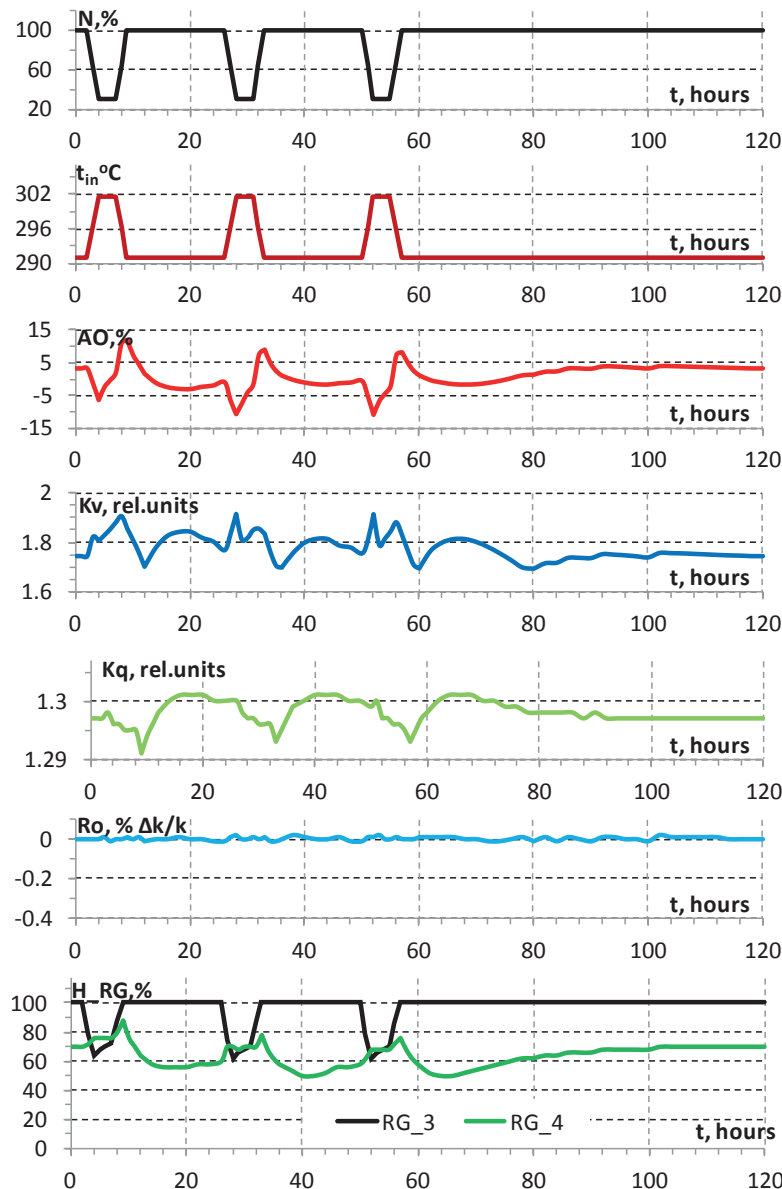


Figure 13: Power maneuvering at BOC. Mode " $t_{av} = \text{const}$ "

So boron-free control is characterized by the well negative TCR which is practically constant during the fuel burn-up that is preferable in contrast to the variant of boron control where TCR is significantly changed during burn-up.

$K_{eff}$  and TCR are compared in the Table 1 in some conditions for two variants with the following deductions:

- for variant of the boron-free control it is possible to achieve MCL at  $200^\circ\text{C}$  and further heating-up up to  $279^\circ\text{C}$  accomplish by the nuclear reaction instead of by RCPs (as usual), that gives an economical advantage. Safety in diapason  $200-279^\circ\text{C}$  is ensured by the strongly negative TCR in contrast to the variant of boron control that one can see from comparison of TCR in the states 6, 7 with 13, 14 in Table 1;

- negative TCR for variant of the boron-free control is realized even for DEC, for example at achievement of critical state at the depoisoning Cold Zero Power in contrast to the variant of boron control with positive TCR (compare states 5 and 11 in Table 1).

Table 1 Comparison of  $K_{eff}$  and TCR in certain conditions for variants of Boron-free Control and Boron Control. BOC, Cold Zero Power, Xenon depoisoning, Sm stationary)

Boron-free Control						Boron Control					
Number	CRs inserted	$t_{in}$ , °C	CB, g/kg	$K_{eff}$	TCR, $10^{-5}$ 1/°C	Number	CRs inserted	$t_{in}$ , °C	CB, g/kg	$K_{eff}$	TCR, $10^{-5}$ 1/°C
1	No	50	0	1.169	-	8	No	50	0	1.239	-
2	All	50	0	1.055	-	9	No	50	1.000	1.116	-
3	All without one CR*	50	0	1.074	-	10	No	50	2.000	1.020	-
4	No	50	2.000	0.960	-	11	No	50	2.233	1.000	4.8
5	No	50	1.531	1.000	-0.3	12	No	50	3.000	0.948	-
6	All, but H_RG_6=58%	200	0.092	1.000	-30.8	13	No	220	2.287	1.000	5.0
7	All, but H_RG_6=58%	220	0	1.000	-36.2	14	No	279	2.277	1.000	-0.7

\*All CRs inserted without one the most effective CR of RG\_8 which stuck in the extreme top position

**Burn-up and efficiency of fuel utilization.** The specific natural uranium consumption has complicated dependence on different factors and it is equal to 0.236 kg U/MW·d(th.) for considered variant with 24-months reactor campaign and 2 fuel reloadings. This is only 3.6% higher than for WWER-1300 with 18-months campaign and 3 fuel reloadings. But this is already 16% higher than for serial WWER-1000 with 12-months campaign and 4 fuel reloadings. This situation reflects the following well-known fact: the shorter reactor campaign and the more fuel reloadings the better fuel utilization but the worse *use factor of installed capacity*. Besides, the less neutron leakage from the core (due to core dimensions and fuel arrangement) and the less average fuel power rating (due to bigger core volume and less installed capacity) the better fuel utilization.

Average burn-up is equal to 32.9 MWd/kg U which is achieved during 700 eff. days for variant of boron-free control (see Figure 5) and 32.0 MWd/kg U which is achieved during 681.9 eff. days for variant of boron control (see Figure 6) at the same average enrichment 3.48%  $^{235}\text{U}$ .

I.e. fuel utilization for boron-free variant is better by 2.6% that is explained by the more flexible regulation by CRs and the smaller radial neutron leakage from the core for concrete realizations of fuel arrangements in considered two variants.

### 3 CONCLUSION

Neutronic characteristics of the core of integral WWER reactor with a small power 600 MW (th.) were analyzed. Variant of boron-free control was compared with usual variant of boron control in the process of burning out of fuel in the base operating mode. Variant of boron-free control uses simplified boron system which is used only for guaranteeing the subcriticality with the failures of mechanical EP system, and also in the cold depoisoning state of reactor, which is realized during the PPRs and fuel reloadings. Some advantages on safety and economy of variant with boron-free control as compared to the variant with boron control were obtained. Nevertheless both variants have right to be realized and in principle can be used as the options taking into account the customer's desire.

The mode of the daily manoeuvring was also analyzed for variant of boron-free control and with use of additional regulation by various primary coolant temperatures (modes "P<sub>2</sub>=const", "t<sub>in</sub>=const", "t<sub>av</sub>=const").

The positive results were obtained, with conclusion about the relatively simple feasibility of WWER technology in the integral small-power reactor.

## ACRONYMS AND CONVENTIONAL SYMBOLS

ALARA – as low as reasonably achievable  
ATWS – anticipated transient without scram  
BOC – beginning of cycle  
BA – burnable absorber  
CPS – control and protection system  
CR – control rod  
DEC – design extension condition  
EOC – end of cycle  
EP – emergency protection  
EUR – European Utilities Requirements  
FA – fuel assembly  
FR – fuel rod  
HA – hydro-accumulator  
IFBA – integrated with fuel burnable absorber  
LBLOCA – large break loss of coolant accident  
LOCA – loss of coolant accident  
MCL – minimally controlled level  
NPP – nuclear power plant  
PPR – planned preventive repair  
PWR – pressurized water reactor  
RCP – reactor coolant pump  
RP – reactor plant  
TCR – temperature coefficient of reactivity  
WWER – water-water energy reactor  
eff.d. – effective days

AO – axial offset of power in the core, %  
CB – concentration of natural boron in the coolant, g/kg  
H – height of the core, % from the bottom  
H<sub>RG</sub> – height of RG in the core, % from the bottom  
K<sub>eff</sub> – effective multiplication factor, rel. units  
K<sub>q</sub> – power peaking factor by FAs in the core, rel. units  
K<sub>v</sub> – power peaking factor by the nodes in the core, rel. units  
N – neutron power of reactor, % of nominal power  
"P<sub>2</sub>=const" – mode of power maneuvering with maintaining of constant secondary pressure  
RG<sub>i</sub> – regulative group of CRs CPS with number *i*  
Ro – reactivity, %Δk/k  
T – time of reactor campaign, eff. d.  
t – time of Xenon transient during power manoeuvring, hours  
t<sub>in</sub> – coolant temperature at the core entrance, °C  
"t<sub>av</sub>=const" – mode of power maneuvering with maintaining of constant average by the core coolant temperature  
"t<sub>in</sub>=const" – mode of power maneuvering with maintaining of constant coolant temperature at the core entrance

## REFERENCES

- [1] EUR. European Utility Requirements for LWR Nuclear Power Plants. Volumes 1&2 Revision D October 2012.

## Study of the Allegro Core Performance

**Ján Haščík, Štefan Čerba, Jakub Lúley, Branislav Vrban**

Institute of Nuclear and Physical Engineering, Slovak University of Technology in Bratislava  
Ilkovičova 3, 812 19 Bratislava, Slovakia

jan.hascik@stuba.sk, stefan.cerba@stuba.sk, jakub.luley@stuba.sk, branislav.vrban@stuba.sk

### ABSTRACT

The presented paper is related to introduction of the design and neutronic characterization of the start-up core developed for Gas cooled Fast Reactor (GFR) demonstrator. Slovak University of Technology in Bratislava joined the project ALLEGRO in last decade within the consortium of middle-European institutions. In the development plan of the GEN IV GFR the ALLEGRO demonstrator is one of the most necessary steps. The ALLEGRO reactor is small helium cooled 75 MW<sub>th</sub> thermal power unit. Its main objective is to demonstrate the key GFR technologies and to perform tests of innovative materials. The reactor core is based on the standard and MOX pin type fuel in the first phase of the project. The active core of a large GFR 2400 makes use of ceramic materials, but in the first ALLEGRO core MOX fuel will be used. It will be mainly to demonstrate the viability of the technology and to acquire necessary experimental data for further research. In the presented works are identified the main discrepancies between ALLEGRO and GFR 2400 designs, the sensitivity analysis was performed for both reactors. Neutronic characterization is aimed to determination of the standard neutronic parameters using conventional computational systems. The results of sensitivity and uncertainty calculations are presented in conjunction with similarity analysis.

**Keywords:** *Neutronics, MOX type fuel, Code Validation, GFR demonstrator*

### INTRODUCTION

The Gas-cooled Fast Reactor (hereinafter the GFR) is one of the six most promising reactor concepts selected by the Generation IV International Forum (GIF) [1]. The design of this reactor may partially benefit from previously proposed but not realized conceptions of the Sodium-cooled Fast Reactor (SFR) and the Very High Temperature Reactor (VHTR). Despite the extensive research done into the GFR technology, no gas cooled fast reactor has ever been built. In the development plan of the GEN IV GFR the ALLEGRO demonstrator is one of the most necessary steps. The ALLEGRO reactor is small helium cooled 75 MW<sub>th</sub> thermal power unit. Its main objective is to demonstrate the key GFR technologies and to perform tests of innovative materials. The active core of a large GFR 2400 makes use of ceramic materials, but in the first ALLEGRO core MOX fuel will be used. It will be mainly to demonstrate the viability of the technology and to acquire necessary experimental data for further research. In order to identify the main discrepancies between ALLEGRO and GFR 2400 designs, the sensitivity analysis was performed for both reactors. The obtained results predict approach how to design and optimize the ALLEGRO core for testing of experimental assemblies. ALLEGRO core is characterized by standard mixed oxide (MOX) assemblies consisting of fuel pins with stainless steel cladding operated at an average coolant temperature around 400°C. In contrast, GFR 2400 core is based on carbide pin fuel type with the application of refractory metallic liners used to enhance the fission product retention of the SiC cladding.

The main principles of fast reactor systems are rather well understood, however, their optimization, in order to comply more effectively with requirements and their timely deployment, requires the research in nuclear data. Although most nuclear data are by and large available in modern data files, their accuracy and validation is still a major concern. The main source of uncertainty in the calculated core responses is due to uncertainties in evaluated nuclear data such as microscopic cross sections (XS), fission spectra, neutron yields, and scattering distributions that are contained in cross section evaluations. These uncertainties are governed by probability distributions which are unknown, but the evaluated data values are assumed to represent the mean of the distribution. TSUNAMI-IP utility available in SCALE system [2] computes the contribution to the response uncertainty due to the cross-section covariance data with the use of sensitivity profiles of the investigated system. The results of this uncertainty analysis of ALLEGRO MOX core are given and discussed in this paper. In addition the neutronic similarity of ALLEGRO MOX core to the several hundred critical benchmark experiments specified in the ICSBEP Handbook [3] is evaluated by the use of three integral indices.

The ALLEGRO reactor is expected to be built in the central European region, thus the research of this reactor is the driving mechanism for Slovak institutions to participate in research projects and in the development of GEN IV fast reactors.

## **1 GENERAL DESIGNS OVERVIEW**

### **1.1 ALLEGRO core specification**

The ESNII+ ALLEGRO MOX starting core configuration is an experimental unit with thermal power of 75 MW<sub>th</sub> characterized by standard Mixed OXide (MOX) fuel assemblies consisting of fuel pins with stainless steel cladding operating at an average helium coolant temperature around 400 °C. The 120 degree symmetric core includes 81 fuel assemblies, with 169 fuel pins. The average PuO<sub>2</sub> content of the heavy metal material in the fuel pin is 25.5%vol. In addition, the ALLEGRO MOX core features 6 in-core dummy assemblies made of special steel alloy 15-15Ti (AIM1) so far assumed homogeneous in geometry and composition. The control rod system is composed of 4 Diverse Shutdown Devices (DSD) and 6 Control and Shutdown Devices (CSD). The absorber rods in both groups are composed of boron carbide. The core fuel region is surrounded by four additional rings of reflector assemblies (80% vol. AIM1 + 20% vol. He at 70 bar) in the radial direction and by the 30.2 cm high axial reflectors of almost the same material placed above and below the fission gas plenums. Additional three rings of shielding assemblies are placed around the reflector in the radial direction. Axial shielding placed just under and above the axial reflector region uses a lower amount of B<sub>4</sub>C. In order to ensure adequate heat transfer the primary coolant pressure during normal operation is 7 MPa. Three decay heat removal loops with helium-gas heat exchangers are available to mitigate core melting accidents. The global primary arrangement is based on two main helium-water loops (2x38 MW<sub>th</sub>), each fitted with one intermediate heat exchanger (IHX) blower unit. The produced heat is finally transferred by air coolers from the secondary circuit to the atmosphere as the ultimate heat sink.

### **1.2 GFR 2400 Core Specification**

The GFR 2400 reactor is considered as a conceptual design of a large scale power GFR. This design is based on the foregoing concepts and experiences of all GoFastR [4] participants. In European FP7 programme, the GoFastR project was the Euratom contribution to the Gen IV gas cooled fast reactors (GFR). The GFR 2400 design is a large scale power unit with thermal power of 2400 MW<sub>th</sub>. This fast-spectrum reactor is a helium-cooled system and it works with a closed fuel cycle. Primary coolant pressure during normal operation reaches 7 MPa in order to ensure adequate heat transfer. Due to safety reasons, the coolant volume fraction in a core is high. This fact allows

maintaining the natural circulation of coolant under pressurized conditions even if active systems are not available. Three decay heat removal loops (each 100% capacity) with heat exchangers and forced convection devices are available and six additional gas reservoirs are prepared in case of emergency to mitigate core melting accident. The global primary arrangement is based on three main loops ( $3 \times 800 \text{ MW}_{\text{th}}$ ), each fitted with one IHX blower unit, enclosed in a single vessel. The current choice of power conversion system is the indirect Brayton cycle operated with He-N<sub>2</sub> mixture. The planned cycle efficiency is approximately 45%. Since the GFR 2400 components need to withstand high temperatures, ceramic compositions are under investigation as a promising solution for used materials. The pin type fuel of active length of 165cm consists of uranium plutonium carbide (UPuC) and it is surrounded by tungsten-rhenium compound (W14Re) and rhenium (Re) refractory liners to ensure fission products confinement within the pins. The gap between fuel and liners is filled with helium gas of 1MPa pressure. The use of a SiC<sub>f</sub>/SiC material for fuel cladding is the latest and very promising solution, where the SiC fibers are improving the mechanical properties of the fuel pin. The active core consists of two zones. The PuC volumetric content in inner core fuel assemblies (FA) reaches 14.2%, and 17.6% in the outer core. The isotopic composition of uranium corresponds to natural abundance of its isotopes while plutonium composes of the twice recycled MOX fuel, expected to be available in France from 2016 [5]. The core fuel region is surrounded by six rings of Zr<sub>3</sub>Si<sub>2</sub> reflector assemblies in the radial direction and by the 1m high axial reflectors of the same material placed above and below the fission gas plenums. The general views of ALLEGRO MOX and GFR 2400 core designs can be found in Figure 1.

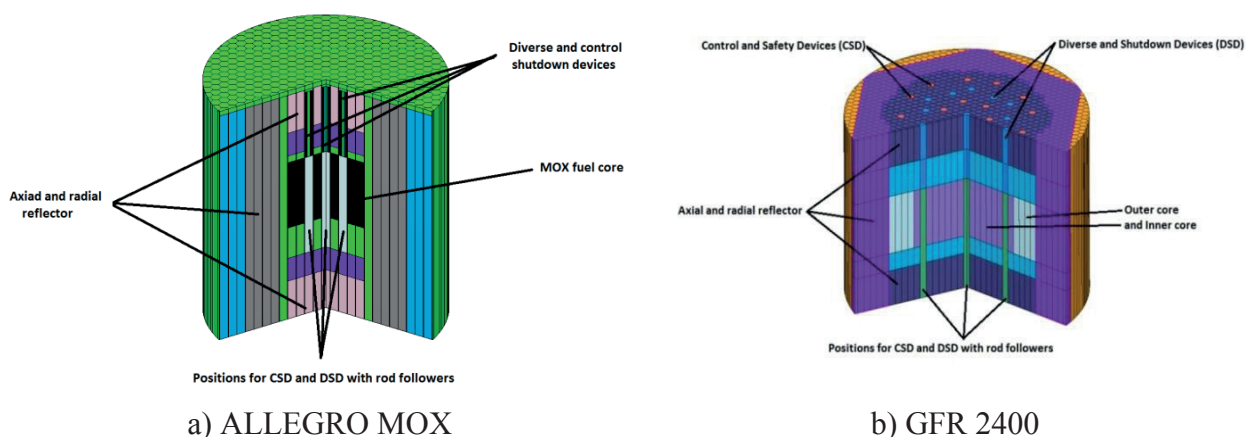


Figure 1: 3D cross-sectional views of ALLEGRO MOX and GFR 2400 core designs

## 2 CALCULATION METHODOLOGY

The sensitivity and uncertainty analysis of ALLEGRO MOX and GFR 2400 cores were performed by using two computational tools. In the first case, the TSUNAMI-3D code was utilized using ENDF/B-VII [7] 238 group cross section data and 44groupcov covariances. Forward and adjoint transport calculations were carried out with KENO6 and the sensitivity coefficients were computed by the SAMS module. For the neutron flux calculations square mesh was placed through the core with a uniform step of 1.5 cm in the fuel region. In other parts of the core, the size of the mesh was directly proportional to the distance from the core centre. In the second case, self-developed perturbation PORK code was used which is interconnected with the diffusion flux solver DIF3D [6] and ZZ-KAFAX-E70 [8] based ENDF/B-VII nuclear data library collapsed from 150 to 25 groups. Due to the multi-group cross section data used in both computational routes, in a process of cross section preparation the resonance self-shielding calculation had to be performed. SCALE system is capable to perform only cell calculation at the level of fuel pin with definition of cladding and coolant in an infinite lattice, but with an option where the spectral calculation can be carried out by using CENTRUM code. Methods used in the multi-group cross sections processing procedures

for DIF3D calculation allow us to take into account resonance self-shielding effect as well as the spatial boundary effects. In this case, two level of cross section calculation was necessary to perform, where in the second level the cross sections were condensed from 150 to 25 groups structure by using regional-wise neutron flux from RZ transport calculation. Sensitivity coefficients calculated by TSUNAMI-3D were collapsed to 25 group structure.

TSUNAMI-IP utility uses sensitivity data generated by TSUNAMI-1D and/or TSUNAMI-3D sequences and cross section-covariance data stored in the 44GRPCOV library. TSUNAMI-1D/3D are sequences that execute modules to determine response sensitivities and uncertainties. The linked computations perform the cross section self-shielding operations, forward and transport calculations, computation of sensitivity coefficients and calculation of the response uncertainty. The SCALE covariance library is based on several different uncertainty approximations with varying degrees of fidelity to the actual nuclear data evaluation. The library includes evaluated covariances obtained from ENDF/B-VII, ENDF/B-VI, and JENDL3.3 for more than 50 materials. It is assumed that covariances taken from one data evaluation such as ENDF/B-VI or JENDL-3.3, can also be applied to other evaluations of the same data, such as ENDF/B-VII. If this is done judiciously for cases in which the nuclear data evaluations are similar, then the covariances taken from one source should be a reasonable representation of uncertainties for the other evaluations. ORNL has a database of pre-calculated sensitivity profiles for several hundred critical benchmark experiments specified in the ICSBEP Handbook. These sensitivities may be input to TSUNAMI-IP utility, along with calculated sensitivity profile of application system. In our case 494 benchmark experiments with various energy group structures were used.

Three global integral indices [2] are used in the analysis to assess the similarity of ALLEGRO MOX neutronic core design (hereinafter application – index  $a$ ) and a single experiment ( $e$ ) on a system-wide basis for all nuclides and reactions. Each integral index is normalized such that a value of 1.0 represents complete similarity between ALLEGRO MOX core design and specific benchmark experiment and the value of 0.0 indicates no similarity. The uncertainty of the integral response  $\Delta R$  (for instance  $k_{eff}$ ) on the target integral parameter by the use of XS sensitivity coefficients denoted by symbol  $S$  and XS covariance matrix  $M$  can be evaluated by the well-known sandwich formula:

$$\Delta R^2 = S_R M S_R^T, \quad (1)$$

where the impact of the individual reactions and energy groups can be evaluated separately. The diagonal elements of the resulting matrix, defined as the solution of Eq. (1), represent the relative variance values for each of the system under consideration. The off-diagonal elements are the relative covariances between given experiments. Following the SCALE methodology, these covariances transformed to correlation coefficients ( $ck$ ) describe the degree of correlation (coupling) in the uncertainties between the two specific systems. This correlation (coupling) demonstrates the level of similarity in the predicted response biases between various systems in the frame of XS induced uncertainties. The  $E$  parameter given by Eq. (2) assesses similarity between two systems based on the magnitude and shape of all sensitivity profiles.

$$E = S_a S_e^T / |S_a| |S_e|. \quad (2)$$

If the group-wise sensitivity data for all nuclides and reactions for each system are considered as a vector, the index  $E$  is the cosine of the angle between the two sensitivity vectors. If these vectors are parallel ( $E=1$ ), the systems are proportional. The  $G$  index assesses the similarity of two systems based on normalized differences in the energy dependent sensitivity data for fission, capture and scatter. A physical interpretation of the  $G$  index is the ratio of the sum of the sensitivity

coefficients of the application that are covered by the experiment to the sum of the sensitivity coefficients of a given application. The  $G$  index is defined as follows:

$$G = 1 - \frac{\sum_n \sum_x \sum_j (S_{x,j}^{a,n} - S_{x,j}^{e',n})}{\sum_n \sum_x \sum_j (S_{x,j}^{a,n})}, \quad (3)$$

where the symbol  $n$  stands for the number of application system nuclides,  $x$  represents the reaction and  $j$  the summation which is performed over all energy groups. As it can be seen from Eq. (3), a  $G$  value of 1 indicates complete similarity and a  $G$  value of 0 indicates no similarity. The nuclide-reaction specific partial integral index based on the same coverage criteria as  $G$  is denoted  $g$ .

### 3 RESULTS

Mentioned above, both investigated systems (ALLEGRO starting core and GFR 2400) are characterized by different material composition. ALLEGRO is composed from MOX fuel with steel type cladding and reflector. Although the GFR 2400 uses carbide fuel with SiC cladding and zirconium based reflector, these differences may not necessarily result in a totally different performance of both cores initiated by a same event. First, the spatially averaged neutron spectra were compared in Figure 2. In the energy region above 1 MeV, the shape and magnitude of the neutron flux is almost identical. Maximum of the spectrum observable below this energy is more significant for ALLEGRO core. In the case of GFR 2400, neutrons from this energy area are moved to lower energies probably due to slowing down on carbon nuclides. This effect can be seen also in the energy region between 1keV and 50keV, where the magnitude of GFR 2400 flux spectra is higher compare to ALLEGRO and the maximal value is slightly higher than the maximum which lies near 500 keV energy. A valuable neutron population in resonance energies is the result of competitive interactions of neutrons with carbon and not only with uranium. Material with similar properties like carbon is missing in the core composition of ALLEGRO MOX core therefore the neutron spectra is harder.

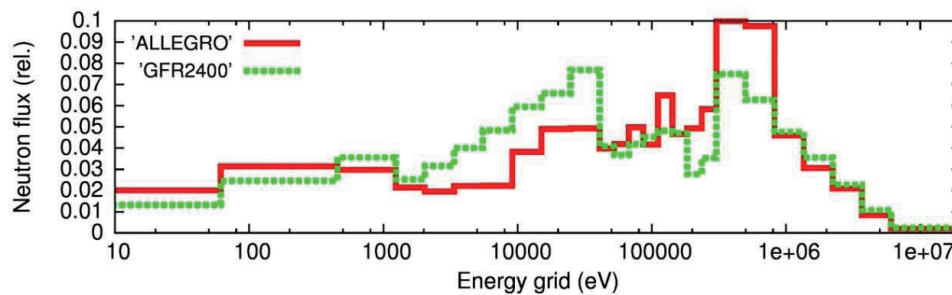


Figure 2: Normalized neutron flux spectrum from DIF3D calculation

The first group of analyzed nuclides consists of fissile nuclides. In this case, the composition of fuel vector for both systems was the same. The difference was just in plutonium isotopes enrichment. The good agreement between the shape of sensitivity profiles and neutron flux can be seen on the sensitivity profiles of  $^{239}\text{Pu}$  and  $^{235}\text{U}$ , which are presented in Figure 3-a and b. In the case of Pu, the shape of sensitivity profiles is consistent with Figure 2. A little different case is U, where the shape of GFR 2400 sensitivity profile is comparable to neutron flux spectrum but it is intensified by increasing value of  $^{235}\text{U}$  fission cross section towards lower energies which ultimately results in notable overestimation compare to ALLEGRO MOX sensitivity profile. From the global view to fissile nuclides, the multiplication properties of both systems are very similar, because they are led by  $^{239}\text{Pu}$  (almost equal integral sensitivity coefficient of fission), but with different consequences during transients. In case of a power excursion where the fuel temperature increases, neutron absorption in the resonance region becomes dominant reaction due to Doppler broadening

which will result in a more negative temperature reactivity effect for GFR 2400 core compared to ALLEGRO MOX core.

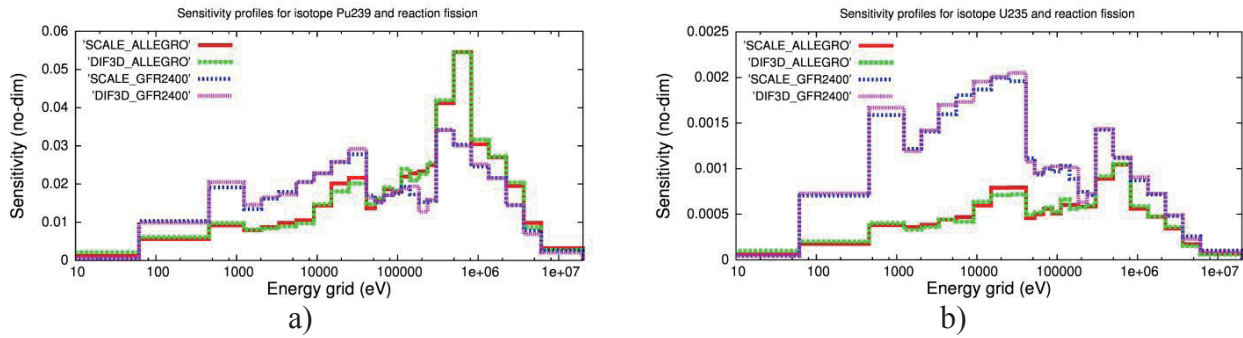
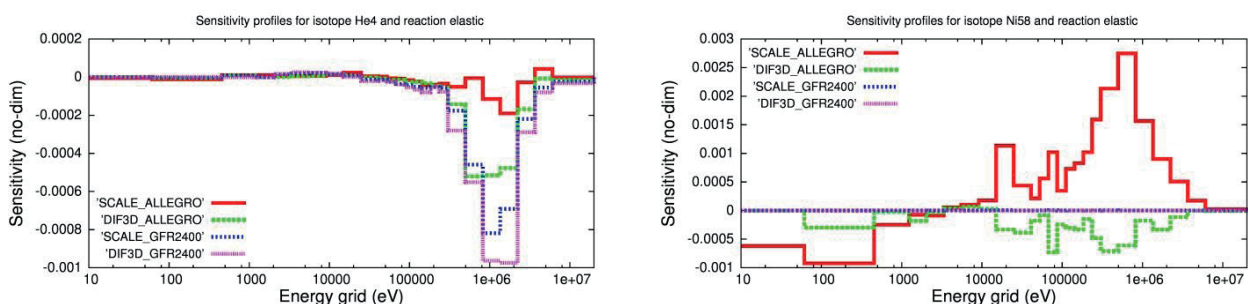


Figure 3: Sensitivity profiles of fissile nuclides and reaction fission

A special attention within sensitivity analysis was paid to structural materials including also a reflector material and coolant. For this group of isotopes it is impossible to expect some comparable results because each core is based on different sets of materials but their individual contribution to the multiplication properties of corresponding system may identify unique processes hidden in integral parameters. Comparison of sensitivity profiles of  $^4\text{He}$  and elastic scattering, presented in Figure 4-a, identifies discrepancy between these profiles both at the level of comparison between the systems, as well as within comparison between used code schemes. The main inconsistency is in case of ALLEGRO MOX core where the shape of sensitivity profile calculated using DIF3D code scheme (green dot line) is comparable with the sensitivity profiles of GFR 2400 core but the sensitivity profiles calculated using SCALE system (red line) is depressed close to zero value which makes ALLEGRO MOX core almost insensitive to change in He composition. Main consequence of this inconsistency could be improper estimation of void effect by SCALE system or overestimation of the same effect in DIF3D. In a certain way, similar behavior was noticed for structural materials of ALLEGRO MOX core as Fe, Cr or Ni, and elastic scattering reaction. GFR 2400 core contains a minimal amounts of these isotopes therefore sensitivity profiles presented in Figure 4-b are almost zero. The sensitivity profiles of  $^{58}\text{Ni}$  and elastic scattering for ALLEGRO MOX core, shown in Figure 4-b, illustrate a different response to change in elastic scattering cross section based on computational scheme. In case of SCALE system, sensitivity profile is mainly positive and peak-oriented around energy 600 keV with small negative contribution in lower energies. However, the sensitivity profile calculated by DIF3D scheme is purely negative. Shape of both profiles can be considered with some simplifications as a comparable but the main inconsistency is related to an absolute magnitude of individual sensitivity coefficients. The source of discrepancies presented in Figure 4-a and b are related to diffusion solution used in DIF3D. Information about non-symmetric angular distribution of elastic scattering related to border effect near fuel-reflector interface is probably lost by using scalar flux during sensitivity calculation. Within comparison of sensitivity profiles between systems, contribution of for GFR 2400 total sensitivity is almost ten times higher than in case of ALLEGRO which is slightly surprising due to absence of materials with moderator properties. This effect can be explained by an effective contribution of fission in lower energies of GFR 2400 core.



a) b)

Figure 4: Sensitivity profiles of chosen nuclides and elastic scattering reaction

The last set of sensitivity profiles is focused on capture reaction. In Figure 5, results for  $^{238}\text{U}$  and  $^{238}\text{Pu}$  are presented. In the case of  $^{238}\text{U}$ , based on the high sensitivity in resonance energy region for GFR 2400 in connection with sensitivity of  $^{239}\text{Pu}$  fission, stronger temperature reactivity effect can be expected compared to ALLEGRO MOX core. Based on this different sensitivity in the resonance region, extrapolation of Doppler coefficients determined for ALLEGRO MOX core to GFR 2400 will be incorrect.

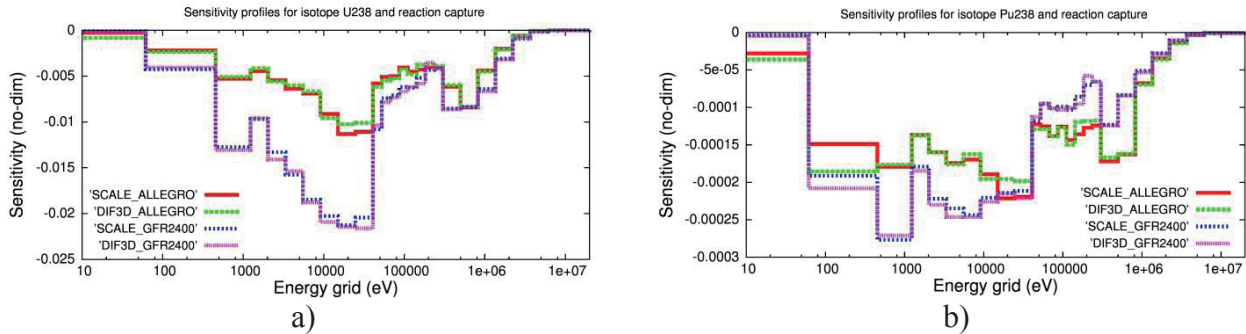


Figure 5: Sensitivity profiles of chosen nuclides and reaction capture

As it was mentioned above, the TSUNAMI sequence computes the contributors to the application response uncertainty due to the XS covariance data. The relative standard deviation of ALLEGRO MOX  $k_{eff}$  due to XS covariance data is 1.04%. Table 1 lists the top 16 covariance matrices that contribute to the  $k_{eff}$  uncertainty. These contributors represent more than 98% of the total uncertainty induced by XS data. The  $k_{eff}$  in the case of 238 energy group calculation with control and safety rods reaches  $1.02534 \pm 0.00019$ .

Table 1: Uncertainty contribution in ALLEGRO MOX  $k_{eff}$

No.	Covariance Matrix		Contributions to Uncertainty in $k_{eff}$ (% $\Delta k/k$ )	No.	Covariance Matrix		Contributions to Uncertainty in $k_{eff}$ (% $\Delta k/k$ )
	Nuclide-Reaction	Nuclide-Reaction			Due to the Matrix	Nuclide-Reaction	
1	$^{239}\text{Pu}$ nubar	$^{239}\text{Pu}$ nubar	6.7999E-01	9	$^{238}\text{U}$ n,gamma	$^{238}\text{U}$ n,gamma	1.5155E-01
2	$^{238}\text{U}$ n,n'	$^{238}\text{U}$ n,n'	5.0948E-01	10	$^{238}\text{U}$ nubar	$^{238}\text{U}$ nubar	1.1712E-01
3	$^{240}\text{Pu}$ nubar	$^{240}\text{Pu}$ nubar	2.3377E-01	11	$^{56}\text{Fe}$ elastic	$^{56}\text{Fe}$ elastic	9.6235E-02
4	$^{239}\text{Pu}$ n,gamma	$^{239}\text{Pu}$ n,gamma	2.3310E-01	12	$^{56}\text{Fe}$ n,gamma	$^{56}\text{Fe}$ n,gamma	7.5133E-02
5	$^{239}\text{Pu}$ chi	$^{239}\text{Pu}$ chi	2.1225E-01	13	$^{241}\text{Pu}$ fission	$^{241}\text{Pu}$ fission	6.7164E-02
6	$^{238}\text{Pu}$ fission	$^{238}\text{Pu}$ fission	2.0489E-01	14	$^{240}\text{Pu}$ fission	$^{239}\text{Pu}$ fission	5.8365E-02
7	$^{238}\text{U}$ elastic	$^{238}\text{U}$ n,n'	1.9741E-01	15	$^{52}\text{Cr}$ elastic	$^{52}\text{Cr}$ elastic	5.4093E-02
8	$^{239}\text{Pu}$ fission	$^{239}\text{Pu}$ fission	1.8240E-01	16	$^{239}\text{Pu}$ n,n'	$^{239}\text{Pu}$ n,n'	5.4073E-02

The top contributor to  $k_{eff}$  uncertainty is the  $^{239}\text{Pu}$  nubar value. This is due to the large  $\text{PuO}_2$  volume fraction (25.5%) in the MOX fuel and, as can be seen in Figure 6, also due to the high sensitivities above 100 keV threshold. In case of  $^{238}\text{U}$  n,n' reaction there are large negative sensitivities in the energy range above 1 MeV burdened with significant relative standard deviation of XS data (20 - 35%). Although the  $k_{eff}$  sensitivities to  $^{239}\text{Pu}$  n,gamma reaction are in magnitude much smaller than  $^{238}\text{U}$  n,n' and  $^{239}\text{Pu}$  nubar, the uncertainty associated to XS data is large and varies between 5 to 45% in the relevant energy range. The similarity assessment procedure identified three groups of potential experiments, where the values of the  $ck$  coefficients got over 0.4.

However, as it can be seen in Figure 7-a), only one experiment (MIX-COMP-FAST-001-001) [3] reached  $ck$  greater than 0.9.

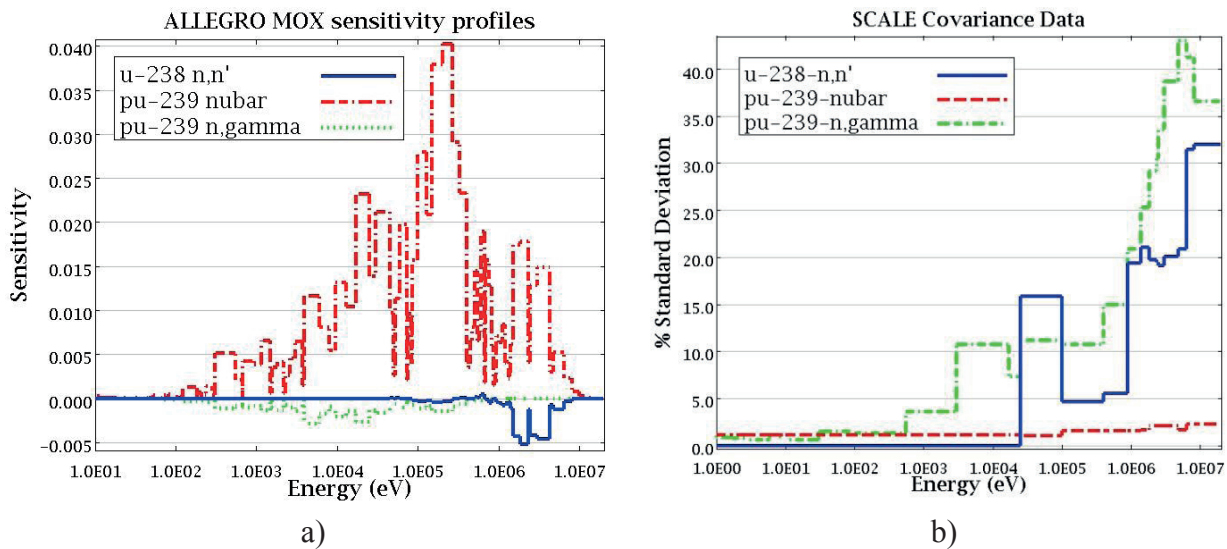


Figure 6: Application sensitivity profiles and covariance data

The good similarity results are mainly driven by the type of fuel (MOX) and fuel cladding material used in the ALLEGRO MOX model and in the MIX-COMP-FAST-001-001 experiment. Although the  $E$  coefficient reaches the quite high value (0.95), the big portion (25%) of ALLEGRO sensitivity profiles is uncovered ( $G$ ) by this experiment.

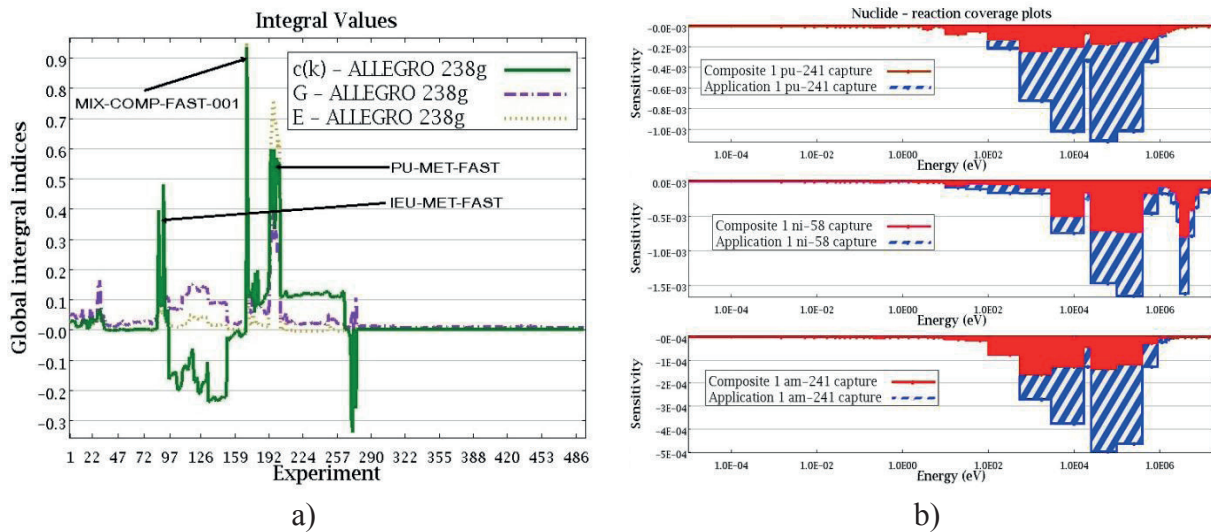


Figure 7: Integral indices and coverage plots

This is mainly caused by different construction materials and coolants (helium vs sodium) used in adopted models resulting to dissimilar neutron spectra. The short characteristics of other identified experiments are shown in the following Table 2.

From Table 2 we can conclude that the majority of identified experiments, except MIX-COMP-FAST-001-001, are simple plutonium metal systems. The average fission group energy in these systems is quite high due to the absence of moderator and structural materials (over 1 MeV). Due to their simplicity, the  $G$  values get very low for all cases. The values of  $g$  indices for nuclide – reaction pairs, having a great impact on the neutron balance of the active core, are given in Table 3. The data presented in Table 3 highlight those nuclide – reaction pairs which are not sufficiently covered by the MIX-COMP-FAST-001-001 experiment.

Table 2: Integral indices for similar experiments in relation to ALLEGRO MOX

ID	ICSBEP ID	Fissile material	Moderator	Average Fission Group Energy	Neutron Flux $\wedge$ 100 keV	Capture $\wedge$ 100 keV	Cladding	Reflector	$ck$	$E$	$G$
171	MIX-COMP-FAST-001-001	MOX	Na	99.8 keV	57%	22%	SS	Depl. U	0.93	0.95	0.75
197	PU-MET-FAST-008-001	Pu Metal	-	1.08 MeV	95%	80%	-	Th	0.60	0.68	0.30
194	PU-MET-FAST-002-001	Pu Metal	-	1.28 MeV	97%	85%	-	-	0.60	0.62	0.30
199	PU-MET-FAST-018-001	Pu Metal	-	913 keV	92%	57%	-	Be	0.57	0.67	0.30
201	PU-MET-FAST-023-001	Pu Metal	-	1.17 MeV	97%	83%	-	Gr	0.56	0.63	0.26
202	PU-MET-FAST-024-001	Pu Metal	-	647 keV	95%	45%	-	PE	0.54	0.62	0.27
193	PU-MET-FAST-001-001	Pu Metal	-	1.28 MeV	97%	86%	-	-	0.54	0.60	0.26
200	PU-MET-FAST-022-001	Pu Metal	-	1.26 MeV	97%	86%	-	-	0.54	0.60	0.26
196	PU-MET-FAST-006-001	Pu Metal	-	1.11 MeV	94%	75%	-	Nat. U	0.47	0.77	0.42

Figure 7-b) shows the coverage of the most problematic nuclide – reaction sensitivity profiles by the use of all experiments involved in our calculations. The hashed area of sensitivity profiles highlights the importance of experimental verification of used nuclear data in energies in the interval between 100 keV and 1 MeV.

Table 3: The results of nuclide-reaction specific partial integral index  $g$

ID	$^{238}\text{U}$ capture	$^{238}\text{U}$ total	$^{239}\text{Pu}$ capture	$^{238}\text{U}$ n,n'	$^{240}\text{Pu}$ capture	$^{56}\text{Fe}$ capture	$^{58}\text{Ni}$ capture	$^{238}\text{U}$ scatter	$^{241}\text{Pu}$ capture	$^{16}\text{O}$ capture	$^{241}\text{Am}$ capture
171	1.00	0.99	0.98	0.99	0.46	0.90	0.47	0.96	0.20	1.00	0.35

Despite the different used fuel types (MOX vs UPUc) and reflector materials (AIM1 vs  $\text{Zr}_3\text{Si}_2$ ) the similarity assessment of ALEGRO MOX and GFR 2400 core designs show quite high values of  $ck$  (0.85) and  $E$  (0.92) coefficients. The variations in material compositions are reflected by the low value of integral index  $G$  (0.65) where almost 35% of GFR 2400 sensitivity profiles are uncovered by ALLEGRO MOX core design. The fact that C and  $^{28}\text{Si}$  isotopes are in ALLEGRO MOX core found in minimal amounts was confirmed by more detailed calculation of the partial integral indices. The coverage plots of specific nuclide – reaction pairs of other important contributors to integral index  $G$  are shown in Figure 8.

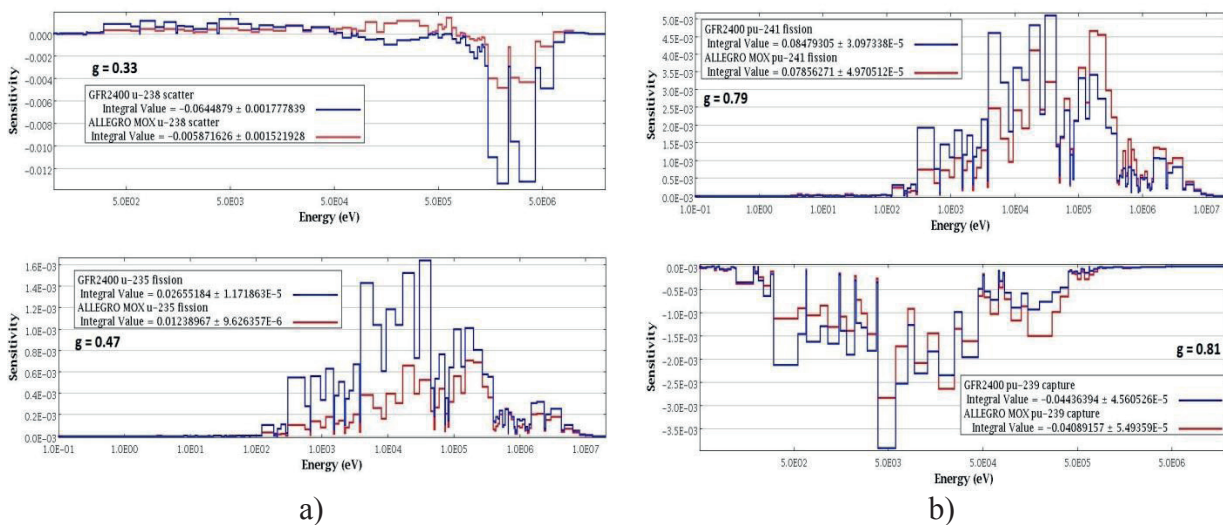


Figure 8: Coverage plots of specific nuclide – reaction pairs

## 4 CONCLUSION

Sensitivity analysis of GFR 2400 and ALLEGRO MOX core was performed using two computational schemes where the first was based on the Monte Carlo method and second on the deterministic approach to determine spatial and energy flux distribution. Both systems are defined with different material compositions and hence by different mean neutron flux spectrum.

However the developed philosophy joins these two systems to the structure where one system serves to prove viability and feasibility of the second system. Based on this structure, some similarities in a response to change in basic data were expected which was not fulfilled on satisfactory level. In many cases, the shape of sensitivity profiles was consistent between both systems, but different absolute value of a magnitude of investigated sensitivity profiles produce presented discrepancies. The sensitivity profiles are able to predict the behaviour of a system during transients but in case of ALLEGRO MOX core and temperature reactivity effect, calculated data cannot be extrapolated for GFR 2400 core. Nevertheless, calculated database of sensitivity profiles is a useful clue for optimization process of ALLEGRO MOX core performance close to GFR 2400 or for development of experimental assembly construction. Appropriate combination of materials with moderation properties in ALLEGRO MOX core is a way how to form neutron flux spectrum to be more representative for GFR 2400 development. From the global point of view, higher sensitivity coefficients of GFR 2400, which was calculated almost in all cases, resulted to the higher uncertainty of  $k_{eff}$  induced by cross section data. This uncertainty for ALLEGRO was determined to 1.04% and for GFR 2400 the uncertainty reaches 1.67%. Special outcome of this analysis was definition of constraints in a usage of diffusion solution in perturbation theory for ALLEGRO MOX core. The similarity and uncertainty analysis of the ESNII+ ALLEGRO MOX core has identified specific problems and challenges in the field of neutronic calculations.

The similarity assessment identified 9 partly comparable experiments where only one reaches  $ck$  and  $E$  values over 0.9. However the Global Integral Index  $G$  remains still low (0.75) and cannot be considered as sufficient. The uncertainty analyses shoes that the main contributors to ALLEGRO  $k_{eff}$  uncertainty are  $^{239}\text{Pu}$  nubar and  $^{238}\text{U}$  inelastic scattering. The additional margin from uncovered sensitivities was determined to be 0.28%. The identified low number of similar experiments prevents the use of advanced XS adjustment and bias estimation methods. It can be concluded that more experimental data are needed. The presented results may serve as a basic step in the development of the necessary critical assemblies. Although exact data are not presented in the paper, faster 44 energy group calculation gives almost the same results in similarity analysis in comparison to more complex 238 group calculation.

The results of the similarity assessment of ALLEGRO MOX and GFR 2400 cores confirmed the adequacy of ALLEGRO MOX starting core design for the development of the commercial gas cooled fast reactor design. The real operation of ALLEGRO MOX demonstrator unit may bring new specific knowledge to the field of fast neutron reactor physics and computational methods.

Finally, it was demonstrated that TSUNAMI-IP utility can play a significant role in the future fast reactor development in Slovakia and in the Visegrad region. Clearly a further R&D and strong effort should be carried out in order to receive more complex methodology consisting of more plausible covariance data and related quantities.

## ACKNOWLEDGMENTS

This study has been financially supported by the Slovak Research Development Agency No. APVV-0123-12.

## REFERENCES

- [1] P. Anzieu, R. Stainsby, K. Mikityuk: GIF Symposium in Paris, France (9-10 September, 2009)
- [2] SCALE: A Comprehensive Modeling and Simulation Suite for Nuclear Safety Analysis and Design, ORNL/TM-2005/39, Version 6.1.3, Oak Ridge National Laboratory, Oak Ridge, Tennessee (2011).
- [3] OECD Nuclear Energy Agency, "International Handbook of Evaluated Criticality Safety Benchmark Experiments", 2010.
- [4] E. Temesvári: ALLEGRO Core Specification, Deliverable D6.6.1-2, Issued by CER, 15.10.2014
- [5] W. van Rooijen and J. Kloosterman, "Closed Fuel Cycle and Minor Actinide Multirecycling", Science and Technology of Nuclear Installations, 2009.
- [6] K. L. Derstine: DIF3D 10.0, Argonne National Laboratory, Argonne, IL, 2011
- [7] M. B. Chadwick et al., "ENDF/B-VII.0: Next Generation Evaluated Nuclear Data Library for Nuclear Science and Technology", *Nuclear Data Sheets*, vol. 107, no. 12, 2006, p. 2931
- [8] D.H. Kim et al., "Validation Tests of the Multigroup Cross Section Libraries for Fast Reactors", PHYSOR -2006, Vancouver, BC, Canada, 2006

## I<sup>2</sup>S-LWR Activation Analysis of Heat Exchangers Using Hybrid Shielding Methodology With SCALE6.1

Mario Matijević, Dubravko Pevec, Radomir Ječmenica

University of Zagreb, Faculty of Electrical Engineering and Computing,

Department of Applied Physics

Unska 3, 10000 Zagreb, Croatia

mario.matijevic@fer.hr, dubravko.pevec@fer.hr, radomir.jecmenica@fer.hr

### ABSTRACT

The Integral Inherently Safe Light Water Reactor (I<sup>2</sup>S-LWR) concept developed by a team lead by Georgia Tech is a novel PWR reactor delivering electric power of 1000 MWe while implementing inherent safety features typically reserved for Generation III+ small modular reactors. The main safety feature is based on an integral primary circuit configuration, bringing together a compact core design with 121 fuel assemblies (FA), control rod drive mechanism (CRDM), 8 primary heat exchangers (PHE), 4 passive decay heat removal systems (DHRS), 8 pumps, and other integral components. A high power density core based on uranium silicide fuel (U<sub>3</sub>Si<sub>2</sub>) is selected to achieve high thermal power which is extracted with PHEs placed in the annular region between the barrel and the vessel. The compact and integrated design of I<sup>2</sup>S-LWR leads to activation of integral components, mainly made from stainless steel, so accurate and precise Monte Carlo (MC) simulations are needed to quantify potential dose rates to personnel during routine maintenance operation. This shielding problem is therefore very challenging, posing a non-trivial neutron flux solution in a phase space. This paper presents the performance of the hybrid shielding methodologies CADIS/FW-CADIS implemented in the MAVRIC sequence of the SCALE6.1 code package. The main objective was to develop a detailed MC shielding model of the I<sup>2</sup>S-LWR reactor along with effective variance reduction (VR) parameters and to calculate neutron fluence rates inside PHEs. Such results are then utilized to find the neutron activation rate distribution via <sup>60</sup>Co generation inside of a stack of microchannel heat exchangers (MCHX), which will be periodically withdrawn for the maintenance. <sup>59</sup>Co impurities are the main cause of (n,γ) radiative gamma dose to personnel via neutron activation since <sup>60</sup>Co has half-life of 5.27 years and is emitting high energy gamma rays (1.17 MeV and 1.33 MeV). The developed MC model was successfully used to find converged fluxes inside all 8 stacks of PHEs with respect to MC statistics using the FW-CADIS methodology. For that purpose the S<sub>N</sub> module Denovo, based on forward-adjoint transport theory, was used to find VR parameters (importance map and biased source) to effectively bias MC simulation. Further research is required to account for other activation pathways, i.e. isotopes of iron which may generate <sup>59</sup>Co through neutron activation and beta decay.

**Keywords:** I<sup>2</sup>S-LWR, PWR, shielding, Monte Carlo, activation, SCALE6.1, FW-CADIS.

### 1 INTRODUCTION

The SCALE6.1 code package [1] with hybrid shielding sequence MAVRIC based on CADIS and FW-CADIS methods developed at Oak Ridge National Laboratory (ORNL) was used for I<sup>2</sup>S-

LWR [2],[3],[4] modeling. Automatic, adjoint and mesh-based variance reduction preparation has nowadays become a standard when dealing with complex MC models posing deep penetration shielding problem. Such hybrid shielding method utilizes a two-step approach [5],[6]: (1) deterministic transport theory solution for the VR preparation (forward-adjoint multigroup fluxes); (2) accelerated and optimized MC solution using these VR parameters. A well known methodology CADIS [7] (Consistent Adjoint Driven Importance Sampling) from ORNL was developed for shielding problems involving answers in localized regions of phase-space such as point/region detectors. The discrete ordinates  $S_N$  solver Denovo [8] is used in CADIS for a quick approximation of space-energy adjoint flux which is subsequently used for VR construction: mesh importance map and biased source. This gives in turn effective biasing of MC simulation towards one specific, localized space region. With the computer hardware advance, it is now possible to handle huge MC models even on workstations, so a slight change of MC paradigm was introduced over the last decade. The MC method has nowadays become routine engineering tool for seeking not only (traditional) point detector results, as illustrated for the PCA benchmark [9] analyses in [10],[11], but radiation field in a sense of phase-space distributions, a characteristics historically typical to deterministic solvers. Following these computing trends, a generalization of the aforementioned ORNL method known as FW-CADIS [12] was developed to address real life MC models with uniformly small errors over large problem domains [13],[14].

Due to the integral configuration of  $I^2S$ -LWR, variation of the neutron flux by many orders of magnitude and complex spatial distribution is expected. To assert confidence in obtained results, shielding analyses were performed independently by two groups, at the Georgia Institute of Technology [15],[16] and at the University of Zagreb. Such parallel work in two independent groups allowed consistent cross-verification of the shielding results.

This paper presents results obtained at the University of Zagreb for the updated shielding model of the  $I^2S$ -LWR with reactor pressure vessel (RPV), integrated components and biological shield. More specifically, the performance of the SCALE6.1/MAVRIC code was investigated to find well converged neutron fluxes inside stacks of homogenized PHEs. The CADIS and FW-CADIS methodologies were used for the PHX irradiation problem, where the objective was to optimize the fast fluence rate ( $E > 1$  MeV) simultaneously at 8 PHX locations. The focus was on homogenized microchannel material to assess the MAVRICs effectiveness for deep penetration shielding problem and  $^{60}Co$  generation which presents activated gamma source. The integral configuration of the  $I^2S$ -LWR reactor introduces large modular units, such as PHEs, which will most likely be activated by neutrons during reactor operation. Such internal components, made from steel alloys, will introduce potential dose rates to working personnel during routine maintenance operation and periodical core refueling. Thus neutron activation via  $(n,\gamma)$  reactions inside heat exchangers needs to be well known because of its radiological importance. Such complex reactor configuration in shielding terms can only be addressed by modern MC codes with advanced VR schemes, utilizing a very detailed level of 3D geometry, which is necessary to capture fine space-energy physics (i.e. phase space) of the reactor model [17],[18].

This paper is organized as follows. Section 2 gives the description of the SCALE6.1 code package with focus on hybrid shielding capabilities in the MAVRIC sequence. Section 3 shows MAVRIC model of the  $I^2S$ -LWR reactor concept with computational parameters. Section 4 gives shielding analysis of the PHEs irradiation problem with different approaches (CADIS vs. FW-CADIS). Section 5 gives PHE activation analysis results. Section 6 gives discussion and conclusions while the referenced literature is given at the end of the paper.

## 2 THE SCALE6.1 CODE PACKAGE

The SCALE6.1 code package is still the latest production version of the ORNL's computing software platform developed in support for the U.S.NRC needs. In the present form the code has versatile ability to perform a whole spectrum of different calculations pertinent for nuclear

engineering activities in wide areas. Some of the possibilities are: criticality, shielding, radiation source term, burnup/depletion and nuclear decay, reactor physics, and sensitivity/uncertainty analyses using well established analytical sequences. The main shielding sequence is MAVRIC, based on the CADIS and FW-CADIS methods utilizing  $S_N$  solver Denovo for VR calculation and subsequent accelerated MC Monaco particle transport. The Denovo code is a fast and robust deterministic program utilizing Koch-Baker-Alcouffe transport sweep algorithm with Krylov multigroup iteration over the orthogonal meshes [8]. A variety of  $S_N$ -like options are available, such as numerical convergence criterion, spatial differencing, within-group acceleration, etc. Inherent flux solution positivity of Step Characteristic (SC) spatial differencing is the best and most important feature of Denovo, which in turn gives the numerical stability for Monaco code. When one looks for a solution in a form of multiple point detectors or over millions of spatial mesh cells, it is necessary to use FW-CADIS which demands for extra forward  $S_N$  run. Such forward solution is used for preparing inversely weighted adjoint source, placed in the region of users interest. For both CADIS and FW-CADIS the particle average weight is inversely related to adjoint flux value throughout phase-space, so locations of high importance (i.e. adjoint flux) will have low-weighted particles and vice versa. This implies that adjoint source location with optimized MC results will present spatial attractor for the source particles, giving "reasonable" MC results in-between regions. This approach was used in  $I^2S$ -LWR shielding calculations presented in the following chapters.

### 3 THE $I^2S$ -LWR MC MODEL WITH SCALE6.1/MAVRIC

The Integral Inherently Safe Light Water Reactor ( $I^2S$ -LWR) is an integral reactor concept developed by Georgia Institute of Technology (Georgia Tech) implementing inherent safety features and delivering an electric power of large PWR (1000 MWe) [2]. Integral primary circuit configuration is limited in size and thus requires a compact design and optimized layout. A novel high power density core based on silicide fuel is composed from 121 fuel assemblies inside reactor pressure vessel. Internal primary heat exchangers are grouped in 4 pairs (8 units in total), based on new micro-channel technology and placed in the annular region between the core barrel and RPV. The control rod drive mechanism and supporting plates are placed above the core. Total of four passive decay heat removal units are also placed outside the core in the annular region, giving passive natural recirculation in case of hypothetical transient scenario. The design details on other reactor vessel internals with CAD images can be found in available  $I^2S$ -LWR papers [3],[4]. The updated MAVRIC model of the  $I^2S$ -LWR is depicted in Figures 1 and 2, where one can notice the location of the PHEs.

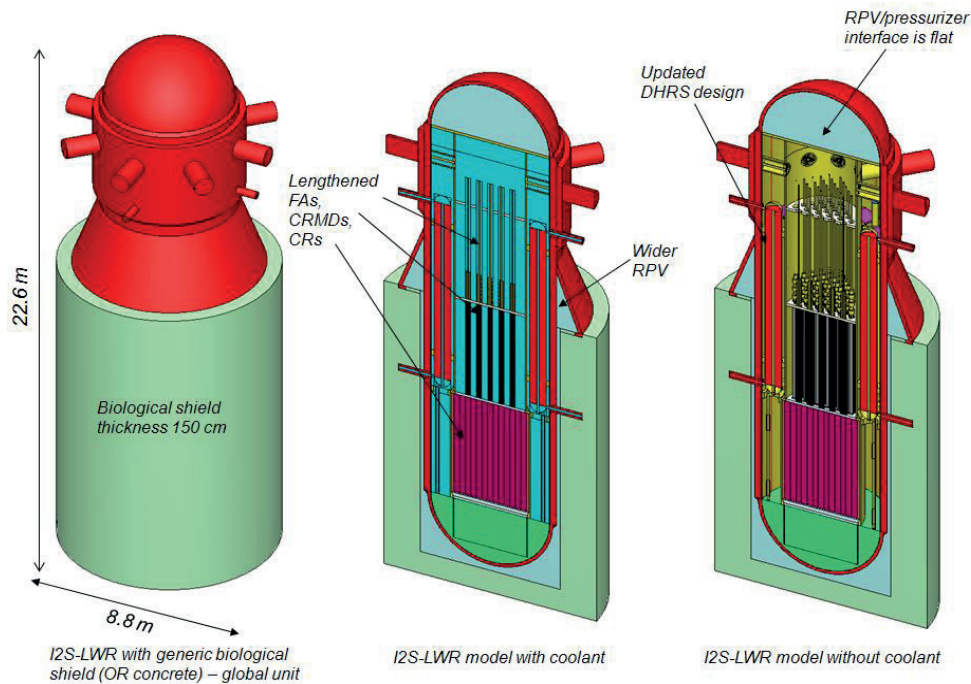


Figure 1: I<sup>2</sup>S-LWR MAVRIC model (with and without water)

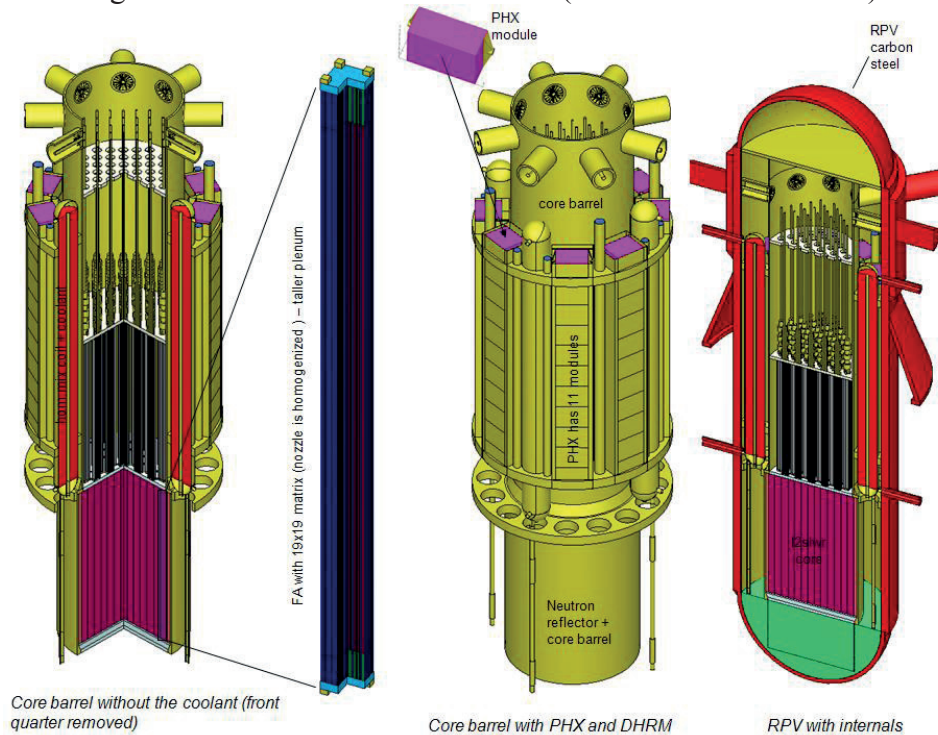


Figure 2: I<sup>2</sup>S-LWR MAVRIC model internals with PHEs

The SCALE6.1/MAVRIC sequence was used on a workstation with 32 GB of RAM and Core i-5 CPU. CADIS and FW-CADIS methods were explored for PHEs irradiation problem, where we calculated the neutron fast fluence rate ( $E > 1$  MeV) simultaneously at 8 PHE locations. The focus of calculations was on homogenized MCHX material inside PHEs, since that result is useful for later  $^{59}\text{Co}$  activation calculations. The adjoint source was thus set as PHE stacks with energy spectrum of fast neutron spectra. That spectra was later changed to  $^{59}\text{Co}(n,\gamma)^{60}\text{Co}$  cross section (in barns) for the purpose of activation calculation. The silicide fuel in heterogeneous FAs (FA depicted in Figure 2) was uniformly sampled with  $^{235}\text{U}$  fission spectrum and with nu-bar of 2.5. The total thermal power of 2850 MW was halved to mimic neutron spatial gradient on core periphery.

This shielding problem with multiple region tallies (i.e. PHE stacks) requires advanced VR parameters, since internal configuration and water coolant massively attenuate neutrons from the reactor core. The computational  $S_N$  mesh with  $S_{12}/P_1$  parameters completely covers global unit with  $135 \times 135 \times 310$  voxels. The Monaco was used with 4000 batches/15000 neutrons per batch and with mesh tally of  $100 \times 100 \times 260$  voxels. The same broad-group shielding library "v7\_27n19g" in SCALE6.1 was used for both Denovo and Monaco modules, derived from ENDF/B-VII.0 data [19]. One has to note that  $S_N$  solver accuracy for a hybrid shielding is not a paramount criterion, since only crude spatial flux profile is good enough for MC acceleration, but that knowledge is not a priori known. In order to benefit from a more accurate  $S_N$  solution without raising memory demanding  $S_N/P_N$  parameters, Denovo was used with macromaterial option which represents the voxel material as a volume-weighted mixture of elementary (user) materials. With "mmTolerance=0.005" option and about 20 elementary materials, the macromaterial table contained 1013 pseudo materials, which will mitigate rapid changes in  $S_N$  flux solution between neighboring cells. The macromaterial option in Denovo solver is a very elegant way to refine  $S_N$  solution without calling for extra memory by increasing  $S_N/P_N$  parameters.

#### 4 ANALYSIS OF PHE IRRADIATION PROBLEM

Two different shielding methodologies (CADIS and FW-CADIS) were investigated with MAVRIC sequence. The adjoint source was defined as PHE stacks with focus on MCHX material. The aim was to calculate a well converged fast fluence rate above 1 MeV, which is radiologically important issue. The mesh-based importance map (i.e. weight windows) derived from such adjoint source represent a "recipe" how to bias transport of source neutrons towards desired locations of PHEs. This transport biasing is in strict (i.e. consistent) accordance with source biasing governed by neutron importance function [1].

##### 4.1 CADIS solution for PHEs irradiation

The  $S_N$  representation of the CADIS adjoint source distribution is depicted in Figure 3. One can notice the absence of spatial gradient, which means constant adjoint source intensity in phase-space by definition of method [7]. Since I<sup>2</sup>S-LWR massively attenuates neutrons outside of the core, spatial shadowing is expected along axial direction of PHE stacks. The axial and radial reactor midplanes of fast neutron fluence rates are depicted in Figures 4 and 5. The detailed mesh tally covering one PHE is depicted on Figure 6. The adjoint  $S_N$  calculation took 1.88 h while final Monaco took 19.3 h.

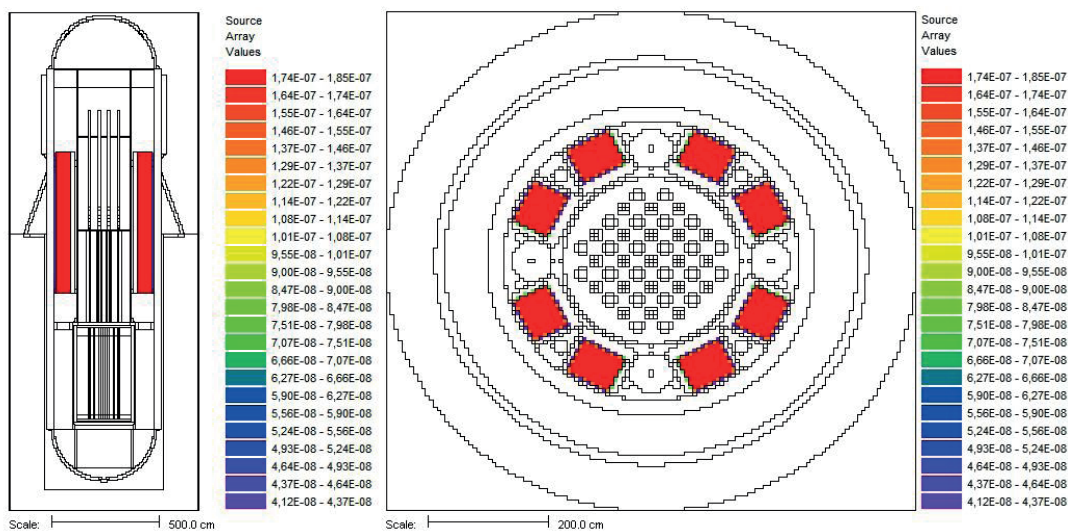


Figure 3: CADIS adjoint source through PHX stacks

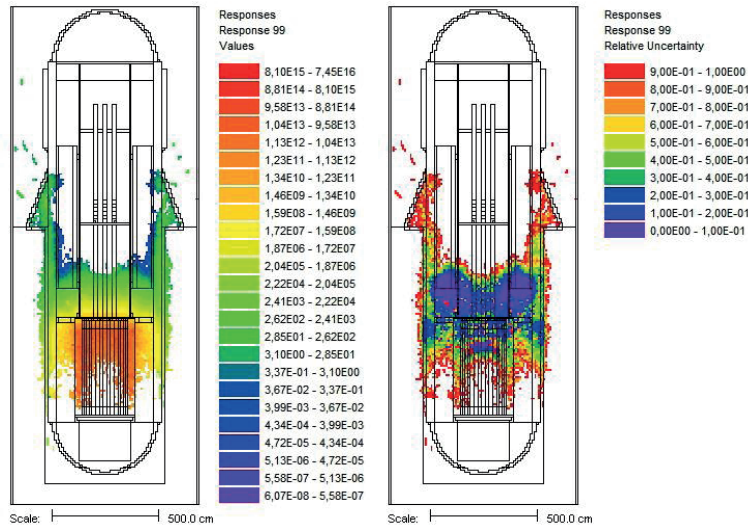


Figure 4: Monaco fast fluence rate ( $E > 1$  MeV) and relative errors

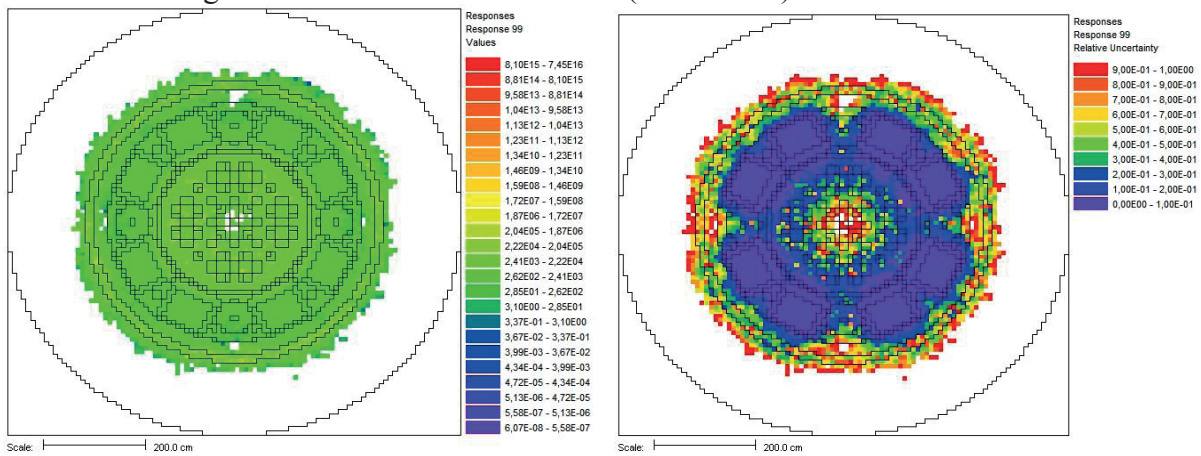


Figure 5: Monaco fast fluence rate ( $E > 1$  MeV) and relative errors (bottom of the first PHX module)

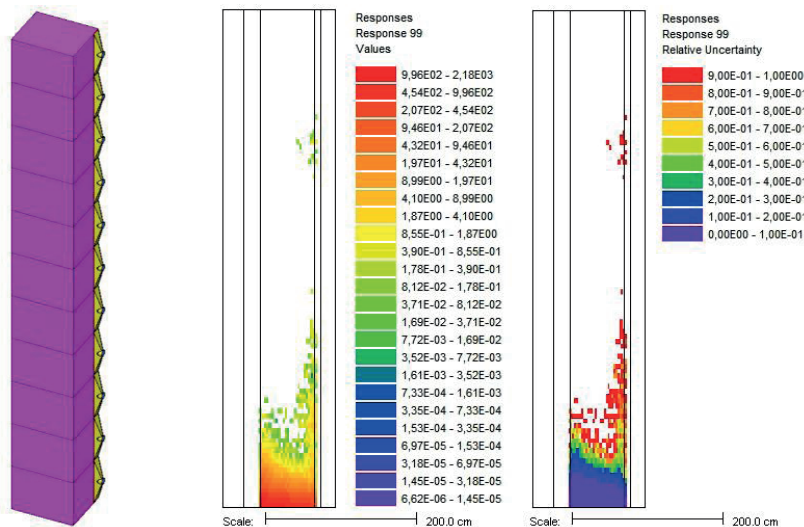


Figure 6: Monaco fast fluence rate ( $E > 1$  MeV) and relative errors inside PHE stack with 11 modules (total height 660 cm)

Maximum neutron fluence rate at the bottom of the first module is about  $2000 \text{ n/cm}^2/\text{s}$  and is falling off rapidly in axial direction. CADIS fluence indicates that  $S_N$  forward flux weighting is necessary step in adjoint source preparation, since only MC reasonable results can be found in the

lowest module closest to the core. No neutron transport can be found beyond the first heat exchanger module. Inherent characteristic of CADIS is spatial shadowing if adjoint source is not highly localized. The first layers of the bottom module will get all the neutrons and prevent deep penetration leaving upper white areas without results. This heavy shielding problem is a suitable test-case for the FW-CADIS methodology.

## 4.2 FW-CADIS solution for PHEs irradiation

From previous MAVRIC calculations it is evident that obtaining fast fluence rate simultaneously at 8 locations of PHE stacks is a significant shielding problem. The motivation for using FW-CADIS is an additional Denovo forward  $S_N$  calculation for redistribution of adjoint source in phase-space. Such DOAS (Distribution of Adjoint Source) is constructed by inverse weighting with integrated forward flux approximation, so that heavy-shielded regions with small neutron population in reality will receive MC particle "boost". With such approach the spatial shadowing in PHE stacks should be eliminated, giving well converged fluxes. The FW-CADIS adjoint source is depicted in Figure 7, covering all 8 PHE units [20]. The forward  $S_N$  calculation took 11 h, the adjoint  $S_N$  calculation took 1.77 h while final Monaco took 3.56 days.

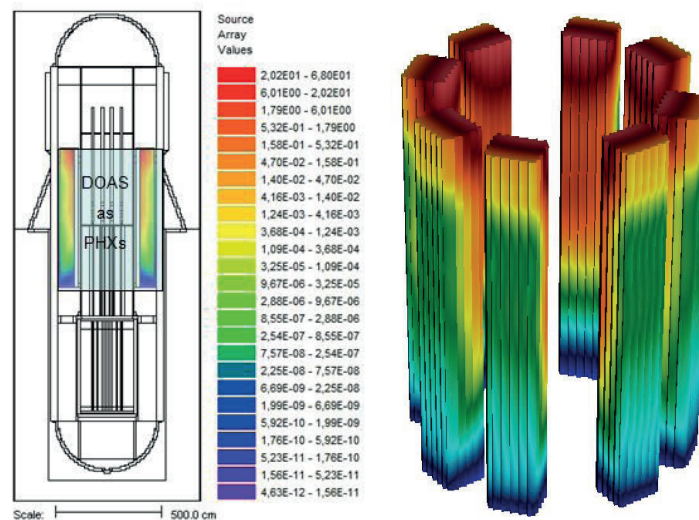


Figure 7: FW-CADIS adjoint source through PHX stacks

One can easily notice the effect of adjoint source redistribution in phase-space. This new adjoint source distribution is in accordance with the independent FW-CADIS calculation which predicts the region between CRDM plate and top CRDM plate as the most problematic one – the PHE stacks as an adjoint source are reinforced in that region. The satisfactory Monaco MC results with uniform relative errors throughout PHEs are depicted in Figure 8. Maximum fluence rate at the bottom of PHE stacks is similar to previous CADIS results.

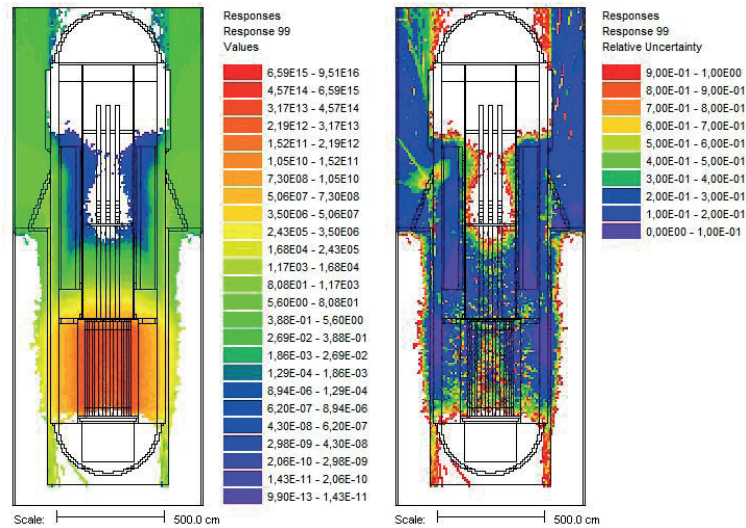


Figure 8: Monaco fast fluence rate with relative errors in  $y = 80$  cm plane using FW-CADIS

Fast fluence rate in some representative reactor axial planes are depicted in Figures 9, 10 and 11. One can notice gradually degradation of MC statistics from the bottom of PHE stacks (below 10% on average) to the top (below 20% on average). Regarding the model complexity and many orders of flux attenuation, one can say that satisfactory, well converged results were obtained in reasonable amounts of time, demonstrating capabilities of SCALE6.1/MAVRIC.

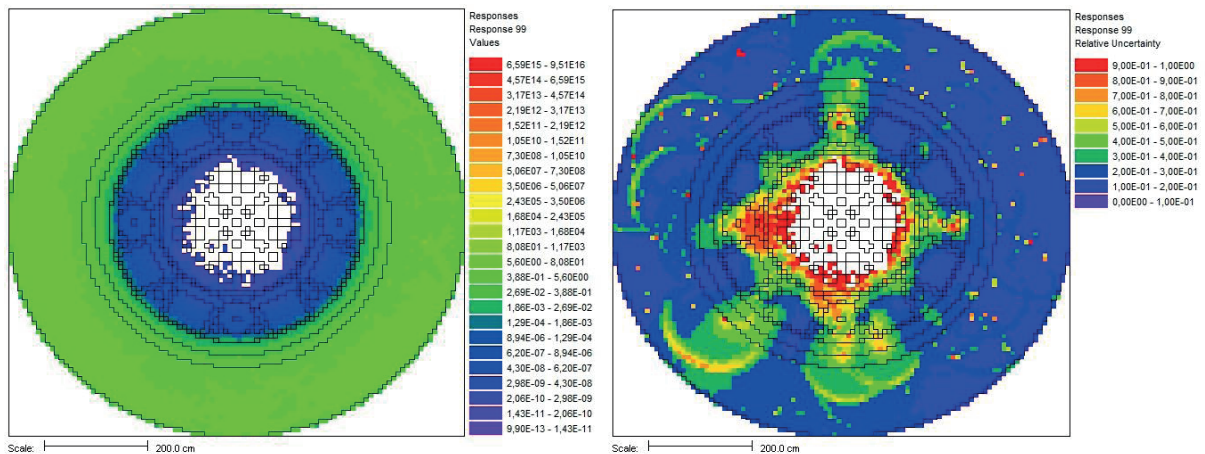


Figure 9: Monaco fast fluence rate with relative errors in PHE planes (top)

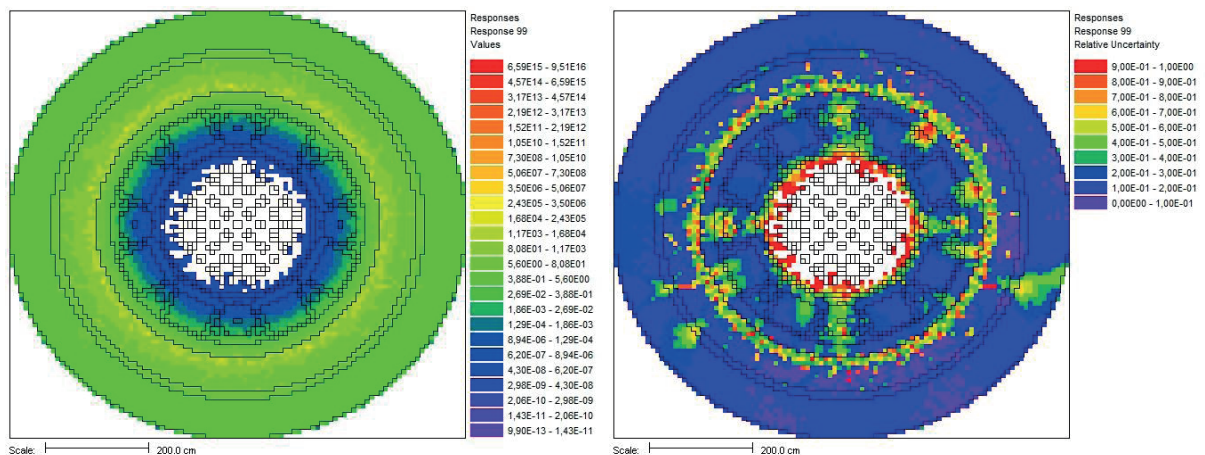


Figure 10: Monaco fast fluence rate with relative errors in PHE planes (midplane)

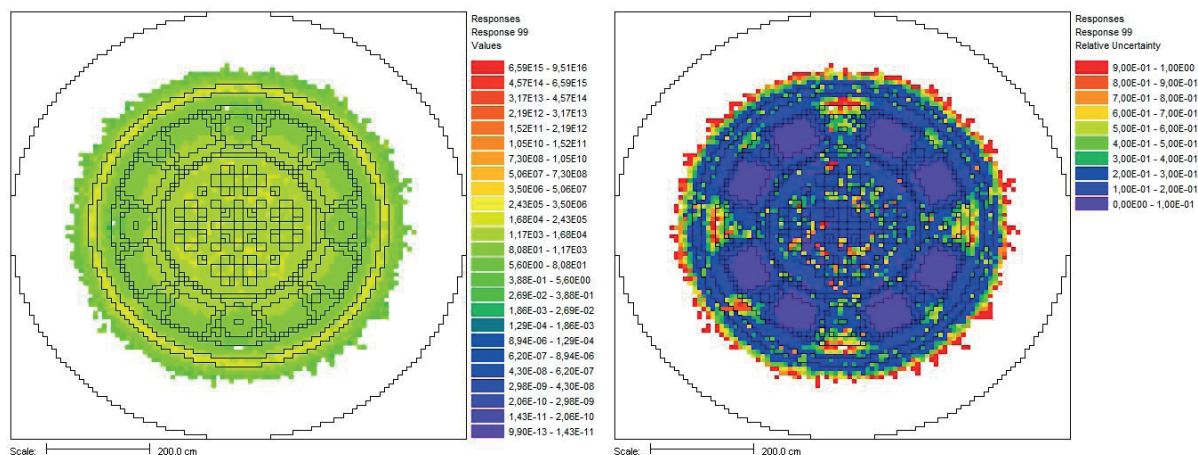


Figure 11: Monaco fast fluence rate with relative errors in PHE planes (bottom)

Important thing to notice is a fast neutron streaming and reflection off the biological shield and from the RPV skirt, giving local amplifications of the neutron field inside MCHX material. This is a major mechanism for activation heat exchangers axially. Since the RPV skirt is a necessary component to bear a reactor weight, suitable neutron absorber should be present in reality to prevent fast neutron leakage, such as additional layer of concrete. The fast neutrons reflection off the RPV skirt is depicted in Figure 12.

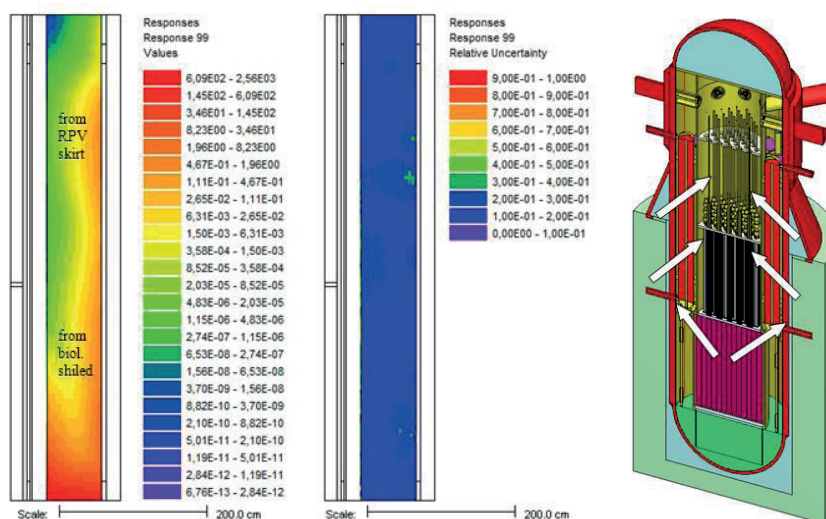


Figure 12: RPV skirt reflection impact on PHEs irradiation

## 5 PHE ACTIVATION CALCULATION

Neutron activation of cobalt impurities inside PHE's steel is a possible source of dose rates to maintenance personnel. The problematic  $^{60}\text{Co}$  is mostly produced via  $(n,\gamma)$  reaction on natural  $^{59}\text{Co}$ , coming as steel impurity, but other pathways exist from iron  $^{58}\text{Fe}$  transmuting again to  $^{59}\text{Co}$ . In this model the presumed level of stable isotope  $^{59}\text{Co}$  in MCHX area of PHEs was 0.05 w/o which is upper limit defined by AP1000 Design Control Document [21]. Fast neutron streaming will produce thermalized neutron spectrum interacting with  $^{59}\text{Co}$  inside PHEs, thus generating radioactive  $^{60}\text{Co}$  which is gamma emitter (1.17 MeV and 1.33 MeV) with half-life 5.27 years. The short half-life and high energy gamma ray emission makes the  $^{60}\text{Co}$  very important isotope to track during reactor operation. In this study a fixed neutron source was used at the moment, without time-dependent burnup effects inside reactor core. The continuous  $(n,\gamma)$  cross section [22] for  $^{60}\text{Co}$  formation is

shown in Figure 13, while multigroup representation in v7\_27n19g shielding library is shown in Figure 14.

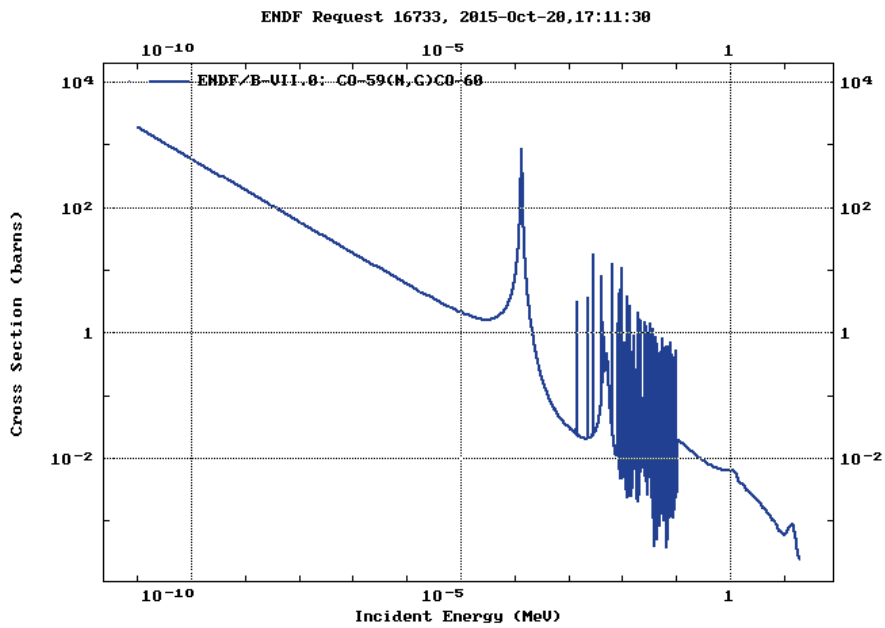


Figure 13: Cross section  $^{59}\text{Co}(n,\gamma)^{60}\text{Co}$  important for thermalized neutrons

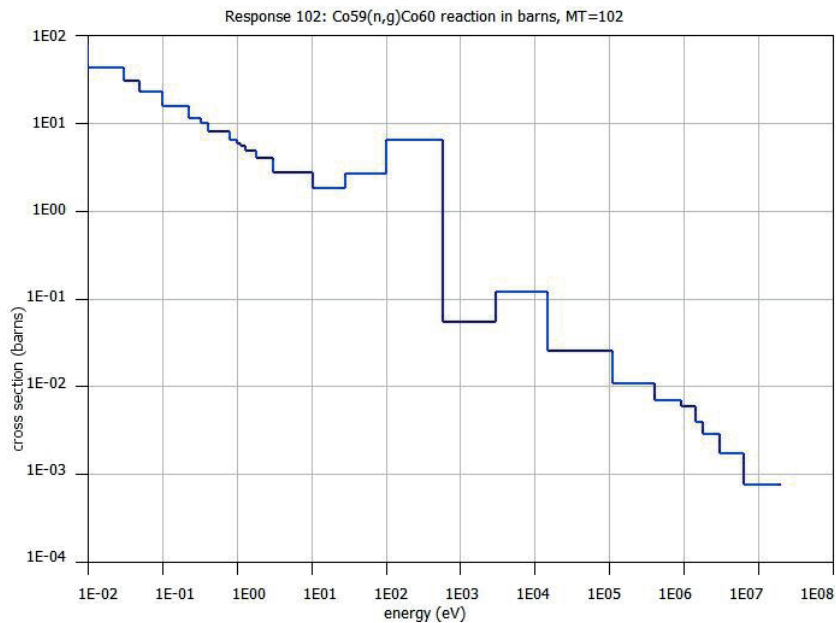


Figure 14: Multigroup representation of the  $^{59}\text{Co}(n,\gamma)^{60}\text{Co}$  cross section

The MAVRIC sequence was used with PHE stacks as adjoint sources with  $^{59}\text{Co}(n,\gamma)^{60}\text{Co}$  reaction as neutron spectrum (response function number MT=102). The forward  $S_N$  calculation took 11 h, the adjoint  $S_N$  calculation took 4 h while final Monaco took 2.3 days. The mesh tally results covering one of the PHE stack is shown in Figure 15.

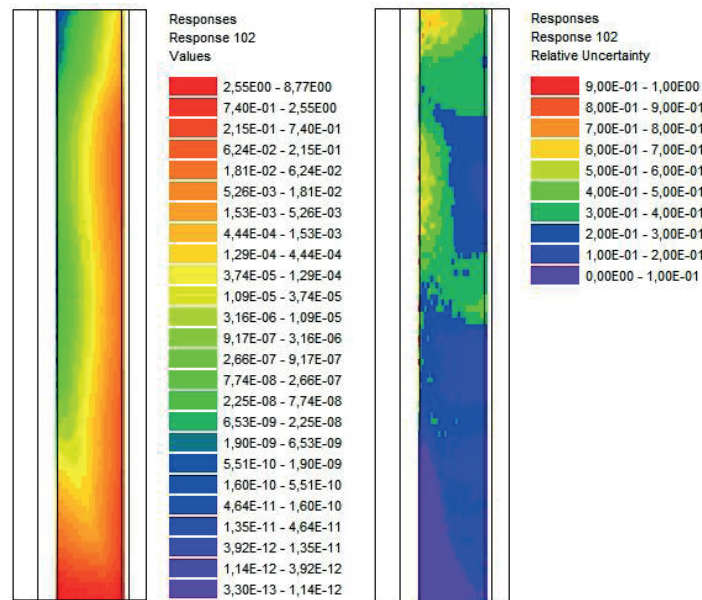


Figure 15: Reaction rates  $^{60}\text{Co}(n,\gamma)^{60}\text{Co}$  (n-barn/cm<sup>2</sup>/s) and relative errors in PHX stack

A detailed MCHX steel activation study was performed by Georgia Tech taking into account time-dependent decay and isotope activation tracking using ORIGEN-S depletion sequence [1],[23]. This method used a problem-dependent decay library with 1-group cross section derived from multigroup libraries weighted with correct neutron spectrum. Conclusion was that  $^{60}\text{Co}$  was 6 orders less than the initial impurity  $^{59}\text{Co}$ , but still emitting radiologically important high energy photons. Using such detailed gamma source in separate shielding calculations, where PHE was isolated in dry air, the maximum gamma dose rate obtained at the bottom of PHE was  $0.127\pm 0.3\%$  mrem/h [21].

## 6 DISCUSSION AND CONCLUSION

The updated shielding model of the I<sup>2</sup>S-LWR reactor was prepared to reflect the necessary design changes within the RPV and integrated components. The SCALE6.1/MAVRIC shielding sequence was used for simulation of the PHEs irradiation problem. The objective was to find fast neutron fluence and  $^{60}\text{Co}$  activation rates in all 8 PHE units simultaneously. The aforementioned hybrid  $S_N$ -MC methods (CADIS and FW-CADIS) were used to calculate radiation field distributions. The CADIS method demonstrated serious limitations in form of spatial shadowing inside PHEs, since adjoint source wasn't highly localized. This was a good example of a very difficult shielding problem which could be solved only by means of FW-CADIS and adjoint source redistribution in phase-space. The Monaco converged results over all 8 PHE stacks were found to be acceptable with respect to MC statistics. The specific task was to investigate the neutron activation in the MCHX part of PHE since it is a component likely to be handled during routine maintenance/refueling activities. Fast neutron streaming in the cavity region was identified as an important factor for MCHX activation, since the RPV skirt and biological shield reflect neutrons back inside the vessel. In reality a suitable neutron absorber will fill such void space beneath the RPV skirt. Such shielding calculations are important part of the overall I<sup>2</sup>S-LWR design process, since they identify potential radiological issues important for achieving ALARA (As Low As Reasonably Achievable) principle in practice.

## ACKNOWLEDGMENTS

This work was supported by the Croatian Science Foundation under the grant number 3522.

## REFERENCES

- [1] "SCALE: A comprehensive Modeling and Simulation Suite for Nuclear Safety and Design", ORNL/TM-2005/39, Version 6.1, June 2011. Available from Radiation Safety Information Computational Center at Oak Ridge National Laboratory as CCC-785.
- [2] B. Petrovic, "Integral Inherently Safe Light Water Reactor (I<sup>2</sup>S-LWR) Concept: Extending SMR Safety Features to Large Power Output", *Proc. International Congress on Advances in Nuclear Power Plants (ICAPP'2014)*, April 6-9, 2014, American Nuclear Society (2014).
- [3] B. Petrovic, "The Integral Inherently Safe Light Water Reactor", *Nuclear Engineering International*, 26-30 (2014).
- [4] M. J. Memmott, M. Marchese, B. Petrovic, "Integral Inherently Safe Light Water Reactor (I<sup>2</sup>S-LWR) Concept: Integral Vessel Layout", Proceedings of ICAAP 2014, Charlotte, USA, April 6-9 2014, Paper 14313.
- [5] G. I. Bell, S. Glasstone, "Nuclear Reactor Theory", Van Nostrand Reinhold Company, New York, 1970.
- [6] E. E. Lewis, W. F. Jr. Miller, "Computational Methods of Neutron Transport", American Nuclear Society, Illinois, 1993.
- [7] J. C. Wagner, A. Haghghat, "Automated Variance Reduction of Monte Carlo Shielding Calculations Using the Discrete Ordinates Adjoint Function", *Nuclear Science and Engineering*, 128, 1998, pp. 186-208.
- [8] T. M. Evans, A. S. Stafford, R. N. Slaybaugh, K. T. Clarno, "Denovo: A New Three-Dimensional Parallel Discrete Ordinates Code in SCALE", *Nuclear Technology*, 171, 2010, pp. 171-200.
- [9] I. Remec and F. B. K. Kam, "Pool Critical Assembly Pressure Vessel Facility Benchmark", Tech. Rep. NUREG/CR-6454, Oak Ridge National Laboratory, Oak Ridge, TN, USA (July 1997).
- [10] T. Flaspohler, B. Petrovic, "Validating Scale6.1/MAVRIC with Two Reactor Pressure Vessel Dosimetry Benchmarks", *Trans. Am. Nucl. Soc.*, **106**, (2012).
- [11] M. Matijević, D. Pevec, K. Trontl, "Modeling of the ORNL PCA benchmark using SCALE6.0 hybrid deterministic-stochastic methodology", *Science and Technology of Nuclear Installations*, 2013, DOI:10.1155/2013/252140.
- [12] J. C. Wagner, E. D. Blakeman, D. E. Peplow, "Forward-Weighted CADIS Method for Global Variance Reduction", *Transactions of American Nuclear Society*, 97, 2007, pp. 630-633.
- [13] J. C. Wagner, D. E. Peplow, S. W. Mosher, "FW-CADIS Method for Global and Regional Variance Reduction of Monte Carlo Radiation Transport Calculations", *Nuclear Science and Engineering*, 176, 2014, pp. 37-57.
- [14] J. C. Wagner, D. E. Peplow, S. W. Mosher, T. M. Evans, "Review of Hybrid (Deterministic/Monte Carlo) Radiation Transport Methods, Codes, and Applications at Oak Ridge National Laboratory", *Progress in Nuclear Science and Technology*, 2, 2011, pp. 808-814.

- [15] T. Flaspöehler, B. Petrovic, "Radiation Damage Assessment in the RPV of the Integral Inherently Safe Light Water Reactor (I<sup>2</sup>S-LWR)", *15th Intl. Symp. On Radiation Dosimetry (ISR-15)*, Aix-en-Provence, France, May 18-23, 2014; Published as a monograph/book *European Physics Journal Web of Conferences*, Vol. **106**, 03004 (2016).
- [16] B. Petrovic, T. Flaspöehler, "Feasibility of Ex-Core In-Vessel Nuclear Instrumentation for Integral Inherently Safe Light Water Reactor (I<sup>2</sup>S-LWR)", *Intl. Conf. on Applications of Nuclear Techniques (CRETE15)*, Crete, Greece, June 14-20, 2015.
- [17] M. Matijević, D. Pevec, K. Trontl, "Dose rates modeling of pressurized water reactor primary loop components with SCALE6.0", *Nuclear Engineering and Design*, 283, 2015, pp. 175-192, DOI: 10.1016/j.nucengdes.2014.07.013.
- [18] B. Petrovic, D. Hartmangruber, "Some considerations in devising effective SCALE6/MAVRIC models for large shielding applications", *Progress in Nuclear Science and Technology*, 2, 2011, pp. 427-431.
- [19] M. B. Chadwick, et al, "ENDF/B-VII.0: next generation evaluated nuclear data library for nuclear science and technology", *Nuclear Data Sheets* 107(12), 2006, pp. 2931-3060.
- [20] "VisIt: An End-User Tool For Visualizing and Analyzing Very Large Data", Lawrence Livermore National Laboratory, VisIt Getting Started Manual, February 2003, UCRL-MA-148506-REV-1, Version 2.7.3.
- [21] I<sup>2</sup>S-LWR Project Team: "FY2015\_Q2 Quarterly Progress Report (January-March 2015)", I<sup>2</sup>S-TR-15-04, Rev.0 (April 2015).
- [22] IAEA Nuclear Data Services. Website: <https://www-nds.iaea.org/>
- [23] I<sup>2</sup>S-LWR Project Team: "FY2015\_Q4 Quarterly Progress Report (July-September 2015)", I<sup>2</sup>S-TR-15-07, Rev.0 (October 2015).

## Spent Fuel Pool Dose Rate Calculations Using Point Kernel and Hybrid Deterministic-Stochastic Shielding Methods

**Mario Matijević, Radomir Ječmenica**

University of Zagreb, Faculty of Electrical Engineering and Computing,  
Department of Applied Physics, Unska 3, 10000 Zagreb, Croatia  
mario.matijevic@fer.hr, radomir.jecmenica@fer.hr

**Davor Grgić**

University of Zagreb, Faculty of Electrical Engineering and Computing,  
Department of Energy and Power Systems, Unska 3, 10000 Zagreb, Croatia  
davor.grgic@fer.hr

### ABSTRACT

This paper presents comparison of the Krško Power Plant simplified Spent Fuel Pool (SFP) dose rates using different computational shielding methodologies. The analysis was performed to estimate limiting gamma dose rates on wall mounted level instrumentation in case of significant loss of cooling water. The SFP was represented with simple homogenized cylinders (point kernel and Monte Carlo (MC)) or cuboids (MC) using uranium, iron, water, and dry-air as a bulk region materials. The pool is divided on the old and new section where the old one has three additional subsections representing fuel assemblies (FAs) with different burnup/cooling time (60 days, 1 year and 5 years). The new section represents the FAs with the cooling time of 10 years. The time dependent fuel assembly isotopic composition was calculated using ORIGEN2 code applied to the depletion of one of the fuel assemblies present in the pool (AC-29). The source used in Microshield calculation is based on imported isotopic activities. The time dependent photon spectrum with total source intensity from Microshield multigroup point kernel calculations was then prepared for two hybrid deterministic-stochastic sequences. One is based on SCALE6.2b3/MAVRIC (Monaco and Denovo) methodology and another uses Monte Carlo code MCNP6.1.1b and ADVANTG3.0.1. code. Even though this model is a fairly simple one, the layers of shielding materials are thick enough to pose a significant shielding problem for MC method without the use of effective variance reduction (VR) technique. For that purpose the ADVANTG code was used to generate VR parameters for the MCNP fixed-source calculation using continuous energy transport. ADVANTG employs a deterministic forward-adjoint transport solver Denovo which implements CADIS/FW-CADIS methodology. Denovo uses a structured, Cartesian-grid SN solver based on the Koch-Baker-Alcouffe parallel transport sweep algorithm across x-y domain blocks. This was our first application of ADVANTG/MCNP hybrid sequence for this type of calculation and the results were compared to SCALE/MAVRIC sequence which we regularly use for similar calculations. The comparison of gamma dose rates on different point detector locations (central above pool and at the top of pool periphery) showed a good agreement between Microshield (point-kernel) and deterministic-stochastic shielding methodologies for the cylindrical approximation of the pool geometry. More complicated cases for model with multi-source option and for cuboids showed very good agreement between SCALE/MAVRIC and ADVANTG/MCNP calculations.

**Keywords:** *pool dose rate, point kernel, hybrid deterministic-stochastic, Microshield, SCALE/MAVRIC, MCNP, ADVANTG, FW-CADIS.*

# 1 INTRODUCTION

Routine shielding calculations are typically performed using deterministic (SN) or Monte Carlo (MC) algorithms when the objective is to find well converged fluxes on point detectors or inside small localized regions. With a fast computer development the MC method was shifted from expensive and complicated approach to routinely used engineering tool. Modern shielding problems are frequently addressing geometry-large problems of obtaining the global radiation field which is a challenging task for a MC method with standard VR techniques. The hybrid shielding methodology, combining SN and MC approach, was developed especially for that purpose. It is based on forward and adjoint SN transport calculation to generate space-energy based variance reduction (VR) parameters for final (optimized) MC calculation.

This paper presents evaluation of spent fuel pool (SFP) radiation dose rates of the Krško Power Plant using conservative assumptions, simplified geometry and different computational shielding methodologies. Auxiliary structures such as transfer canal and cask loading area for underwater nuclear fuel handling and transport were not modeled at the moment. The SFP was represented with homogenized bodies, such as cylinders and cuboids, preserving original material fractions of uranium, iron, water, and dry-air. Such computational model is a fairly simple one, but effective layers of shielding materials are thick enough to pose a significant shielding problem for the MC method in general, without the use of advanced VR techniques. Comparison of such MC calculations using SN mesh-based VR parameters to more traditional point-kernel calculations was investigated for this simplified SFP.

The general objective was to compare dose rates on point detectors using modern hybrid shielding sequence with more traditional approach using point-kernel method. The specific task was to identify limiting gamma dose rates on wall mounted level instrumentation in case of significant loss of cooling water with presumption that the integrity of the fuel rods is not compromised. The comparison of gamma dose rates on different point detector locations (central above pool and at the top of pool periphery) showed a good agreement between Microshield (point-kernel) and deterministic-stochastic shielding methodologies for the cylindrical approximation of the pool geometry. More complicated cases for a model with multi-source option and for cuboids showed very good agreement between SCALE/MAVRIC and ANDVANTG/MCNP calculations.

This paper is organized as follows. Section 2 gives the description of the modern computational tools SCALE/MAVRIC and ADVANTG/MCNP implementing hybrid shielding methodologies. Section 3 gives the description of the Microshield point-kernel code. Section 4 shows SFP computational model with computational parameters. Section 5 gives shielding analysis of the SFP dose rates with different computational approaches. Section 6 gives discussion and conclusions while the referenced literature is given at the end of the paper.

## 2 HYBRID SHIELDING COMPUTATIONAL TOOLS

Both hybrid shielding tools SCALE/MAVRIC and ANDVANTG/MCNP use a deterministic forward-adjoint transport solver Denovo as a mean for automatic, adjoint and mesh-based VR generation. With such VR parameters the final (optimized) MC calculation is done. Denovo is implemented with Consistent Adjoint Driven Importance Sampling (CADIS) and Forward Weighted CADIS (FW-CADIS) methodologies, developed at Oak Ridge National Laboratory (ORNL). Denovo is a very fast and robust SN solver, working over a structured Cartesian-grids and based on the Koch-Baker-Alcouffe parallel transport sweep algorithm across x-y domain blocks. The most important feature is a multigroup flux positivity when using Step Characteristic (SC) spatial differencing option, which is paramount factor for numerical stability of the MC calculation.

## 2.1 The SCALE/MAVRIC shielding sequence

The SCALE6.2b3 code package is the beta version of the latest ORNL's computing software platform developed in support for the U.S. NRC needs. In the present form the code has versatile ability to perform a whole spectrum of different calculations pertinent for nuclear engineering activities in wide areas. Some of the possibilities are: criticality, shielding, radiation source term, burnup/depletion and nuclear decay, reactor physics, and sensitivity/uncertainty analyses using well established analytical sequences. The main shielding sequence is MAVRIC, based on the CADIS and FW-CADIS methods utilizing SN solver Denovo for VR calculation and subsequent accelerated MC Monaco particle transport. When one looks for a solution in a form of multiple point detectors or over millions of spatial mesh cells, it is necessary to use FW-CADIS which demands for extra forward SN run. Such forward solution is used for preparing inversely weighted adjoint source, placed in the region of users interest. For both CADIS and FW-CADIS the particle average weight is inversely related to adjoint flux value throughout phase-space, so locations of high importance (i.e. adjoint flux) will have low-weighted particles and vice versa. This implies that adjoint source location with optimized MC results will represent spatial attractor for the source particles, giving "reasonable" MC results in-between regions. This approach was used in SFP shielding calculations presented in the following chapters.

## 2.2 The ADVANTG/MCNP sequence

The ADVANTG3.0.1 is an automated tool for generating variance reduction parameters for fixed-source continuous-energy Monte Carlo simulations with MCNP code, based on approximate 3-D multigroup discrete ordinates adjoint transport solutions generated by Denovo. The VR parameters generated by ADVANTG consist of space-energy dependent weight-window bounds (WW) and biased source distributions (SB), which are output in formats that can be directly used with unmodified version of MCNP. ADVANTG has been applied to neutron, photon, and coupled neutron-photon simulations of real-world radiation detection and shielding scenarios. ADVANTG is compatible with all MCNP geometry features and can be used to accelerate cell tallies (F4, F6, F8), surface tallies (F1 and F2), point-detector tallies (F5), and Cartesian mesh tallies (FMESH). ADVANTG implements CADIS/FW-CADIS methods for generating VR parameters which provide a prescription for generating space-energy dependent WW targets and a consistent biased source distribution (SB cards in SDEF and WWINP file). The CADIS method was developed for accelerating individual tallies, whereas FW-CADIS can be applied to multiple tallies and mesh tallies. The MCNP6.1.1b [6] is a general-purpose Monte Carlo N-Particle code that can be used for neutron, photon, electron, or coupled neutron/photon/electron transport. The MCNP treats an arbitrary three-dimensional configuration of materials in geometric cells bounded by first- and second-degree surfaces and fourth-degree elliptical tori. For neutrons, all reactions given in a particular cross-section evaluation (such as ENDF/B-VI) are accounted for. Thermal neutrons are described by both the free gas and  $S(\alpha,\beta)$  models. Important standard features that make MCNP very versatile and easy to use include a powerful general source, criticality source, and surface source; both geometry and output tally plotters; a rich collection of variance reduction techniques; a flexible tally structure; and an extensive collection of cross-section data. Energy ranges are from 10<sup>-11</sup> to 20 MeV for neutrons with data up to 150 MeV for some nuclides, 1 keV to 1 GeV for electrons, and 1 keV to 100 GeV for photons. Pointwise cross-section data were used within MCNP. Auxiliary program MAKXSf prepares cross-section libraries with Doppler broadening.

## 3 POINT-KERNEL COMPUTATIONAL TOOL

MicroShield is a photon/gamma ray shielding and dose assessment program developed by Grove Software [14]. It is interactive, easy to use, and utilizes extensive input error checking.

Integrated tools provide material and source file creation, dose calculation and plotting of the results. The code has capability to model simple three-dimensional geometries, and the most simple situation is when specific source material is within cylindrical body oriented such that the axial length of the cylinder is in the positive y-axis direction, with the center of the cylinder's bottom placed at the origin. The appropriate layers of side shielding with their respective thicknesses can surround the cylinder in the radial and z-axis direction, or planar shields can be placed at cylinder top (y-axis direction).

MicroShield uses a method called Gauss quadrature for point-kernel numerical integration for integration calculations. In this method, the source is separated into a number of kernels determined by the quadrature order. In general, the greater the quadrature order, the more precise results will be output. The default values of quadrature orders used in the integrations are [14]: radial 10, circumferential 10, and axial 20. In this calculation the number of subdivisions is increased two times in each direction without significant change in calculated dose rates. The code calculates dose rates without and with build-up factors. Dose buildup factors depend on photon energy, the mean free path traveled by a photon in the material of consideration, geometry of the source, and geometry of the attenuating medium. Build-up is calculated automatically by the code for a shield material specified by the user (closest to the detector point). All results used for further comparison are results with build-up included.

#### 4 THE SFP COMPUTATIONAL MODEL

The realistic SFP walls are made of concrete (1.83 m thick) with stainless steel liner plates (0.6 cm thick). Normal water level in the pool is at elevation 115 m which is a 0-level on the water level indicator. The FA is standard 16x16 Westinghouse PWR with cross section 19.718x19.718 cm<sup>2</sup>. Maximum design enrichment is  $\leq 5$  w/o in <sup>235</sup>U and design licensed burnup is 60 GWD/MTU. The FAs are stored in the racks divided in old section (left) made of stainless steel and new section (right) made of borated high density stainless steel. The old and new sections accommodate 621 and 1073 cells, respectively. The total usable capacity of all racks installed in the SFP is 1694 cells. The detailed information about geometry configuration and other dimensions can be found in reference [13]. The MAVRIC model of the SFP with heterogeneous racks is depicted in Figure 1 while the Figure 2 gives the cross sectional view of the different unit cells in the old and the new section.

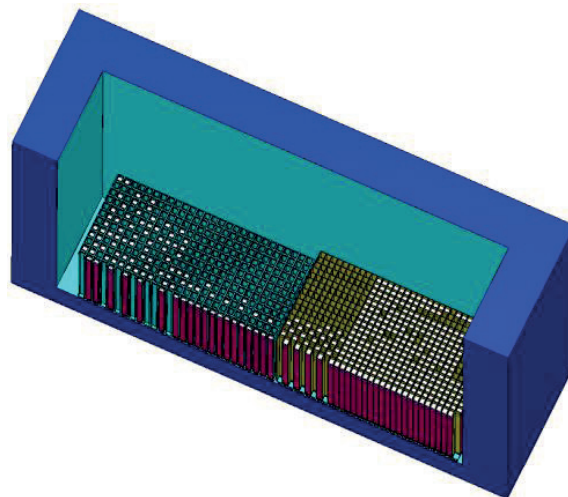


Figure 1: Front view of realistic Krško SFP model with old and new racks (water removed)

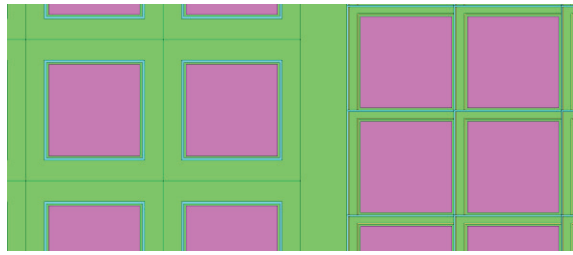


Figure 2: Unit cells of the old (left) and the new (right) section

Preliminary calculations were performed using described realistic model, but because still some important data are missing (mostly related to pool inventory), we have decided to first perform calculations using simplified model of the pool, and compare results against available point-kernel code results.

Simplified SFP computational model uses homogenized regions representing fuel assemblies (source), top shielding layer (homogenized FA nozzles and water), and varying layer of water above it. Locations of interest are at top pool elevation, in the middle of the pool and at pool periphery (potential location of wall mounted level detector). The old section has three additional subsections representing fuel assemblies (FAs) with different burnup/cooling periods of 60 days, 1 year and 5 years. The new section represents the FAs with the average cooling time of 10 years. The time dependent FA isotopic composition was calculated using ORIGEN2 code applied to the depletion of one representative FA present in the SFP (AC-29). The obtained isotopic activities were then used for the source preparation in the point-kernel code Microshield. The source in a form of time dependent, multigroup photon spectrum with known intensity was easy to implement in subsequent hybrid deterministic-stochastic sequences using gamma line spectra with known emission probabilities.

Average density of old SFP racks active part (621 rack locations occupied), with active height of 365.76 cm, was calculated to be 2.5 g/cm<sup>3</sup>. This section is composed of water (84.67%), UO<sub>2</sub> (14.83%) and other heavy metals (0.5%). The material selected in the model is uranium. Average density of new SFP racks active part (1073 rack locations occupied) with active height of 365.76 cm was calculated to be 4 g/cm<sup>3</sup>. This section is composed of water (73.2%), UO<sub>2</sub> (24.4%) and other heavy metals (8.4%). Above the fuel active height there is an additional 10 cm thick homogeneous layer (top nozzle and water) with an average density of 1.4 g/cm<sup>3</sup> (material selected in model is iron). Depending on calculation scenario there is a layer of water of varying thickness above it (results for 0 and 1 m of waters are presented). Rest of the model is filled with air (density 0.00122 g/cm<sup>3</sup>). The bottom cross section of the model is depicted in Figure 3.

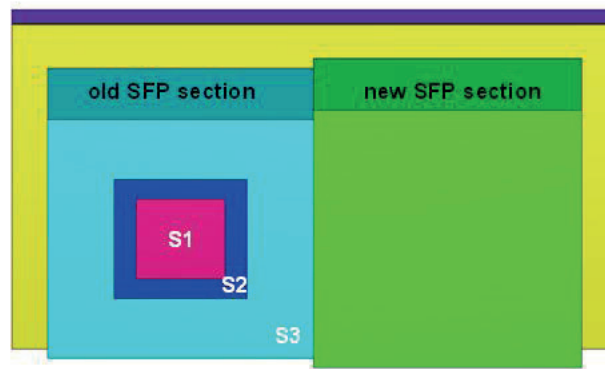


Figure 3: Bottom view of the simplified SFP sections: old (S1, S2, S3) and new section

In the middle of the old section there are 64 FAs (8x8) with the cooling time of 60 days (S1). They are surrounded by 80 FAs with the cooling time of 1 year (S2), which are again surrounded by

432 FAs with the cooling time of 5 years (S3). For these three sections the gamma intensities were  $2.38 \cdot 10^{18}$  phot/s,  $1.04 \cdot 10^{18}$  phot/s,  $1.91 \cdot 10^{18}$  phot/s, respectively. This gives total of 576 FAs in total of 621 rack positions. The new section gamma intensity was  $2.64 \cdot 10^{18}$  phot/s. Dose rates were calculated at the center and the edge of the old and new SFP sections at the elevation 1193.76 cm. The point-kernel model uses cylinder source having the same volume as homogenized cuboid. MC runs are performed for the same type of the geometry in order to be able to compare results. Additional MC runs using cuboids are performed to check influence of geometry change. Final multisource MC runs were beyond capabilities of point-kernel code and they are used for comparison between two MC codes. For simple geometry two detector points were used, one at the middle of the section and one at the side of the model, both at the top of the pool (11.93 m above bottom). For MC codes 4 point detectors were used with the following coordinates: new section middle Pd1 (0, 0, 1193.76), new section side Pd2 (0, 355.68, 1193.76), old section middle Pd3 (735.36, 0, 1193.76) and old section side Pd4 (735.36, 384.2, 1193.76). These point detectors represent point adjoint sources in hybrid shielding sequences with spectrum of ANSI-ANS-1977 gamma dose rates (built in function ID=9504 in rem/hr).

## 5 THE SFP DOSE RATES

Series of shielding calculations were performed for two basic cases: no water above the top FA nozzle and with 1 m of water layer above the top FA nozzle. Separate calculations were performed for each subsection of the old SFP section (S1, S2, S3) and for the new SFP section using cuboidal and cylindrical geometry representation of homogenized regions with the same volumes (i.e. material mass). Obtained MC dose rates with different geometry (cylinders vs. cuboids) and different MC codes showed small difference compared to Microshield. As an example, gamma dose rates for the SFP new section (cylindrical geometry) without and with water layer above the FA nozzle (Figure 4) are shown in Table 1. Gamma dose rates for the smallest old pool section (Figure 5) are shown in Table 3. The differences are reasonable, but it should be mentioned that point-kernel code predictions are not always conservative in terms of calculated gamma dose rate. MC code results for cuboid-based geometry are given in Table 2 and Table 4. The differences in calculated dose rates are small, usually giving lower doses in the middle and higher in the periphery of the model compared to cylinder case.

Table 1 SFP dose rates (rem/h) in the new section

Cylindrical geometry	ADVANTG/MCNP	SCALE/MAVRIC	Microshield
	0 m water layer	0 m water layer	0 m water layer
Pd1	$1.14 \cdot 10^3 \pm 0.15\%$	$1.17 \cdot 10^3 \pm 0.08\%$	$1.39 \cdot 10^3$
Pd2	$8.48 \cdot 10^2 \pm 0.19\%$	$8.68 \cdot 10^2 \pm 0.10\%$	$7.81 \cdot 10^2$
	1 m water layer	1 m water layer	1 m water layer
Pd1	$3.22 \pm 0.19\%$	$3.72 \pm 0.24\%$	5.99
Pd2	$2.07 \pm 0.25\%$	$2.38 \pm 0.27\%$	2.56

Table 2 SFP dose rates (rem/h) in the new section (MC geometry)

Cylindrical geometry	SCALE/MAVRIC	SCALE/MAVRIC
	0 m water layer	1 m water layer
Pd1	$1.17 \cdot 10^3 \pm 0.08\%$	$3.72 \pm 0.24\%$
Pd2	$8.68 \cdot 10^2 \pm 0.10\%$	$2.38 \pm 0.27\%$
Cubical geometry	0 m water layer	1 m water layer
Pd1	$1.15 \cdot 10^3 \pm 0.08\%$	$3.63 \pm 0.22\%$
Pd2	$9.17 \cdot 10^2 \pm 0.09\%$	$2.59 \pm 0.27\%$

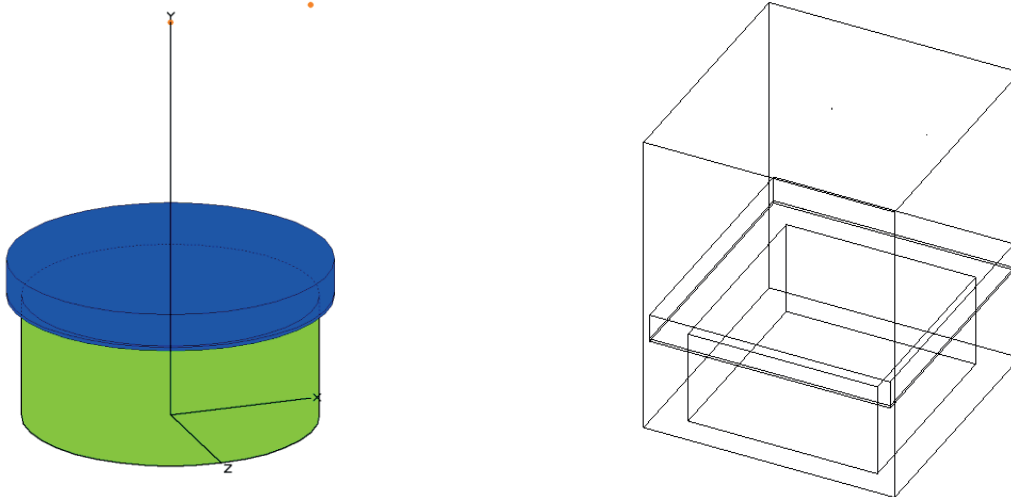


Figure 4: Microshield ( $r_{eq} = 4.25$  m) and SCALE geometries for the new SFP section

Table 3 SFP dose rates (rem/h) in the inner part of the old section

Cylindrical geometry	ADVANTG/MCNP	SCALE/MAVRIC	Microshield
	0 m water layer	0 m water layer	0 m water layer
Pd1	$3.14 \cdot 10^3 \pm 0.22\%$	$3.15 \cdot 10^3 \pm 0.08\%$	$3.11 \cdot 10^3$
Pd2	$2.61 \cdot 10^3 \pm 0.18\%$	$2.63 \cdot 10^3 \pm 0.09\%$	$2.79 \cdot 10^3$
	1 m water layer	1 m water layer	1 m water layer
Pd1	$1.53 \cdot 10^1 \pm 0.19\%$	$1.75 \cdot 10^1 \pm 0.15\%$	$1.66 \cdot 10^1$
Pd2	$8.80 \pm 0.19\%$	$1.02 \cdot 10^1 \pm 0.34\%$	8.48

Table 4 SFP dose rates (rem/h) in the inner part of the old section (MC geometry)

Cylindrical geometry	SCALE/MAVRIC	SCALE/MAVRIC
	0 m water layer	1 m water layer
Pd1	$3.15 \cdot 10^3 \pm 0.08\%$	$1.75 \cdot 10^1 \pm 0.15\%$
Pd2	$2.63 \cdot 10^3 \pm 0.09\%$	$1.02 \cdot 10^1 \pm 0.34\%$
Cubical geometry	0 m water layer	1 m water layer
Pd1	$2.72 \cdot 10^3 \pm 0.08\%$	$1.49 \cdot 10^1 \pm 0.23\%$
Pd2	$2.63 \cdot 10^3 \pm 0.08\%$	$1.40 \cdot 10^1 \pm 0.25\%$

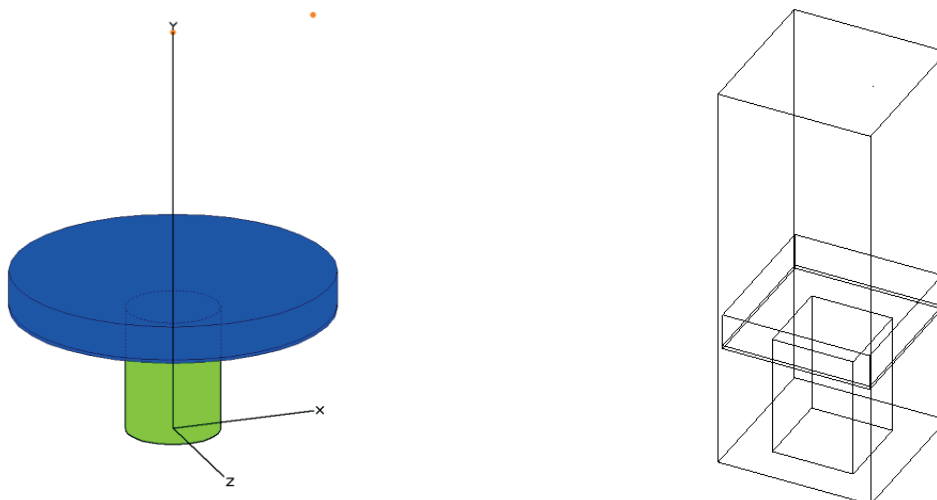


Figure 5: Microshield ( $r_{eq} = 1.36$  m) and SCALE geometries for the inner part of the old SFP section

The final, multisource model (Figure 6 and Figure 7) was prepared implementing all SFP sections and corresponding gamma sources. The obtained gamma dose rates are shown in Table 5 and Table 6. The difference in calculated dose rates is generally small. For the case with 1 m water layer SCALE predictions are always higher than MCNP predictions. For the case without water layer MCNP calculates higher dose rates for new section (old fuel) and SCALE for old section of the pool (new fuel). As expected, overall difference is larger when water layer is present.

The distribution of gamma dose rates and relative uncertainties in the MCNP model are shown in Figure 8 and Figure 9.

Table 5 SFP dose rates (rem/h) with ADVANTG/MCNP using multisource

Cuboidal geometry	SFP total dose rates (rem/h) with rel. error	
	0 m	1 m
Pd1	$5.81 \cdot 10^3 \pm 0.31\%$	$15.28 \pm 0.55\%$
Pd2	$4.52 \cdot 10^3 \pm 0.30\%$	$9.66 \pm 0.81\%$
Pd3	$2.92 \cdot 10^3 \pm 0.33\%$	$4.55 \pm 0.52\%$
Pd4	$2.36 \cdot 10^3 \pm 0.30\%$	$3.28 \pm 0.51\%$

Table 6 SFP dose rates (rem/h) with SCALE/MAVRIC using multisource

Cuboidal geometry	SFP total dose rates (rem/h) with rel. error	
	0 m	1 m
Pd1	$5.50 \cdot 10^3 \pm 0.07\%$	$16.35 \pm 0.08\%$
Pd2	$4.28 \cdot 10^3 \pm 0.04\%$	$10.33 \pm 0.08\%$
Pd3	$3.06 \cdot 10^3 \pm 0.06\%$	$5.65 \pm 0.16\%$
Pd4	$2.46 \cdot 10^3 \pm 0.05\%$	$4.06 \pm 0.13\%$

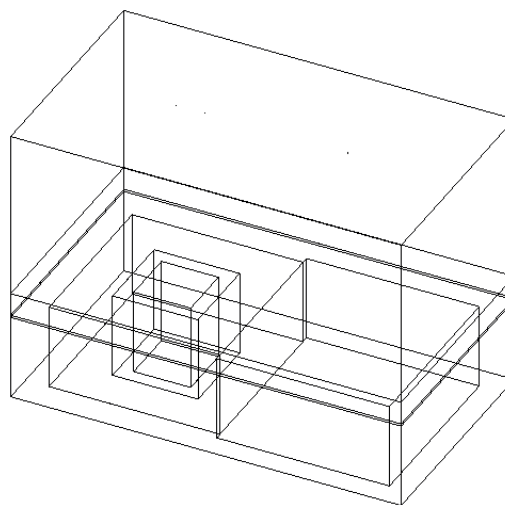


Figure 6: Simplified MC geometry of the whole pool

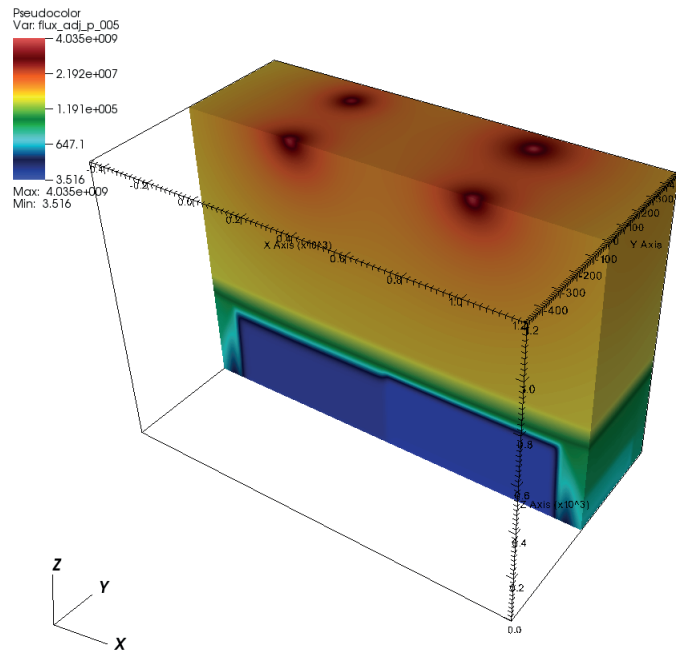


Figure 7: Point detectors as adjoint sources in hybrid shielding methodology using ADVANTG

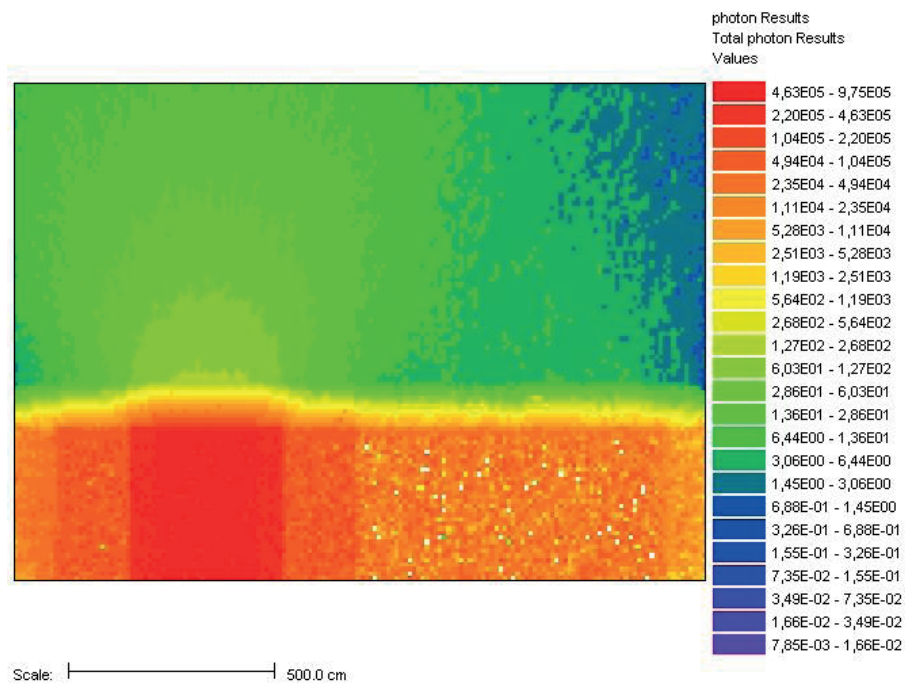


Figure 8: Mesh tally of gamma dose rates (rem/hr) calculated with MCNP6.1.1b

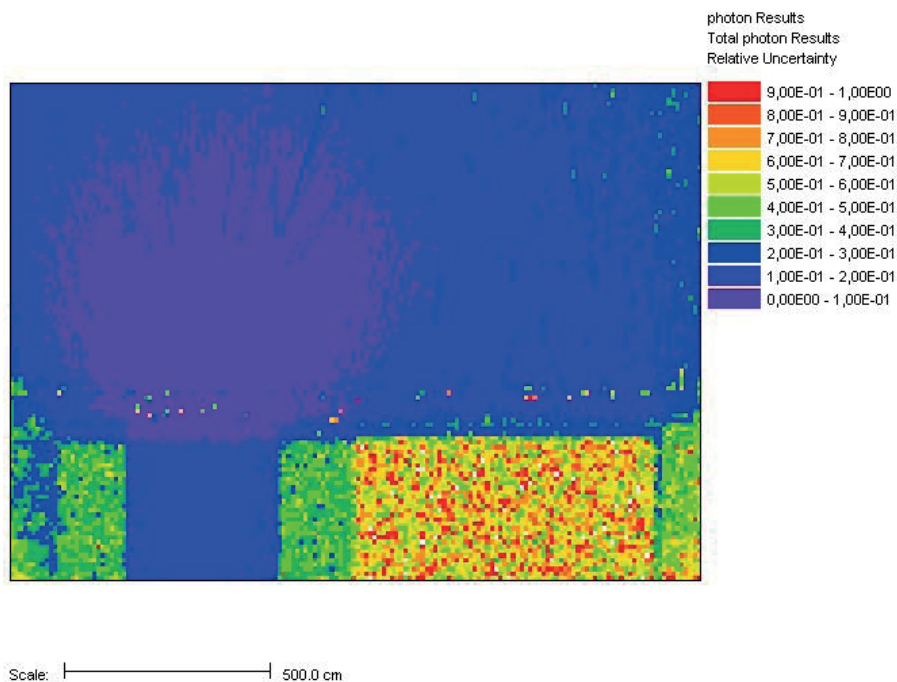


Figure 9: Mesh tally of gamma dose rates relative errors calculated with MCNP6.1.1b

## 6 DISCUSSION AND CONCLUSIONS

The shielding model of the simplified Krško Power Plant SFP was prepared based on homogenized regions representing old and new FA racks. Every section of the SFP was modeled with different gamma source spectrum based on ORIGEN2 depletion calculations of representative FA AC-29. The hybrid shielding sequences (SCALE/MAVRIC and ADVANTG/MCNP) were used for point detector calculations at center and edge of pool sections at elevation 1193.76 cm. Obtained gamma dose rates were compared to a more traditional approach using point-kernel code Microshield. A good agreement between point-kernel and MC calculations is obtained for cylindrical mono source cases, where both type of the codes should perform similarly. Still, it should be mentioned that point-kernel code predictions in terms of calculated dose rates are not always conservative. Different geometrical representation with cylinders or cuboids, gives similar results (slightly lower in the middle and slightly higher at the cuboid periphery compared to cylinder) if equivalence is performed properly. Both MC calculation sequences calculated similar dose rates for multisource whole SFP model. As expected the difference is larger when water layer is present. Monte Carlo codes with implemented VR are reasonable alternative to engineering point-kernel calculation if the geometry is starting to be more complicated.

## REFERENCES

- [1] "SCALE: A comprehensive Modeling and Simulation Suite for Nuclear Safety and Design", ORNL/TM-2005/39, Version 6.1, June 2011. Available from Radiation Safety Information Computational Center at Oak Ridge National Laboratory as CCC-785.
- [2] G. I. Bell, S. Glasstone, "Nuclear Reactor Theory", Van Nostrand Reinhold Company, New York, 1970.
- [3] E. E. Lewis, W. F. Jr. Miller, "Computational Methods of Neutron Transport", American Nuclear Society, Illinois, 1993.

- [4] J. C. Wagner, A. Haghghat, "Automated Variance Reduction of Monte Carlo Shielding Calculations Using the Discrete Ordinates Adjoint Function", *Nuclear Science and Engineering*, 128, 1998, pp. 186-208.
- [5] T. M. Evans, A. S. Stafford, R. N. Slaybaugh, K. T. Clarno, "Denovo: A New Three-Dimensional Parallel Discrete Ordinates Code in SCALE", *Nuclear Technology*, 171, 2010, pp. 171-200.
- [6] M. Matijević, D. Pevec, K. Trontl, "Modeling of the ORNL PCA benchmark using SCALE6.0 hybrid deterministic-stochastic methodology", *Science and Technology of Nuclear Installations*, 2013, DOI:10.1155/2013/252140.
- [7] J. C. Wagner, E. D. Blakeman, D. E. Peplow, "Forward-Weighted CADIS Method for Global Variance Reduction", *Transactions of American Nuclear Society*, 97, 2007, pp. 630-633.
- [8] J. C. Wagner, D. E. Peplow, S. W. Mosher, "FW-CADIS Method for Global and Regional Variance Reduction of Monte Carlo Radiation Transport Calculations", *Nuclear Science and Engineering*, 176, 2014, pp. 37-57.
- [9] J. C. Wagner, D. E. Peplow, S. W. Mosher, T. M. Evans, "Review of Hybrid (Deterministic/Monte Carlo) Radiation Transport Methods, Codes, and Applications at Oak Ridge National Laboratory", *Progress in Nuclear Science and Technology*, 2, 2011, pp. 808-814.
- [10] M. Matijević, D. Pevec, K. Trontl, "Dose rates modeling of pressurized water reactor primary loop components with SCALE6.0", *Nuclear Engineering and Design*, 283, 2015, pp. 175-192, DOI: 10.1016/j.nucengdes.2014.07.013.
- [11] M. B. Chadwick, et al, "ENDF/B-VII.0: next generation evaluated nuclear data library for nuclear science and technology", *Nuclear Data Sheets* 107(12), 2006, pp. 2931-3060.
- [12] "VisIt: An End-User Tool For Visualizing and Analyzing Very Large Data", Lawrence Livermore National Laboratory, VisIt Getting Started Manual, February 2003, UCRL-MA-148506-REV-1, Version 2.7.3.
- [13] "SFP DOSE RATE EVALUATION", NEK Report number NEK ESD-TR-11/11, Rev.0.
- [14] MicroShield User's Manual, Version 10, Grove Software, 2014.

## Nuclear and thermal hydraulic calculation of a representative I<sup>2</sup>S-LWR first core

**Radomir Ječmenica, Davor Grgić, Mario Matijević**

University of Zagreb Faculty of Electrical Engineering and Computing  
Unska 3, 10000 Zagreb, Croatia  
radomir.jecmenica@fer.hr, davor.grgic@fer.hr, mario.matijevic@fer.hr

**Bojan Petrović**

Georgia Institute of Technology, Nuclear and Radiological Engineering  
770 State St., Atlanta, GA 30332-0745, USA  
bojan.petrovic@gatech.edu

### ABSTRACT

The Integral Inherently Safe Light Water Reactor (I<sup>2</sup>S-LWR) concept developed by Georgia Tech is a novel PWR reactor delivering electric power of 1000 MWe while implementing inherent safety features typical for Generation III+ small modular reactors. The main safety feature is based on integral primary circuit configuration, bringing together compact design of the reactor core (121 fuel assembly), control rod drive mechanism (CRDM), 8 primary heat exchangers (PHE), 4 passive decay heat removal systems (DHRS), 8 pumps, and other integral components. A high power density core based on silicide fuel and APMT (FeCrAl) stainless steel cladding is selected to achieve a high thermal power. Initial representative first core nuclear design is proposed by Westinghouse. Full core 3D depletion calculation was performed using PARCS code. The cross section library is prepared using FA2D code and verified using Polaris sequence from SCALE 6.2 beta5. The axial and radial reflectors are assumed to be homogeneous water-APMT mixtures. The axial reflectors are both assumed to be 12 inch (30.48 cm) sections composed of 30% APMT steel by volume. The radial reflector is assumed to be 90% APMT steel by volume. The reflector constants were calculated using SCALE TRITON sequence. The thermal hydraulic part of the model is based on COBRA subchannel code coupled to PARCS code. Initial depletion calculation is based on one thermal hydraulics channel per fuel assembly approach. The hot fuel assembly is determined using separate pin-by-pin COBRA subchannel model and pin power reconstruction data from PARCS. The objective of the paper is demonstration of LWR design methodology applicability to silicide fuel and identification of possible improvements in the first core design.

**Keywords:** I<sup>2</sup>S-LWR, core design, PARCS, COBRA, SCALE, FA2D

### 1 INTRODUCTION

The Integral Inherently Safe Light Water Reactor (I<sup>2</sup>S-LWR) concept [1][2] developed by team led by Georgia Tech is a novel PWR reactor delivering electric power of 1000 MWe while implementing inherent safety features typical for Generation III+ small modular reactors. The main safety feature is based on integral primary circuit configuration, bringing together compact design of the reactor core (121 fuel assembly), control rod drive mechanism (CRDM), 8 primary heat exchangers (PHE), 4 passive decay heat removal systems (DHRS), 8 pumps, and other integral

components. The objective of the paper is to calculate 3D fuel depletion for one of the proposed 1<sup>st</sup> core concepts.

## 2 I<sup>2</sup>S-LWR FIRST CORE CONFIGURATION

The I<sup>2</sup>S-LWR core contains 121 fuel assembly (FA) with active height of 365.76 cm which is typical value for standard 2-loop PWRs [3]. The major difference compared to standard PWR FA is its higher power rating, giving I<sup>2</sup>S-LWR core thermal power of 2850 MWth. To accommodate such power increase, specific design features are introduced, such as 19x19 square pitch lattice, U<sub>3</sub>Si<sub>2</sub> fuel and advanced stainless steel cladding and grids. The denser FA matrix with increased heat transfer surface area will provide slightly higher average heat flux compared to typical 4-loop PWR core which benefits DNB performance. Novel, high-conductivity, silicide fuel allows a reasonable margin against fuel melting during hypothetical accidents giving core dimensions compatible for integral configuration (Table 1).

Silicide fuel was selected as the primary option for several reasons, most important are higher heavy metal (H/M) ratio (about 17%) and higher thermal conductivity, compared to UO<sub>2</sub> fuel. These characteristics are enhancing fuel cycle and operational performance. Current design includes smaller pellet-gap compared to initial one (enabled by better understanding of fuel swelling under irradiation) and elimination of inner voids in pellets (Table 2). Safety considerations dictate the choice of advanced cladding steels (APMT), which must withstand high temperature (above 1200 °C) steam-water mixture without high oxidation rates and hydrogen generation customary for zirconium alloys. The corrosion resistance can be enhanced from properly tailoring the steel composition, together with mechanical properties (even compared to Zircaloy) and higher thermal conductivity under irradiation. On the other hand, some of the isotopes in the steel (especially Fe and Cr) have high neutron absorption cross-sections which lead to a significant reactivity penalty compared to Zr. Silicon carbide cladding has better neutronic properties than Zr and represents the secondary option for the I<sup>2</sup>S-LWR cladding material.

Table 1. Fuel property comparison: U<sub>3</sub>Si<sub>2</sub> vs UO<sub>2</sub>

Fuel	U <sub>3</sub> Si <sub>2</sub>	UO <sub>2</sub>
Theoretical density (TD) (g/cm <sup>3</sup> )	12.2	10.98
HM TD (g/cm <sup>3</sup> )	11.3	9.68
Thermal conductivity (W/mK)	9 - 20 (300 - 1200 °C)	5 - 2 (300 - 2000 °C)
Specific heat (J/kgK)	230 - 320 (300 - 1200 °C)	280 - 440 (300 - 2000 °C)
Melting point (unirradiated) °C	1665	2840

Table 2. Fuel assembly main characteristics

Lattice type	19×19, square
Fuel/Cladding material	U <sub>3</sub> Si <sub>2</sub> / APMT
Fuel rods per assembly	336
Fuel rod outer diameter (mm)	9.144
Cladding thickness (mm)	0.406
Pellet-clad gap width (mm)	0.1143
Pellet outer diameter (mm)	8.1026
Fuel rod pitch (mm)	12.116
Assembly pitch (mm)	231

Most of the core design effort within I<sup>2</sup>S-LWR project was spent on equilibrium core. We have decided to analyze first core design. Initial representative first core nuclear design is proposed by Westinghouse [3]. Full core 3D depletion calculation was performed using PARCS code [4]. The cross section library is prepared using FA2D code and verified using Polaris sequence from SCALE 6.2 beta5. Small benchmarking at Fuel Assembly (FA) level has been performed using SCALE TRITON and Polaris [5], SERPENT 2.1 [6], and FA2D. Both infinite multiplication factor and cross section data were reasonably similar (Figure 1).

The axial and radial reflectors are assumed to be homogeneous water-APMT mixtures. The axial reflectors are both assumed to be 12 inch (30.48 cm) sections composed of 30% APMT steel by volume. The radial reflector is assumed to be 90% APMT steel by volume. The reflector constants were calculated using FA2D and SCALE TRITON sequence.

The thermal hydraulic part of the model is based on COBRA subchannel code coupled to PARCS code. Initial depletion calculation is based on one thermal hydraulics channel per fuel assembly approach.

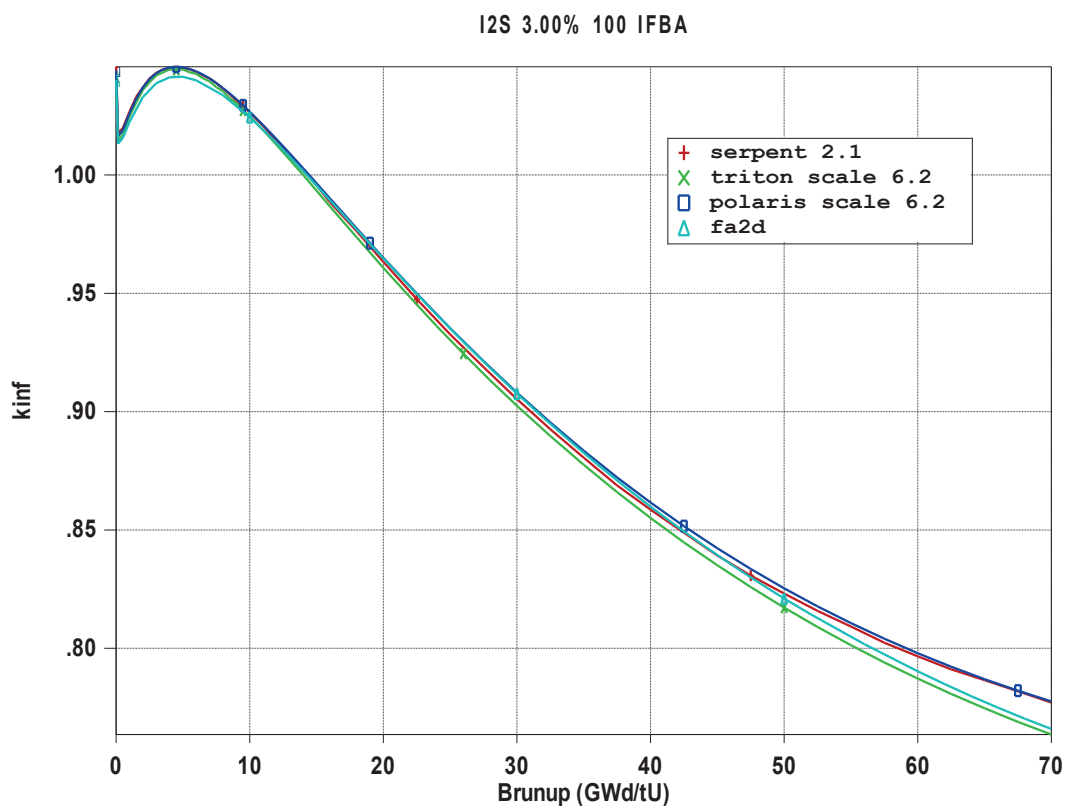


Figure 1: Fuel assembly calculation and cross section preparation benchmarking

Initial core loading scheme is shown in Figure 2. FAs labeled with A have enrichment of 2.5%, labeled with B have enrichment 3.0% and assemblies labeled with C have enrichment 4.0%. All fuel assemblies have axial blankets enriched at 2.5%. IFBA burnable absorbers were used in the core design (batch A has 84 IFBAs, batch B has 100 and 156 IFBAs, and batch C has 100 IFBAs). Classical Westinghouse scheme with IFBA layer in the middle of the assembly was initially used (6-6-120-6-6 inches), Figure 3. Due to higher than wanted Axial Offset (AO) values the IFBA layer is shifted toward bottom for 6 inches, and then optimization is performed for additional 6 inches IFBA segment at the top. If we take geometry shown in Figure 3 as a reference it is possible to add additional 6 inches to the top of shifted 120 inches layer and then perform sensitivity calculation by decreasing that length in steps of 1 inch from 6 inches to 0 inch. That was done in our calculation uniformly across all IFBA FAs. In original WEC design additional 2 inches were present for 2.5%

84-IFBA and 3.0% 100-IFBA assemblies, and additional 4 inches for 3.0% 156-IFBA and 4.0% 100-IFBA assemblies (that was obviously result of additionally performed nuclear peaking factor optimization done by WEC).

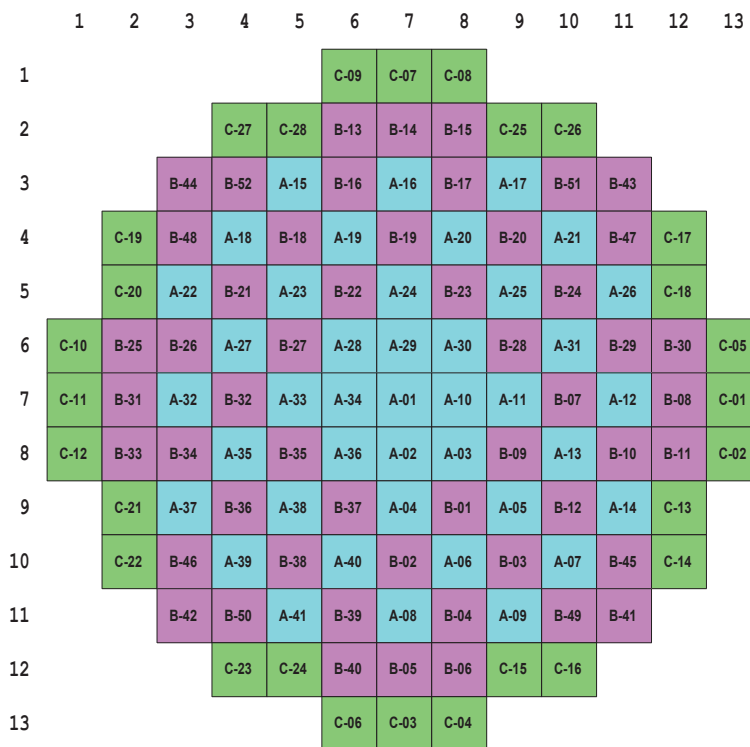


Figure 2: I<sup>2</sup>S first core loading pattern

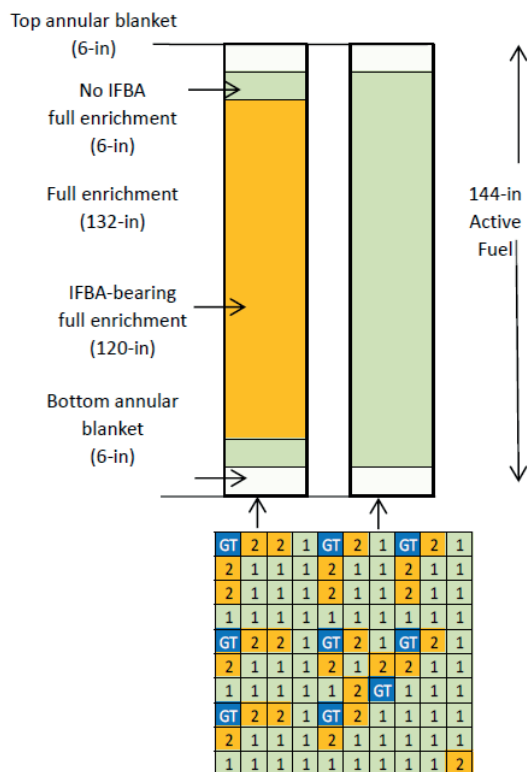


Figure 3: Axial representation of Westinghouse IFBA and non-IFBA fuel assembly

### 3 ANALYSIS AND RESULTS

Initial PARCS calculation was performed for loading scheme proposed by Westinghouse, but with classical symmetric IFBA layer. In following figures that case was labeled with *ori*. For all additional cases two numbers were used to describe analyzed configuration. First number is length of node without IFBA layer at original FA enrichment and second number is length of node with IFBA layer (cases **6-6**, **5-7**, **4-8**, **3-9**, **2-10**, **0-12**). The sum of two numbers is always 12 inches. The case **6-6** is with additional 6 inches IFBA layer (total length 126 inches) and **0-12** is case with shift of original 120 inches IFBA layer for 6 inches down. Label *wec* means Westinghouse results are used when available.

Boron concentration versus burnup is shown in Figure 4. It is clear that small variation in IFBA layer length and position has limited influence on overall reactivity of the core. In addition results compare reasonably with WEC results. In Figure 5, showing AO versus burnup, it is clear that AO is very sensitive to variation in IFBA layer length and position. AO can be very negative (-20%) for classic central IFBA layer or very positive (+25%) if IFBA layer is just shifted toward bottom. Our case **4-8** is close to WEC case with variation of IFBA layer length depending on position, enrichment and number of IFBAs.

The results for total and axial peaking factors are shown in Figure 6 and Figure 7. The variation in IFBA layer length again has significant influence on power peaking values both before and after IFBA depletion. The differences between our **4-8** and *wec* case are small for axial peaking factor and rather large, early in cycle, for total peaking factor. That is due to radial peaking factor that is additionally optimized in WEC case by variation of IFBA length depending on enrichment and number of IFBAs. It should be mentioned that radial core peaking factor (not shown) is rather insensitive to the described variation in IFBA layer.

The corresponding relative axial power distribution for selected cases for 0.15 and 13 GWd/tU are shown in Figure 8. The influence of IFBA axial variation is significant before IFBA depletion and small later. Using the proposed scheme it is possible to keep it within allowable range.

Rather symmetric radial power and burnup distributions at EOL conditions are presented in Figure 9 and Figure 10. The temperature of fuel rod centre line (one average rod per FA) is shown at EOL in Figure 11. It is as expected lower than for UO<sub>2</sub> fuel due to better thermal conductivity of used fuel. The results of pin power reconstruction calculation for beginning of life (0.15 GWd/tU, first core quadrant) and for end of life (13 GWd/tU, forth core quadrant) are shown in Figure 12 and Figure 13, respectively. Rather large variation in power distribution is initially present, but within allowable values. For end of life conditions due to depletion of both fuel and IFBA usual, more flat, distribution is obtained. The obtained pin powers can be used for detailed hot fuel assembly calculation in COBRA subchannel code.

### 4 CONCLUSION

The objective of the paper is to demonstrate applicability of our LWR design methodology to silicide fuel and to identify possible improvements in the first core design. We were able to apply classical PWR core design calculation methodology, with some adjustments of fuel and cladding thermal properties, to I<sup>2</sup>S-LWR calculation. Obtained length of the cycle and most of the calculated core parameters are acceptable for an initial first core development. Axial power distribution was proven to be sensitive to change in initial core axial properties. The variation in IFBA layer position and size, proposed by WEC, can be an effective way to control axial power shape, but some additional optimization will be needed. Another observation, as expected, is a significant influence of steel reflector on overall core reactivity, and need for careful preparation of reflector cross sections.

I2S C01

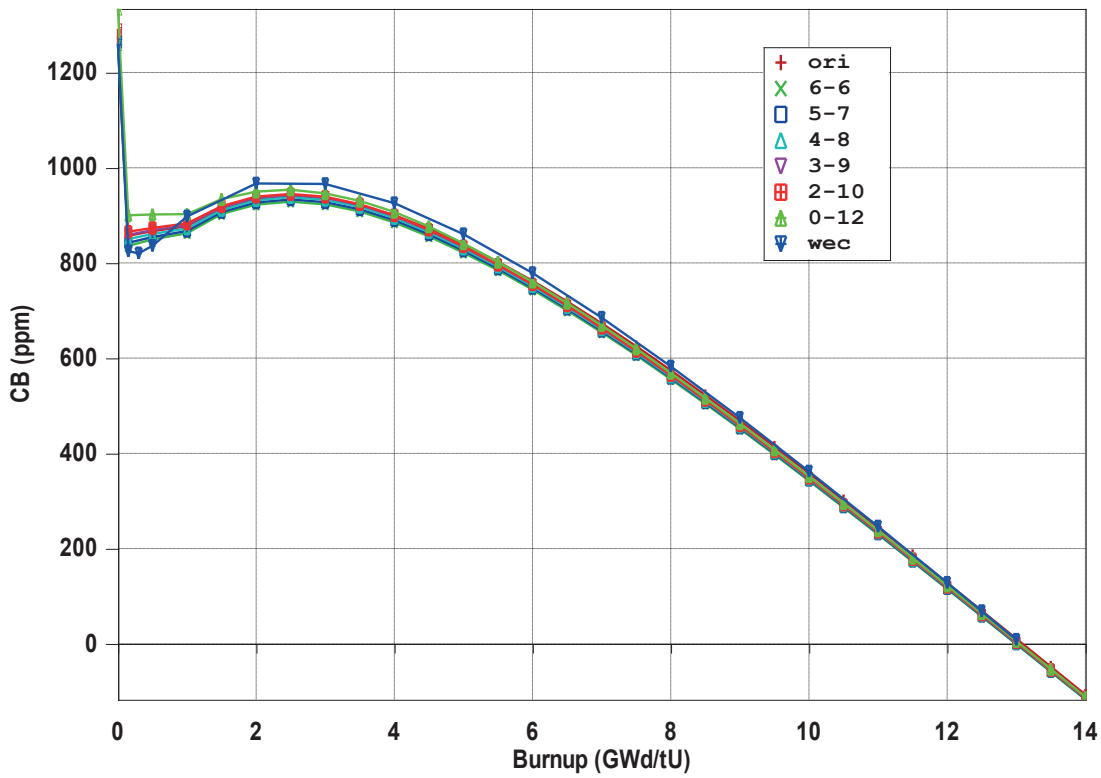


Figure 4: Boron concentration vs. burnup

I2S C01

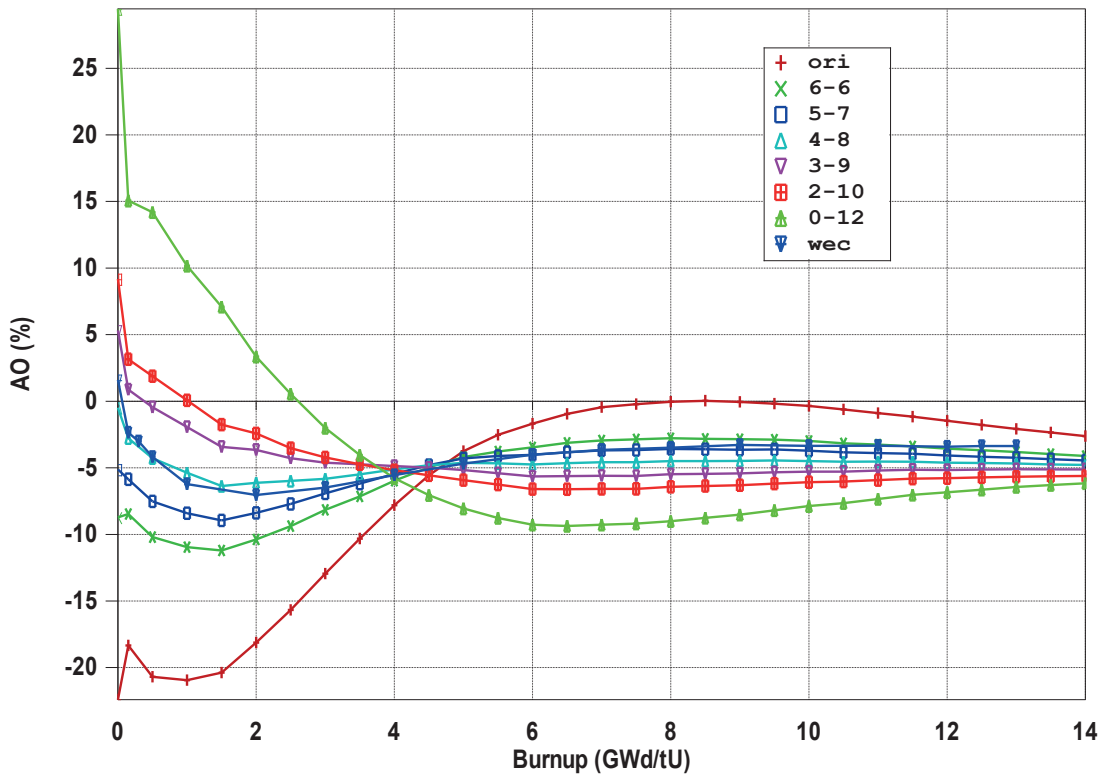


Figure 5: Axial Offset vs. burnup

I2S C01

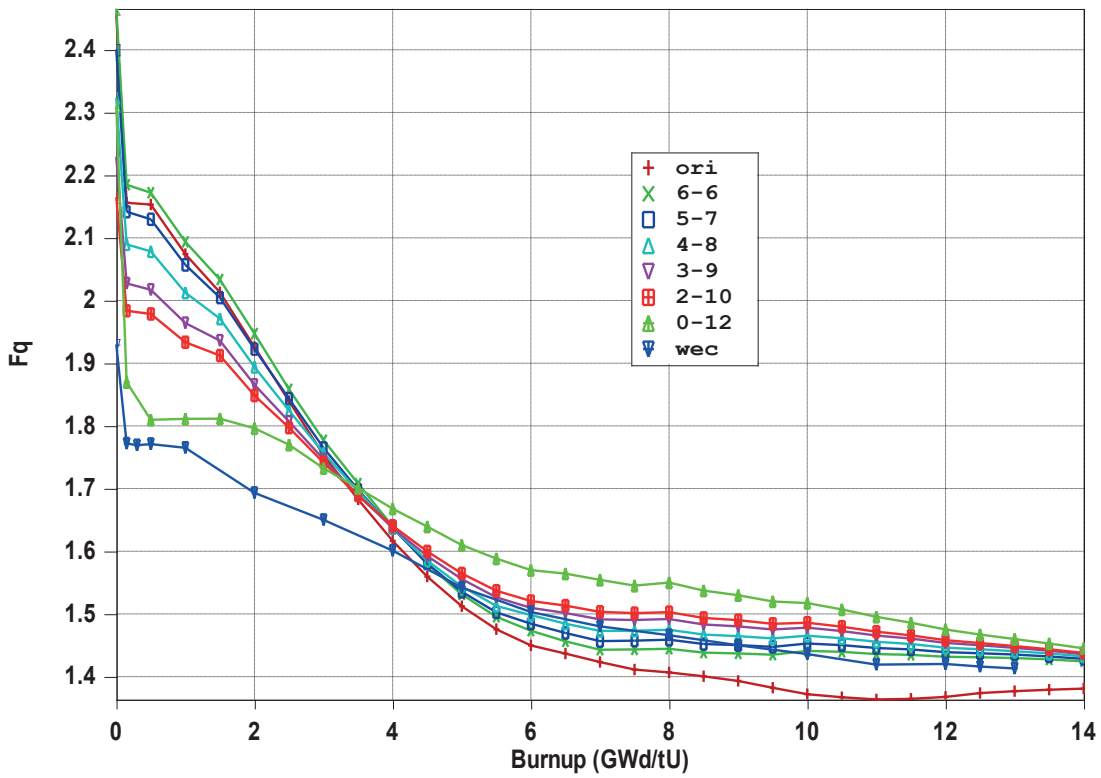


Figure 6:  $F_q$  vs. burnup

I2S C01

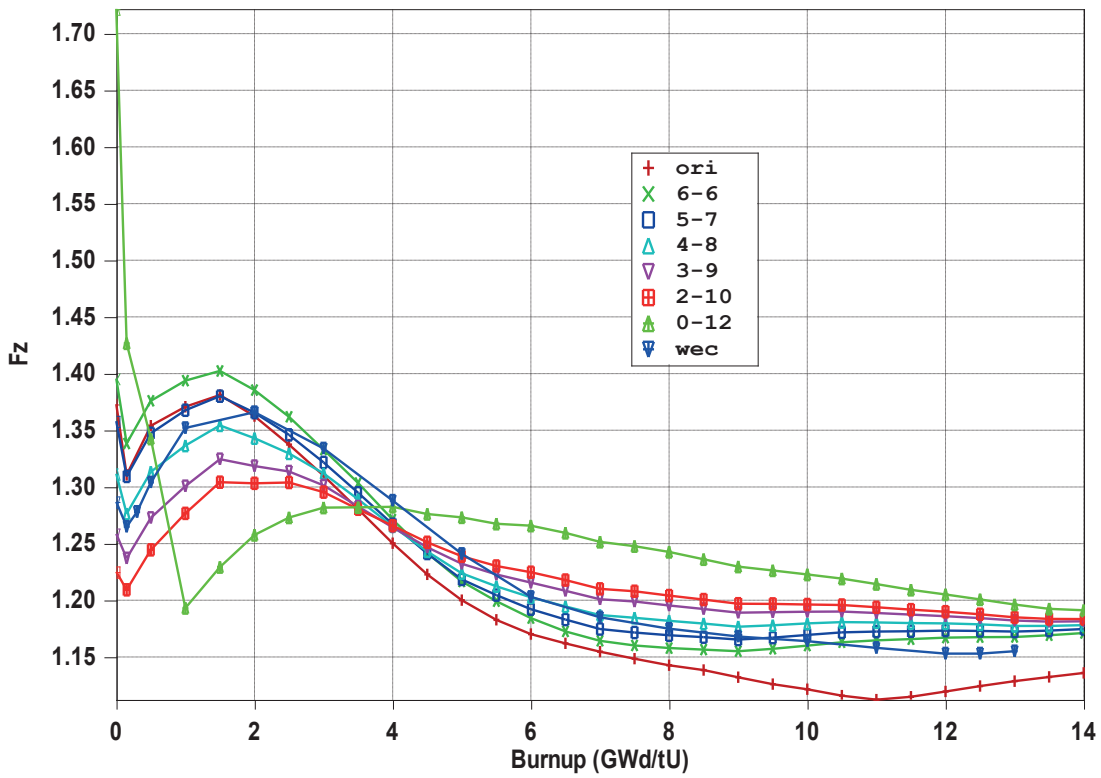


Figure 7:  $F_z$  vs. burnup

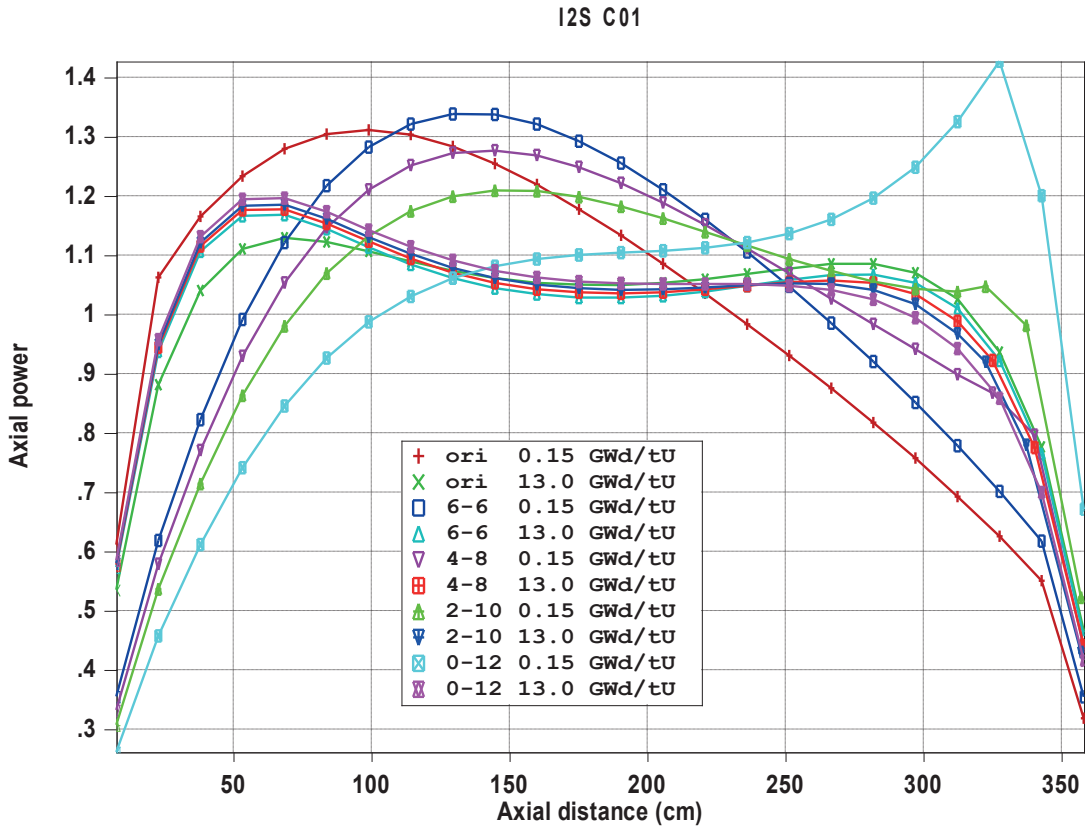


Figure 8: Axial power distribution

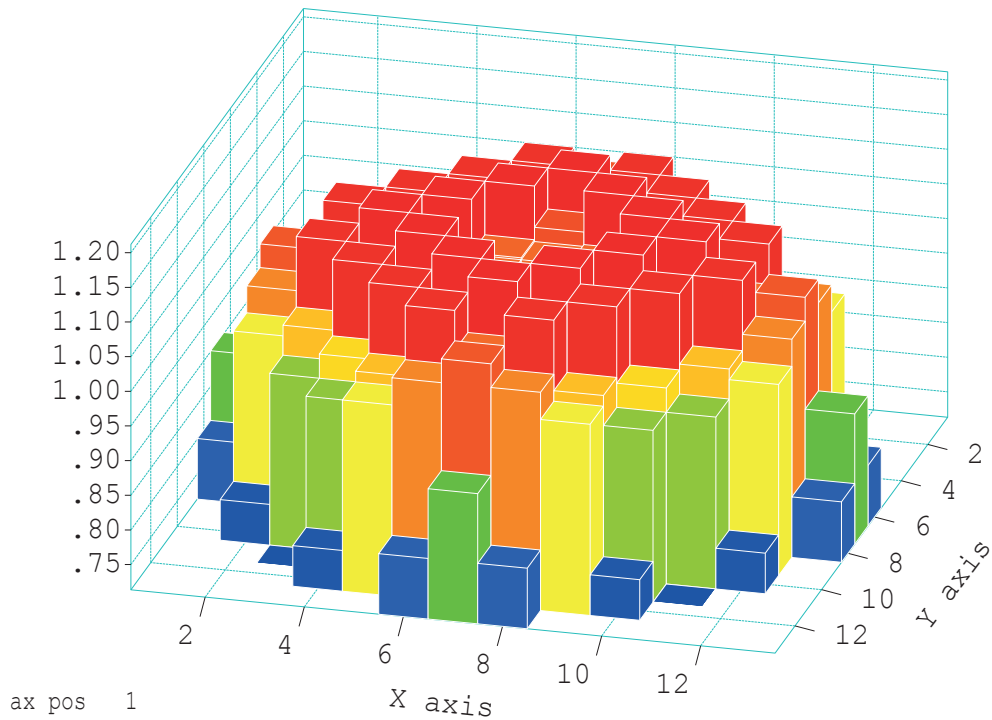


Figure 9: Relative power distribution at Bu = 13 GWd/tU

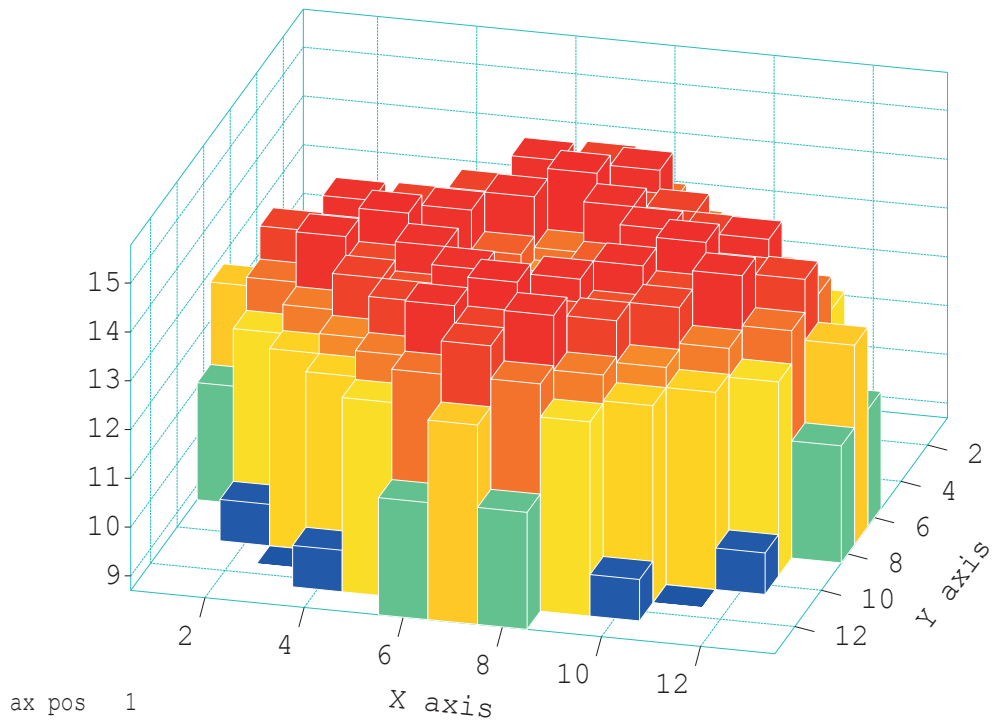


Figure 10: Burnup distribution at Bu = 13 GWd/tU

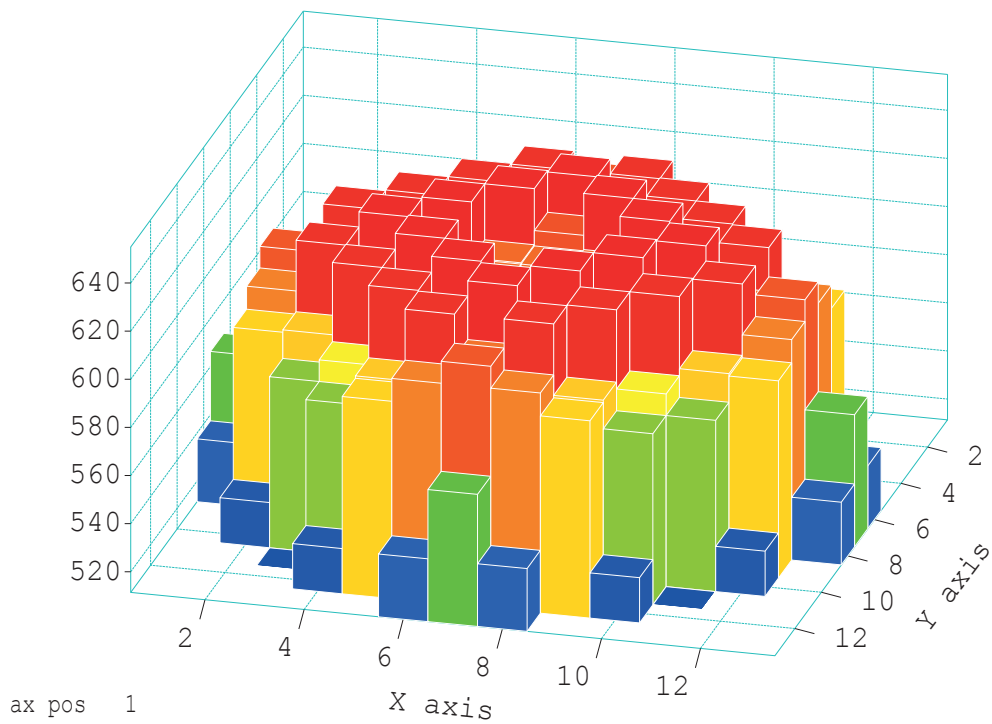


Figure 11: Fuel center line temperature distribution at Bu = 13 GWd/tU

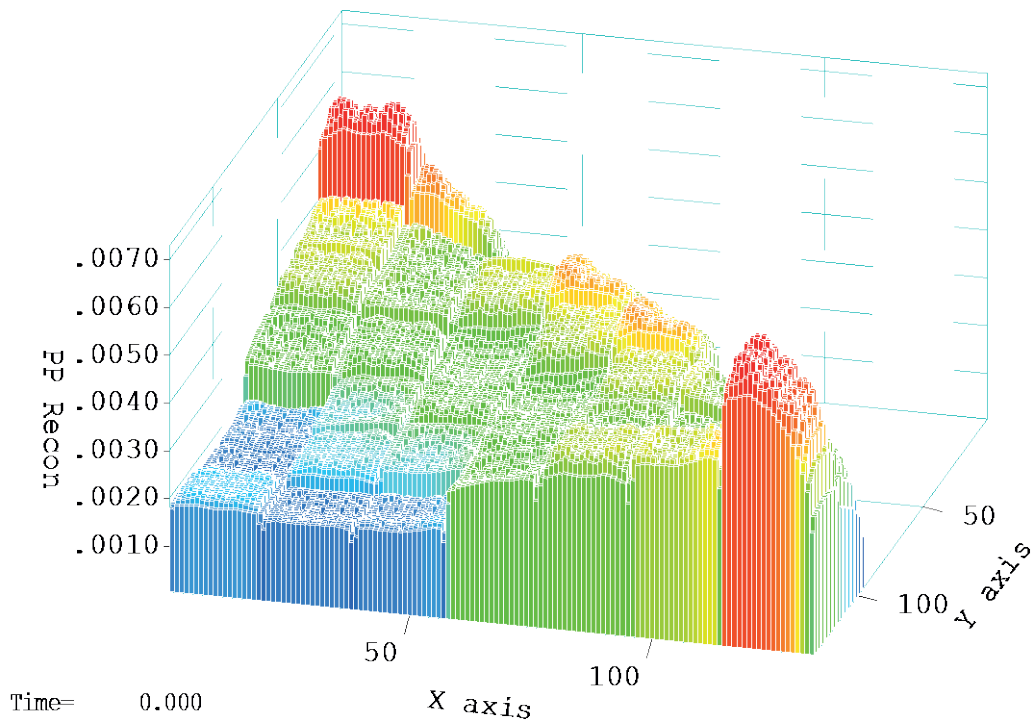


Figure 12: Relative pin powers at  $Bu = 0.15$  GWd/tU, 1<sup>st</sup> quadrant

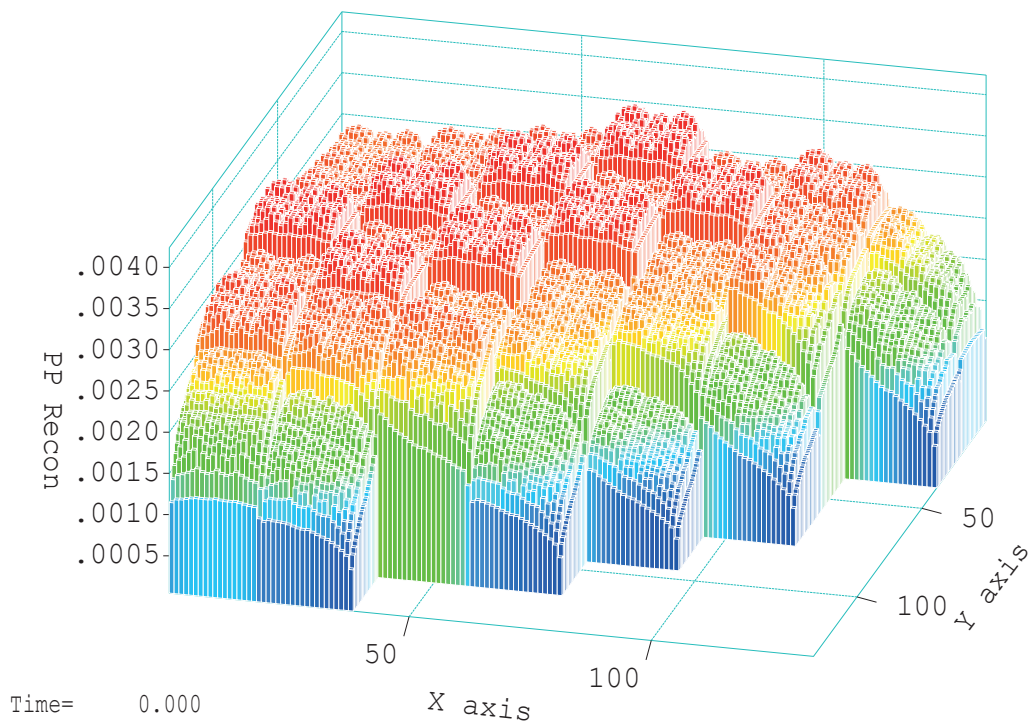


Figure 13: Relative pin powers at  $Bu = 13$  GWd/tU, 1<sup>st</sup> quadrant

## REFERENCES

- [1] B. Petrovic, "Integral Inherently Safe Light Water Reactor (I<sup>2</sup>S-LWR) Concept: Extending SMR Safety Features to Large Power Output", *Proc. International Congress on Advances in Nuclear Power Plants (ICAPP'2014)*, April 6-9, 2014, American Nuclear Society (2014).
- [2] B. Petrovic, "The Integral Inherently Safe Light Water Reactor", *Nuclear Engineering International*, 26-30 (2014).
- [3] B. Petrovic, F. Franceschini, P. Ferroni, "Fuel Cycle Cost Trade-off Studies for I<sup>2</sup>S-LWR (Integral Inherently Safe LWR) Fuel Design Selection", LWR Fuel Performance Meeting, Top Fuel 2013, 603-610.
- [4] H. Joo, Barber, D., Jiang, G., Downar, T., "PARCS: A Multi-Dimensional Two-Group Reactor Kinetics Code Based on the Nonlinear Analytic Nodal Method", *PU/NE-98-26*, Purdue University, 1998.
- [5] "SCALE: A Comprehensive Modeling and Simulation Suite for Nuclear Safety and Design", ORNL/TM-2005/39, Version 6.1, June 2011. Available from Radiation Safety Information Computational Center at Oak Ridge National Laboratory as CCC-785.
- [6] Jaakko Leppänen, "Serpent – A Continuous-Energy Monte Carlo Reactor Physics Burnup Calculation Code", User's Manual, June 18, 2015.

## Possible Used Fuel Management Options For A Single Reactor Utility

Vanessa Vo Van, Peter Breitenstein

AREVA NC

Tour AREVA, 1 Place Jean Millier, 92 400 Courbevoie La Defense, France

[vanessa.vovan@areva.com](mailto:vanessa.vovan@areva.com), [peter.breitenstein@areva.com](mailto:peter.breitenstein@areva.com)

### ABSTRACT

Used nuclear fuel generated by the operation of Nuclear Power Plants (NPP) needs to be managed in a safe, responsible and effective way. Whereas utilities managing several NPP can implement large scale used fuel management operations, a single reactor utility will chose solutions adapted for relatively low amount of used fuel.

There are currently two different approaches for managing used fuel:

- Open fuel cycle, or “once-through” strategy, where used fuel is considered to be waste and disposed of after wet or dry interim storage following in-reactor use;
- Closed fuel cycle, or “recycling” strategy, where used fuel is considered as valuable material as it mainly contains reusable uranium and plutonium and thus recycled; such strategy can be implemented directly after in-reactor use without interim storage step and can also be put in place after interim storage; by treating used fuel, 96% of the nuclear material is recovered and recycled as Mixed OXide (MOX) fuel and Enriched Reprocessed Uranium (ERU) fuel; the remaining 4% of non-recyclable material, as well as cladding and structural elements of fuel assemblies, are packaged for final disposal.

In addition, long term interim storage of used fuel has been retained by some states until decision is made for one or the other of the two available options, keeping in mind that interim storage, even long term, is a waiting solution and not a sustainable one.

For all options, disposal is the final radioactive waste management step: either direct disposal of used fuel or disposal of final residual waste remaining after used fuel treatment.

The purpose of the paper is to present the possible used fuel management options for a single reactor utility, clarifying advantages and drawbacks of each of them according to following criteria: safety, security, sustainable development, environment protection, non-proliferation, public acceptance, economy.

*Keywords:* used fuel, sustainable, radioactive waste, open fuel cycle, closed fuel cycle

### 1 INTRODUCTION

With sustainable development, environment protection, and public acceptance in mind, single reactor utilities (and states) are looking into their options for used nuclear fuel (UNF) management. UNF needs to be managed in a safe, responsible and effective way.

There are two options for UNF management: open fuel cycle with direct disposal and closed fuel cycle with recycling of UNF (see Figure 1).

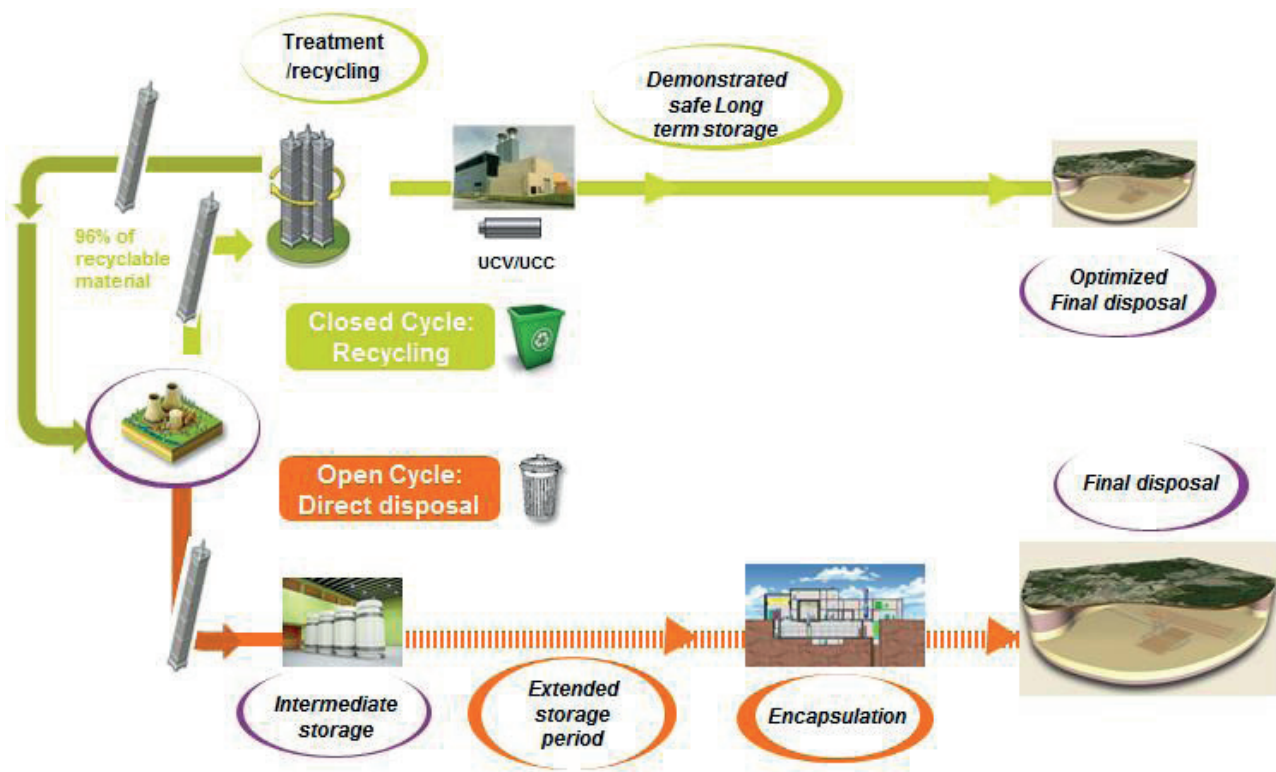


Figure 1: Two options for UNF management, direct disposal and recycling

These options can be implemented either in the state itself or in the framework of an international cooperation program: for example, ERDO working group in which a number of European countries/utilities currently take part, is aiming at investigating the feasibility of implementing shared solutions for safe and very long-term management of long-lived nuclear waste.

In addition, long term interim storage of UNF has been retained by some states until decision is made for one or the other of the two available options, keeping in mind that interim storage, even long term, is a waiting position and not a sustainable solution.

For all options, disposal is the final radioactive waste management step: either direct disposal of UNF or disposal of final residual waste remaining after used fuel treatment. It is widely accepted in the technical community that the only currently feasible method to ensure very long-term safety for High Level Waste (HLW) or UNF is isolation in deep, stable geological formations, usually several hundred meters or more below the surface

The paper presents a panorama of UNF management available options for utilities operating a single reactor or a small fleet of reactors, clarifying advantages and drawbacks of each of these options according to following criteria: safety, security, sustainable development, environment protection, non-proliferation, public acceptance, economy.

The following factors may especially influence the decisions to make:

- Remaining reactor lifetime, lifetime extensions
- Need for extended interim storage of UNF before availability of a definitive solution
- Uncertainty concerning geological disposal availability (incl. schedule).

## 2 OPEN FUEL CYCLE: ADVANTAGES AND DRAWBACKS

In case of open fuel cycle, or “once-through” strategy, used fuel is considered as waste and disposed of after several decades of extended wet or dry interim storage (see Figure 2) which have been following in-reactor use. There are two main reasons for this need to extend the initially designed storage capacity on reactor site before evacuation of UNF to the final repository can be implemented:

- Developing a final repository is a very long process
- 40 to 60 years of storage are mandatory for the UNF to be cooled enough so that there is no need to include forced ventilation system in the disposal.

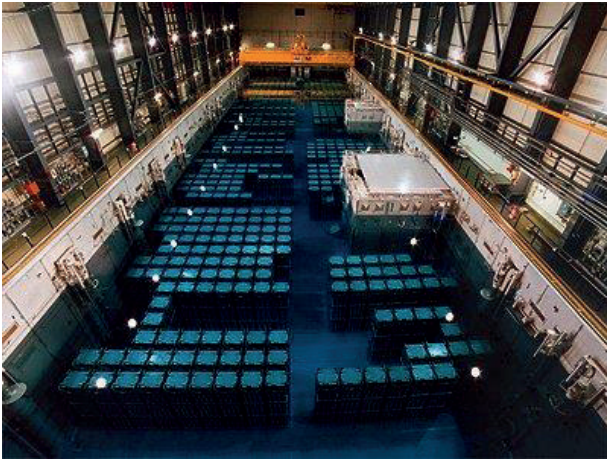


Figure 2: Examples of UNF interim storage: centralized pool and dry storage casks

After storage and before disposal, the UNF needs to be encapsulated in a corrosion resistant and mechanically stable container, which will provide isolation for thousands of years.

Most programmes under development worldwide for direct disposal of UNF consist in deep geological disposal either in clay or granite. Tuff was the host rock for Yucca Mountain project in the US, and salt is still considered as a possible option in the US as well as in Germany and Spain.

The most advanced states in the process of setting a final repository for UNF are Finland and Sweden which are considered as benchmark for other states.

As open fuel cycle strategy states, Finland and Sweden have been developing the KBS-3 approach: UNF first is encapsulated in copper, and the copper canisters then are placed in granite basement rock at a depth of about 500 meters and surrounded by bentonite clay.

In addition, final repositories for UNF require implementation of safeguards in order to comply with non-proliferation objectives aiming at detecting any diversion of declared nuclear material or any undeclared nuclear material activity. The IAEA figure 3 below illustrates control points that could be implemented in the framework of a deep geological repository including used nuclear fuel.

It is to be noted that this figure does not show the virtual containment controls that are to be implemented according to IAEA once the repository will be closed.

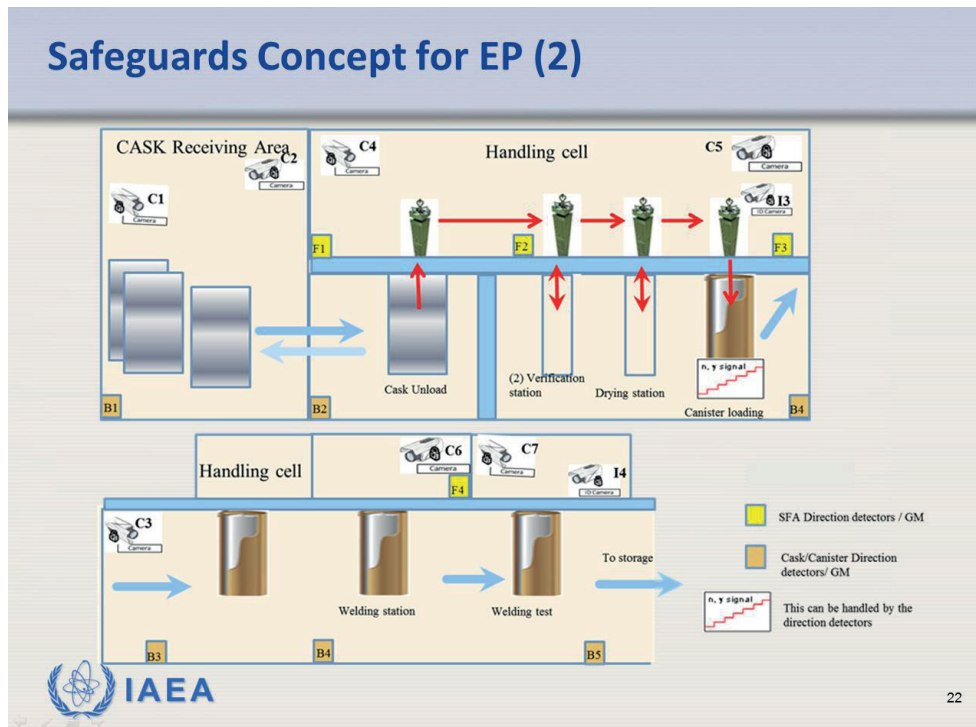


Figure 3: Safeguards control points in UNF deep geological repository concept [1]

Compared with a closed fuel cycle, a direct disposal approach presents several drawbacks as it leaves to future generations:

- Surveillance of very long-lived high level radioactive waste (need for one million years for UNF to reach ore radioactivity level) and proliferating material (security of used fuel inventories becoming a challenge taking into account terrorist attacks context), during extremely long periods of time
- Management of large majority of the safety and economical risks.

On the other hand, the open fuel cycle strategy has several advantages:

- It does not require separation of plutonium which is, in some societies, a benefit regarding public acceptance
- The high expenses are significantly postponed as majority of the back-end management funding is required for the encapsulation, the geological repository and the long-time surveillance.

A utility/state operating a single reactor or a small fleet of reactors can chose the open fuel cycle strategy with the objective of developing with others an international disposal. During such development, the utility would need to implement interim storage of UNF. Depending on requirement for flexibility, modularity, security, short-term cost effectiveness, the utility will chose among the various available solutions: dry storage casks, vault dry storage, wet storage.

### 3 CLOSED FUEL CYCLE: ADVANTAGES AND DRAWBACKS

In case of closed fuel cycle, or “recycling” strategy, used fuel is considered as valuable material as it mainly contains reusable uranium and plutonium and is thus recycled. Such strategy can be implemented directly after in-reactor use without interim storage step and can also be put in place after interim storage. By treating used fuel (see figure 4), 96% of the nuclear material is recovered and recycled as Mixed OXide (MOX) fuel and Enriched Reprocessed Uranium (ERU) fuel; the remaining 4% of non-recyclable material, as well as cladding and structural elements of fuel assemblies, are packaged for final disposal.

## 96% of the content of used nuclear fuel is recyclable

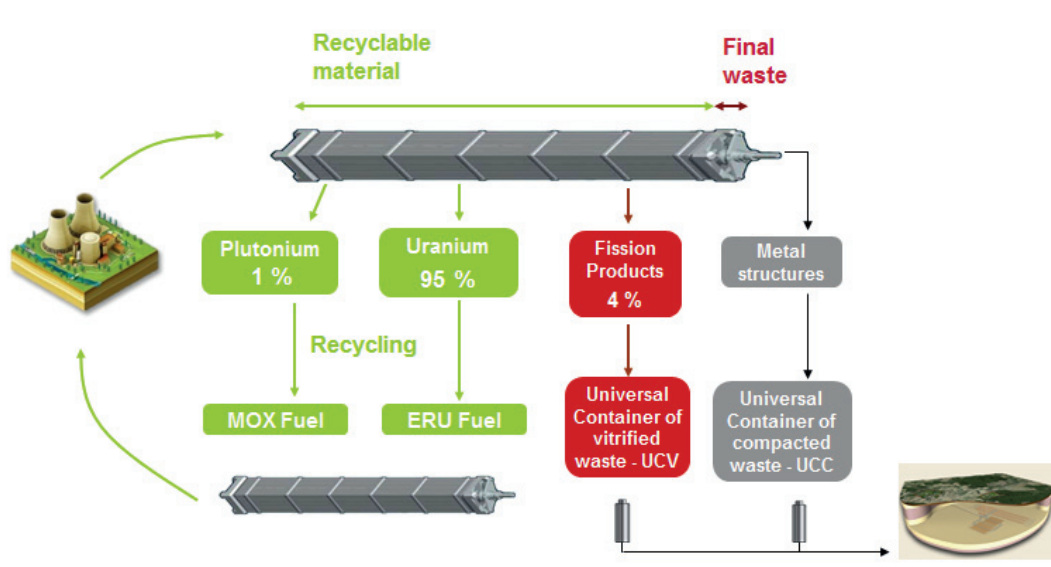


Figure 4: UNF recycling – 96% of the nuclear material is recovered

Several states have chosen the closed fuel cycle strategy including a state with a small fleet of reactors: France, Russia, China, India, Japan, the Netherlands.

After recycling of UNF, the residual waste is conditioned in very stable form and stored while waiting for final disposal either in vault storage or in dry storage casks facility.

The most advanced state in the process of setting a final repository for universal canisters is France, considered as benchmark for other states: the project consists in deep geological disposal in clay.

UNF recycling brings huge benefits on final repository as it:

- Leads to a drastic reduction of the volume of conditioned/packaged HLW and long-lived intermediate level radioactive waste (LL-ILW) for disposal, thanks to the removal of uranium and plutonium
- Decreases the long-term radiotoxicity as well as the short-term heat load of HLW to be disposed of
- Eases final repository design as safeguards are not required thanks to uranium and plutonium removal from final waste; this advantage coupled with the reduction in waste volume, long-term radiotoxicity and short-term heat load of HLW lead to a strong optimisation of the final repository
- Gives additional time for implementing the final disposal repository taking into account the demonstrated stability of final waste (stored pending disposal) and ease of above ground storage
- Eases public acceptance process in the framework of final repository implementation
- Reduces the risks associated with the uncertainty surrounding final disposal costs.

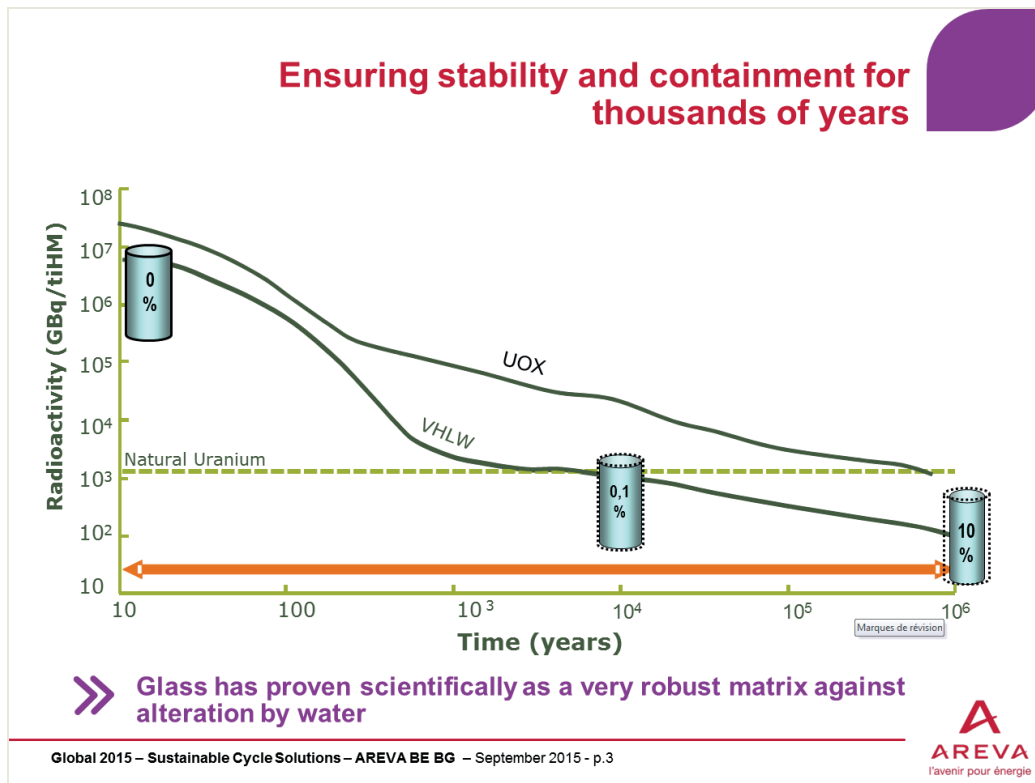


Figure 5: UCV radioactivity decrease and glass matrix robustness [2]

Recycling approach presents two main difficulties:

- Public acceptance may not be in favour of the recycling activity, with a misled but usual perception that plutonium is “produced” in the treatment facility, rather than retrieved and reused in recycled fuels (plutonium being in fact produced through irradiation in reactors)
- Strong financing must be implemented upfront: an important share of the back-end management funding is required for recycling the fuel, while funds dedicated to further storage and disposal are more limited as volumes and risks significantly decrease vs open cycle options.

On the other hand, the advantages of closed fuel cycle strategy are numerous:

- It is highly sustainable as it removes for future generations the burden related to management of very long-lived high level radioactive waste (meaning the long-lived HLW to manage reaches uranium ore activity level in 2,000-3,000 years as compared to UNF activity which needs about  $10^6$  years for getting to uranium ore activity level, see figure 5), proliferating material, and economical risks
- It facilitates the public acceptance about final repository implementation and strongly optimizes its design thanks to
  - no requirement for safeguards
  - drastic reduction in waste volume, long-term radiotoxicity and short-term heat load of HLW
  - no conditioning or repacking facility needed.

A utility/state operating a single reactor or a small fleet of reactors can choose the closed fuel cycle strategy by implementing recycling with a recycling services provider like AREVA in France.

Uranium and plutonium recovered from UNF recycling can then be reused either in the utility own reactor(s) or in third party reactor(s), depending on utility reactor’s lifetime.

One to two decade(s) after recycling, the utility will receive the final waste remaining after UNF treatment, conditioned into universal canisters and can store them in vault storage or dry storage casks, both with simplified design compared to UNF storage.

As for the final step of radioactive waste management, the final disposal, the utility/state may develop with others an international disposal, bringing to it the benefits of having recycled UNF.

From a global point of view, it will be technically simpler and economically more effective to implement an international disposal for various types of universal waste canisters than for UNF with various origins.

## 4 CONCLUSION

There are two options for UNF management, each of them presenting several advantages and drawbacks: open fuel cycle with direct disposal and closed fuel cycle with recycling of UNF.

Direct disposal presents several drawbacks as it leaves to future generations a burden related to:

- Surveillance of very long-lived high level radioactive waste and proliferating material
- Management of large majority of the safety and economical risks.

On the other hand, this strategy has several advantages:

- It does not require separation of plutonium which is a benefit regarding public acceptance
- The high expenses are significantly postponed as majority of the back-end management funding is required for the encapsulation, the geological repository and the long-time surveillance.

UNF recycling presents two main difficulties:

- Public acceptance may not be in favour of the recycling activity
- Strong financing must be implemented upfront as large part of the back-end management funding is required for recycling the fuel.

On the other hand, the advantages of closed fuel cycle strategy are numerous:

- It is highly sustainable as it removes now the burden related to management of very long-lived high level radioactive waste, proliferating material, and economical risks
- It facilitates the public acceptance about final repository implementation and strongly optimizes its design.

A utility or state operating a single reactor or a small fleet of reactors will chose the UNF management strategy based on deep assessment of international regulation, own state regulation specificities, economics, certainties, financial and technical risks, energetic independence, sustainability. For this, the utility can benchmark the strategies chosen by others and also use the services providers industrial experience.

## REFERENCES

- [1] Yuri Yudin, IAEA Department of Safeguards, “Developing Safeguards Approaches for Future Encapsulation Plants and Geological Repositories”, Presentation at INPRO Dialogue Forum on Roadmaps for a Transition to Globally Sustainable Nuclear Energy Systems, Vienna, 22 October 2015
- [2] Caroline Drevon, AREVA, “Sustainable Cycle Solutions”, Presentation at Global 2015, Paris, September 2015

Journal  
of Energy

ENERGY